Production of vanillin from lignin present in the Kraft black liquor of the pulp and paper industry

Ph.D. Dissertation in

Biological and Chemical Engineering

Presented by

José Daniel Pacheco Araújo

Department of Chemical Engineering

Faculty of Engineering

University of Porto

August 2008

Acknowledgments

In this section I would like to express myself in a language easier to understand by all the people I want to address my appreciation.

Ao meu orientador Professor Alírio Rodrigues, pela oportunidade que me proporcionou, capacidade de orientação e pelos conhecimentos que me transmitiu ao longo deste trabalho.

A toda a FEUP, e em particular ao Departamento de Engenharia Química, pelo apoio e meios disponibilizados.

A todos os Professores do LSRE, em particular ao Professor José Miguel Loureiro, pelas ajudas que me foram dadas, sugestões e palavras de encorajamento.

Ao Sr. Nelson Neves, pelo excelente trabalho que realizou na construção da coluna de borbulhamento, e pela disponibilidade que sempre revelou para a resolução de problemas.

To Westvaco Co., for the kindly offer of the raw material (Indulin AT) used in the experimental part of this work.

À Fundação para a Ciência e a Tecnologia, pelo financiamento da bolsa de Doutoramento PRAXIS/BD/21501/99 e do projecto POCTI/1999/QUE/33198.

A todo o grupo de trabalho da SNF/Ambientágua, pelo apoio que me foi dado durante a minha presença na empresa, amizade e incentivo na resolução dos problemas diários.

Ao meu amigo (e irmão) Carlos Grande, pela sua importantíssima ajuda na realização deste trabalho, e pelo seu altruísmo, com o qual nunca me deixou desistir, mesmo nos momentos mais difíceis e de menor motivação. Ao Eduardo Oliveira, pela sua amizade incondicional e empenho constante para ajudar os que o rodeiam.

Aos meus amigos e colegas – Mafalda, Eduardo Borges, Simone, Paulo, Filipe Lopes, Paula, Marta, Rui, Filipe Cunha, Nabil, Ricardo, Peter, Rodrigo, Nuno e José Augusto – que de uma forma directa ou indirecta contribuíram para que fosse capaz de concluir este trabalho.

Ao meu pai, pela sua dedicação e perseverança para que realizasse os objectivos a que me tinha proposto. Muito obrigado por toda a ajuda que me deste, muitas das vezes em teu próprio prejuízo, e pelo teu contributo fundamental para que crescesse como pessoa. Sem isso, nunca teria conseguido.

A toda a minha restante família, em particular à minha mãe, pelo seu carinho, força, atenção e enorme paciência. Mereces todos os agradecimentos e dedicatórias possíveis.

MUITO OBRIGADO A TODOS!

Abstract

In this work, the main objective was to produce vanillin from the Kraft lignin present in the *black liquor* of the pulp and paper industry. Vanillin is one of the most popular flavouring agents in food industry and its wide range of application also spreads to the fields of perfumery and pharmaceutical intermediates.

Batch experiments of lignin oxidation were performed with the purpose of determine the vanillin yield obtained with the Kraft lignin supplied by Westvaco Co., and compared to the results achieved in previous studies. The vanillin yields obtained were around 3.5% of the initial lignin mass – in extreme oxidative conditions it is admitted that a maximum of only 13% of the lignin mass can be converted into vanillin – which is approximately half of the levels achieved by Dr. Álvaro Mathias. This fact supports the idea that the lignin available for this work is different, leading to an adjustment in the values of two parameters of the original kinetics of lignin oxidation already developed at the LSRE.

A complete setup to promote the lignin oxidation with oxygen, in continuous mode, was designed and constructed during this thesis. The heart of this apparatus is a bubble column reactor with a capacity of 8 liters, and it is prepared to work in very alkaline media with temperatures up to 170ºC and pressures up to 15 bar. This reaction unit was also filled with three modules of Mellapak 750.Y structured packing from Sulzer Chemtech (Switzerland).

To evaluate the performance of the continuous gas-liquid reactor regarding the vanillin yield, experiments of Kraft lignin oxidation and vanillin oxidation were performed in two different configurations – empty column (BCR) and column filled with structured packing (SPBCR). In this experimental work, the effect of the liquid flow rate, oxygen partial pressure and gas flow rate was studied within the setup operation limits. For the lignin oxidation, the highest value achieved for the vanillin concentration in the outlet stream was 0.89 g/l (11.4% of a complete lignin oxidation). When compared to the BCR configuration, the structured packing enhanced the oxygen mass transfer to the liquid, although only a small increase in the volumetric mass transfer coefficient was observed (1.35 times).

A mathematical model to describe the continuous reactor was developed, and simulation studies on the influence of the operating conditions were performed to improve the levels of vanillin yield achieved in the experimental work. The best result for the steady state vanillin concentration in the exit stream was 1.8 g/l, which is 23% of a complete lignin oxidation and 85% of the maximum levels obtained in the batch reactor for the same lignin source. The respective set of conditions is: liquid flow rate of 10 l/h; set point of the thermostatic bath of 433 K; oxygen partial pressure of 10 bar; total pressure of 10 bar; and gas flow rate of 40000 ml_{NTP}/min.

Resumo

O principal objectivo deste trabalho foi a produção de vanilina, a partir da lenhina Kraft presente na corrente de licor negro da indústria de pasta de papel. A vanilina é um dos aromatizantes mais populares da indústria alimentar, mas a sua vasta gama de aplicação também abrange as áreas da perfumaria e intermediários para produtos farmacêuticos.

Foram realizadas experiências de oxidação de lenhina, em reactor fechado, com o propósito de determinar o rendimento de vanilina obtida a partir da matéria-prima fornecida pela Westvaco Co., e comparar esse valor com resultados de estudos anteriores efectuados para diferentes lenhinas. Foi obtida uma conversão de 3.5% da massa inicial de lenhina em vanilina – em condições extremas de oxidação, admite-se que, apenas 13% da massa de lenhina se poderá converter em vanilina – cujo valor é aproximadamente metade dos níveis atingidos por Álvaro Mathias. Este facto suporta a ideia de que a lenhina disponível para este trabalho é diferente da utilizada anteriormente no LSRE, o que levou a um ajustamento de dois parâmetros da cinética de oxidação de lenhina neste trabalho.

Durante esta tese foi projectada e construída uma instalação completa para promover a oxidação de lenhina com oxigénio, em modo de operação contínuo. O coração desta instalação é uma coluna de borbulhamento com uma capacidade de 8 litros, que está preparada para trabalhar em meios fortemente alcalinos, com temperaturas e pressões que poderão ir até aos 170ºC e 15 bar, respectivamente. Foram também colocados, no interior desta unidade de reacção, três módulos de enchimento estruturado do tipo Mellapak 750.Y da Sulzer Chemtech (Suiça).

Para avaliar o desempenho do reactor em contínuo foram efectuadas experiências de oxidação de lenhina Kraft e de oxidação de vanilina, para duas configurações diferentes do reactor – coluna vazia (BCR) e coluna preenchida com enchimento estruturado (SPBCR). Neste trabalho experimental foram estudados os efeitos do caudal de líquido, pressão parcial de oxigénio e caudal de gás, dentro dos limites de operação da instalação. Nas experiências de oxidação de lenhina, a concentração de vanilina mais alta, obtida na corrente de saída do reactor, foi de 0.89 g/l (11.4% de uma oxidação completa de lenhina). Comparando os resultados obtidos para as duas configurações do reactor, verifica-se que o enchimento estruturado melhora a transferência de oxigénio para o líquido, apesar de se observar um pequeno aumento no respectivo coeficiente de transferência de massa.

Foi desenvolvido um modelo matemático para descrever o reactor gás-líquido, e foram também efectuadas simulações para estudar a influência das principais condições operatórias, de modo a melhorar os valores atingidos no trabalho experimental, em termos de produção de vanilina. O melhor resultado destas simulações, relativamente à concentração de vanilina na corrente de saída do reactor, foi de 1.8 g/l, o que representa 23% de uma oxidação completa de lenhina, e 85% do máximo obtido para a mesma fonte de lenhina no reactor fechado. Para obter este resultado as condições operatórias são as seguintes: 10 l/h de caudal de líquido; banho termostático a 433 K; 10 bar pressão total de gás (utilização de oxigénio puro); 40000 ml_{PTN}/min de caudal de gás.

Résumé

Dans cette étude, l'objectif principal était de produire de la vanilline à partir de la lignine de Kraft présent dans la liqueur noire de l'industrie papetière. La vanilline est l'un des aromatisants les plus populaires dans l'industrie alimentaire et son large champ d'application s'étend jusqu'au domaine du parfum et des intermédiaires pharmaceutiques.

Les expériences en réacteur fermé de l'oxydation de la lignine ont été réalisées dans le but de déterminer les rendements de vanilline obtenus à partir de la lignine de Kraft fournie par Westvaco Co., et de comparer ces résultats avec ceux issus des précédentes études. Les rendements de vanilline obtenus étaient alors proches de 3,5 % de la masse de lignine initiale - dans des conditions oxydatives extrêmes, il est admis que 13 % maximum de lignine peut être convertie en vanilline - ce qui correspond approximativement à la moitié des niveaux atteints par le Dr. Alvaro Mathias. Ce fait conforte l'idée que la lignine employée dans cette étude est différente et nécessite par conséquent un ajustement des valeurs de deux paramètres de la cinétique originale de l'oxydation de la lignine initialement développée au LSRE.

Une installation expérimentale complète a été conçue et construite durant cette thèse pour favoriser l'oxydation de la lignine avec l'oxygène. Le cœur de cette installation est un réacteur de type colonne à bulles d'une capacité de 8 litres et aménagé pour travailler dans un milieu très alcalin à des températures pouvant atteindre 170 °C avec des pressions allant jusqu'à 15 bar. Ce réacteur a également été rempli avec trois modules de garnissage structuré Mellapak 750.Y fournis par Sulzer Chemtech (Switzerland).

Pour évaluer la performance de ce réacteur continu gaz-liquide en fonction du rendement de vanilline, les expériences d'oxydation de la lignine de Kraft et celles d'oxydation de la vanilline ont été réalisées suivant deux configurations différentes – une colonne vide (BCR) et une colonne avec un garnissage structuré (SPBCR). Dans ce travail expérimental, plusieurs paramètres ont été étudiés tels que l'influence du débit liquide, de la pression partielle d'oxygène ou encore le débit du gaz. Pour l'oxydation de la lignine, la plus grande valeur atteinte en termes de concentration de vanilline dans le courant de sortie, était de l'ordre de 0,89 g/l (11,4 % de l'oxydation complète de la lignine). En comparaison avec une configuration BCR, le garnissage structuré a permis d'accroître le transfert de matière de l'oxygène vers le liquide, malgré une faible augmentation du coefficient de transfert de matière volumétrique (1,35 fois).

Un modèle mathématique a été développé pour décrire le réacteur continu et des simulations ont été réalisées pour étudier l'influence des conditions opératoires afin d'améliorer les rendements de vanilline dans le travail expérimental. La plus grande concentration de vanilline à l'état stationnaire obtenue dans le courant de sortie était de 1,8 g/l, soit 23% d'une oxydation complète de vanilline et 85 % des niveaux maximums atteints dans un réacteur fermé avec la même source de lignine. Les conditions respectives étaient les suivantes : débit liquide de 10 l/h ; point de consigne du réacteur thermostatique de 433 K ; pression partielle de l'oxygène de 10 bar ; pression totale de 10 bar ; et un débit de gaz de 40000 ml_{NTP}/min.

Table of contents

List of Figures

Chapter 1

Chapter 2

Chapter 3

Chapter 4

Chapter 5

Appendix B

Appendix C

Appendix D

List of Tables

Chapter 1

Chapter 2

Chapter 3

Chapter 4

Chapter 5

Appendix B

Appendix C

Appendix D

Appendix E

1. Introduction

1.1 Relevance and Motivation

Vanillin (4-hydroxy-3-methoxybenzaldehyde) is the major flavour constituent of vanilla. It has a wide range of applications in food industry as a flavour agent and in perfumery as an additive. Other applications are as chemical precursor in the pharmaceutical industry, ripening agent, antifoaming agent in lubrification oils, brightener in zinc coating baths, vulcanization inhibitor, and starting material for insecticides and herbicides (Mathias, 1993; Villar et al., 1997).

There are around 150 varieties of vanilla, but only two of them are grown commercially – Bourbon and Tahitian vanilla (McGregor, 2005). Vanilla has it origins on Mesoamerican Mexico, with this country dominating the world production until the late 19th century. Since then, the focus of development was shifted to the former French colonies, in particular Madagascar, Comoros, Reunion and Tahiti. Nowadays, vanilla is grown on numerous countries, with data from 2005 indicating that Madagascar was the largest producer, accounted for around 60% of the world production, followed by Indonesia and China, with 23% and 10%, respectively (http://faostat.fao.org). Looking at the last 20 years, the vanilla production has oscillated between 1200 and 4000 tonnes, with a world consumption varying from 1800 to 3000 tonnes (McGregor, 2005).

The natural vanilla market is characterized by very volatile prices. Normally the price pattern of vanilla is made up of high peaks and prolonged periods of relatively low prices. These prices have been particularly sensitive to events affecting a single country – Madagascar. From 1989 to 1995, the vanilla market was regulated by the Univanille

cartel, an alliance of vanilla exporters. The major buyers and producers, principally Madagascar, met annually to determine demand and export pricing. In Figure 1.1 is schematically shown the evolution on the market prices of natural vanilla, since the early 1990's to the first half of 2005.

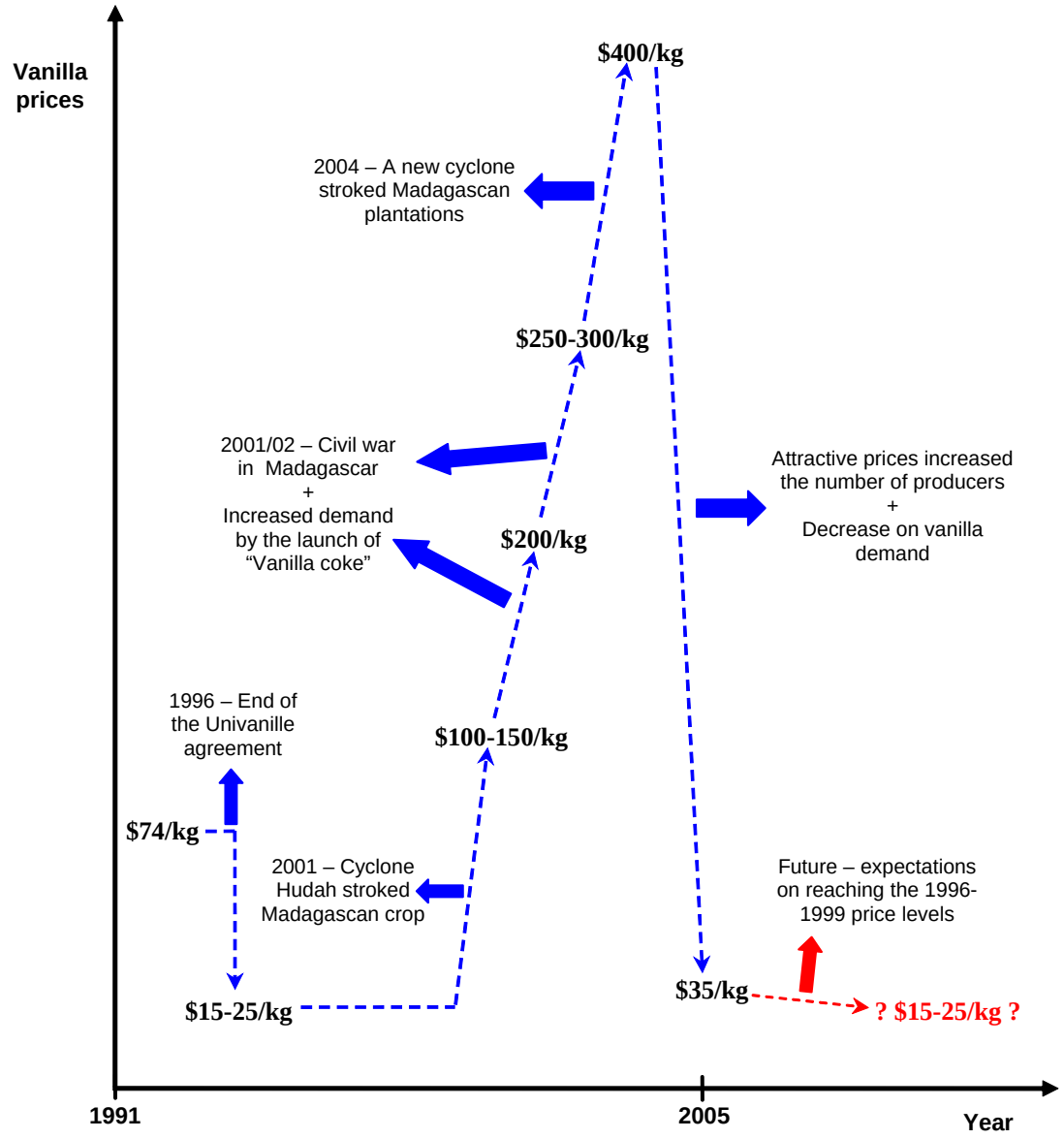

Figure 1.1. Evolution of natural vanilla prices since the early 1990's to 2005 (based on Jaeger (2005)).

Vanilla does not consist of vanillin alone, but contain several tens of aromatic compounds. For example, the vanilla world trade in 2001 (2300 tonnes) represents less than 50 tonnes of natural vanillin (Loeillet, 2003), which only constitutes a yield around

2%. Historically, the production of vanillin was its direct extraction from vanilla beans. However, according to the constantly increasing markets, new chemicals routes were developed. Synthetic vanillin became widely used and competition of markets is longstanding and turns more fierce when prices of natural vanilla rockets.

Vanillin was first produced by Haarmann and Reimer in the late 1800's, using guaiacol from phenol. This was the main route for more than 40 years, until it was discovered that vanillin could be produced from lignin present in the waste liquor of pulp and paper industry. The commercial production of vanillin from lignin started in 1937. This process become the dominant one for many years, with 80% supply ratio of the synthetic vanillin market (Triumph Venture Capital, 2004b). However, in the 1980's some changes in the processes of pulp and paper industry led to a decrease in the available raw material required by the vanillin plants. The traditional calcium sulphite pulping process produced huge amounts of disposable effluents, that combined with the growing public awareness on environmental issues were leading to unsustainable waste treatment costs. These mills started to close, or were converted to new technology that allowed the recycling of the waste liquors for chemical recovery and thus making these by-products streams not available for vanillin production. Since 1993, only Borregaard was producing vanillin from lignin. Nowadays the synthesis of vanillin from guaiacol accounts for 85% of the world supply, with the remaining 15% being produced from lignin (Triumph Venture Capital, 2004b).

Commercial users can choose between natural vanilla (very expensive and used only in niche markets), synthetic vanillin and artificial vanilla flavour (ethyl vanillin). Synthetic vanillin is a cost effective alternative to vanilla and is increasingly substituting the natural product. It not only substitutes vanilla, but also supplements adulterated vanillin extracts. Natural vanilla flavouring constitutes less than 5% of the

world market (Triumph Venture Capital, 2004b). Global demand for synthetic vanillin currently is around 16000 tonnes per year (http://www.foodnavigator.com/news/ng.asp?id=72634-borregaard-vanillin-vanilla), but there are only a few significant manufacturers of this product in the world.

Rhodia SA dominates the world vanillin market using the catechol-guaiacol process (http://www.rhodia.com). Rhodia entered the USA vanillin market in 1986 with the purchase of the Monsanto plant. This plant was subsequently closed down in 1991. In November 1993, Rhodia purchased the ITT Rayonier vanillin business and immediately closed the plant. After that, their main target has been China. First they gained control of the guaiacol market in China with the opening of the Jade Fine Chemical Company plant at Wuxi in 1999, as the result of a 60/40 joint venture between Rhodia and Ube. In 2000 Rhodia acquired the Xuebao vanillin plant, forming a new subsidiary called Ruohai Fine Chemicals Company. This vanillin is marketed mostly on China and other Asian countries. In addition to synthetic vanillin, Rhodia manufactures a bio-based vanillin (Rhovanil Natural), at its facility in France, with a fermentation process using ferulic acid. The product was launched in Europe in 2000 and priced at $700.00/kg (Triumph Venture Capital, 2004b).

Borregaard (Norway), the second largest vanillin producer, is the only remaining producer of lignin vanillin (http://www.borregaard.com). The company also has guaiacol vanillin and ethyl vanillin production capacity as it acquired Eurovanillin in 1995 (Triumph Venture Capital, 2004b). Borregaard mainly supplies the European market and its lignin vanillin production is almost exclusively for large costumers under long-term contracts.

The market for vanillin consists mainly of large multinational holders, such as the major international flavour and fragrance houses (e.g. IFF, Givaudan, Quest,

Danisco, Symrise), the bigger producers of ice cream (such as Unilever) and chocolate (Nestle, Cadbury, Suchard), and producers of pharmaceutical active ingredients such as L-methyl dopa (Merck). Other users include hundreds of small and medium companies, and producers of baked goods and confectionary.

Vanillin is sold on the merchant market as a crystalline solid in two grades, technical and Food Chemicals Codex (FCC) grade. The synthetic vanillin FCC grade requires a minimum assay of 97.0% on dried basis (Food Chemical Codex, 2003). The technical grade is usually applied when there are no official standards for quality and impurity levels, and generally sells for about $2.00/kg less than FCC grade.

In 1995 Rhodia's vanillin price was $17.50/kg, decreasing to about $11.00/kg in 2001, due to the liberalization of the Chinese economy (Triumph Venture Capital, 2004b). It is highly likely the stranglehold that Rhodia exerts on guaiacol market in China will allow this company to continue to dominate the world vanillin market and set price levels. This factor associated with a significant higher energy and raw material (for the catechol-guaiacol process is benzene) costs led to price increases for vanillin. In the middle of 2005, market prices of vanillin reached the range of $15.00/kg (http://www.blonnet.com/2005/06/14/stories/2005061401521000.htm). Lignin based vanillin is in high demand in certain market sectors, particularly the perfume industry, European chocolate manufacturers, and the Japanese market, and as such tends to command a price premium. The price of lignin vanillin is consistently maintained at about $1.00 to $2.00 per kg above that of guaiacol based vanillin (Triumph Venture Capital, 2004b). The ethyl vanillin price follows the same basic trend as the vanillin price. It is maintained at about twice that of vanillin, but as it has about three times the flavour intensity of vanillin there is a cost saving associated with substituting vanillin with ethyl vanillin.

Lignin is the most abundant aromatic substance present in the biosphere. It is an organic amorphous polymer constituted by phenylpropanoid units linked to each other through a variety of non-hydrolysable C-C and C-O-C bonds (Mathias et al., 1995). The fundamental building units (precursors) that compose the structure of lignin are conyferil, sinapyl and p-coumaryl alcohols (Kirk-Othmer Encyclopedia, 2005).

The main source of pure lignin is the pulp and paper industry, where nowadays the Kraft process prevails with approximately 80% of the world chemical pulp production (Ullmann's Encyclopedia, 2003). A by-product stream of this process, known as *black liquor*, contains typically 30 to 34% of lignin in dry solid weight basis. This stream is burned to provide energy for mill operations, and to facilitate the recovery of pulping chemicals. Due to the complex energetic integration of the Kraft process, an expansion in the production of pulp implies a revamp in the burners. An alternative plant design to the burners revamp will be a utilization of the increased amount of black liquor in the production of high-added value products and the elimination of a production bottleneck at the recovery boiler (Axelsson et al., 2006). In this work, the focus is on the production of synthetic vanillin from lignin obtained from black liquor.

A flow sheet of a process to produce synthetic vanillin from lignin in a pulp and paper industrial unit is proposed in Figure 1.2. A portion of the by-product stream, black liquor, is processed to extract lignin. This extraction can be done by the traditional acidification/precipitation followed by separation, or using an improved method similar to one developed by a Swedish group and known as LignoBoost (Öhman et al., 2006). After obtaining purified lignin, the subsequent process is based on three main steps studied in LSRE. The first step consists on the alkaline lignin oxidation in a bubble column reactor, which is the main subject of this thesis. Then, the mixture obtained in

the reaction passes through a membrane ultrafiltration process where the bigger molecules of degraded lignin are retained. Sodium vanillate (salt of vanillin) and other low molecular weight species goes to the permeate stream (Zabkova, 2006). Finally, the permeate containing smaller molecules and excess NaOH flows through a packed bed on acid resin in H^+ form, in order to convert the sodium vanillate into vanillin (Zabkova et al., 2007). This ion exchange step is accompanied by neutralization reaction resulting in a lower *pH* for the product exit stream.

In order to have a reference point for the results to achieve, it is important to refer a study developed in South Africa that revealed a benchmark final vanillin concentration was 4.2 g/l, for a production process based on Kraft black liquors (Triumph Venture Capital, 2004a). A process which final product has a concentration below this value should not be very competitive in the present scenario of the synthetic vanillin market.

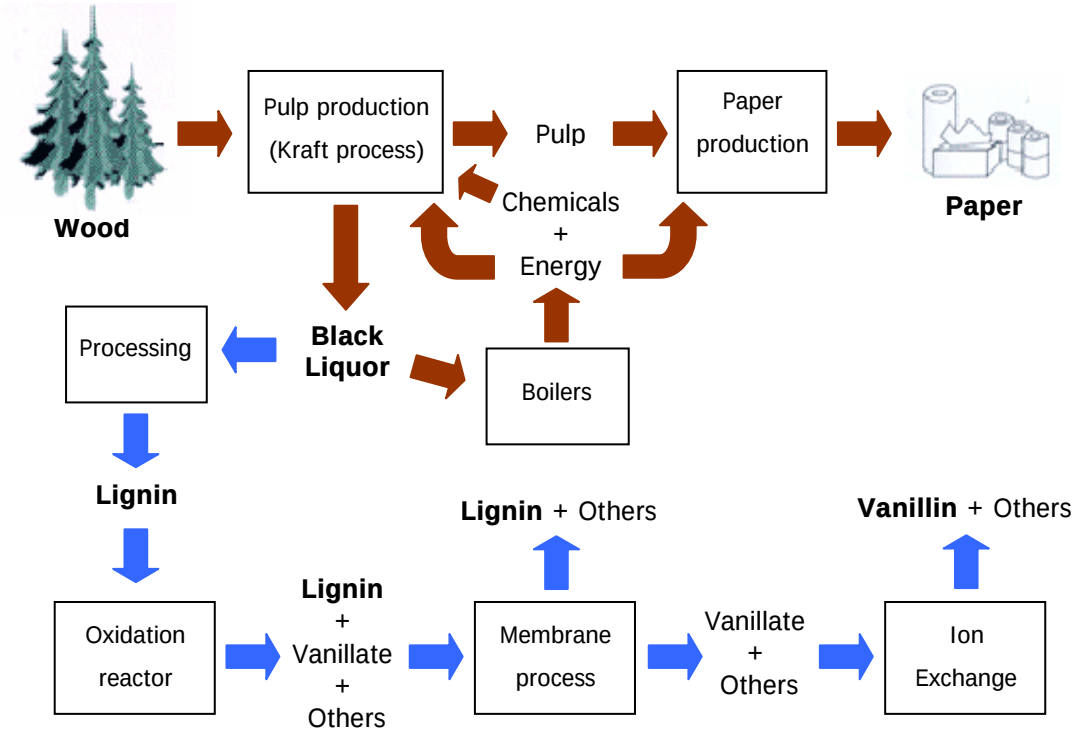

Figure 1.2. Flow sheet of a process for vanillin production integrated in a pulp and paper mill (Zabkova, 2006).

The most important raw material for pulp production is wood, in which cellulose, hemicelluloses and lignin are the main components. This complex mixture of polymers varies in composition, but can be roughly divided into (Chenier, 2002): 40% of cellulose, 30% of hemicelluloses, 28% of lignin and 2% of extractives (terpenes, fats, waxes, phenols, etc).

Softwoods (coniferous woods) have the most homogeneous structure. They consist on more than 90% of cells with an average length of 3 mm and a width of 30 - 50 μm. These cells have a length-to-width ratio greater than 100:1, which is ideally suited for papermaking. The hardwoods, such as birch, beech, eucalyptus and poplar, have a structure much more heterogeneous, where the major type of cells accounts for 40–60% of the tissue of most of these trees. The average length of hardwood cells is usually less than 1 mm, and their width varies greatly, in the range 10 – 40 µm, depending on the type of wood. In addition, hardwoods contain a considerable percentage of very voluminous cells, with relatively thin and partially perforated walls and a low length-to-width ratio that does not contribute for good technological properties of the resultant pulp.

Softwoods (coniferous woods) are normally preferred for the production of pulp, especially spruce and pine, because of their favourable morphological structure. However hardwoods (deciduous woods) have gained an increased importance in this industry. In particular the importance of eucalyptus should grow steadily on this chemical processes, because of its high growth rate and the excellent technical properties of the pulp made from this wood. Some other differences in the use of softwoods and hardwoods in the pulp industry are detailed in Table 1.1 (Ullman´s Encyclopedia, 2003).

Whereas lignin content within a plant species is reasonably constant, there may be considerable variation among species. Normally, in softwoods the amount of lignin varies between 25 and 35%, while in the hardwoods the amounts range from 18 to 25% (Wool and Sun, 2005). The chemical structure of lignin also shows a great heterogeneity between species. The lignin of softwoods and hardwoods differ with regard to their content on guaiacyl (3-methoxy-4-hydroxyphenyl), syringyl (3,5-dimethoxy-4-hydroxyphenyl) and 4-hydroxyphenyl units. Coniferous wood lignins are predominantly polymers of coniferyl alcohol, consisting mainly on guaiacyl units, while lignins from hardwoods are composed of guaiacyl and syringyl units in various proportions. The variation of lignin composition is much greater in hardwoods than in softwoods (Ullman´s Encyclopedia, 2003).

Table 1.1. Differences of using softwood and hardwood in pulp and paper industry operations.

	Softwoods	**Hardwoods**
Wood treatment	Usually high productivity More uniform raw material, especially better stem formation, easier to debark, longer fibers, higher yields in acidic cooking	In some cases extremely high productivity (e.g. eucalyptus, poplar), higher stock stability Higher specific weight (e.g. eucalyptus, beech, birch) → lower transport cost → higher digester capacity → high pulp output Lower lignin content → easier to pulp → less energy and chemicals consumption Higher yields in alkaline cooking
Pulp	Better wet web strength, better drainage properties	Requires less beating energy, rapid strength development during beating and better bleachability → fewer bleaching stages → lower chemical demand → less pollution (chlorine-free bleaching possible)
Paper	High strength properties, especially tear strength, better runability	Better sheet formation (higher content of hemicelluloses), usually smoother surface, higher bulk, higher opacity → better printability

For vanillin production from black liquor, it seems to be more suited to use a softwood lignin. Three main reasons can support this assumption:

- Since lignin composition of hardwoods is more variable, softwood should give a more constant chemical basis as starting point.
- Softwood has a bigger amount of lignin than hardwood, which promotes a correspondent black liquor stream more concentrated on the intended feedstock for vanillin production.
- Guaiacyl units are preferred for vanillin formation from lignin. These units derive from coniferyl alcohol and are present in higher extent in softwood lignin.

In the European and world context, it is known that Portugal is a country focused on forestry activities. Forestry is the basis of an important industrial chain that makes Portugal an exporter of forestry products, unlike other EU countries (except Sweden and Finland). Nowadays the forest occupies 38% of the national territory (3.4 million hectares), according to data from the Portuguese General Directorate for Forests (Direcção Geral dos Recursos Florestais, DGRF), with conditions to grow more 1.9 millions hectares, if the extensive uncultivated area available for forestry is used (Resultados do Inventário Florestal Nacional, 2006).

Maritime pine (*pinus pinaster*), cork oak (*quercus suber*) and eucalyptus (*eucalyptus spp.*) are the three species with greater economical interest and dominant in the distribution of the forestry population's area. They occupy 75% of the forestry area, where the maritime pine prevails (especially on the central and northern coastal regions of the country), as can be seen in Table 1.2 (Statistics Reports, 2006).

In the wide scope of the forestry activities the black liquor is obtained as a by-product of the pulp and paper industry. For this reason, this work deals with this industry. Pulp and paper industries are unquestionably of great relevance to the

Portuguese economy. In fact, these sectors are responsible for 4.6% of the Portuguese goods exports (http://www.portucelsoporcel.com) and warranted special attention in the 2000-2006 Strategic Vision of the National Plan for Economic and Social Development.

Table 1.2. Distribution of the forestry area by species, according to the Portuguese General Directorate for Forests (DGRF, 2001).

Forestry species		**% forestry area**	**Area (hectares)**
Maritime pine	*Pinus pinaster*	30.5	976,069
Umbrella pine	*Pinus pinea*	2.4	77,650
Other softwoods		0.8	27,358
Holm oaks	*Quercus rotundifolia*	14.4	461,577
Other oaks	*Quercus spp.*	4.1	130,899
Chestnut	*Castanea sativa*	1.3	40,579
Eucalyptus	*Eucalyptus spp.*	21.0	672,149
Cork oak	*Quercus suber*	22.3	712,813
Other hardwoods		3.2	102,037
Total		100	3,201,131

One of its major points of interest for the country development is that activities are carried out outside the main urban centres, which can contribute for the growing of some economically depressed zones. The sites of the different pulp factories in Portugal are shown in Figure 1.3 while their location and main product identification is presented in Table 1.3.

From the companies pointed out in Table 1.3, it can be emphasized the Portucel Soporcel Group that possesses three mill sites all operating with the Kraft process:

- The Setúbal pulp mill is one of the most important on Southern Europe, both for its size and technology. It includes two integrated industrial units producing bleached eucalyptus pulp and uncoated printing and writing paper. Their production capacities are 340 thousand tonnes per year and 270 thousand tonnes per year, respectively (http://www.portucelsoporcel.com).
- Installed inside the Lavos Industrial Complex at Figueira da Foz is the biggest mill site in Europe for uncoated woodfree paper with an annual production of 750 thousand tones. This capacity is ensured by the integrated production of 550 thousand tonnes of sulphate eucalyptus pulp (http://www.portucelsoporcel.com).
- Located in the heart of the largest area of eucalyptus forest in the country, the Cacia mill was the first ever (1957), at an international level, to produce pulp and paper by the Kraft process using eucalyptus as raw material. This mill produces 260 thousand tonnes per year of pulp designed for special applications, which are very appreciated by demanding costumers from Central Europe (http://www.portucelsoporcel.com).

Pulp and paper sector is also practically auto-sufficient concerning to its raw material. In fact the Portuguese eucalyptus and pine forests manages to supply almost all of the wood resources needed for the pulp and paper industries, where only 1% were imported in 2005 (Statistics Reports, 2006). It is very important to note that the Portuguese pulp and paper industry is responsible for the direct management of about 200 thousand hectares of forest, integrating all the process (from planting trees to final product). Since the demand for paper tends to increase, this factor is crucial for rising industry competitiveness inside the national panorama and for a growing favourable position on the external markets.

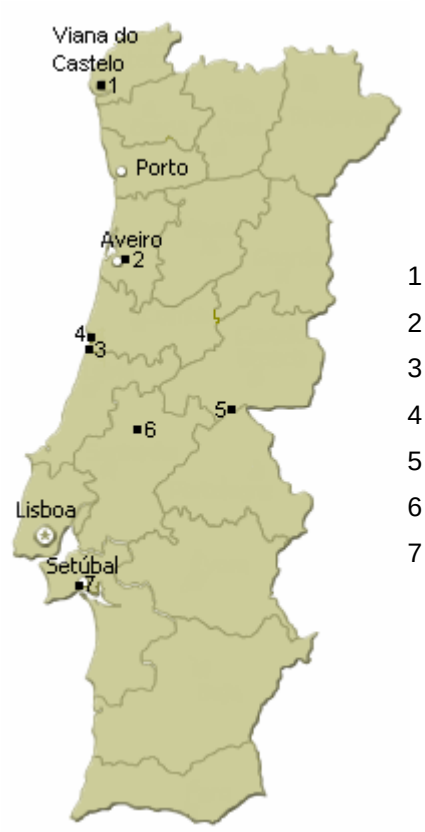

Figure 1.3. Location of the Portuguese pulp and paper mills.

Table 1.3. Portuguese pulp and paper mills.

	Industrial site	**Main product**
Portucel Viana	Deocriste	Unbleached sulfate eucalyptus and pine pulp Recovered paper pulp Kraft liner paper
Portucel Soporcel	Cacia	Bleached sulphate eucalyptus pulp
	Lavos –Figueira da Foz	Bleached sulphate eucalyptus pulp Uncoated printing and writing paper
	Setúbal	Bleached sulphate eucalyptus pulp Uncoated printing and writing paper
Celulose do Caima	Constância	Bleached sulphite eucalyptus pulp
Celbi	Leirosa	Bleached sulphate eucalyptus pulp
Portucel Tejo	Vila Velha de Rodão	Unbleached sulphate eucalyptus pulp

Some relevant details of pulp and paper markets are pointed out next:

- In 2005, the national pulp and paper companies were responsible for the direct employment of 3581 workers (Statistics Reports, 2006).
- The 2005 total Portuguese pulp production was 1.932 million tonnes (Statistics Reports, 2006).
- The 2005 total Portuguese paper production was 1.577 million tonnes (Statistics Reports, 2006).
- In 2004, Portugal was the 3rd larger producer of chemical pulp in the CEPI countries (EU25 + Norway + Switzerland) with 1.949 million tonnes, following Sweden and Finland. In the same universe, Portugal was the 14th producer of paper and board with 1.666 million tonnes (Statistics Reports, 2006).
- The 2003 world pulp production was 188 million tonnes and the paper and board produced worldwide reached the 325 million tonnes (Statistics Reports, 2006).
- In the world context, on 2002, Portugal was the 15th larger pulp producer with 1.1% of the total market. With respect of paper production, in the same year, Portugal was placed on 28th (Statistics Reports, 2005).
- Between 1994 and 1999, the pulp and paper sector was the 4th net exporting branch in the Portuguese economy, after the textile, leather and wood and cork industries (Statistics Reports, 2005).

1.2 Objectives and Outline

Market increase, raise in energy prices and high volatility in natural vanilla prices are a strong driving force to have a deeper understanding of alternative methods to produce vanillin. Vanillin obtained from lignin can employ a low-value fuel to

produce a high-added value and also represents a “green process”, since it is biomass-based. The guaiacol process to produce vanillin employs benzene obtained from a non-renewable source (petroleum). Within this context, the objective of this thesis is the study of vanillin production from lignin and its implementation in a continuous three-phase oxidation reactor. The source of lignin should be black liquor from pulp and paper industries using the Kraft process. In this work it was used lignin from softwood *Pinus spp.*, kindly supplied by Westvaco Co. The target of vanillin concentration to achieve is around 4.0 – 4.2 g/l. The necessary steps to attain this final objective are:

1. Determination of a protocol to characterize appropriate source of lignin: reaction kinetics of lignin oxidation in a batch reactor.
2. Design, build-up and operation of a continuous reactor for lignin oxidation in “hard operating conditions”: 10 bar, *pH* close to 14 and temperature between 120-160ºC.
3. Development of a reliable mathematical model to describe the reactor operation that can allow direct optimization of variables to improve vanillin yield.

This work is not the starting point at the Laboratory of Separation and Reaction Engineering (LSRE) studying the vanillin production from lignin oxidation. In fact an extensive work, including the determination of kinetic laws of lignin and vanillin oxidation by oxygen and optimum conditions for the production of vanillin, was performed by Álvaro Mathias (Mathias, 1993) and Claire Fargues (Fargues et al., 1996a; Fargues et al., 1996b).

This work is divided into six chapters. Chapter 1 is a brief introduction, pointing out the relevance and motivation and the objectives of the work. Chapter 2 describes basic principles and phenomena of pulp and paper industry, Kraft process, vanillin routes of production and final choice of a three-phase reactor for continuous oxidation

of lignin. Chapter 3 contains kinetic data of vanillin and lignin oxidation in a batch reactor describing analytical protocols used for determination of vanillin in reaction media. In Chapter 4 a complete description of the structured bubble column reactor (SBCR) experimental unit built during the course of this thesis. Details about construction and operation of the unit, applied to lignin oxidation for vanillin production are also described in this Chapter. Chapter 5 deals with mathematical modelling of the SBCR and comparison of the mathematical model developed with experimental data collected both for vanillin and lignin oxidation. Finally, Chapter 6 has the conclusions of this work and some suggestions for future work.

1.3 References

1. Axelsson, E.; Olsson, M. R.; Berntsson, T. Increased capacity in Kraft pulp mills: lignin separation and reduced steam demand compared with recovery boiler upgrade. *Nord. Pulp Paper Res. J.*, **2006**, 21 (4), 485-492.
2. Chenier, P. J. *Survey of Industrial Chemistry*, 3rd Edition, Springer-Verlag, **2002**.
3. Fargues, C.; Mathias, A.; Rodrigues, A. Kinetics of vanillin production from Kraft lignin oxidation. *Ind. Eng. Chem. Res.*, **1996a**, 35, 28-36.
4. Fargues, C.; Mathias, A.; Silva, J.; Rodrigues, A. Kinetics of vanillin oxidation. *Chem. Eng. Technol.*, **1996b**, 19 (2), 127-136.
5. *Food Chemical Codex*; 5th Edition, National Academies Press, **2003**.
6. http://faostat.fao.org
7. http://www.blonnet.com/2005/06/14/stories/2005061401521000.htm
8. http://www.borregaard.com/

9. http://www.foodnavigator.com/news/ng.asp?id=72634-borregaard-vanillin-vanilla
10. http://www.portucelsoporcel.com/eng/index.html
11. http://www.rhodia.com
12. Jaeger, P. *Spices*. Issue nº 5, Market News Service, International Trade Centre UNCTAD/WTO, **2005**. (http://www.intracen.org/mas)
13. *Kirk-Othmer Encyclopedia of Chemical Technology*; 5th Edition, John Wiley & Sons, **2005**.
14. Loeillet, D. The international vanilla market – Price is the main handicap. *FruiTrop*, **2003**, 98, 4-8.
15. Mathias, A. L. *Produção de vanilina a partir da lenhina: estudo cinético e do processo.* Ph.D. Dissertation, University of Porto, Portugal, **1993**.
16. Mathias, A. L.; Lopretti, M. I.; Rodrigues, A. E. Chemical and biological oxidation of *Pinus pinaster* lignin for the production of vanillin. *J. Chem. Tech. Biotechnol.*, **1995**, 64, 225-234.
17. McGregor, A. *Diversification into high-value export products: case study of the Papua New Guinea vanilla industry*. AGSF Working Document nº 2, FAO, Rome, **2005**. (http://www4.fao.org/faobib/index.html)
18. Öhman, F.; Wallmo, H.; Theliander, H. *An improved method for washing lignin precipitated from Kraft black liquor – The key to a new bio-fuel.* 5th Conference on Chemical Industry and Environment, Vienna, Austria, 3-5 May, **2006**. (http://www.lignoboost.com)
19. *Resultados do Inventário Florestal Nacional 2005/06*. Direcção Geral dos Recursos Florestais (DGRF), Portugal, **2006**. (http://www.dgrf.min-agricultura.pt)

20. *Statistics Reports 2004*. CELPA – Associação da Indústria Papeleira, Lisboa, Portugal, **2005**. (http://www.celpa.pt)
21. *Statistics Reports 2005*. CELPA – Associação da Indústria Papeleira, Lisbon, Portugal, **2006**. (http://www.celpa.pt)
22. Triumph Venture Capital *Part 2-Aroma chemicals derived from effluent from the paper and pulp industry*. In: Study into the establishment of an aroma and fragrance fine chemicals value chain in South Africa (Final Report), FRIDGE, NEDLAC, South Africa, **2004a**. (http://www.nedlac.org.za)
23. Triumph Venture Capital *Part 3-Aroma chemicals from petrochemical feedstocks*. In: Study into the establishment of an aroma and fragrance fine chemicals value chain in South Africa (Final Report), FRIDGE, NEDLAC, South Africa, **2004b**. (http://www.nedlac.org.za)
24. *Ullmann´s Encyclopedia of Industrial Chemistry*; 7th Edition, Wiley-VCH, Verlag GmbH & Co..KGaA, **2003**.
25. Villar, J. C.; Caperos, A.; García-Ochoa, F. Oxidation of hardwood Kraft lignin to phenolic derivatives. Nitrobenzene and copper oxide as oxidants. *J. Wood Chem. Technol.*, **1997**, 17 (3), 259-285.
26. Wool, R.; Sun, X. S. *Bio-based polymers and composites.* Elsevier, USA, **2005**.
27. Zabkova, M. *Clean technologies for the purification of wastewaters: adsorptive parametric pumping.* Ph.D. Dissertation, University of Porto, Portugal, **2006**.
28. Zabkova, M.; Borges da Silva, E. A.; Rodrigues, A. E. Recovery of vanillin from Kraft lignin oxidation by ion-exchange with neutralization. *Sep. Purif. Technol.*, **2007**, 55, 56-68.

2. State of the art

This chapter is divided into four sections. The first part is focused on the pulp and paper industry. A general description of the physiology and chemistry of wood, and the flow sheet for pulp and paper production are presented; then each process step is briefly explained with particular attention to Kraft pulping since it is the source of lignin used in this thesis.

A viable technology of making vanillin from lignin will have the final purpose of being integrated in pulp mills as a complement, improving the profitability of the by-products from the original plant, leading to a decrease in the levels of air and water pollution, and adding capacity to explore new product fields. Since the subject of this thesis is about the first step in the road to that objective, it becomes relevant to provide a basic background for a general understanding on the pulp and paper industries. In fact, if a vanillin production setup is fitted in this sector of the chemical industry, the starting point to obtain this aromatic compound will be the wood that goes through several physical and chemical treatments whose concepts and phenomena need to be reviewed.

In the second part the raw material of this work (lignin) is presented. Some general aspects are pointed out, along with physical properties, commercial forms, characteristic reactions and applications in industry or under development.

A revision about the desired product, vanillin, is made in the third section. Besides general features and applications, the different routes of production (natural,

chemical and biotechnological), including research and patents about these subjects are described.

Finally, in the last section the decision about the type of configuration for the developed continuous reactor, along with alternatives and basic fundamentals is discussed.

2.1 Pulp and paper industry

2.1.1 History of papermaking

About 4000 years ago, in Egypt was developed a writing surface formed from pounding repeatedly strips of papyrus plants. The word paper derives from the Greek term for this ancient Egyptian writing material (Kirk-Othmer Encyclopedia, 2005).

However, paper is defined as a sheet material resulting from individualized fibres brought together by the removal of water. According to this definition, paper manufacture began in China, around the year of 105 AD, when Ts'ai Lun created a sheet of paper from mulberry, old rags and hemp mixed with water (Ciullo, 1996; Kirwan, 2005).

The Arabs first paper mill started in Baghdad, at 759, where they invented a method to produce thicker sheets of paper. With the golden age of Islamic culture they spread papermaking to Damascus and Egypt in the 10th century, and Morocco by 1100. Finally it entered the frontiers of Europe by the Iberian Peninsula, when in 1151 the Arabs build a paper mill in Xativa near Valencia (http://www.handpapermaking.org). From there, papermaking spread throughout the Europe and by the 14th century a large number of paper mills were established particularly in Spain, France, Italy and Germany. The raw materials for these mills were essentially hemp, linen and cotton rags (Sixta, 2006).

In 1450, Johann Gutenberg invented the moveable type printing press, causing a huge impact in society since written communication became more accessible to the masses (http://www.adeq.state.ar.us).

The paper sheet formation process was handmade, until 1798, when Nicolas Louis Robert, in France, constructed a machine that could produce paper in continuous operation mode (Ciullo, 1996; http://www.britannica.com). This machine consisted on a moving endless belt that received a mixture of pulp and water, delivering it to a pair of rollers that squeezed out the excess water, forming a continuous sheet of paper for further drying by suction, pressure and heat.

Since the invention of the printing press, the demand for paper experienced a continuous increase and during the first half of the 19th century the waste of the textile industry could no longer satisfy the production needs. It became imperative to develop a process based on a more abundant material. From this necessity, the wood fibres emerged as the preferred raw material for paper production. At this point several pulping processes started to be developed following two distinct paths. One consisted on the separation of wood fibres by mechanical means, and the other resulted from the exposition of wood to chemical solutions that dissolved lignin and left cellulose fibres free for further treatment. The 19th century was very rich on events related to this evolution of papermaking technology, such as (Sixta, 2006):

- In 1840 the German Friedrich Gootlob Keller designed an equipment to mechanically turn wood into pulp. The mechanical pulping process did not find considerable application until 1870, when a step of steam pre-treatment of wood was introduced.

- The first chemical pulping process was developed in 1851 by Hugh Burgess and Charles Watt. It was called soda process because the wood chips were boiled with a solution of sodium hydroxide.
- Shortly after, a US chemist named Benjamin Tilghman invented the sulphite pulping process and in 1867 issued a patent (Tilghman, 1867). The cooking used solutions of sulphur dioxide and hydrogen sulphite ions at high temperature and pressure.
- Fry and Eckman carried studies to improve the sulphite process leading to the first commercial sulphite mill, built in Sweden in 1874, which used rotary digesters and indirect heating to make magnesium bisulphite pulp.
- In 1880 the German sulphite pulping industry was based on a process developed by Alexander Mitscherlich. In this process the cooking was made on calcium hydrogen sulphide solutions with an excess of dissolved sulphur dioxide.
- Carl Dahl in Danzig concluded that a stronger pulp was produced by substitution of the soda ash by sodium sulphate, in the soda pulping recovery system. This discovery was patented in 1884, and the correspondent pulping process called sulphate or Kraft, deriving from the German term for strong.

In 1925, the sulphite pulping process prevailed with 60% of the total chemical wood pulp production, leaving the remaining 40% evenly distributed by the soda and Kraft processes (Sixta, 2006). This predominance resulted from the low costs of the chemicals applied in the preparation of sulphite pulp and its good bleachability, in contrast to the dark colour and the difficulty of the bleaching of the Kraft pulp. However, since 1937 this scenario started to change, supported on the advances achieved in the areas of combustion furnaces, white liquor recovery system and continuous multi-stage bleaching. Nowadays, the Kraft process accounts for

approximately 80% of the world pulp production (Chenier, 2002; Ullmann's Encyclopedia, 2003), enabling the usage of practically all species of wood as raw material.

In the last decades the pulp and paper industries are putting a lot of effort on the development and application of some of their by-products, such as (Brady et al., 1998; Nalco Company, 1988): turpentine for the paint and coatings industry; tall oil for producing chemical intermediates; lignosulphonates as surface active agent and dispersant, and for the production of vanillin, acetic acid, activated carbon and alcohol. Recently, a new technology was developed in Sweden, by Lignoboost AB, consisting on the extraction of lignin from *black liquor* into the form of compact cake or pellets (www.lignoboost.com). This product can be used as a bio fuel or raw material for the production of chemicals.

Probably, like no other industrial sector, the pulp and paper industry have shown a growing concern for the recycling of waste products. In fact, recovered paper accounted for about 45% of the fibres used in 2001 for paper production (Kirwan, 2005).

2.1.2 Raw material – wood

Due to its composition and versatile properties, wood is one of the most valuable renewable resources of the planet, being used in several important applications such as raw material for pulp production, structural timber, furniture, panels and production of various composites (Criss, 1999; Ullmann's Encyclopedia, 2003). By definition, wood is the interior tissue of stems, branches and roots of perennial plants. It performs vital functions for the plants, like providing mechanical stability, transport of water and minerals, and storage of material. Trees are the most important woody plants for the

purpose of pulp and paper industry. A cross sectional segment of a tree stem is showed in Figure 2.1, where it can be seen its main tissue sections:

- Pith is a core of tissue located in the middle of the stem or branches and represents the initial times of wood growth.
- Wood or xylem is composed by growth rings that may determine the age of the plant. The xylem is divided into heartwood (inner part) and sapwood (outer part). Heartwood consists only of dead tissue and is dark coloured generally due to the presence of extractives. Sapwood is lighter in colour and contains living tissue responsible for the transport of water.
- The cambium zone is a very thin layer of living cells present between the wood and the bark. The cell division that occurs on this layer is the cause of the radial growth of bark and wood.
- Bark or phloem is the exterior layer of the stems and branches, protecting the plant from the environmental conditions. It is divided into an inner living part and an outer corky dead part.

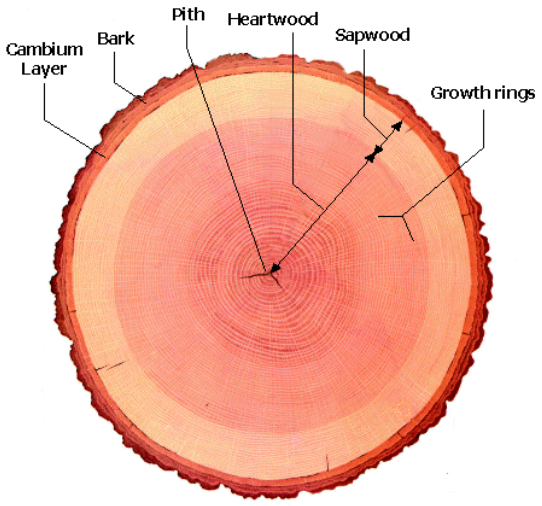

Figure 2.1. Representation of a cross sectional segment of a tree (based on http://www.hoganhardwoods.com).

Woody plants are divided in two botanical classes: softwoods (*gymnosperms*) and hardwoods (*angiosperms*). The softwoods are characterized by needle-like leaves that stay green during all year, while hardwoods have broad leaves that normally turn brown in winter and fall off (Criss, 1999).

The elemental units that compose the wood tissue are wood cells. They have different shapes and sizes and are cemented together by a layer called middle lamella. These cells can be separated into four types: *tracheids*, *fibers*, *parenchyma* cells and *vessels* (Ullman's Encyclopedia, 2003). *Tracheids* are elongated cells with a length of 3 mm and width of 30-50 μm, resulting in a length-to-width ratio higher than 100, which is ideal for papermaking. They are predominant in softwoods and have a dual function of water transport and mechanical support of the wood. *Parenchyma* cells participate in several metabolic pathways, short distance transport and storage. The length-to-width ratio of these cells is around 3, making them inappropriate to use in paper production. *Fibers* are present only in hardwoods and provide them with mechanical support. *Vessels* are cells with relatively large diameter and partially perforated walls, responsible for long distance transport of water and minerals in hardwoods. Because of their low length-to-width ratio, these cells are not suitable for papermaking (Ullman's Encyclopedia, 2003).

Softwoods exhibit a very homogeneous structure. Their composition has only two types of cells: longitudinal *tracheids* that constitutes over 90% of the volume of the softwoods; and *parenchyma* cells (Kolppo, 1994). The structure of hardwoods is much more heterogeneous, containing *fibers* (40% to 60% in most hardwoods), *parenchyma* cells and *vessels*. The presence of *vessels* and *parenchyma* cells in a higher percentage, in comparison with softwoods, provides the hardwoods with cell properties less suitable

for application in the paper industry (Ullman's Encyclopedia, 2003). Pictures of typical cell arrangements in softwood and hardwood are presented in Figure 2.2.

The chemistry of wood is very complex because it consists on a large number of substances varying their composition with the plant species, within each species, within each part of the plant and within the cell wall. However, the wood chemical structure is divided into four main components: cellulose, hemicelluloses, lignin and extractives.

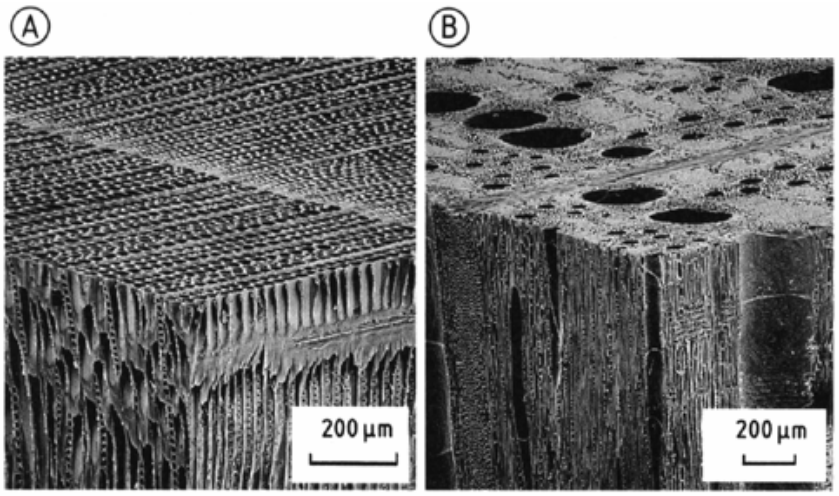

Figure 2.2. Comparison between the cell arrangements in softwood and hardwood by SEM (Scanning Electron Micrograph). A) *Cedrus libani* - softwood; B) *Quercus cerris* - hardwood (Ullman's Encyclopedia, 2003).

Cellulose is the major constituent of wood, making up about 40 to 50% of the wood dry weight (Criss, 1999). The structure and composition of cellulose is independent of the type of tree source (softwood or hardwood). It is a linear polysaccharide derived from β-D-glucose monomers linked together by (1-4) glycosidic bonds (Figure 2.3). Because of this fact, the cellulose macromolecules have a highly ordered structure and are bonded together by intermolecular hydrogen bonds. The degree of polymerization of native cellulose is between 10000 and 14000 (Ullman's Encyclopedia, 2003).

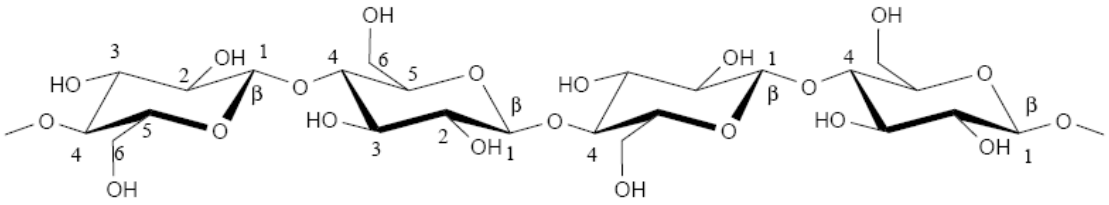

Figure 2.3. Representation of the chemical structure of cellulose (Laine, 2005).

The hemicelluloses are branched polysaccharides with lower molecular weight than cellulose, consisting of several different combinations of pentose and hexose sugar monomers (xylose, galactose, arabinose, mannose, glucose). The structure and composition of the hemicelluloses varies with the tree species, but in average they represent about 25 to 35% of the wood weight (Chenier, 2002; Ullman's Encyclopedia, 2003). The degree of polymerization ranges from 50 to 200. Unlike cellulose, hemicelluloses are not crystalline, have low chemical resistance to acids and alkalis, and are partially soluble in certain solvents. As an example, the structure of the major hemicelluloses in softwoods (galactoglucomannans) is represented in Figure 2.4.

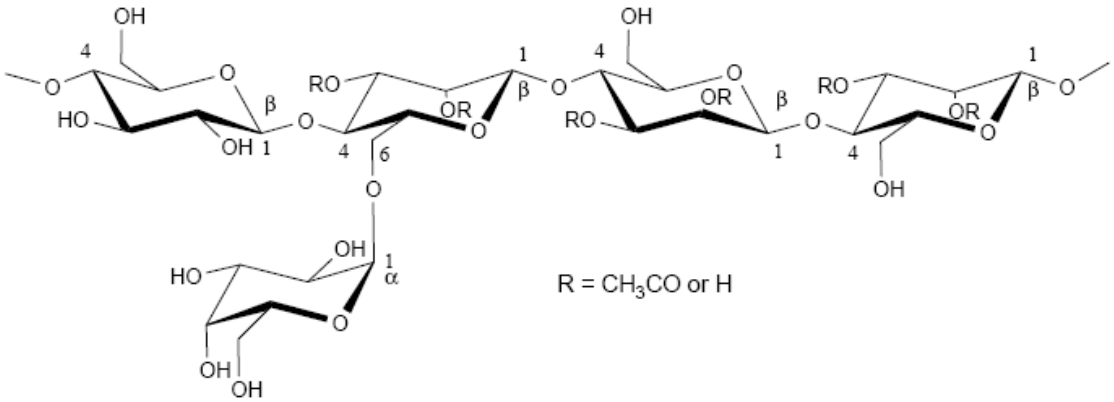

Figure 2.4. Structural unit of a softwood galactoglucomannan molecule (Laine, 2005).

Lignin constitutes 25 to 35% of the wood substance in softwoods and 18 to 25% in hardwoods (Wool and Sun, 2005). The chemistry of lignin is very complex, since it is a cross-linked polymer of phenylpropane units joined together in a 3-D structure by various ether and carbon bonds. The lignin structure and composition is different

between softwoods and hardwoods, as it will be described later in this chapter. Looking to the microstructure of wood, lignin is mainly concentrated between the cells, binding them together, which gives the trees their strength and rigidity. Lignin can be degraded in the presence of strong alkalis, acid sulphite solutions and other oxidizing agents.

The fraction of wood (1-3 wt %) that can be extracted with organic solvents (alcohol, benzene, acetone, ether) or hot water is called extractives (Chenier, 2002; Ullman's Encyclopedia, 2003). Extractives are low molecular mass compounds that include terpenes, fats, waxes, phenols, tannins and inorganic salts. They contribute to some properties of wood such as colour, odour, taste, density, biodegradability, hygroscopicity and flammability.

2.1.3 Process

A complete integrated process for paper production contains a complex set of unit operations. It can be divided in four major steps: wood preparation; pulp production and chemical recovery; pulp bleaching; stock preparation and paper manufacturing. A simplified scheme is presented in Figure 2.5.

2.1.3.1 Wood preparation

Before being processed in the pulp mills, the wood is stored for a period of time after its harvesting. In this period, as a result of the respiration of living cells, micro-organisms attack and chemical auto-oxidative reactions, the wood suffers some degradation of its constituents, strength loss and temperature increase. The temperature of the stored wood can rise to values near 60ºC in one to two weeks, or even to 90ºC, which are conditions that can promote spontaneous ignition (Ullman's Encyclopedia, 2003).

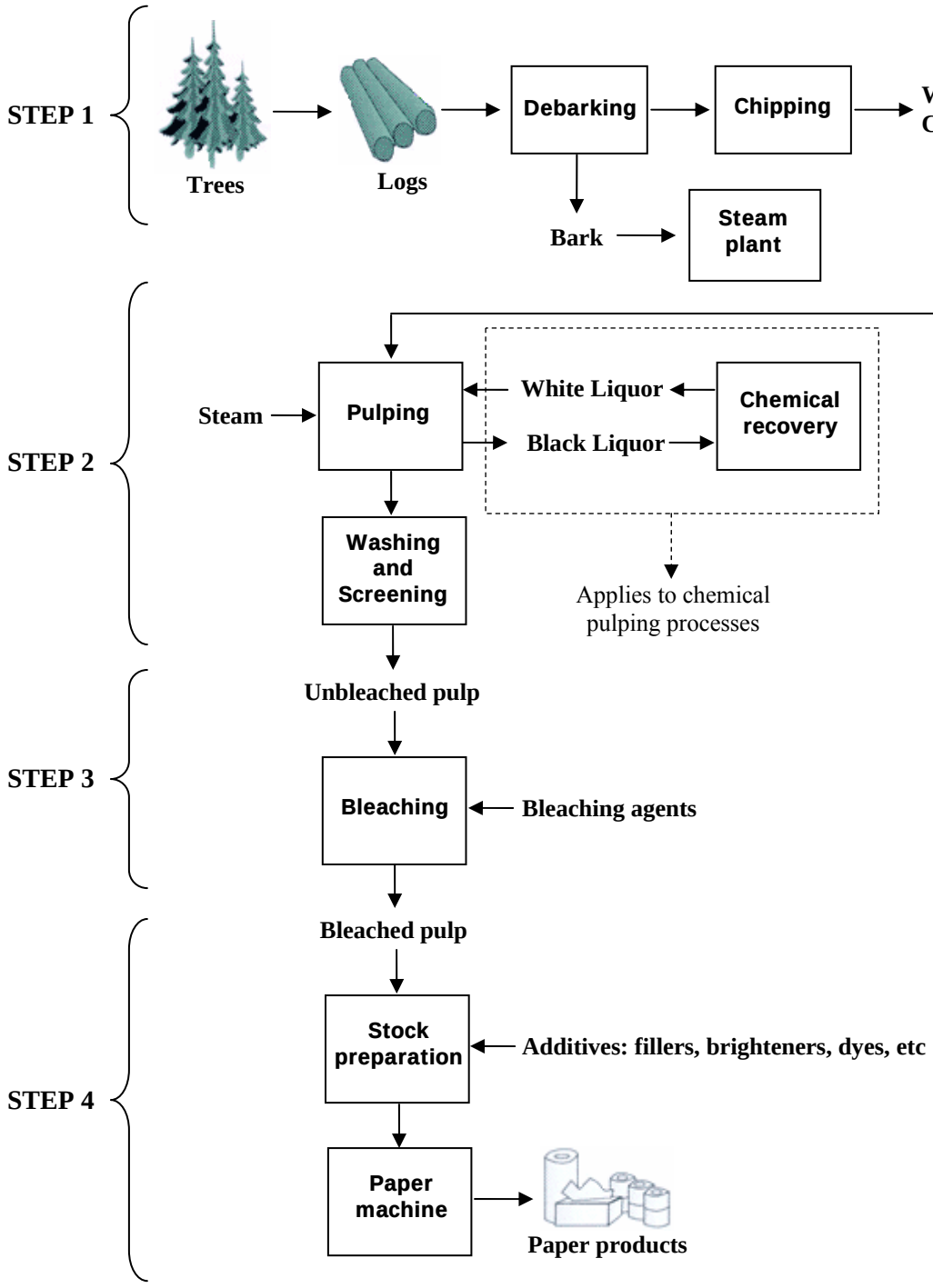

Figure 2.5. Scheme of an integrated process for paper production.

It is estimated that the wood losses are more or less 1% for each month in storage. In order to prevent excessive damage, the storage period should not be higher than two or three months (Ullman's Encyclopedia, 2003).

The first stage of the pulp and paper production process is the debarking of the logs (Cleveland, 2004). The need to remove the bark, that constitutes 10 to 20% of the tree trunk, is related to the problems it causes on the digestion procedure and the subsequent reduction of the yield and quality of the pulp. One of these problems is that the bark contains coloured substances, normally phenolic compounds, which react with lignin and prevents its dissolution by the sulphite pulping process. In the Kraft pulping this dissolution problem is not so severe, since most of the bark components are soluble in alkali.

The debarking units more frequently applied are the drum barkers and the ring barkers (appropriate for logs with large diameter). The rejected bark is dewatered, pressed, and fed to appropriate boilers as fuel for steam generation. The efficiency of the debarking should be around 85 to 95%, depending on the subsequent pulping process (Ciullo, 1996; Ullman's Encyclopedia, 2003).

The debarked logs need to be chipped to a size small enough that guarantees a sufficient impregnation in the wood by the digestion chemicals in the pulping stage. However, this operation also brings the disadvantage of possible damages on the wood structure and fibres. It is assumed that the chip dimensions should be around 25 to 35 mm of length and a thickness of 3 to 7 mm (Ullman's Encyclopedia, 2003). The chipping machines most used are disk chippers, but it can also be focused the drum chippers, headrige cutter and the CCL chippers.

2.1.3.2 Pulping

Commercially, the term pulping refers to processes in which the wood fibres are separated from each other. Industrial pulping processes are generally divided into three main classes: mechanical, semi-chemical and chemical. The most prevalent is the chemical pulping accounting for more than 80% of the worldwide pulp production (Chenier, 2002; Cleveland, 2004).

Mechanical pulping consists on using pressure, high temperatures and/or steam to physically separate the wood fibres. This kind of process is cheaper than chemical pulping, but the fibres suffer some damage, which reduces considerably their quality and the strength of the correspondent produced paper. The resulting pulp contains all the initial wood chemical components, including a substantial fraction of the lignin, which gives these processes high yields on the utilization of wood mass, in the range of 90-95% (Jones, 1999; Nalco Company, 1988). However, the paper produced from mechanical pulps is opaque and easily turns yellow when exposed to light, heat or after aging. Newspapers and paperboards are the typical main applications of the mechanical pulping (Ciullo, 1996; Cleveland, 2004).

Semi-chemical pulping combines chemical and mechanical treatments. The wood chips are partially cooked with inorganic chemical solutions, in smaller amounts and in less severe conditions compared to full chemical pulping. The remainder of the pulping is achieved by a refining mechanical step. The most common process is called neutral sulphite semi-chemical (NSSC), where the wood is digested at 180ºC and the cooking liquor is a sodium sulphite solution, buffered by sodium carbonate, bicarbonate, and hydroxide to maintain a *pH* approximately neutral. This type of processes present yields around 70% (Ciullo, 1996; Nalco Company, 1988), and the

corresponding pulps have chemical and strength properties intermediate between mechanical and full chemical pulps.

In chemical pulping the wood chips are placed in large digester tanks and cooked with chemical solutions and steam at high temperature and pressure. The optimum cooking time can vary between two to six hours, depending on the chemical process used, the extent of delignification to achieve and the type of wood to be pulped (http://student.britannica.com). The main goal of the chemical pulping processes is the dissolution of as much lignin as possible from the chips to the cooking liquor, particularly from the middle lamella of the wood cells, without attacking the carbohydrate components. This lignin removal is called delignification and promotes the dissolution of about 50 to 60% of the initial wood mass (Brady et al., 1998). Delignification allows the wood fibres to easily separate from each other, forming a pulp with superior properties for paper production than the ones obtained by mechanical or semi-chemical pulping.

The extent of delignification is generally determined using the *Kappa number*, which is a parameter regularly used in pulp and paper industry to quantify the lignin content of a pulp. According to standard methods, the *Kappa number* is determined by the volume of potassium permanganate consumed by one gram of dry pulp, which is related to the number of oxidizable structures in the pulp (Mielenz, Klasson, Adney and McMillan, 2007). The higher the *Kappa number*, the higher will be the lignin content of the pulp. For example, traditional values of this parameter for bleachable softwood and hardwood pulps are 30-40 and 18-20, respectively (Kirk-Othmer Encyclopedia, 2005). Delignification should not be extended too much to prevent unwanted degradation of cellulose by the chemical components of the cooking medium.

There are three chemical pulping processes that can be pointed out: soda, sulphite and Kraft.

The soda process was introduced in the pulp and paper production over 150 years ago (http://www.britannica.com; Sixta, 2006). It is the simplest alkaline pulping process, where the wood is treated with aqueous solution of sodium hydroxide under temperature conditions between 150ºC and 170ºC (Kirk-Othmer Encyclopedia, 2005). Low selectivity is observed, since not only lignin is degraded but also cellulose, lowering the strength properties of the produced pulp.

In the sulphite pulping process the active species for delignification are free sulphur dioxide, SO_2, hydrogen sulphite ions, HSO_3^-, and sulphite ions, SO_3^{2-}. These chemical conditions can be attained with mixtures of sulphurous acid and bisulphate in the form of calcium, magnesium, sodium or ammonium. The digestion is normally promoted in pressure vessels built in acid resistant materials and prepared to deal with high temperatures (around 150ºC).

Originally the sulphite process was applied almost worldwide using acid cooking liquor based on calcium bisulphate (Ciullo, 1996; Woodings, 2001). However this reaction medium revealed inappropriate for posterior chemicals recovery and brought very high levels of water pollution. This lead to the emerging of a process based on a pulping medium with magnesium bisulphate and acid *pH*, which allowed some liquor recovery and was less water pollutant.

Nowadays, it is called sulphite process to a great number of cooking liquor variations, especially due to its versatility with respect to the *pH*. In fact, it is possible to work with this kind of pulping process in almost the entire *pH* range, only by manipulation of the composition and concentration of the two main starting chemicals (Ullman's Encyclopedia, 2003). These possibilities can be subdivided in:

1. Acid bisulphite pulping – has a *pH* around 1 to 2, as a consequence of large excess of free SO_2. Almost all the bisulphate forms referred above can be used.
2. Bisulphite pulping – there is no excess of free SO_2, and the *pH* is between 2 and 6. Magnesium is the base commonly used in this pulping, and in some cases ammonium and sodium bisulphate can also be applied.
3. Neutral sulphite pulping – the *pH* is in the range of 6 to 9 and was already referred earlier in this chapter as semi-chemical process.
4. Alkaline sulphite pulping – the cooking liquor consists on sodium sulphite, sodium hydroxide and/or sodium carbonate. The working *pH* is between 9 and 13. This type of delignification is usually catalyzed with anthraquinone.

2.1.3.3 Kraft pulping

Kraft pulping is emphasized in this chapter since it is the source of raw material for the process studied in this thesis. This pulping process was first industrially applied in Jonkoping (Sweden), in the year of 1891 (Li, 1997). Since that date, the Kraft process has suffered huge developments that resulted in the dominance of the pulp market, with more than 95% of the chemical pulp production in the recent years. Data from the Food and Agricultural Organization of the United Nations (FAO) for the year of 2006 reveals that 9.8×10^7 tonnes of Kraft pulp were produced in worldwide developed countries, from a chemical pulp total production of 1.03×10^8 tonnes (www.fao.org/forestry).

The stronger points arising in the Kraft process are: good flexibility towards the raw material – basically the cooking can manage almost all types of woody materials including bark and extractives; high energetic efficiency and good capability on recovering the pulping chemicals, which is very interesting in the economical

perspective; good technological properties of the resulting pulps, specially the pulp strength. However, it has some disadvantages namely the unpleasant smell from the sulphur gases liberated, the darker colour of the obtained pulps, compared with the sulphite pulps, and the consequent higher difficulty on bleaching. Nowadays, this last factor is largely suppressed, but it is still necessary to use chlorine bleaching agents that are very water pollutant.

There are three main parts in which the Kraft pulping can be divided (Brady et al., 1998): digestion of the wood; separation of the black liquor and pulp washing; and chemicals recovery from the black liquor. The Kraft pulping process is represented on Figure 2.6.

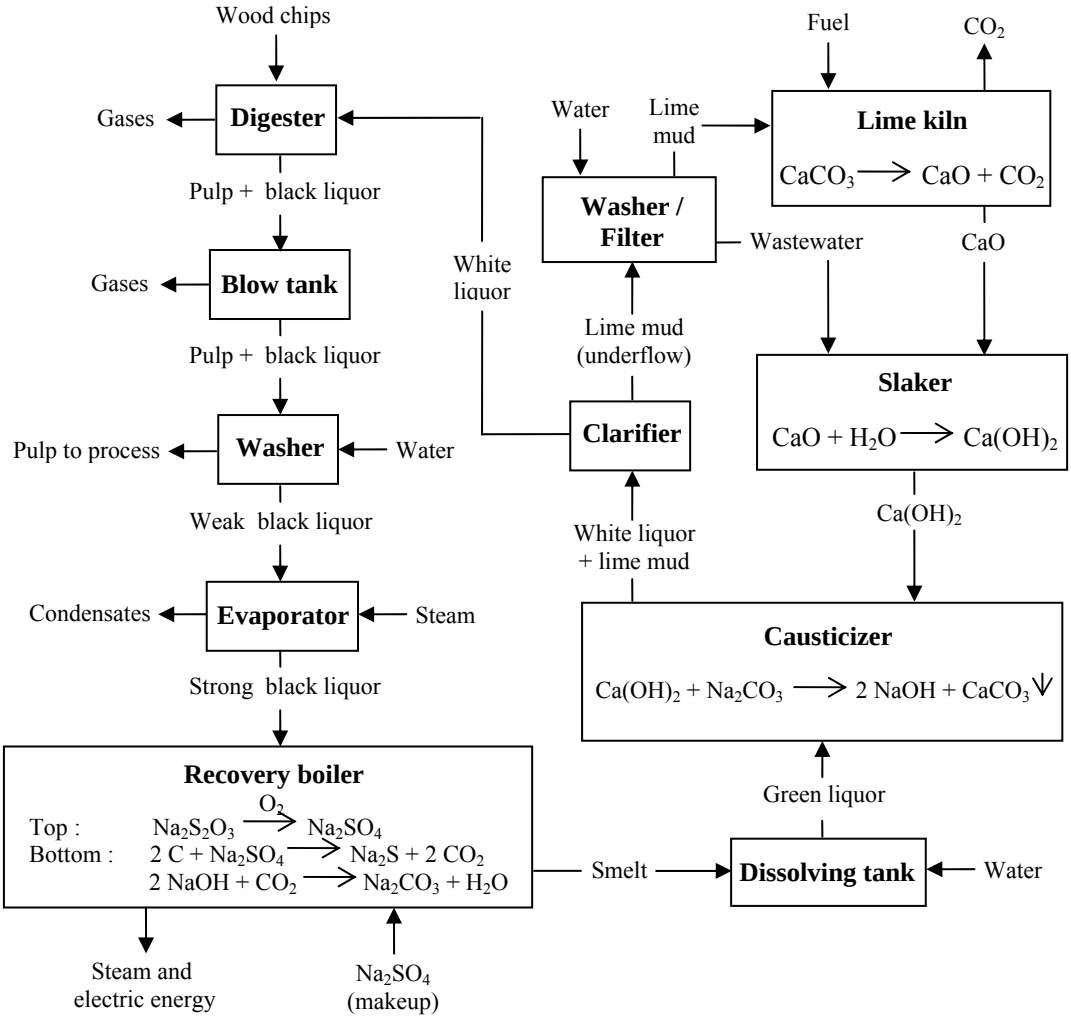

Figure 2.6. Flow sheet of the Kraft pulping process (Nalco Company, 1988).

The digestion of the wood chips takes place in a pressure vessel that can operate in batch or continuous mode. The chips are mixed with the white liquor in a weight ratio (liquor weight/ wood weight) that can vary from 1 to 4. This white liquor is an alkaline digestion solution where the active chemical species are NaOH and Na_2S. Kraft cooking generally takes place at pressures of 7 to 9.5 bar and temperatures that reach 170ºC (Speight, 2002). Nowadays, the pulping technology is dominated by the Kamyr digester that consists on a cylindrical tower operating as a continuous moving bed reactor (Fernandes and Castro, 2000).

There are two important pulping parameters related to the chemical composition of the white liquor: active alkali, that represents the total amount of sodium hydroxide and sodium sulphide; and sulphidity, defined as the ratio of the Na_2S to active alkali. Normally, for a Kraft process, the active alkali should be around 15-20% and the sulphidity in the range of 25-35%, which represents approximately a 3:1 ratio of NaOH to Na_2S (Kirk-Othmer Encyclopedia, 2005). The sulphur present in the Na_2S is a key factor for the Kraft pulping, since it is responsible for a faster and more selective delignification when compared to the usage of only NaOH. As a result, the Kraft process can operate with lower cooking times, producing pulps with higher cellulose content and consequent higher strength. However, the optimal sulphidity should result of a trade-off between these advantages and the fact that the higher the content of Na_2S in the system, the more malodorous sulphur gases are liberated and more corrosive are the correspondent white liquors.

At the start up of the pulping, the *pH* of the cooking medium is very high (in the range of 13 to 14), decreasing along the digestion with the formation of organic acids from the lignin and carbohydrates degradation (Ullman's Encyclopedia, 2003).

The Kraft delignification of the wood can be divided into three phases: initial, bulk and residual delignification. The initial phase occurs at temperatures below 140ºC and is controlled by diffusion phenomena. When this temperature is achieved, the dissolution of lignin enters the bulk phase. The rate of delignification becomes controlled by chemical reactions and increases steadily with the cooking temperature, remaining at a high value until 90% of the lignin have been removed from the fibres (Chakar and Ragauskas, 2004; Kirk-Othmer Encyclopedia, 2005; Li, 1997). Then it starts the last phase, the residual delignification, which is much slower than the bulk phase and has a very poor selectivity. In fact, the cook should be stopped with some residual lignin present, for example around 4-5% when using softwood, to avoid excessive degradation of polysaccharides (Chakar and Ragauskas, 2004). This residual lignin can be removed by bleaching treatments.

Most of the lignin and some hemicellulose are dissolved in the aqueous phase, which at the end of digestion is called black liquor, leaving pulps with typical kappa numbers of 25-30 for softwoods, and 15-20 for hardwoods (Ullman's Encyclopedia, 2003). These pulps normally contain around 40 to 50% of the initial mass of wood (Ciullo, 1996; Yang, 1998). When the cooking is finished, the pulp and the correspondent black liquor are discharged from the digester into a blow tank. From there, the pulp advances to screening and washing procedures. The pulp washing is performed with water to remove the black liquor present in the pulp. The resulting stream of diluted black liquor goes to the chemical recovery process.

Relief gases are liberated during the cooking and the blow down of the digester. They contain vapours that can be used for heating purposes, and recuperation of a by product called turpentine and non condensable gases such as H_2S and SO_2 that must be treated to control sulphurous emissions.

An important feature for the success of the Kraft process is that the active species of the white liquor can be recovered from the black liquor and recycled, adding only a chemical makeup of sodium sulphate (Na_2SO_4). The alternative term for Kraft process – sulphate process – derives from this chemical makeup. The chemical recovery sequence can be observed in Figure 2.6, where the complete Kraft pulping process is shown.

The first stage of the chemical recovery consists on the concentration of the black liquor stream from approximately 15% of total solids to 65% (Ciullo, 1996). This removal of excess water is performed by a series of evaporators.

There are some studies on additives for reduction of black liquor viscosity, which can allow the increase of evaporation levels to the range of 70-85% on dry solids without the appearance of the correspondent problems in processing, such as pumping difficulties, plugging of operation units and pipelines (Llamas et al., 2007). Beyond the fact that they do not affect the Kraft process medium, these additives can also have a very positive influence in the process, especially by increasing steam and energy generation, reducing the gas emissions and promoting easier operation conditions.

The concentrated or strong black liquor is then sprayed into a recovery boiler, to produce energy and steam by burning the organic solids. In the present mills, the boilers mostly used are Tomlinson type. Salt cake (Na_2SO_4) is also added to the boiler as a makeup to compensate the chemical losses throughout the entire pulping process. Nowadays these losses can achieve 10 to 20 kg of Na_2SO_4 per tonne of produced pulp, which represents more than 90% of the chemicals (Chakar and Ragauskas, 2004).

Inside the boiler, carbon dioxide is formed from the combustion of the organic material. The contact of this gas with NaOH can convert it to sodium carbonate. The sulphates are reduced back to sulphides, the initial state of sulphur in this pulping

process. Due to the high temperatures of combustion, around 900ºC (http://etcpitea.se/blg/document/PBLG_or_RB.pdf), the remaining inorganic chemicals are present in the form of a molten smelt, which consist essentially on Na_2S and Na_2CO_3. This material is collected at the bottom of the boiler and flowed to a dissolving tank, where water is added to produce the green liquor.

The green liquor must be converted into white liquor to allow the recycling of this stream to the wood digester. This step is called causticizing and consists of adding calcium hydroxide to the green liquor (Ciullo, 1996; Speight, 2002). The reaction transforms the sodium carbonate into NaOH and forms a precipitate of calcium carbonate. This precipitate is called lime mud and is separated from the solution of white liquor, washed and filtered before being fed to a lime kiln. Inside this operation unit the calcium carbonate is burnt and reconverted to CaO. The calcium oxide is then slaked to calcium hydroxide, which is recycled to the causticizing step.

In Kraft pulp mills, the capacity of the recovery boiler is very often a limiting factor to the increase of the pulp production. This bottleneck can be overcome by two different approaches as suggested by Axelsson et al. (2006): upgrade or change the boiler system to deal with higher quantities of black liquor; or extract lignin from the black liquor stream, before entering the boiler, to compensate for the increase on organic load resulting from higher production levels.

Until several decades ago, the first option was the only alternative, although it represents very high capital investments. The possibility of lignin extraction from black liquor seems to be much more attractive, either for energy production or combustion elsewhere, or to serve as feedstock for chemicals production. A lot of research effort has taken place in the areas of lignin separation from black liquor, specially using precipitation (Norgren, 2001; Norgren and Edlund, 2003; Sun et al., 1999) and ultra

filtration methods (Bhattacharjee et al., 2006; Holmqvist et al., 2005; Liu et al., 2004; Wallberg et al., 2003; Wallberg et al., 2005; Wallberg et al., 2006), and, as focused earlier, new lignin applications and chemical processes using lignin. The work of this thesis is intended to fit in this two purpose scenario of presenting alternatives to the pulp and paper industry for the utilization of lignin and producing high added value chemicals from renewable biomass materials.

In Figure 2.7 is shown a picture from above of the Cacia Kraft pulp mill (Portugal) from the Portucel group just to give an idea of the dimension of the processes described.

Figure 2.7. View from above of the Cacia pulp mill in Aveiro (Portugal).

2.1.3.4 Bleaching

After cooking, the first chemical treatment in the pulp line of a paper production process is bleaching, to improve the purity and optical properties of the pulp by removing the residual lignin still present in the fibres, or at least eliminating its chromophoric groups. These groups can be formed during pulping, particularly Kraft pulping, and are responsible for an increase in pulp colour producing a non permanent brightness that disappears from exposure to oxygen and light. In contrast, when the bleaching treatment also removes the residual lignin, the paper has higher and lasting levels of brightness but has lower sheet strength.

Bleaching is normally a multiple stage process where, in each stage, the pulp is treated with a chemical and the final mixture is washed with water. A bleaching stage is composed by a tower, where the chemical treatment takes place, a washer to remove the bleaching agents and degraded lignin from the pulp, and a tank to collect the washing stream. The optimal combination of chemical stages, called bleaching sequence, depends essentially on the type of wood, previous pulping process and the quality desired for the bleached pulp. As an example, some years ago, in the Soporcel mill the bleaching sequence had five steps and was composed with chlorine dioxide (D) followed by alkaline extraction with NaOH (E), DEDED (Curto, 2003).

There are several chemical agents used in pulp bleaching, but most commonly applied are chlorine, chlorine dioxide, oxygen, hydrogen peroxide and sodium hydroxide. Chlorine is a bleaching agent that is rather selective for lignin with fast reactions carried out at low temperatures, approximately 30ºC (Ullman's Encyclopedia, 2003). However, a very negative fact, from the environmental point of view, is that are produced some toxic and carcinogenic chlorinated compounds almost impossible to remove via biological process from the waste effluents.

Chlorine dioxide (ClO_2) is an expensive bleaching agent; however, it is even more selective than chlorine, produces smaller amounts of chlorinated compounds and the resulting pulps present higher brightness.

Oxygen can be applied in the first stages of bleaching eliminating the problems of equipment corrosion brought by ClO_2. It is a cheap reactant, not selective to lignin and requires pressurization of the medium to dissolve in adequate quantities in water.

Hydrogen peroxide can be used in final stages of bleaching sequences, it is very effective on the elimination of the chromophoric groups present in lignin, giving high levels of brightness stability to the correspondent pulp.

The sodium hydroxide is used in extraction steps, to dissolve the degraded residual lignin present in the pulp fibres during bleaching treatment. This need for alkali is more important when dealing with Kraft pulps.

The detection of toxic substances (e.g. dioxins and furans) in bleaching effluents, in 1986, and also in the paper products give birth to important environmental and health issues, which lead to an increase of the development and application of alternatives for benign bleaching agents and processes (Jones, 1999). The alternative processes can be classified as Elemental Chlorine Free (ECF) or Totally Chlorine Free (TCF). In ECF processes the chlorine treatment is replaced by ClO_2, promoting wastewater streams with lower amounts of toxic chlorinated compounds. The TCF bleaching waste stream is completely clear of these substances, since it eliminates the chlorinated agents from the pulp treatment. This kind of "cleaner" approach to bleaching sequences can be applied to sulphite pulps. However, the majority of the Kraft mills were converted to ECF since the correspondent pulps are harder to bleach.

2.1.3.5 Stock preparation and papermaking

The stock preparation consists of a series of unit operations to improve the pulp properties, specially the bonding between fibres before they enter the paper machine. The composition of this series of unit operations is not unique and greatly depends on the pulp to be treated and the desired paper quality. However, there is a major step on the stock preparation called refining. Refining is a mechanical treatment of the fibres, in the presence of water, that makes them swell, increases their flexibility and sometimes reduces their length. This treatment causes an improvement of the strength of the paper sheet.

In the stock preparation some chemicals can also be added to provide specials properties to the final product. These additives include:

- Fillers: they are mineral powder products (Kaolins, calcium carbonate, titanium dioxide, synthetic silicas and aluminas). In terms of quantities, they are normally one of the most important additives to fibre slurry, achieving frequently 5 to 50% of the paper weight, depending on the kind of paper (Ciullo, 1996). Fillers decrease the cost of the product, since they are cheaper than the fibres (with the exception of TiO_2). They also improve the print quality, smoothness, brightness and opacity of the paper.
- Sizing agents: they are intended to increase the resistance of paper to liquids penetration. The most common sizing agents are rosins, alkyl ketene dimmer and alkenyl succinic anhydride (Holmberg, 2002).
- Optical brighteners: substances used to increase the whiteness and luminous appearance of the paper (derivatives of diaminostilbenedisulfonic acid).

- Dry strength additives: these agents are added to increase the natural capacity of the cellulose fibres to bond each other when paper is being dried. Cationic starch is the major substance used for this objective.
- Wet strength additives: they help to maintain, permanently or temporarily, part of the original paper strength and integrity, even when it is completely soaked. They include poly(ethylene imines), polyamides, and urea-formaldehyde condensates (Ullman's Encyclopedia, 2003).
- Dyes: they are used to attribute the desired colour to the paper product.

After stock preparation procedure, the fibre slurry is fed to a paper machine to produce the final sheet product. There the slurry will pass through several steps: sheet forming, pressing, drying, sizing and calendering. Since the start of papermaking history this process sequence has not changed; however, technology evolved so much that nowadays the modern paper machines can have 10 meters wide, operate at speeds over 2000 m/min and produce more than 2000 tonnes per day (Ciullo, 1996; Ullman's Encyclopedia, 2003).

Sheet forming consists on filtering the water from the slurry, leaving it uniformly distributed over the web. Then the slurry advances to the press section where it is compressed between rolls. The objective is to mechanically dewater the fibre slurry as much as possible, in order to save energy in the subsequent drying section. The dry content after the press section can achieve values around 55% (Ullman's Encyclopedia, 2003). In the drying section the slurry will suffer a heating treatment to evaporate the major part of the remaining water. After this treatment, the dry content of the fibre sheet reaches 92-95% (Ciullo, 1996). In sizing, some additives like starch or pigments can be added to improve even more the paper strength and its surface properties. Finally, in

calendering the surface of paper is smoothed, and sometimes its thickness is reduced, using compressing rolls and temperature treatments.

2.1.3.6 Alternative pulping processes

A great deal of effort has been made in developing alternative competitive processes, in order to minimize the environmental problems and high investment costs of the traditional pulping processes (Kraft and sulphite). The most relevant of those alternative routes are organosolv pulping and the application of catalysts in traditional pulping (Kirk-Othmer Encyclopedia, 2005; Sixta, 2006; Ullman's Encyclopedia, 2003).

Organosolv pulping consists on using organic solvents to help on the extraction of lignin from wood. Examples of organosolv methods are:

- ASAM process: it is based on the conventional alkaline sulphite process, where sodium sulphite is used as pulping agent with the addition of anthraquinone and methanol (Kirk-Othmer Encyclopedia, 2005; Ullman's Encyclopedia, 2003).
- Organocell process: it has two pulping stages. In the first stage the wood is cooked with a 50:50 mixture of methanol and water, at temperatures around 190ºC. Then, in the second stage the wood extensively delignified using pulping liquor with NaOH, anthraquinone and 35% in methanol (Ullman's Encyclopedia, 2003).
- Alcell process: the wood pulping is performed by mixtures of ethanol and water.

The organosolv pulping seems to have some strong advantages over Kraft pulping, namely in the areas of chemicals recovery, since the solvents seems to be easily recovered by simple distillation; in the environmental area, eliminating the emissions of sulphur and using less aggressive chemical conditions; and in the production of larger

amounts of valuable biomass by-products. However, the organosolv pulps normally have a lower quality comparing to Kraft pulps, especially in the strength properties.

Anthraquinone is the catalyst most applied in traditional pulping processes. In soda pulping it accelerates the delignification, but the produced pulp can not compete with Kraft pulp, in terms of quality and price. It can also be used in alkaline sulphite pulping with very good results on pulp strength. Studies using anthraquinone and polysulfide (Na_2S_x), together as additives in Kraft pulping, showed improvements in the pulp yield and in carbohydrate retention (Li, 1997). In fact the combined application of these additives revealed a so called synergistic effect, since the improvements referred were higher than the sum of the correspondent gains, over the conventional Kraft pulping, when they are used alone.

In spite of all the work for alternative processes focused above, the Kraft technology has also been evolving in a clear indication that Kraft pulping will prevail in a foreseeable future.

2.2 Starting material: Lignin

2.2.1 General features and molecular structure

In 1838, Anselme Payen treated wood with nitric acid followed by an alkaline solution, which yielded an insoluble fraction, named cellulose, and a soluble fraction that he called *incrustant* (Norgren, 2001; Wool and Sun, 2005;). In 1857, this soluble material was designated 'lignin' by the German scientist F. Schulze (Norgren, 2001).

Lignin is one of the most important constituents of biomass and, among the group of renewable polymers, only cellulose overcomes its natural abundance. The biosphere contains $3x10^{11}$ tons of lignin and annually it increases around $2x10^{10}$ tons

(Gregorová et al., 2006). Lignin can be defined as a three-dimensional amorphous macromolecule made of phenylpropane units that arise from the copolymerization of three primary precursors: coniferyl alcohol, sinapyl alcohol and *p*-coumaryl alcohol (Figure 2.8). The common notation used for addressing to the different carbon atoms within each phenyl propane unit is shown in Figure 2.9.

The biosynthesis pathway of lignin is initiated with enzymatic dehydrogenation of the monomers presented in Figure 2.8 with the formation of correspondent phenoxy radicals. Each of these free radicals is highly resonance-stabilised, as a result of its possible mesomeric forms (Figure 2.10).

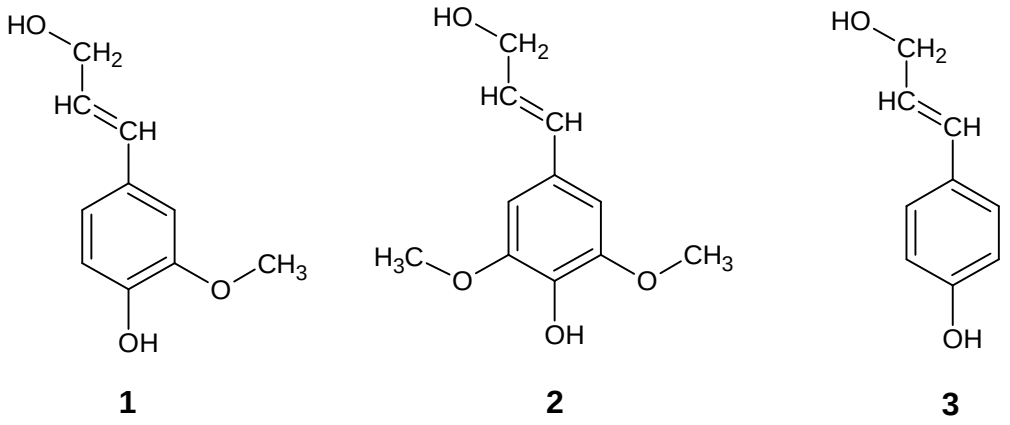

Figure 2.8. Primary percursors of lignin: (1) coniferyl alcohol, (2) sinapyl alcohol and (3) *p*-coumaryl alcohol.

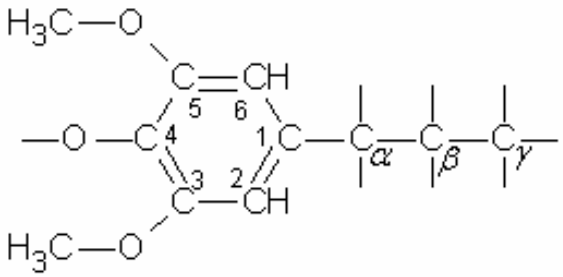

Figure 2.9. Common notation for addressing to the carbon atoms within each phenylpropane unit (Wool and Sun, 2005).

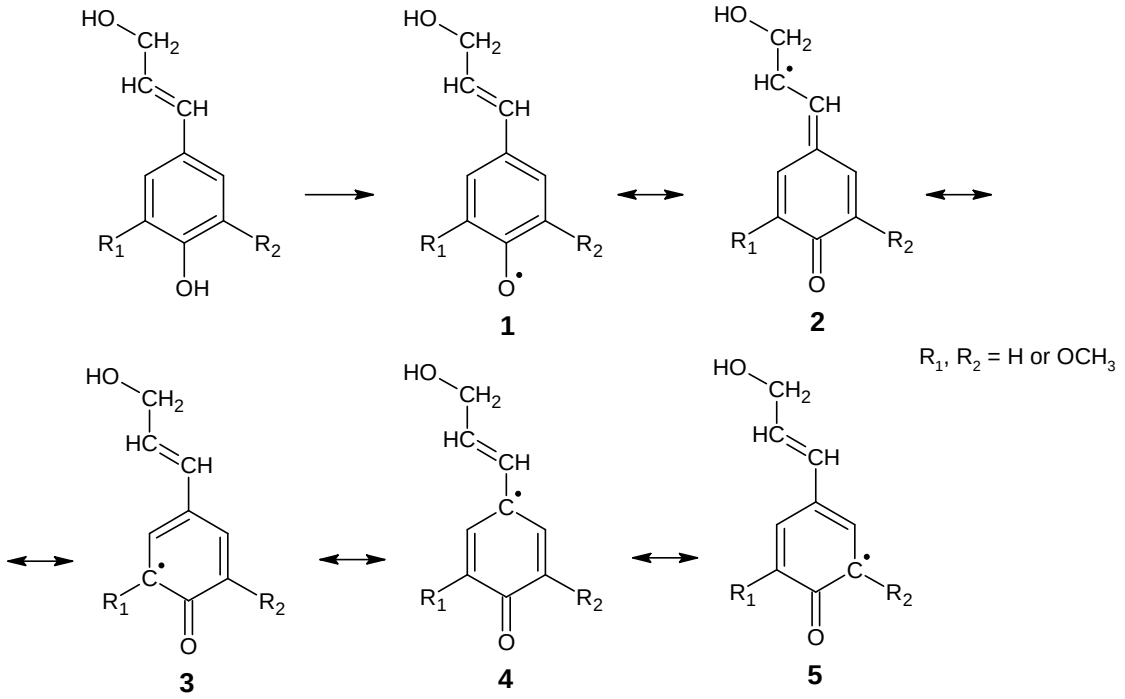

Figure 2.10. Mesomeric forms of the phenoxy radicals derived from the lignin precursors (Bjørsvik and Minisci, 1999).

The random coupling reactions between the radicals presented in Figure 2.10 result in structures disposed in very complex three-dimensional networks and with high heterogeneity in respect to its composition, size, cross-linkages and proportion of the characteristic functional groups (hydroxyl, carbonyl and carboxyl). Because of this, it is not possible to attain a definite structural model for the molecule of lignin in its native form. The most common of these models is the Adler's structure for native lignin that is shown in Figure 2.11.

The building blocks of lignin structures are bonded together by several types of carbon-carbon and ether (β-O-4, α-O-4, 4-O-5) linkages of remarkable stability, that gives the biopolymer high resistance against degradation, with the exception of the weak and hydrolysable α-aryl ether bonds (Wool and Sun, 2005). Normally, the β-O-4 ether bond is predominant on the lignin molecules from wood, with around 48-60% of the linkages between the phenyl propane units (Mathias, 1993).

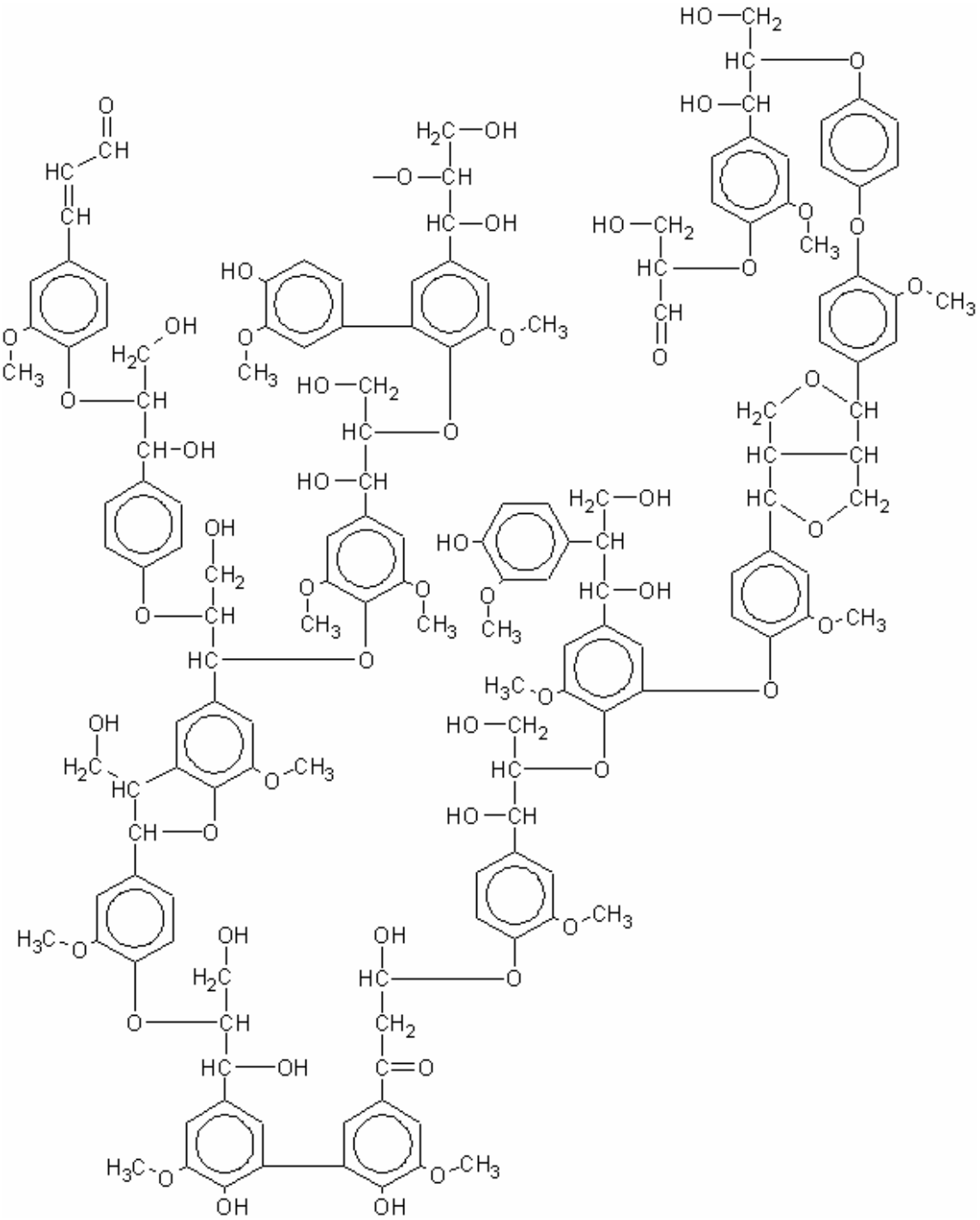

Figure 2.11. Structure of native lignin according to Addler (Glasser and Sarkanen, 1989).

Lignin is one of the main constituents of woody plants. The lignin content in wood varies greatly with species but also with the environment and conditions in which the plant develops. Lignin contributes with around 25-35% and 18-25%, respectively, to the dry weight of softwoods and hardwoods (Wool and Sun, 2005).

The chemical composition of lignin is also irregular showing variations in the relative amounts of the phenyl propane monomers with and within a plant, depending on its species, age, and morphological location. However, it is commonly recognized that the lignins from softwoods (gymnosperms) are predominantly based on structural units derived from coniferyl alcohol (guaiacyl units), in quantities usually higher than 90%, with the remainder small percentages of structural units being attributed to the *p*-coumaryl alcohol precursor (Kirk-Othmer Encyclopedia, 2005). On the other hand, hardwood (angiosperms) lignins are polymers that present structures with much broader chemical compositions, consisting in varying proportion ratios of guaiacyl and syringil (derived from sinapyl alcohol monomer) units.

Lignin plays a very important role in plants life performing several functions indispensable for their survival. It is distributed between and in the cell walls acting like a glue or cement on binding the wood fibres together, which gives the rigidity and mechanical resistance to compression, impact and bending that are well known in wood materials. Lignin also acts as a water sealant across the cell walls playing a decisive part in the control of the internal transport of water, nutrients and metabolites. Finally, lignin makes the woody tissue more resistant against biological attacks by obstructing microorganisms penetration.

2.2.2 Lignin reactions

The combination of the functional groups comprised in each structural unit of native lignin provides this macromolecule with a great potential to participate in a wide spectrum of reactions. Some of these lignin-based reactions are pointed out below (Kirk-Othmer Encyclopedia, 2005):

- Electrophilic substitution in the aromatic rings by chlorination, nitration and ozonation. Chlorination mainly occurs in bleaching sequences of chemical pulps when chlorine is introduced into the aromatic rings, and nitration consists on substitution in the aromatic rings with nitro groups when lignin reacts with nitrogen dioxide.
- Conversion of aromatic rings to non-aromatic cyclic and acyclic structures by the action of some oxidants like chlorine, hypochlorite, chlorine dioxide, oxygen and hydrogen peroxide. The aromatic ring converts into an *o*- or *p*-quinoid structure that can suffer further oxidative splitting into an acyclic structure.
- Ring coupling and condensation reactions that result from the combination of free radicals in lignin.
- Cleavage of ether bonds in the α- and β- carbon positions of the phenyl propane units. These linkages are the most abundant between the lignin building blocks and their cleavage is the main step in the degradation and dissolution of lignin occurring on the chemical pulping processes.
- Rupture of carbon-carbon bonds in the propanoid side chains of the phenyl propane units. These reactions only occur in particularly aggressive treatments such as bleaching of chemical pulps, and some chemical and biological degradation.
- Substitution reactions in the propanoid side chains and mainly in the benzyl carbon. This carbon in the α- position is the most reactive of the side chain and may undergo substitution reactions by the attack of nucleophilic agents.
- Formation and elimination of multiple bonds have a major effect on the colour of lignin, particularly important for the requirements of pulp

bleaching processes. Examples of these reactions are the reduction of carbonyl groups to alcohols and the transformation of olefinic groups into their saturated derivatives.

2.2.3 Commercial lignins

The lignin present in wood cells, generally known as native lignin or protolignin, is almost impossible to isolate without changing its original structure. The less aggressive procedure to extract native lignin consists in contacting finely ground wood meal with a mixture of dioxane with water. This procedure attains low extraction yields, and the isolated lignin, known as milled wood lignin (MWL), is commonly used in lignin studies and chemical analyses.

The more efficient reagents and solvents used in industrial delignification processes promote significant structural changes in the native lignin, especially through bond cleavages, condensation reactions and attack to some functional groups. The lignins that results from these industrial processes are called commercial or technical lignins.

Technical lignins can be divided into two categories. The first category includes the sulphur-free lignins, which are the technical lignins that resemble more closely to the original structure of native lignins. Sulphur-free lignins are mainly obtained from three sources: biomass conversion technologies mainly focused on biofuel production; organosolv pulping processes; and soda pulping based on alternative resources like agricultural residues and non-wood fibres (Lora and Glasser, 2002).

The second category consists on the sulphur containing lignins, which result essentially from Kraft and sulphite pulping processes. This category comprises almost the totality of the market of commercially available lignins. However, it is estimated

that 98-99% of the lignin separated from wood in the sulphite pulping, and especially in the Kraft pulping, are burned for energy and chemicals recovery or disposed of in waste streams (Lora and Glasser, 2002). The remaining amount is isolated from the spent pulping liquors and sold for specialty applications, which normally is around 1 million tons per year worldwide (Lora and Glasser, 2002; Thielemans et al., 2001). In Table 2.1 are presented some values on the annual capacity of the major producers of technical lignin in Europe and North America.

Table 2.1. European and North American major producers of technical lignins (Kirk-Othmer Encyclopedia, 2005).

Producer		**Annual capacity (tons/year)**
Borregaard LignoTech	Europe *	400,000
	U.S.	70,000
Tembfibre	Europe	40,000
	Canada	40,000
Fraser Paper	U.S.	50,000
Tolmozzo	Europe	35,000
Westvaco *	U.S.	30,000
Inland Paper	U.S.	20,000
Others		100,000
Total		**785,000**

* Produces Kraft lignin; the rest of the companies only produces lignosulphonates.

Technical lignins obtained from sulphite pulping are called lignosulphonates or sulphite lignins. They can be obtained in several forms such as calcium, sodium, magnesium and ammonium lignosulphonates, depending on the correspondent type of pulping process (Kirk-Othmer Encyclopedia, 2005).

Lignosulphonates can be isolated from spent pulping liquors by various methods. In industry, the most widely used is the Howard process, where excess lime is added to precipitate the lignosulphonates to achieve recoveries around 90-95% (Kirk-Othmer Encyclopedia, 2005).

Kraft lignins or sulphate lignins, are present in a by-product stream of the Kraft pulping process known as black liquor. They are precipitated and extracted from black liquor in a two-step acidification process. First, carbon dioxide is used to reduce the *pH* of the liquor to 9-10, and about 75% of the lignin is precipitated as a sodium salt (Kirk-Othmer Encyclopedia, 2005). For further purification, this lignin is suspended in water and acidified with H_2SO_4 to a *pH* lower than 3. The commercial Kraft lignins are generally sold in the sulfonated form or as lignin amines.

2.2.4 Physical properties

The real molecular mass of lignin in wood is undetermined, since all of the methods to isolate protolignin promote alterations on its molecular structure. As already been mentioned, to overcome this limitation is commonly used milled wood lignin in characterization studies of protolignin. The weight average molecular mass (M_w) of softwood MWL is reported to be around 20,000, with a polydispersity of 2.5, whereas hardwood MWL present lower values of M_w (Ullman's Encyclopedia, 2003).

Lignin is a polymer that exhibits thermoplastic behaviour and has a glass transition temperature (T_g) around 440 ºK (Kirk-Othmer Encyclopedia, 2005). This parameter is greatly affected by moisture content and posterior isolation and heat treatments.

Frequently the analytical data of lignins is expressed in C_9 formulae, since its structural blocks (phenyl propane units) contain nine carbons. For example, the elementary analysis of MWL from softwood *Picea abies* and hardwood *Eucalyptus regnans* gave, respectively, the C_9 formulae of $C_9H_{8.3}O_{2.7}(OCH_3)_{0.97}$ and $C_9H_{8.7}O_{2.9}(OCH_3)_{1.58}$ (Ullman's Encyclopedia, 2003).

Good solvents for milled wood lignin and Kraft lignin are those having a Hildebrand's solubility parameter (δ) of 10-11 $(cal/cm^3)^{0.5}$, and also with a good capacity to form hydrogen bonds, such as methyl cellosolve and pyridine.

Besides methyl cellosolve and pyridine, other solvents such as dioxane, dimethylformamide (DMF) and acetone are able to dissolve Kraft lignins. In aqueous systems with low hydroxide ion concentrations (pH < 10.5), high ionic strengths or at elevated temperatures, Kraft lignins self-associate to form colloidal particles and sometimes also precipitate (Norgren, 2001; Norgren and Edlung, 2003; Norgren et al, 2002a; Norgren et al, 2002b).

Kraft lignins have number average molecular weight (M_n) in the range of 2000-3000 and polydispersities between 2 and 3 (Kirk-Othmer Encyclopedia, 2005). For a typical softwood Kraft lignin its was reported a C_9 formulae of $C_9H_{7.759}O_{2.479}N_{0.006}S_{0.065}(OCH_3)_{0.597}$ corresponding to a monomer molecular weight of 176.09 (El Mansouri and Salvadó, 2006). The content in free phenolic hydroxyl groups is especially rich with values around 3.1 meq g^{-1} (Ullman's Encyclopedia, 2003). This functional group plays as important role in the dissolution of macromolecules.

Lignosulphonates are characterized by a molecular polydispersity much higher than Kraft lignins, and their M_n is normally in the interval of 20,000 to 50,000 (Kirk-Othmer Encyclopedia, 2005). The C_9 formulae of a softwood lignosulphonate was reported as $C_9H_{11.18}O_{4.94}N_{0.003}S_{0.40}(OCH_3)_{0.73}$ with a monomer molecular weight of 220.89 (El Mansouri and Salvadó, 2006). The content in free phenolic hydroxyl groups is approximately 0.5 meq g^{-1} (Ullman's Encyclopedia, 2003). Lignosulphonates are soluble in water in all pH range but insoluble in common organic solvents.

Comparing the properties of Kraft lignins and lignosulphonates, besides the differences on polidispersity and solubility behaviour, lignosulphonates have

considerably higher molecular weights and lower content in free phenolic hydroxyl groups, both of these factors a consequence of a more extensive attack and cleavage of the lignin in the Kraft pulping process. In Table 2.2 are compiled some of the discussed physical properties for softwood Kraft lignins and softwood lignosulphonates.

Table 2.2. Properties of softwood Kraft lignins and softwood lignosulphonates.

Property	Kraft lignins	Lignosulphonates
Molecular weight	2,000 – 3,000	20,000 – 50,000
Polydispersity	2 – 3	6 – 8
C_9 formulae	$C_9H_{7.759}O_{2.479}N_{0.006}S_{0.065}(OCH_3)_{0.597}$	$C_9H_{11.18}O_{4.94}N_{0.003}S_{0.40}(OCH_3)_{0.73}$
Molecular weight of C_9 unit	176.09	220.89
Phenolic hydroxyl (meq/g)	3.1	0.5
Sulphur (%)	1 – 1.5	4 – 8
Solubility	Soluble in alkali (pH>10.5), acetone, pyridine, DMF, methyl cellosolve	Soluble in water in all *pH*'s, insoluble in organic solvents
Colour	Dark brown	Light brown

2.2.5 Applications

Nowadays, the major slice of the lignin residues in industry, particularly in pulp and paper mills, is burned as a valuable fuel for energy recovery. However, there is a growing interest and concern on exploring the potential of lignin and its derivates as raw materials in the polymer industry and other chemicals.

The chemical utilization of lignin involves some difficulties like its molecular complexity and polydispersity that poses difficulties in quality control, high oxygen content and higroscopicity, low solubility and high thermal glass transition temperature

(Glasser and Sarkanen, 1989; Hu, 2002). On the other hand, there are a lot of attractive factors favouring chemical utilization of lignin (Glasser and Sarkanen, 1989; Hu, 2002):

- easily obtainable in industry and in large quantities;
- reduction of its disposal as a pulp mill waste and the correspondent environmental problems;
- interesting energetic value due to its high aromatic content;
- good colloidal and rheological properties;
- compatible with important chemical products;
- large number of reactive points on its molecular skeleton where it can occur several kinds of reactions.

Technical applications of industrial lignins include the areas of thermoplastics, adhesive resins, carbon fibres, cement additives, sorption-active materials, medicinal antioxidants, automotive brakes, sealants, polyurethane foams, rubber fillers, surfactants, dispersants, electrical shielding, storage battery plates and many others (Dizhbite et al., 1999; El Mansouri and Salvadó, 2006; Glasser and Sarkanen, 1989; Hu, 2002; Košíková et al., 2006; Thielemans et al., 2001).

Lignin utility in polymeric applications is commonly dependent on the incorporation of some functional groups in its structure. This is called chemical modification and the purposes are to obtain higher polymer-lignin compatibility, improve lignin solubility or miscibility behaviour and introduce reactive sites in the molecule. Due to the large number of functional groups of technical lignins, almost endless possibilities exist for chemical modification. However, the prominent alternatives are esterification, etherification and acetylation of the hydroxyl groups, addition of double-bond functionality, sulphonation, amination and nitration.

Engineering plastics and thermosetting resins are two fields with higher perspectives for utilization of lignin and its derivatives. Several studies have been done on the use of lignin in adhesives like phenol-formaldehyde, urea-formaldehyde resorcinol-formaldehyde and epoxy resins, mainly to apply in wood based products such as plywood, particleboard and fibreboard (Hu, 2002). The most investigated area has been the utilization of lignin in phenol-formaldehyde adhesives, since lignin being a phenolic polymer is considered as a possible replacement for phenol in this type of adhesives.

A good example is the study of El Mansouri and Salvadó (2006), which characterized different types of technical lignins to incorporate into phenolic resins. They concluded that Kraft and soda-anthraquinone lignins may be good raw materials for lignin-based phenol-formaldehyde resins. This kind of resins were also prepared without the carcinogenic formaldehyde, substituted by glyoxal, a non-volatile and non-toxic aldehyde, and tested for application to wood panels with good strength and reactivity results (El Mansouri et al., 2007). Lora and Glasser (2002) reported some industrial applications for sulphur-free lignin such as partial substitute for phenolic resins, incorporation in epoxy resins and polyurethane foams, and production of bio-dispersants.

The addition of lignin to polyolefins aims to improve their mechanical properties, stability or provide biodegradability (Hu, 2002). Gregorová et al. (2005) investigated the influence of a sulphur-free lignin on the oxidative stability of polypropylene and recycled polypropylene. The results showed that lignin acts as an antioxidant on both of them when used as a dry powder up to 5 wt%.

Lignin can also be used as a filler in rubber materials. In fact, it has been proved that natural rubber, polybutadiene, nitrile rubber, neoprene and styrene-butadiene rubber

are compatible with lignin to form polymer blends. A recent study revealed that a carbon black filled natural rubber attained similar stabilization improvements when incorporated with a commercial rubber antioxidant known as IPPD (*N*-phenyl-*N*-isopropyl-*p*-phenylene diamine) or with a sulphur-free lignin (Gregorová et al., 2006). The stabilizing effects exerted by lignin where maximum under concentrations of 2-5 wt%. Moreover, the activity of commercial rubber antioxidant IPPD could be enhanced with the addition of lignin.

An interesting application of lignin polymer blends is their potential use as precursor for carbon fibres. For this purpose, Kadla et al. (2002) produced carbon fibres for the first time from a commercially available Kraft lignin, without any chemical modification, by blending lignin with less than 5% of poly(ethylene oxide) and subjecting the blend to thermal spinning followed by carbonization.

A completely different field is related to exploring the sorption capacities of lignin. The presence of a significant amount of oxygen-containing groups in the cross-linked structure of lignin is a prerequisite for sorption activity by mechanisms such as physical adsorption, hydrogen bonding, coordination and covalent linking, and acidic-basic interactions. Dizhbite et al. (1999) investigated the sorption properties of hydrolysis lignin, a by-product of wood conversion to ethanol, modified with quaternary ammonium compounds and amino groups. The first were effective on sorption of organic compounds of aromatic nature, while amino-lignins revealed good sorption activity towards heavy metals, bile acids and cholesterol. In fact, the capacity of aminolignins for bile acids (140 mg g^{-1}) and cholesterol (80 mg g^{-1}) surpassed the correspondent one of commercial Bilignin, used for sorption of these species from blood.

Vanillin and dimethyl sulphoxide are the only two low molecular mass chemicals produced in large quantities from technical lignins, particularly lignosulphonates. The reaction of sulphide or elemental sulphur with lignosulphonates, at 215ºC, produces dimethyl sulphide and methyl mercaptan (Kirk-Othmer Encyclopedia, 2005). Dimethyl sulphide can be further oxidized to dimethyl sulphoxide, a useful industrial solvent (Kirk-Othmer Encyclopedia, 2005).

Industrially, softwood spent sulphite liquors or isolated lignosulphonates are oxidized, in alkaline media, by oxygen or air to produce vanillin (Bjørsvik and Minisci, 1999). The goal of this thesis fits in this kind of lignin application, but instead of using lignosulphonates, the vanillin production is based on isolated lignin from the largely available Kraft pulping waste liquor, although knowing that this is a raw material with less quality for this production process.

2.3 Target product: Vanillin

2.3.1 General features

Vanillin is the common name for 4-hydroxy-3-methoxybenzaldehyde, also known as vanillic aldehyde, vanillaldehyde, 3-methoxy-4-hydroxybenzaldehyde, methyl-protocatechualdehyde and *p*-vanillin (Washburn, 2003; Mathias, 1993). This organic compound possesses the aldehydic, etheric and phenolic functional groups, and its molecular formula is $C_8H_8O_3$ corresponding to a molecular weight of 152.15 (Washburn, 2003). The chemical structure and geometry of vanillin are presented in Figure 2.12. Some relevant physical properties of vanillin are shown in Table 2.3.

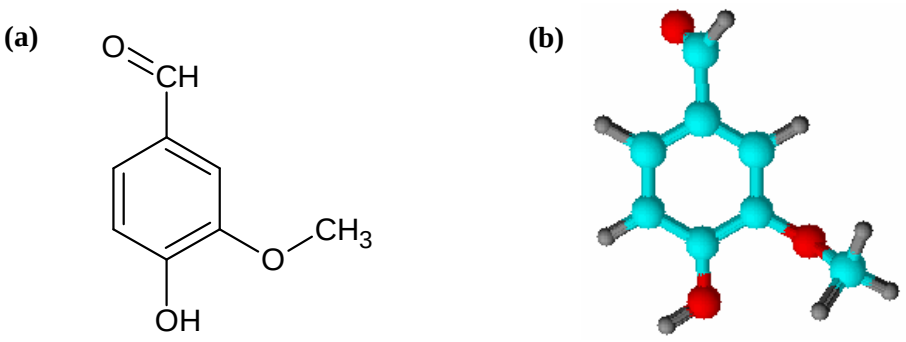

Figure 2.12. Chemical structure (a) and geometry (b) of vanillin molecule.

Vanillin occurs widely in nature, especially in the cured beans of the tropical *Vanilla* orchids. It is the major component among about 200 other flavour compounds found in these beans (Walton et al., 2003). Isolated vanillin occurs in the form of white needle-like crystalline powder with a pleasant aromatic vanilla odour and an intensively sweet taste, which are the main reasons for its widespread demand.

Table 2.3. Physical properties of vanillin.

Property	Value	Reference
Melting point	81-82 ºC	Perry, Green and Maloney, 1997
Boiling point at 760 mmHg	285 ºC	Perry, Green and Maloney, 1997
Density at 20ºC	1.056	Perry, Green and Maloney, 1997
Water solubility at 25ºC	10 g/l	The Merck Index, 2001
Vapour pressure at 25ºC	2.2×10^{-3} mmHg	Perry, Green and Maloney, 1997
Heat of solution in water	-21.8 kJ mol^{-1}	Washburn, 2003
pH of an 5% aqueous solution	4.3	http://www.chem.unep.ch
Odour threshold in water	2×10^{-1} ppm	http://www.buetzer.info
Odour threshold in air	1.10×10^{-8} ppb	http://www.buetzer.info

In terms of toxicity, vanillin does not present any particular risk for humans. However, vanillin can promote dermal reactions in people already sensitized to other

compounds like balsam of Peru, benzoin, rosin, benzoic acid, orange peel, cinnamon and clove (http://www.buetzer.info).

2.3.2 Applications

The world market of vanillin can be divided in three main applications: flavouring agent, fragrance and pharmaceutical intermediate.

Vanillin is one of the most popular flavouring agents in the food industry. It is widely used as an additive in chocolates, ice creams, confectionery, baked goods and beverages, with normal concentrations in the range of 50 to 1000 ppm, depending on the product category (Kirk-Othmer Encyclopedia, 2005). In 2004, this kind of application accounted for 82% of the total vanillin demand (Triumph Venture Capital; 2004).

In addition to its use as a fragrance ingredient in perfumes and cosmetics, vanillin has become an important deodorant to mask unpleasant odours of medicines, cleaning products, and many manufactured goods, such as paper products, plastics, rubber goods, etc.

Besides its flavour and fragrance qualities, vanillin is also very useful in the synthesis of several pharmaceutical chemicals, namely, L-methyldopa, L-dopa, trimethoprim, cyclovalone and etamivan (Bjørsvik and Liguori, 2002; Walton et al., 2003). These chemicals cover a large spectrum of medical applications: L-methyldopa is an antihypertensive drug; L-dopa is an agent on the treatment of Parkinson's disease; trimethoprim is used in the treatment of upper respiratory tract infections and some venereal diseases; cyclovalone is a digestant or choleretic; and etamivan is analeptic and a central nervous system and respiratory system stimulant (Bjørsvik and Liguori, 2002; Mathias, 1993). The pharmaceuticals production was responsible for the consumption

of a share of 13% of the 2004 worldwide market for vanillin (Triumph Venture Capital; 2004).

Smaller scale applications for vanillin include the production of antifoaming agents, brightener and activator in zinc coating baths, agent in the prevention of mouth roughness by smoking tobacco, attractant in insecticides, solubilization agent for riboflavin and catalyst in the polymerization of methyl methacrylate (Mathias, 1993).

Vanillin reveals antioxidant and antimicrobial properties allowing a potential use in food preservation. In fact, it was shown that vanillin acts as an antioxidant in complex foods containing polyunsaturated fatty acids, and more recently were reported promising results in the inhibition of food spoilage yeasts and moulds in fruit purees and fruit based agar systems (Cerrutti et al., 1997; Fitzgerald et al., 2003; López-Malo et al., 1998).

2.3.3 Production routes

The methods to obtain vanillin can be divided in three main classes: natural, chemical synthesis and biotechnological routes.

2.3.3.1 Natural route

The most relevant natural source of vanillin are the beans, or pods, of the tropical *Vanilla* orchids, principally the *Vanilla planifolia* species. The flowers of this plant have a closed structure that makes self pollination almost impossible. Artificial pollination is the only solution and to attain reasonable yields it is manually made, which is a very laborious task that discourages the cultivation of these plants in a very large scale (Rao and Ravishankar, 2000).

Around six to eight months after fertilization, the green vanilla beans are harvested (Walton et al., 2003). At this point the beans display an unpleasant odour, and like the other flavour compounds present, vanillin is in the β-d-glycoside form. Then the beans are submitted to a multi-step curing process, where they develop the characteristic vanilla aroma as a result of the enzymatic action of β-d-glycosidases to obtain vanillin and the other flavour compounds in their free form. The techniques of curing process can differ from one country to another, but they consist basically of four steps: scalding or killing, sunning or sweating, drying and conditioning. The complete curing process can have up to six months of duration (Dignum et al., 2001; Walton et al., 2003).

The cured vanilla beans contain about 200 components, where the most abundant aromatic is vanillin with 2% of the dry matter, followed by *p*-hydroxybenzaldehyde and vanillic acid with 0.2% and 0.1%, respectively (Rao and Ravishankar, 2000). Commercially, natural vanillin is sold as a dilute ethanolic extract, and is responsible for the supply of less than 1% of the total vanillin demand.

2.3.3.2 Chemical synthesis route

Synthetic vanillin produced by chemical routes is responsible for the supply of almost the entire market of this substance. The first chemical process to obtain vanillin was based on eugenol as raw material (Kirk-Othmer Encyclopedia, 2005). Nowadays, this process has only historical interest as synthetic vanillin is produced, in a commercial scale, from either the petrochemical guaiacol or from lignin.

There are several possibilities to synthesize vanillin from guaiacol, however, at the present time the most competitive technology consist on using guaiacol and glyoxylic acid (Kirk-Othmer Encyclopedia, 2005). This is a two-step process that starts

with a condensation reaction, in alkaline media, between guaiacol and glyoxylic acid. The resulting vanilmandelic acid is then converted to vanillin by oxidative decarboxylation. This sequence of reactions is represented on Figure 2.13.

In the industrial process, the condensation of the glyoxyl radical with the aromatic ring of guaiacol occurs, in alkaline media, almost entirely in the *para* position referent to the phenolic hydroxide group. Crude vanillin is then obtained by oxidation, acidification and simultaneous decarboxylation of the vanilmandelic acid. The vanillin is formed with nearly absence of by-products, simplifying the role of the subsequent separation procedure, which gives a very attractive advantage for this kind of production process. However this process is dependent on petroleum derived compounds such as guaiacol, in opposition to the biomass based lignin oxidation process.

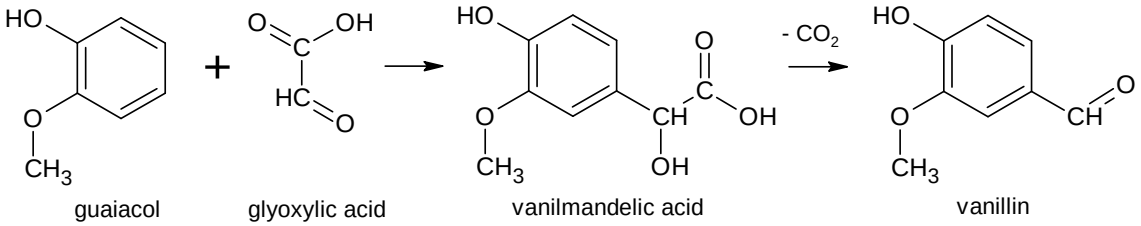

Figure 2.13. Chemical reaction sequence for producing vanillin from guaiacol (based on Kirk-Othmer Encyclopedia (2005)).

Alternatively to this guaiacol based process, lignin can be used as raw material to produce vanillin. Lignin is an important biomass component that finds its major industrial source on a by-product stream of pulp and paper mills, called black liquor, as already described earlier in this chapter. This vanillin synthesis route consists on treating an aqueous solution of lignin with oxidants, at very alkaline *pH*, and high temperatures and pressures. These oxidants can be air, oxygen, nitrobenzene or metallic oxides, with or without the help of catalysts (Mathias, 1993). Lignin is degraded and oxidized, producing vanillin along with other by-products. Besides lignin fragments,

typical compounds that may be present in a product stream of lignin oxidation can be observed on Figure 2.14 (Bjørsvik and Liguori, 2002; Mathias, 1993). The presence of these contaminants with chemical structure close to vanillin requires the use of much more intensive purification procedures, when compared to the guaiacol process. These procedures have a determinant role on the economical competitiveness of the lignin-based process, and breakthroughs in this field will lead to major positive impacts to its expansion in the industrial panorama.

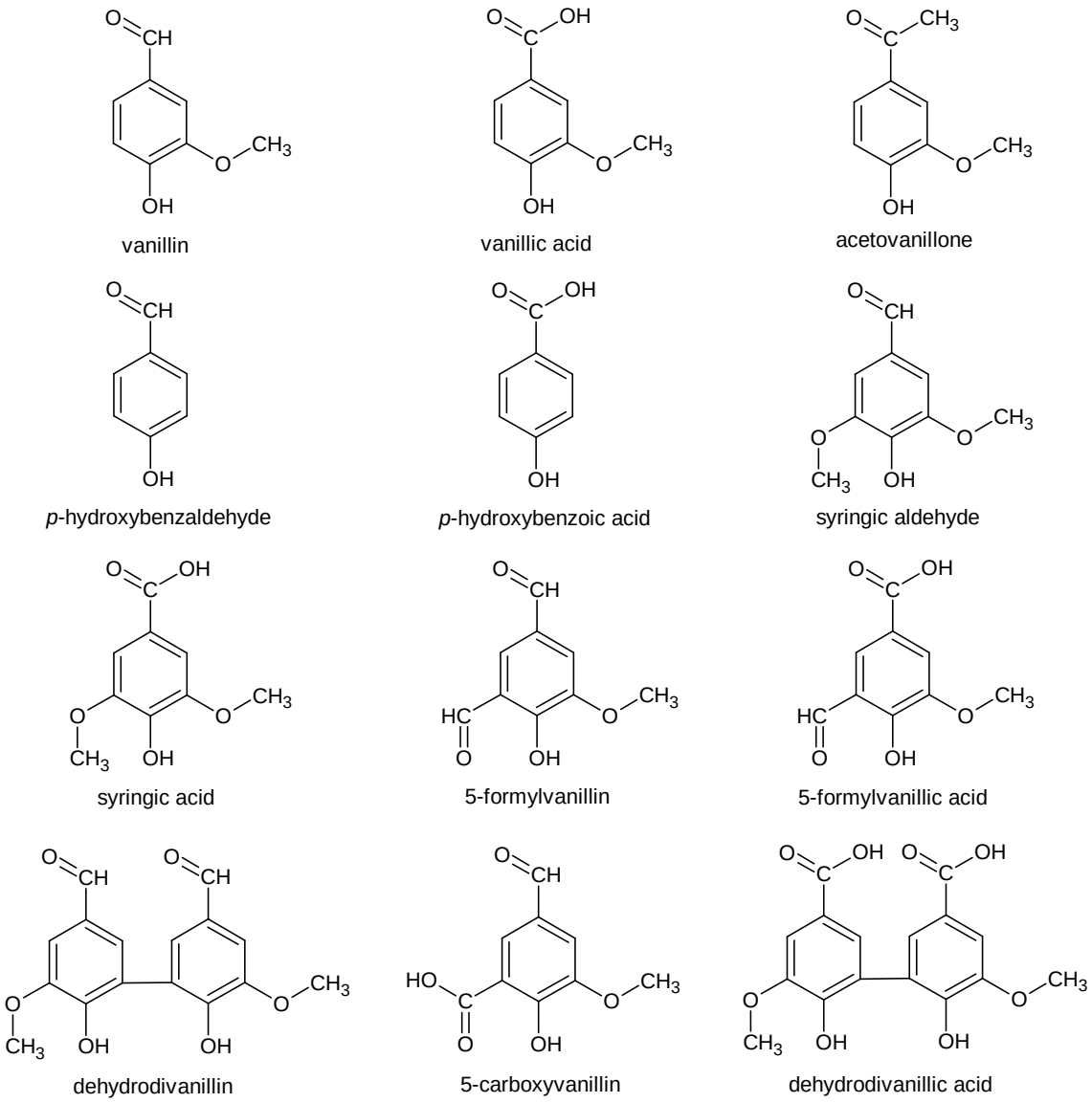

Figure 2.14. Aromatic compounds formed during lignin oxidation.

The only lignin-based process industrially implemented is supported on alkaline oxidation of lignosulphonates, collected from sulphite pulp mills, in the presence of air. In 2004, it was responsible for the supply of 15% of the synthetic vanillin market (Triumph Venture Capital; 2004). Besides the separation steps, there are several windows for research and improvement, especially regarding the use of Kraft black liquor as raw material, instead of the conventional application of lignosulphonates, since Kraft process prevails in the pulp and paper industry.

The subject of vanillin formation from lignin oxidation is not very rich on specific available literature. However is should be pointed out some studies developed on the last 15 years.

First of all, the work of Laboratory of Separation and Reaction Engineering (LSRE) in the area of vanillin chemical production from Kraft lignin oxidation started up some years ago (Fargues et al., 1996a; Fargues et al., 1996b; Mathias, 1993; Mathias et al., 1995; Mathias and Rodrigues, 1995). In this important work it was performed a complete kinetic study of lignin and vanillin oxidation by O_2, in alkaline medium, which included the effect of the most relevant operating conditions (namely temperature, total pressure, oxygen partial pressure, initial lignin concentration and initial sodium hydroxide concentration) and the proposal of the correspondent kinetic laws. It was reported that the optimum conditions for vanillin production from this route were: temperature of 130°C, oxygen partial pressure of 3 bar, total pressure of 9 bar, and lignin concentration of 60 g/l in an alkaline medium of 80 g/l of NaOH (Fargues et al., 1996a). The evolution of vanillin concentration with time showed a maximum at 35 minutes of reaction, corresponding to a yield of 10% over the initial lignin mass, and also that vanillin suffers oxidative degradation under these conditions.

Tarabanko et al. (1995a) presented a study about the influence of lignin origin and its conditions of production and pre-treatment on the yields of vanillin and syringaldehyde obtained by lignin oxidation. For this purpose, four different raw materials were oxidized with O_2 under alkaline conditions, and in the presence of $Cu(OH)_2$ catalyst (optimum concentration of 4 g/l): rotten pine wood, native pine wood, native asp wood and lignosulphonates from some Russian pulp mills. The results reflected the existence of a competition between condensation of lignin fragments and oxidation into aldehydes. Beyond the fact that hardwoods produced more syringaldehyde than vanillin, they also provided higher total yields of aldehydes than softwoods since syringil fragments have higher stability to condensation when compared to guaiacyl fragments. When lignins undergo pre-treatment stages they are also subject to condensation processes, decreasing their capability of producing vanillin, as it is supported by the experimental results obtained on the vanillin yield: 23% for native lignin; 20% for fermentative lignin; and 17% for lignosulphonates.

Related to the oxidation of native lignin sources, a flowsheet was developed for direct hardwood conversion into the fine chemicals vanillin, syringaldehyde and levulinic acid (Tarabanko et al., 2000). The first step of the process consists in catalytic oxidation of wood by oxygen, in alkaline medium, carried out at 150-200ºC and working pressures around 2-5 MPa. Cellulose is obtained along with an aqueous solution of vanillin, syringaldehyde and by-products of lignin and hemicellulose oxidation. The cellulose is treated with acid to give levulinic acid. The process is concluded with separation and purification steps, giving total yields of 1.5% of vanillin, 4% of syringaldehyde and 12% of levulinic acid, based on the initial wood weight.

An approach to a reaction mechanism that accounts the catalysts effects in the vanillin formation via lignin oxidation with O_2, in an alkaline medium, has been

proposed by Tarabanko et al. (1995b) and (1997). The catalysts of transition-metals (Cu, Co, Mn oxides) increase considerably the yields of this kind of oxidations. The influence of the $Cu(OH)_2$ concentration, *pH* and temperature in the vanillin production and O_2 consumption, referent to catalytic oxidation of commercial lignosulphonates, was experimentally studied for validation of the mechanism proposal. It was also concluded that the main role of the catalyst is to change the selectivity of fragmentation of a hydroperoxide intermediate rather than accelerate the oxidation.

More recently, Tarabanko and Petukhov (2003) proposed a new version of the mechanism of lignin oxidation based on different assumptions from the ones previously reported. In the present hypothesis it is attributed a key role to the γ-carbon atoms of the phenylpropanoid units, and in its final step occurs the formation of vanillin through a retro-aldol cleavage of substituted coniferyl aldehyde (Figure 2.15).

Besides considering the catalyst effect on the process, the mechanism on Figure 2.15 also supports the verified necessity for strongly alkaline medium and the formation of aceto derivatives as by-products, whose explanations were absent from earlier presented hypothesis. The proposed oxidation mechanism was validated by a number of experiments, which included the effect of *pH* on the vanillin yield and rate of oxygen absorption, and the oxidation of simple model compounds, like eugenol, for detection of postulated intermediates.

Villar et al. (1997) presented a work on Kraft lignin oxidation, in alkaline medium, using oxidants more selective than oxygen. A hardwood Kraft lignin was oxidized with nitrobenzene and copper oxide, to obtain phenolic compounds like syringaldehyde, vanillin, syringic acid and vanillic acid. The effects of temperature, reaction time and oxidants concentration on the yield of the phenolic compounds were studied. Some previously reported results for nitrobenzene and CuO oxidation of lignins

from different sources are also shown, revealing that the less transformations or chemical treatments a lignin suffers, the more useful it becomes for producing phenolic aldehydes.

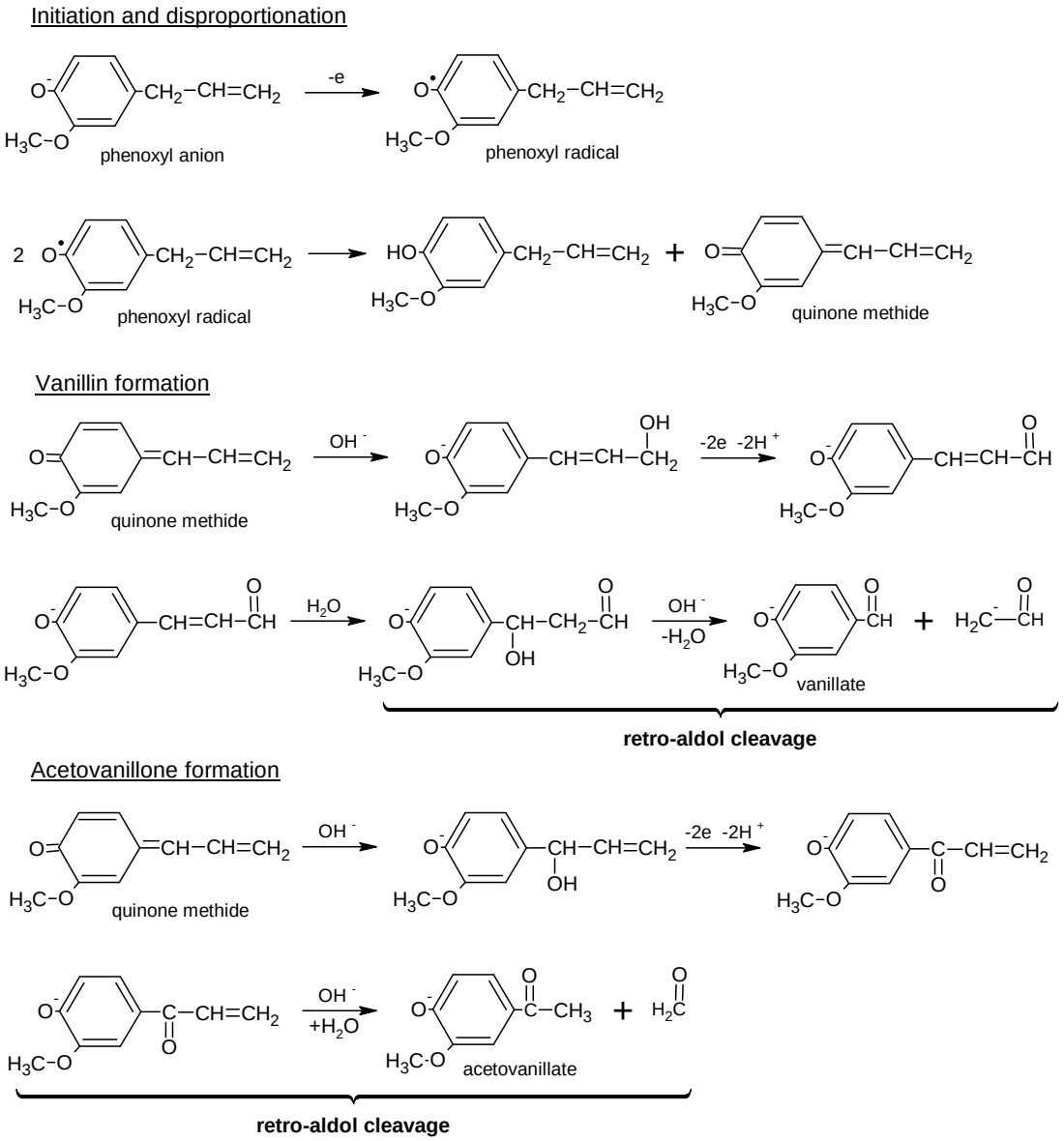

Figure 2.15. Approach for the reaction mechanism of oxidative cleavage of lignins into aromatic aldehydes (Tarabanko and Petukhov, 2003).

From this idea, also corroborated in Tarabanko et al. (1995a), the lignin used in the experimental work was precipitated from Kraft black liquor, not by the traditional acid treatment, but with the addition of a calcium salt dissolved in a water soluble

alcohol. This prevented some lignin condensation that occurs under acidic precipitation, which improved the phenolic aldehydes yields of subsequent lignin oxidation with nitrobenzene and CuO. The syringaldehyde presented individual yields approximately five times greater than the correspondent ones for vanillin. The maximum yields for the total phenolic aldehydes (syringaldehyde + vanillin) were 14% from nitrobenzene oxidation (40 min of reaction, 190ºC, 2 N of NaOH and 6 ml of nitrobenzene per gram of initial lignin) and 8% from CuO oxidation (70 min of reaction, 190ºC, 2 N of NaOH and 4 mol CuO per mol of initial lignin). Nitrobenzene seemed to be the most effective oxidation, however its reduction products are harmful, and CuO can be easily separated and regenerated, making this oxidant more attractive to commercial application.

A similar study was developed for oxygen as oxidant in the presence of a catalyst (Villar et al., 2001). The catalysts tested were Cu and Co salts, and two commercial platinum-alumina. The copper salts produced better results, however they were similar to the aldehyde yields obtained in the absence of a catalyst. Moreover, cobalt and platinum-alumina catalysts showed a negative effect on lignin conversion, suggesting that they catalyzed undesirable reactions with production of non-phenolic derivatives. Opposing to the study using nitrobenzene and CuO as oxidants (Villar et al., 1997), in this work the calcium precipitated Kraft lignins showed no appreciable improvement on the final aldehyde yield when comparing to acid precipitated lignins. Under optimum conditions, the O_2 oxidation of Kraft lignin produced only 4% of phenolic aldehydes, a low amount that can be partially explained by lignin transformation into the correspondent low molecular weight acids.

Also in the field of catalytic investigation, Bjørsvik and Minisci (1999) tested several systems for oxidation of lignosulphonates to vanillin, and applied multivariate mathematical and statistical modelling to optimize the yield of this process. Before the

addition of catalyst to start-up the oxidation step, the experiments contained a preheating step at high temperature (160-200ºC) to hydrolyze the lignosulphonates. The catalytic systems tested were persulphate, nitrobenzene and 1,3,5-trinitrobenzene combined with Cu salt, and O_2 with metal salts (Cu, Ce and Co). For the oxidation with oxygen, the efficiency of copper and cesium salts were approximately the same, however it was a little faster when using Cu. With the developed multivariate model it was performed the optimization of the reaction conditions for oxidation by O_2 with copper salt, achieving an increase of the vanillin yield from 4.1% (reference procedure) to 7.2%, corresponding to a 75% of relative improvement.

Sales et al. (2004) developed a work on catalytic wet-air oxidation of lignin obtained from sugar-cane bagasse by the Organosolv acid process, with the goal of producing vanillin, syringaldehyde and *p*-hydroxybenzaldehyde in continuous operation mode. The catalyst used was palladium (2.85%) supported on γ-alumina. The catalyst revealed very effective on increasing the rate of formation of desirable aldehyde compounds, 10 to 20 times higher compared to the correspondent non-catalytic reactions, and on decreasing the rate of formation of undesirable products, representing a significant improvement to the selectivity of the process. The maximum experimental yield on the aldehydes formation was 12% of the lignin feed concentration, obtained when operating the reactor with an air flow rate of 1000 l/h, a liquid flow rate of 5 l/h, 4 bar of pressure, a catalytic loading of 4% and a temperature of 393 K. The complete study about the referred kinetic model was later published by Sales et al. (2006).

The studies presented in last pages about alternative oxidants and catalysts for lignin oxidation have interesting results in the point of view of laboratory scale production. However in a perspective of industrial application they may not be advantageous when compared to simple oxidation with O_2 because of three factors:

catalysts or alternative oxidants are expensive; difficulties on separating these compounds from the product media; and some of these catalysts are very aggressive and the correspondent processes would be far for been considered "clean" or "green" processes such as the objective of the oxidation with O_2.

2.3.3.3 Biotechnological route

The high market prices and limited supply of natural vanillin, isolated from plants, along with a worldwide increasing concern for health and nutrition has encouraged the research for alternative means of natural flavour production. The label "natural" can be attributed when a product is derived from natural raw materials by biosynthesis, according to the European Union and United States food legislation. Following this trend, a large number of studies have been recently developed on the field of biotechnological processes for vanillin production.

Most of these biotechnological processes are based on the application of fungi, bacteria, plant cells (Rao and Ravishankar, 1999; Suresh et al., 2003) or genetically engineered microorganisms (Gasson et al., 1998; Plaggenborg et al., 2006; Yoon et al., 2005), to produce vanillin, an intermediate of the biodegradation of several substrates, such as ferulic acid (Gasson et al., 1998; Hua et al., 2007; Lesage-Meessen et al., 1996a; Muheim and Lerch, 1999; Oddou et al., 1999; Plaggenborg et al., 2006; Suresh et al., 2003; Yoon et al., 2005; Zheng et al., 2007), lignin (Mathias et al., 1995), vanillic acid (Lesage-Meessen et al., 1997; Stentelaire et al., 1998), glucose (Li and Frost, 1998), eugenol (Muheim and Lerch, 1999; Plaggenborg et al., 2006), isoeugenol (Rao and Ravishankar, 1999; Zhao et al., 2005; Zhao et al., 2006), vanillylamine (Van den Heuvel et al., 2001) and creosol (Van den Heuvel et al., 2001).

Several reviews have been published with the scope of biotechnological generation of natural flavour compounds with particular emphasis on vanillin (Krings and Berger, 1998; Priefert et al., 2001; Schrader et al., 2004; Walton et al., 2003; Rao and Ravishankar, 2000).

Rao and Ravishankar (2000) reviewed the production of natural vanillin from vanilla pods, the chemical synthesis of vanillin and gave a short overview about the biotechnological methods for vanillin production. Some illustrative examples of bioprocesses currently used or under investigation in industry for the synthesis of natural flavour compounds are compiled in Schrader et al. (2004). This publication also outlines the advances in genetic engineering related with biocatalytic production of natural flavours and its approaches to industrial application. Priefert et al. (2001) presented a detailed review on biotechnological routes of vanillin production, using different substrates and biosynthesis methods, and simultaneously gives a considerable background on patent literature about this subject. It is curious to notice that the first patent that claimed for a microbial process to produce vanillin was published on 1991 (Rabenhorst and Hopp, 1991).

Most bioprocesses are affected by the high toxicity of vanillin that inhibits the performance of the producing microorganisms, and the high chemical reactivity of vanillin, reflected by higher degradation rates than that of substrates. Therefore vanillin is rapidly bio-converted to products like vanillic acid or vanillyl alcohol. To avoid this transformation into undesirable products, some works have been carried out on the application of *in situ* product removal (ISPR) to biotechnological production of vanillin (Hua et al., 2007; Stentelaire et al., 1998; Zhao et al., 2006). These methods consists on the use of adsorbent resins to trap vanillin before its degradation, which by-passes the

formation of unwanted products, lowers the medium toxicity to the fungal metabolism and improves the vanillin recovery and concentration.

The routes involving plant cell cultures and genetically modified organisms are currently not feasible for commercial production, since until now they have not achieved acceptable yields (Krings and Berger, 1998; Schrader et al., 2004). The bioconversion of lignin by white-rot fungi yields several products, including vanillin, however in all the correspondent studies vanillin has been detected in very small quantities (Mathias et al., 1995; Priefert et al., 2001).

The most intensively studied biotransformation to produce vanillin is based on ferulic acid as substrate, since it is considered the only commercial biocatalytic route for this purpose (Schrader et al., 2004). Ferulic acid (Figure 2.16) is an abundant phenolic compound in nature, commonly occurring in plant cell walls, grasses and agricultural residues such as cereal and rice bran and sugar beet pulp. It can be released in its free form combining physical and enzymatic treatments, which provides a sufficient natural source of this compound. A remaining drawback to the use of ferulic acid is that this natural substance is a little expensive, and has not yet been developed an industrial scale process for its isolation from plant material (Priefert et al., 2001).

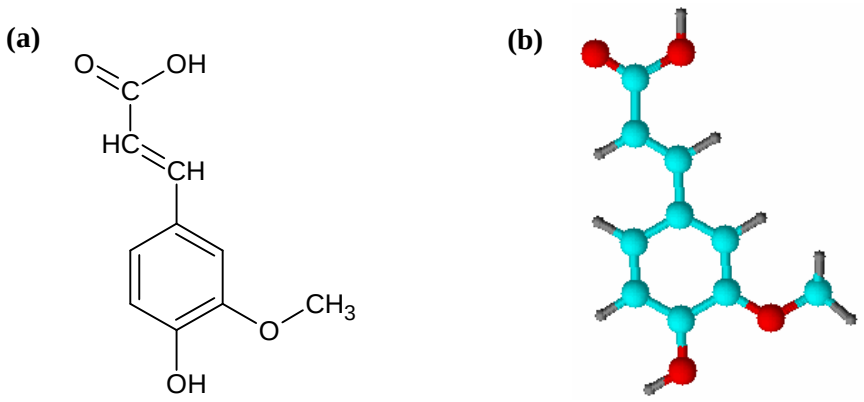

Figure 2.16. Chemical structure (a) and geometry (b) of the ferulic acid molecule.

Eugenol and isoeugenol, derived from essential oils, are more resourceful and more economical precursors for vanillin production. However, until now, the research made about microbial and enzymatic bioconversion of these two natural compounds conducted to rather low vanillin yields, resulting from their toxicity to microorganisms that inhibit cellular growth and metabolism (Zhao et al., 2006).

Muheim and Lerch (1999) compared ferulic acid and eugenol as precursors for microbial production of vanillin. Ferulic acid proved to be a better precursor, since with eugenol the feeding concentrations could not be increased above 1 g/l. Then two different microbes, *Pseudomonas putida* and *Streptomyces setonii*, were studied for their ability in the production of vanillin from ferulic acid. Despite vanillin high reactivity, *Streptomyces setonii* showed not only a high tolerance to the presence of this aldehyde, but also a metabolic bottleneck in the step of oxidation of vanillin to vanillic acid, which promoted the accumulation of vanillin as the main product. When appropriate culture medium was fed with 6 g/l of ferulic acid, and then added more 6 g/l when the first one was consumed, it was obtained a maximum concentration of vanillin of 6.41 g/l, representing a molar yield of 68%.

Lesage-Meessen et al. (1996a) presented a work about the formation of vanillin from ferulic acid in a two-step bioconversion process, where it was applied two strains of filamentous fungi with complementary capabilities. First, ferulic acid was transformed into vanillic acid by *Aspergillus niger*, and then *Pycnoporus cinnabarinus* was used to reduce vanillic acid to vanillin. To improve the yields on the desired products for each step, it was practiced sequential addition of the correspondent precursors. The first step achieved very high yields of ferulic acid consumption (98%) and vanillic acid formation (88%). In opposition, the major product obtained in the last step was methoxyhydroquinone, resulting from the oxidative decarboxylation of vanillic

acid, instead of the desired formation of vanillin that only accounted for 22% of molar yield. This work was also patented by Lesage-Messen et al. (1996b).

A new study was reported on the improvement of the yields of the biological reduction of vanillin acid to vanillin, by diminishing the formation of methoxyhydroquinone (Lesage-Meessen et al., 1997). Again, it was used for this purpose a strain of *Pycnoporus cinnabarinus*, but the carbon source added to the culture medium was changed to cellobiose. With this carbon source, the molar yield of vanillin reached 51.7%, which is more than two-times higher in comparison to the results presented by Lesage-Meessen et al. (1996). Cellobiose appeared to be a carbon source easy to metabolize, and to inhibit the decarboxylation pathway of vanillic acid.

The ability of the combination of the fungal strains *Aspergillus niger* and *Pycnoporus cinnabarinus* to convert ferulic acid to vanillin, in a two-step process, was once again explored and published by Zheng et al. (2007). The substrate, ferulic acid, was prepared from waste residue of rice bran oil. The process was scaled-up to a fermenter of 25 litters and reached a vanillin yield of 2.8 g/l, when 5 g/l of glucose (carbon source) and 25 g of HZ802 resin were added to the bioconversion medium of the second step. The purpose of this resin was to adsorb the vanillin avoiding its toxic effects and the extension of the vanillic acid reduction pathway to the formation of the unwanted vanillyl alcohol.

Van den Heuvel et al. (2001) investigated the synthesis of vanillin using the enzyme flavoprotein vanillyl alcohol oxidase (VAO) with two alternative natural raw materials: creosol, the major product in creosote obtained from heating wood and coal tar; and vanillylamine that can be easily obtained from an enzymatic hydrolysis of the capsaicin, present in nature as the pungent principle of hot red pepper. Similarly to the enzymatic degradation of vannilylamine in mediums with alkaline *pH* (between 9 and

10.5), the VAO conversion of creosol into vanillin reaches yields near 100%, for a *pH* around 7.5. From these two enzymatic routes, the process from capsaicin seemed to be the most effective from the biotechnological and economical point of view.

In order to achieve high levels of vanillin productivity from ferulic acid, Hua et al. (2007) used a batch bioprocess with *Streptomyces* sp. Strain V-1, and studied the possibility of application of an adsorbent resin to remove this flavour compound, during its formation, from the reaction medium. Starting with a ferulic acid concentration of 10 g/l, when the substrate concentration was below 2 g/l (around 12 hours of reaction) it was added 8% of resin DM11, from Shandong Lukang Pharmaceutical Group (Shandong, China) along with a supplement of ferulic acid with 5 g/l. The supplements of substrate were carried out continually every time the ferulic acid was below 2 g/l, and until its total concentration added reached 45 g/l. It was reached a value of 19.2 g/l for total vanillin (aqueous solution + adsorbed in resin) within 55 hours of reaction. This result is very important, since it overcomes the crystallization concentration of vanillin and therefore can create a great impact in the downstream process of purification.

2.3.4 Patents review

Since 1874, a large number of patents related to vanillin production have been developed, presenting inventions in several different fields. Chemical oxidation of the lignin in wood pulping waste liquors was one the most explored of those areas, specially before 1940's, with studies about operating conditions, apparatus to be used and effective oxidizing agents for the achievement of higher vanillin yields. The vanillin purification and extraction from the reaction liquors was also a subject of great concern, where several technologies were developed, based on chemical engineering separation methods like organic solvent extraction, distillation, acidification/precipitation,

bisulphitation, crystallization, supercritical extraction, adsorption and ion exchange. More recently, the focus of the patents have been changed to the biotechnological production of vanillin, in a pursuit for alternative processes to the common *Vanilla planifolia* plant, with higher yields and cheapest "natural" labelled product. Some selected patents are briefly described in Table 2.4.

Table 2.4. Review of patents.

U.S. Patent 2,057,117
Sandborn et al., 1936
Marathon Paper Mills Company
The process starts with the lignin material being subjected to cooking under suitable pressure, in the presence of water and caustic alkali. The cooked medium is discharged to a hot solution of alkali-metal bisulphite salt, with the *pH* maintained below 7 through the addition of SO_2. Some organic material, mainly consisting in degraded lignin, is precipitated and removed, and a solution containing vanillin and other similar compounds in the bisulphite form is also obtained. This solution is treated with an acid to decompose the bisulphite salts present, liberating SO_2 for reuse in the process, and the resultant solution is extracted with benzene to yield an organic phase with vanillin and other benzene soluble organic matter. This organic solution can be further treated with NaOH solutions, in scrubbing units, to recover benzene and to separate vanillin and the other phenolic products into commercial forms. A flow sheet for this entire process of making vanillin is also provided.
U.S. Patent 2,062,205
Boedecker and Volk, 1936
This patent includes a method for preparing vanillin based on the condensation of guaiacol with glyoxylic acid, in alkaline solution, followed by an oxidative decarboxylation with the help of a mild oxidizing agent such as cupric oxide, lead oxide or manganese dioxide.
U.S. Patent 2,187,366
Schulz, 1940
Schimmel & Co. A. G.
In this method the lignin containing substances, such as sulphite waste liquor, are digested in alkaline aqueous medium, at elevated temperatures, and in the presence of an aromatic nitro compound. This compound acts as an oxidizing agent and preferably could be used nitrobenzene. When nitrobenzene is applied the cooking temperature should be in the range of 175ºC to 225ºC. It states that vanillin is formed with a yield averaging from 8 to 10%, based on the weight of the sulphite liquor solids. Vanillin can be recovered from the products by known methods like solvent extraction and crystallization.

Continuation of Table 2.4. Review of patents.

U.S. Patent 3,197,359
Logan, 1965
The Ontario Paper Company Limited
The invention relates to the application of a weakly cationic ion exchange resin, in a plant producing vanillin integrated into a sulphite pulp mill. This resin should be used in a three-step or two-step process, depending if the pulping operations are based on either calcium or sodium, respectively. First, the vanillin reactor effluent goes through the resin, exchanging sodium ions in the aqueous solution with the hydrogen ions of the resin, leaving it in the Na^+ form. Then, if the pulping is calcium based, the resin in the Na^+ form exchanges this sodium ions with the calcium ions present in the waste sulphite pulping liquor. Finally, the resin in the Ca^{2+} form is treated with sulphurous acid to return to its original H^+ state, and produce an effluent of calcium bisulphite. If the pulping is sodium based, the resin in the Na^+ form is treated directly with sulphurous acid to regenerate the resin and obtain sodium bisulphite.
U.S. Patent 3,686,322
Diddams and Renaud, 1972
Sterling Drug, Inc.
Crude vanillin in aqueous mixture with structurally similar compounds is purified by partial extraction with hot hydrocarbon solvent, cooling to crystallize vanillin and repeating this procedure to extract successive portions of vanillin more than 85% pure. The impurities present in the initial mixture are normally referred as 5-formylvanillin, *p*-hydroxybenzaldehyde and acetovanillone. The partial extractions should be carried out at temperatures above 30ºC, and the hydrocarbon solvent is preferably a petroleum cut boiling between 125ºC and 200ºC.
U.S. Patent 4,021,493
Major and Nicolle, 1977
Canadian International Paper Company
Vanillin is isolated from alkaline aqueous solutions, containing chemically similar phenolic impurities, through the application of a process called “extractive bisulphitation”. This process consists on the treatment of the referred alkaline solutions with SO_2 or an acidic salt of sulphurous acid to form water-soluble bisulphite complexes with the aldehydic compounds like vanillin, in the presence of a water immiscible alcohol such as n-butanol. The simultaneous application of an organic solvent represents a new feature that allows the extraction of tars and precipitates of some non-reacting impurities formed as a result of the adjustment of the operation *pH* to the range of 3 to 4.5. The bisulphite complexes in the aqueous solution are decomposed back to its original components by acidification, preferably done with sulphuric acid, promoting the liberation and recirculation of SO_2. Then, the vanillin may be concentrated by solvent extractions, distillations or multi-step crystallizations. It is also provided a flow sheet of the complete process and an illustration of the typical apparatus to be applied.
U.S. Patent 4,277,626
Forss et al., 1981
This patent consists in a method of separation of sodium vanillate from lignin and alkali, present in alkaline solutions, by the adsorption on a cationic ion-exchange resin in its sodium form. When these solutions are fed to a column filled with resin, the lignin material, sodium hydroxide and sodium carbonate leave it before, and the sodium vanillate adsorbed into the surface of the resin can be later eluted with either water or dilute alkali salt solution. This invention is characterised by the ion-exchange resin being in the same form all through the process, which allows the elimination of the regeneration step. The resins can be either of the strong sulphonic acid type or the weak carbonic acid type, preferably a Dowex-50W, X-8.

Continuation of Table 2.4. Review of patents.

U.S. Patent 4,652,684 Derouane and Powell, 1987 Mobil Oil Corporation A spent lignin fermented liquor containing vanillin passes through a fixed bed, filled with a large pore zeolite, to adsorb the desired vanillin. The zeolite should have a high silica/alumina ratio, between 10 and 35, and pores wide enough to admit large semi-polar molecules like vanillin, with a size bigger than 0.7 nm. Preferably, these selective adsorbents can be chosen between Zeolite ZSM-20, Zeolite Beta and dealuminated Zeolite Y. The regeneration of the bed and recovery of the adsorbed vanillin should be performed by feeding a suitable solvent to the bed, normally ethanol, at a temperature between 20ºC and 80ºC.
U.S. Patent 4,847,422 Klemola and Tuovinen, 1989 Yhtyneet Paperihtehtaat Oy This patent introduces the technology of supercritical extraction into a vanillin production process, stating that may replace extraction with an organic solvent and re-extraction to aqueous solution. After the air oxidation of wood pulping waste liquor, under basic conditions, the resulting solution is treated a supercritical carbon dioxide flow at a pressure from 75 to 400 bars and a temperature from 30ºC to 100ºC, extracting vanillin and other chemically related substances. The vanillin dissolved in the CO_2 is separated by passing the gas flow into a receiver with appropriate pressure and temperature conditions. It is also attached the drawings of proposed apparatus.
U.S. Patent 4,898,990 Coenen and Konrad, 1990 Fried. Krupp GmbH The supercritical extraction is combined with bisulphitation treatment to remove vanillin from oxidized sulphite pulping waste liquors. These solutions are treated with supercritical CO_2 at a temperature of 0 to 100ºC and a pressure ranging 30 to 400 bars. The gas flow passes through an aqueous bisulphite solution that dissolves vanillin and liberates the CO_2 for reuse. Subsequently, the aqueous solution containing vanillin-bisulphite adducts is acidified with sulphuric acid to a *pH* value of 2 to 4, and heated to a temperature of 50 to 90ºC. After the breakage of the adducts by acidification, the aqueous solution is cooled off and the vanillin crystallizes well and with an appreciable purity.
U.S. Patent 5,017,388 Rabenhorst and Hopp, 1991 Haarmann & Reimer GmbH This is the first patented process of microbial production of natural vanillin. The precursors are eugenol and/or isoeugenol oxidized by microorganisms from the genera Serratia, Klebsiella or Enterobacter. The microorganisms are cultivated in a proper culture medium, with a substrate concentration regulated between 5 to 50 g/l, a temperature in the range of 25 to 35ºC and a *pH* of 3.5 to 7.5. In order to protect the microorganisms from the toxic effect of eugenol or isoeugenol, it could also be added to the medium some active charcoal or adsorbent resin.

Continuation of Table 2.4. Review of patents.

European Patent WO96/08576
Lesage-Meessen et al., 1996
Institut National de la Recherche Agronomique – I.N.R.A.
A method is claimed for the production of vanillin by bioconversion from ferulic acid, with a culture medium containing phospholipids and at least one kind of microorganism selected from the classes Ascomycetes, Basidiomycetes or Actinomycetes. This medium should also comprise cellobiose as a carbon source and a non-ionic hydrophobic resin to trap the formed vanillin, preventing its further reduction to vanillyl alcohol. It is also claimed that the bioconversion of ferulic acid to vanillic acid, as well as vanillic acid to vanillin, can be performed separately and in consecutive steps, with microorganisms from the classes referred earlier and in appropriate culture medium conditions.
U.S. Patent 5,510,006
Jones et al., 1996
International Flavors & Fragrances Inc.
Vanillin is separated from a second organic chemical with an approximate boiling point, such as *p*-hydroxybenzaldehyde, by azeotropic distillation with the help of an effective azeotropic distillation agent like dibenzyl ether. In a distillation apparatus, the overhead product consists on a single phase mixture of vanillin and dibenzyl ether. This mixture is cooled to promote the precipitation of vanillin crystals that are subsequently removed.
European Patent 0 885 968
Muheim et al., 1998
Givaudan-Rore International S.A.
The inventors claim for a process where a bacterium of the order Actinomycetales, preferably *Streptomyces setonii*, is applied in the production of vanillin from bioconversion of ferulic acid. For the culture medium, glucose is used as the carbon source, and then the ferulic acid is added in the range of about 5-40 g/l. The bioreactor should operate at temperatures between 30 ad 45ºC and a *pH* of 7 to 9. The product recovery consists in the removal of the biomass, followed by a two-step extraction with an organic solvent, preferably methyl-tert-butylether. The first extraction step is carried out at a *pH* of 10 to 11, in the aqueous phase, to extract by-products such as guaiacol. Then, the remaining aqueous solution is acidified to a neutral pH, and the vanillin is selectively extracted from it with the organic solvent. Purification of vanillin can be achieved by recrystallization methods.
U.S. Patent 7,226,783
Havkin-Frenkel and Podstolski, 2007
David Michael & Co., Inc.
The patent is related to novel compositions and methods to improve vanillin production in *Vanilla planifolia* plants. These novel methods comprises the addition to tissue cultures of an elicitor compound selected from the group of malic acid, 3,4-dihydroxybenzaldehyde and glycosylated lysozyme, and subjecting the cultures to heat or mechanical shear stresses. This invention also comprises genetic engineering the *Vanilla planifolia* to overproduce one or more enzymes associated with the vanillin biosynthesis in this plant.

2.4 Continuous oxidation reactor

The main purpose of this thesis is to study the lignin oxidation to obtain high-added value compounds (vanillin). This oxidation reaction must be carried out in gas-liquid environment. As the reaction kinetics of lignin and also vanillin oxidation were already studied (Fargues et al., 1996a; Mathias, 1993), the step to be performed in this thesis is the production of vanillin in a pilot scale production unit. For this purpose, a new reactor unit is required. The design of the reactor was performed based on some considerations based on available literature and will be explained in this section.

Nowadays, in industrial practice the continuous production processes are generally more attractive than batch processing, since they are easier to control and to attain constant product characteristics and also their overall investments and operating costs are usually less (Kirk-Othmer Encyclopedia, 2005; Rase, 1977). Also, as the volumes to be treated in a pulp industry may be relatively high, the choice, either of a batch or a semi-batch unit will be *a priori*, less interesting from an industrial point of view. Based on these principles, it was decided that the reactor to be developed should operate in continuous mode.

2.4.1 Column and tank reactors

The continuous operation units used to promote gas-liquid reactions may be divided into two main types: tower or column reactors and tank reactors. Simple diagrams exemplifying these reactors are presented in Figure 2.17. The tank reactors essentially comprise a pressure vessel, a sparger to feed the gas to the system and a shaft with one or more impellers that mechanically agitates the medium bringing the two phases into more intimate contact.

Tower or column reactors do not apply mechanical agitation, so the interface contacting (gas-liquid) occurs only under the influence of gravity and fluids natural dynamics. They consist on tubular vessels, with a height-to-diameter ratio considerably greater than one and distributor systems for gas and liquid that feed the two phases separately or together, in co-current or counter-current flow configuration.

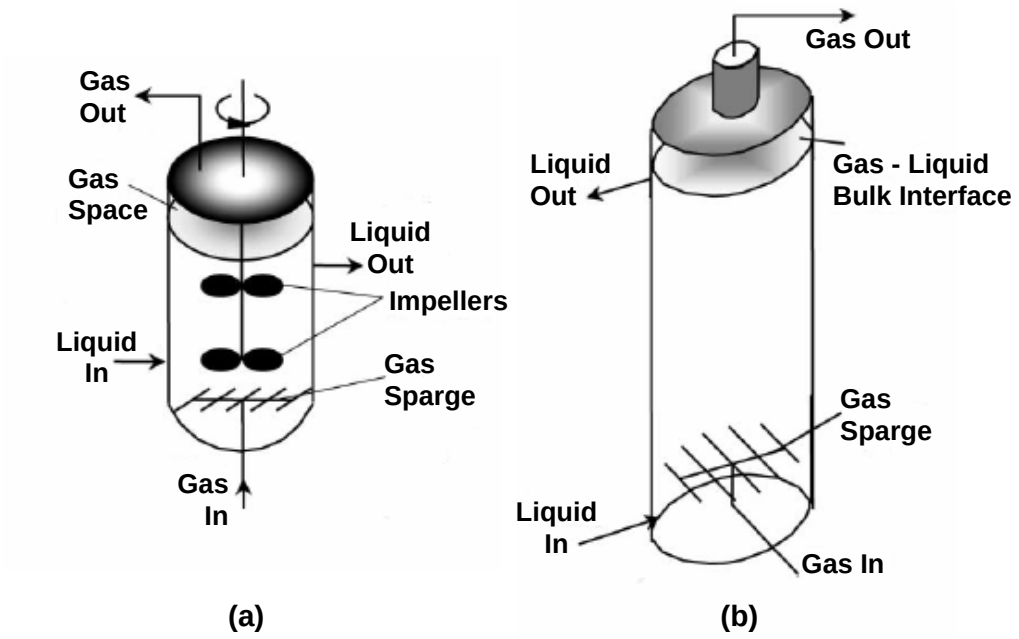

Figure 2.17. Schematic diagram representation of: (a) Stirred tank reactor with gas sparging and dual impeller, and (b) column reactor with the gas and liquid flowing upward and co-currently (Stitt, 2002).

The mechanical agitation in stirred tanks ensures (or at least promotes) that the conditions of the reaction medium are uniform within the vessel. This particular feature is also responsible for high heat transfer rates, which is quite important when dealing with highly endothermic or exothermic reactions. However, as a result of these mixing characteristics of the stirred tank reactors, the residence time of the molecules present a very wide distribution. In fact, a molecule of reactant can leave in the instant it enters the tank or it can stay for an extended period. Similarly, a molecule of product can leave immediately after it is formed or it can have a long residence time. This is inappropriate for systems where the desired product is an intermediate of the reactional sequence

operating in series, presenting a maximum yield at a particular time of reaction and then decreasing for longer times.

Because the composition of mixtures leaving a stirred tank are those within the reactor, the reaction driving forces are low (usually reactant concentrations), and therefore, except for zero or negative order reactions, the stirred tank is the reactor configuration that requires highest volume for a given conversion. Tank reactors are also suitable to work with high liquid holdups or long liquid phase residence time, which can be required for some slow gas-liquid reactions.

A negative aspect of using mechanical agitation is the problems of design and maintenance that are encountered on sealing the shaft of the mixer, especially when dealing with high pressure systems and large industrial scale reactors.

In contrast, the column reactors do not use mechanical agitation, which eliminates the problems related to the shaft sealing and makes them more appropriate to operate with high pressures. These reaction units are simple to build and it may not be a tedious work to add further capacity (revamp) whenever it is needed.

Column reactors are characterized by narrower liquid phase residence time distributions when compared to tank reactors, which makes them more appropriate for obtaining maximum yields of intermediate products in complex reaction schemes.

In order to attain the referred advantages of column reactors, one should be prepared to deal with some negative factors, such as lower heat transfer rates than tank reactors due to the absence of mechanical agitation Also, high pressure drops may be expected in some configurations, especially when using long reactors.

The main incomes and outcomes of using tank or column reactors are summarized in Table 2.5.

In this work, we are interested in vanillin, which is an intermediate product from lignin oxidation: presents a maximum yield during the course of the reaction and then gets degraded. For this reason and also taking into account the aspects related to simplicity of construction and maintenance, the pilot unit will be a column reactor. The next step was to choose a type of column reactor that minimizes the outcomes presented on Table 2.5.

Table 2.5. Advantages and disadvantages of working with tank and column reactors.

	Advantages	**Disadvantages**
Tank reactors	- Capacity to work with high liquid holdups (useful for slow reactions); - High heat transfer rates	- Wide residence time distribution; - Difficult to seal the shaft of the mechanical agitator (particularly for high pressure systems); - Low reaction driving forces (usually reactant concentrations)
Column reactors	- Simple construction and possible to add capacity; - Negligible sealing problems (proper for high pressure systems) and less maintenance; - Narrower residence time distribution than tank reactors (useful when the desired product is an intermediate of a reaction scheme)	- Large pressure drops (at least for some configurations); - Lower heat transfer rates than the ones in tank reactors

2.4.2 Selection of the type of column reactor

Column reactors are characterized for the need of additional devices to enhance contact between gas and liquid phases. Normally this work is performed by the use of internals (rings, plates, honeycombs, etc.) or either liquid or/and gas distributors. The large number of internals and fluid distributors available for the columns, together with the possible combinations of feed flow modes (co-current or counter-current and upward or downward), leads to a multiplicity of column reactor configurations

characterized by completely different gas/liquid volume ratios. The major examples of these configurations for gas-liquid reactions are illustrated schematically in Figure 2.18.

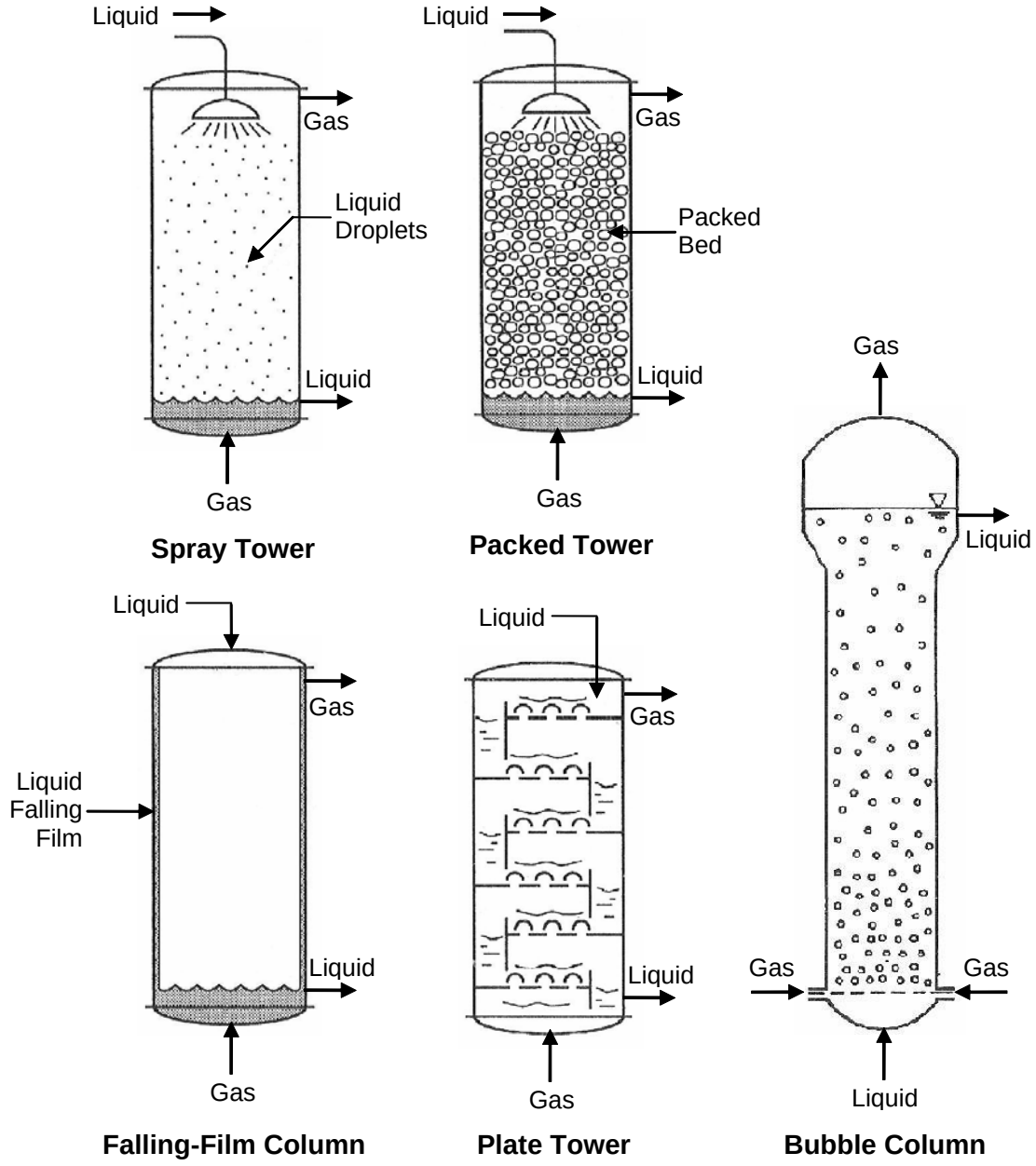

Figure 2.18. Types of column reactor for gas liquid reactions (based on Missen, Mims and Saville (1977); Levenspiel (1999) and Schlüter et al. (1992)).

In a spray tower, the liquid is showered from the top of the column, in the form of droplets, contacting with a gas stream that normally flows in counter-current direction. The gas-liquid interface is large, but the residence time of both phases is relatively small. Another configuration of a tower with no internals is the falling-film

column, where the liquid phase is introduced at the top and falls down the wall as a film counter-currently to the gas phase that flows continuously upward. In this case the interfacial area is very small and the overall mass transfer is consequently low, what explains the fact that this type of contactor is normally used for experimental studies of mass transfer characteristics.

A packed tower is filled with solid shapes made of metal, plastic or ceramic materials to improve the gas-liquid contact. Both phases are normally fed continuously and counter-currently, allowing the gas to rise through the voids of the packing and with the liquid flowing down as a film over the particles surface. In most cases, the packing contains or consists of catalysts particles, like the commonly used trickle-bed reactor.

The plate tower consists in a column with an interior containing sieve plates or bubble caps, placed along its height with fixed distance intervals. The two phases flow counter-currently and in each plate it is assumed that the gas is dispersed in a continuous liquid phase. The gas-liquid interfacial area is relatively large and the mass transfer is very efficient. This kind of configuration is mainly used in extraction rather than reactive processes, where their most common applications are as distillation or gas absorption columns.

Bubble columns are units where a gas is dispersed into a continuous liquid phase, which is the opposite of what happens in spray towers. In its conventional form the bubble column reactor is basically a cylindrical vessel with a gas distributor at the bottom that vary in design. The top of the bubble column is normally widened to facilitate the separation of the gas from the liquid phase.

The gas enters the vessel in the form of bubbles through the distributor and moves upward, while the liquid may be supplied in co-current, counter-current, or even in batch form, resulting in a semi-batch reactor. In contrast to simple mass transfer

operations where is advantageous to work in counter-current (like in plate towers) when reaction occurs the consequent concentration drop is usually sufficient to promote the necessary material exchange, and so counter-current flow offers no significant income for bubble column reactors.

The length-to-diameter ratio of the bubble column, normally called aspect ratio, can vary in a wide range while the most common values are between 3 and 6 but often can reach 10 (Deckwer, 1992). Bubble column reactors are characterized by high gas-liquid interfacial areas, and are desirable for slow reactions or when the rate-limiting step is in the liquid phase (Kirk-Othmer Encyclopedia, 2005).

Since the gas flows upward through a slower moving liquid, the bubbles entrain some liquid with it and the combination rises preferentially through the centre of the column. Then, the liquid proceeds downwards again near the wall transporting some smaller bubbles with it. This characteristic flow pattern of conventional bubble columns forms a kind of circulation that induces some back-mixing in the liquid phase (Deckwer, 1992).

In conclusion, the tower reactor configuration chosen to apply in the work of this thesis was the bubble column reactor. The main aspects of this reactor that contributed for the decision were:

- Higher liquid/gas volume ratio than the falling-flow column, the spray tower and the packed tower configuration presented above. Bubble columns normally operate at liquid volumetric fractions between 60 and 98%, in contrast to the spray towers with 2-20%, and counter-current packed towers with 2-25% (Perry, Green and Maloney, 1997). This is decisive when using gases with low solubility in the liquid, like the case of O_2 in aqueous solutions.

- Simple internal structure, little maintenance, low operating costs and higher compactness than the other configurations.
- Ease to vary the liquid residence time, especially when it is desired to have a relatively high mean residence time for the liquid phase.
- The back-mixing phenomenon enhances the heat transfer rates that are commonly low in tower reactors, which is very important when dealing with exothermic reactions, which is the case of the lignin oxidation.

The bubble column is not a perfect reactor configuration and also has some negative aspects that need to be accounted for and, if possible, minimized. One of them is related to the back-mixing phenomenon that is not proper to achieve high conversion levels, unless the volume reactor is increased accordingly. Other disadvantage is the short gas residence time that results only from the bubble rise velocity. Together with these two aspects, it is also important to know that despite the simple arrangement of the bubble column reactor it provides an environment for extremely complex hydrodynamic interactions, which makes the prediction of the correspondent parameters a very difficult task, at least with a good degree of certainty (Deckwer, 1992).

2.4.3 Bubble column reactors

In chemical industry, bubble columns are widely used as multiphase reactors in several applications. They are used in processes such as oxidation, chlorination, hydrogenation, and polymerization and also increasingly applied in biotechnological processes such as fermentation and biological waste water treatment (Deckwer, 1992; Kantarci et al., 2005). Some very well known applications are the Fischer-Tropsch process that consists in the indirect coal liquefaction, the Wacker-Hoechst process for

production of acetaldehyde by partial oxidation of ethylene, and wet oxidation of heavily polluted liquid effluent (Deckwer, 1992; Kantarci et al., 2005).

The fluid dynamics and performance of bubble column reactors are dependent on the employed flow regime. The classification of the flow regimes is made according to the superficial gas velocity, which is one of the most important parameters on this kind of equipment.

The homogeneous flow regime, also known as bubbly flow regime, occurs when gas velocities are low and is characterized by bubbles with a sharp size distribution that rises through the column at relatively uniform velocities. Bubble coalescence and break-up is almost absent, thus the bubble size mainly depends on the system properties and the gas distributor design.

If the gas velocity is increased, the bubbles start to aggregate forming larger bubbles that rise more rapidly than the smaller ones. This type of flow occurs in the heterogeneous regime, also called churn turbulent. Since the mass transfer is less efficient when operating with non uniform bubble size distribution, the levels of reactant conversion are usually higher in the homogeneous regime (Deckwer, 1992). The superficial gas velocity at which the homogeneous regime is converted into heterogeneous regime has not a fixed value and is a function of the coalescent properties of the system and the kind of gas distribution. However, for a medium with a viscosity level similar to water the reference value is 5 cm/s (Deckwer, 1992).

When using high gas flow rates in small diameter laboratory columns sometimes is observed a particular phenomenon: the larger bubbles of the heterogeneous regime are stabilized by the column walls forming slugs that move upward in piston-like manner. This regime is named slug flow and was reported to happen in column diameter up to 15 cm (Kantarci et al., 2005).

In Figure 2.19 is presented an illustration of the discussed flow regimes where main differences between them can be observed.

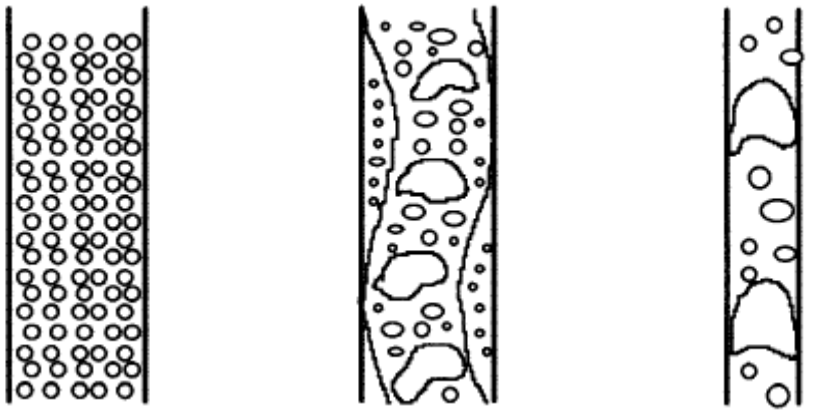

Figure 2.19. Flow regimes in bubble column reactors (Kantarci et al., 2005).

Due to the importance of their industrial application areas, the bubble column reactors have been the subject of an extensive research effort in the last two decades. In fact, a tremendous number of research studies have been developed about several topics, such as mass and heat transfer measurements, effect of column internals and operating conditions, bubble characteristics, flow regimes, and computational fluid dynamic modelling (Kantarci et al., 2005). Some of these studies will be focused on the appropriate chapter of this thesis related to the modelling and simulation of the experimental continuous reactor used for the lignin oxidation (Chapter 5).

2.4.4 Modified bubble column reactors

Finally, to obtain the complete configuration of the continuous reactor to be build within this work, it remains to decide whether a simple bubble column should be used, or if some modification should be applied to the conventional structure.

In order to respond to specific process engineering issues, there are several number of bubble columns types in use, all of them adapted to the correspondent

practical needs and differing in fluid dynamics and internal installations. Some of the most frequent types of modified bubble column are depicted in Figure 2.20.

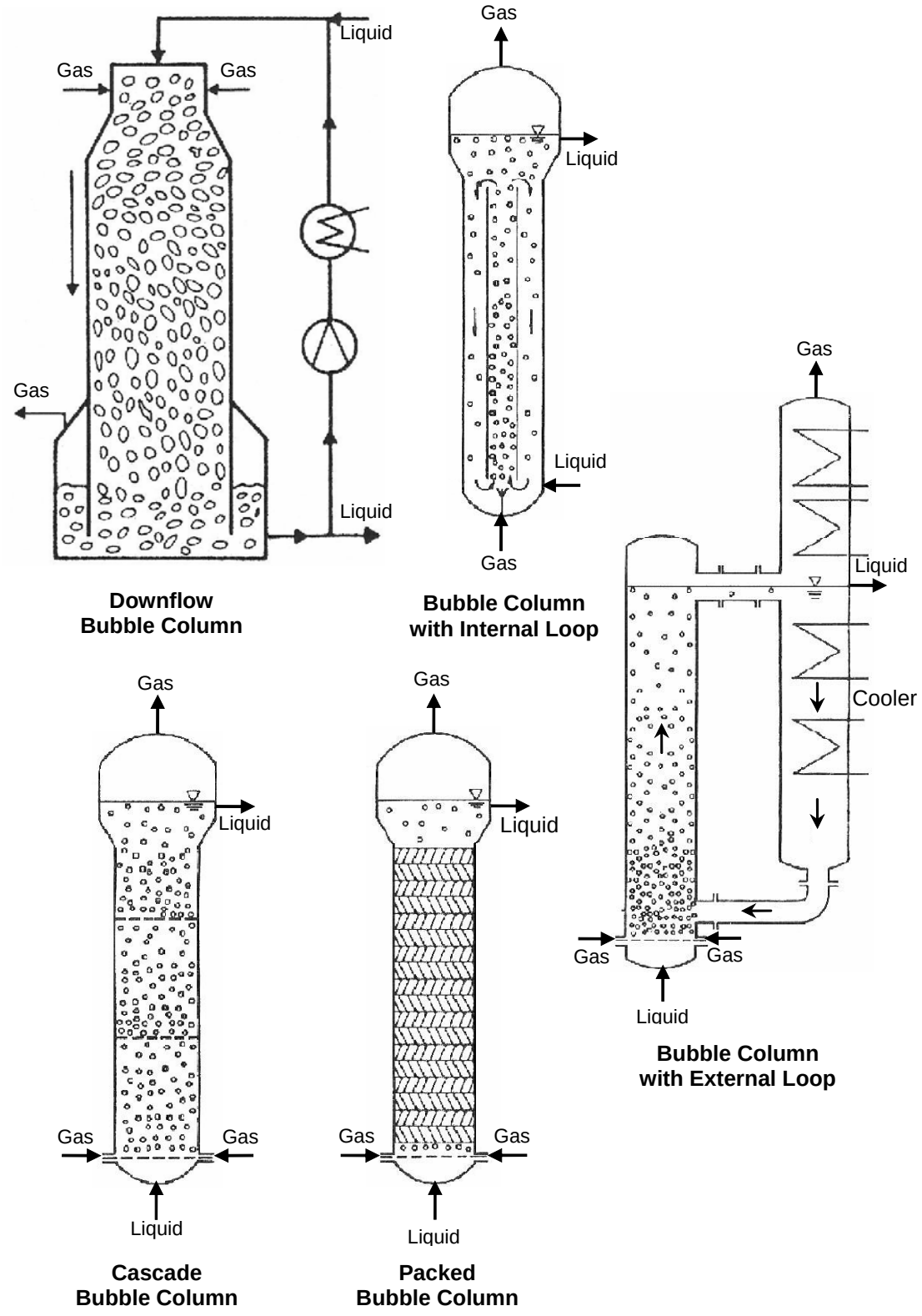

Figure 2.20. Schematic representation of modified bubble columns (based on Deckwer (1992) and Schlüter et al. (1992)).

The downflow bubble column reactor is a pleasant solution that allows working with higher gas residence times than those in the simple configuration. The gas is injected in the top of the column and moves downward forced by the circulating liquid. This liquid phase must move downward with a velocity of at least 21 cm/s in order to avoid bubble rise and coalescence that can build up an undesirable bulk of gas at the column head (Deckwer, 1992). The liquid stream is also fed at the top and is usually a makeup of fresh supply with recycled liquid product from the bottom of the column.

Some types of bubble column incorporate directional fluid circulation by means of inserted loops. These loops reactors can have either internal or external liquid removal lines, as it can be seen in Figure 2.20 and are based in the drag effect of the liquid over the entrained bubbles, together with density gradient between the dispersed gas and the liquid phases. Loop reactors can process large amounts of gas and are characterized by almost absence of concentration gradients resulting from the high rates of circulation. This feature makes them very attractive to biotechnological processes where is decisive to have the biomass in a medium of constant composition.

The conventional bubble column model is converted into a multistage cascade version with the incorporation of internal perforated plates. This modification intends to decrease the fraction of larger bubbles, intensify mass transfer and avoid back-mixing in both phases. Similar effects can also be achieved in packed bubble columns in which their main bodies are filled with random or structured packing usually made in metal, plastic or ceramic materials. Examples of these packings are shown in Figure 2.21.

Structured packings are generally manufactured as cylindrical elements consisting of metal or plastic corrugated sheets arranged in parallel, where successive layers have opposing angles of corrugation. The regular flow channels that result from these arrangements are inclined at an angle to the horizontal that is normally of 45 or 60

degrees (Petre et al., 2003). The structured packing elements tend to eliminate the problems of liquid maldistribution over the entire cross section of the column that are very common to find in beds using conventional random packings. Regular packings also present reductions on energy consumption through the minimization of pressure drop per unit length of column (Petre et al., 2003). These very attractive advantages of structured packings are leading them to an increasingly number of applications such as thermal separation processes, catalyst support in chemical multiphase reactors, oxidation of organic products in bubble columns, support of microorganisms in biofilm reactors and reactive distillation (Cavatorta et al., 1999; Fair et al., 2000; Noeres et al., 2002; Petre et al., 2003; Urseanu et al., 2001).

(a) **(b)**

Figure 2.21. Images of metallic (a) random packings and (b) structured packing element (Khamadieva and Böhm, 2006).

The downflow bubble column requires liquid velocities too high for the system in study that only would be apply able in a very tall unit. This device also includes the recycling of liquid that would be an extra effort in pumping and though, higher operation costs than the simple bubble column may be expected.

In the loop reactors some of the negative features of the tank reactors may occur: wide residence time distribution and the medium as almost uniform composition. These

features do not favour a system were the desired product is an intermediate of the reaction scheme like the case of vanillin production from lignin.

Both cascade and packed bubble column presents a similar type of advantages, although the second option seems to be of simpler construction and maintenance, since the packing elements are internals that can easily be removed and replaced in the column. In a packed bubble column not only the negative influence of back-mixing in the conversion levels is reduced, but also when using metallic packing elements their high thermal conductivity somewhat compensate the decrease of heat transfer effects promoted by the absence of back-mixing.

From the options presented and discussed above the final choice of the continuous reaction configuration reverted to a jacketed bubble column filled with structured packing elements. A detailed description of how this unit was build and also the details about its operation will be described in Chapter 4 and its application in lignin oxidation to obtain vanillin will be focused in Chapter 5.

2.5 References

1. Axelsson, E.; Olsson, M. R.; Berntsson, T. Increased capacity in kraft pulp mills: Lignin separation and reduced steam demand compared with recovery boiler upgrade. *Nordic Pulp Paper Res. J.*, **2006**, 21 (4), 485-492.
2. Bhattacharjee, C.; Sarkar, P.; Datta, S.; Gupta, B. B.; Bhattacharya, P. K. Parameter estimation and performance study during ultrafiltration of Kraft black liquor. *Separ. Purif. Tech.*, **2006**, 51, 247-257.

3. Bjørsvik, H.-R.; Minisci, F. Fine chemicals from lignosulfonates. 1. Synthesis of vanillin by oxidation of lignosulfonates. *Org. Process Res. Dev.*, **1999**, 3 (5), 330-340.

4. Bjørsvik, H.-R.; Liguori, L. Organic processes to pharmaceutical chemicals based on fine chemicals from lignosulfonates. *Org. Process Res. Dev.*, **2002**, 6 (3), 279-290.

5. Boedecker, F.; Volk, H. *Process of producing the m-alkyl-ethers of protocatechuic aldehyde*. U.S. Patent 2,062,205, **1936**.

6. Brady, B.; Brush, S.; Burmark, B.; Corbin, M.; DeMay, J.; Drabek, J.; Figueroa-Kaminsky, C.; Hibbard, R.; Keel, L.; Newman, A.; Otterson, S.; Piliaris, A.; Schweiters, J. *Washington State air toxic sources and emission estimation methods*. Washington State Department of Ecology – Air Quality Program, USA, **1998**.

7. Cavatorta, O.; Böhm, U.; Giorgio, A. M. C. Fluid-dynamic and mass-transfer behavior of static mixers and regular packings. *AIChE J.*, **1999**, 45 (5), 938-948.

8. Cerrutti, P.; Alzamora, S. M.; Vidales, S. L. Vanillin as an antimicrobial for producing shelf-stable strawberry puree. *J. Food Sci.*, **1997**, 62(3), 608-610.

9. Chakar, F. S.; Ragauskas, A. J. Review of current and future softwood kraft lignin process chemistry. *Ind. Crop. Prod.*, **2004**, 20, 131-141.

10. Chenier, P. J. *Survey of Industrial Chemistry* (3rd Edition). Springer-Verlag, **2002**.

11. Ciullo, P.A. *Industrial Minerals and Their Uses - A Handbook and Formulary.* William Andrew Publishing, **1996**.

12. Cleveland, C. J. *Encyclopedia of Energy.* Volumes 1 – 6, Elsevier, **2004**.

13. Coenen, H.; Konrad, R. *Process for the extraction of vanillin*. U.S. Patent 4,898,990, **1990**.

14. Criss, D. L. *Reactions of nonphenolic β-O-4 lignin model compounds: alkaline hydrolysis of γ and/or α-hydroxyl diastereomers and studies of an unusual rearrangement.* Ph.D. Dissertation, Mississippi State University, USA, **1999**.

15. Curto, J. M. R. *Potencial papeleiro do Pinus pinaster.* University of Beira Interior, **2003**.

16. Deckwer, W.-D., *Bubble column reactors.* John Wiley & Sons, England, **1992**.

17. Derouane, E. G.; Powell, R. A. *Vanillin extraction process using large pore, high silica/alumina ratio zeolites*. U.S. Patent 4,652,684, **1987**.

18. Diddams, D. G.; Renaud, N. E. *Process for purifying vanillin*. U.S. Patent 3,686,322, **1972**.

19. Dignum, M. J. W.; Kerler, J.; Verpoorte, R. Vanilla production: technological, chemical, and biosynthetic aspects. *Food Rev. Int.*, **2001**, 17(2), 199-219.

20. Dizhbite, T.; Zakis, G.; Kizima, A.; Lazareva, E.; Rossinskaya, G.; Jurkjane, V.; Telysheva, G.; Viesturs, U. Lignin – a useful bioresource for the production of sorption-active materials. *Bioresour. Technol.*, **1999**, 67, 221-228.

21. El Mansouri, N.-E.; Pizzi, A.; Salvadó, J. Lignin-based wood panel adhesives without formaldehyde. *Holz Roh Werkst*, **2007**, 65, 65-70.

22. El Mansouri, N.-E.; Salvadó, J. Structural characterization of technical lignins for the production of adhesives: Application to lignosulfonate, Kraft, soda-anthraquinone, organosolv and ethanol process lignins. *Ind. Crops Prod.*, **2006**, 24, 8-16.

23. Fair, J. R.; Seibert, A. F.; Behrens, M.; Saraber, P. P.; Olujic, Z. Structured Packing Performances Experimental Evaluation of Two Predictive Models. *Ind. Eng. Chem. Res.*, **2000**, 39, 1788-1796.

24. Fargues, C.; Mathias, A.; Rodrigues, A. Kinetics of vanillin production from Kraft lignin oxidation. *Ind. Eng. Chem. Res.*, **1996a**, 35, 28-36.

25. Fargues, C.; Mathias, A.; Silva, J.; Rodrigues, A. Kinetics of vanillin oxidation. *Chem. Eng. Technol.*, **1996b**, 19 (2), 127-136.

26. Fernandes, N. C. P.; Castro, J. A. A. M. Steady-state simulation of a continuous moving bed reactor in the pulp and paper industry. *Chem. Eng. Sci.*, **2000**, 55, 3729-3738.

27. Fitzgerald, D. J.; Stratford, M.; Narbad, A. Analysis of the inhibition of food spoilage yeasts by vanillin. *Int. J. Food Microbiol.*, **2003**, 86, 113-122.

28. Forss, K. G.; Talka, E. T.; Fremer, K.-E. *Method for the isolation of vanillin from lignin in alkaline solutions*. U.S. Patent 4,277,626, **1981**.

29. Gasson, M. J.; Kitamura, Y.; McLauchlan, W. R.; Narbad, A.; Parr, A. J.; Parsons, E. L. H.; Payne, J.; Rhodes, M. J. C.; Walton, N. J. Metabolism of ferulic acid to vanillin: a bacterial gene of the enoyl-SCoA hydratase/isomerase superfamily encodes an enzyme for the hydration and cleavage of a hydroxycinnamic acid SCoA thioester. *J. Biol. Chem.*, **1998**, 273 (7), 4163-4170.

30. Glasser, W.; Sarkanen, S. *Lignin: properties and materials.* American Chemical Society, **1989**.

31. Gregorová, A.; Cibulková, Z.; Košíková, B.; Šimon, P. Stabilization effect of lignin in polypropylene and recycled polypropylene. *Polym. Degrad. Stab.*, **2005**, 89, 553-558.

32. Gregorová, A.; Košíková, B.; Moravčík, R. Stabilization effect of lignin in natural rubber. *Polym. Degrad. Stab.*, **2006**, 91, 229-233.

33. Havkin-Frenkel, D.; Podstolski, A. *Vanillin production*. U.S. Patent 7,226,783, **2007**.

34. Holmberg, K. *Handbook of Applied Surface and Colloid Chemistry.* John Wiley & Sons, **2002**.

35. Holmqvist, A.; Wallberg, O.; Jönsson, A.-S. Ultrafiltration of Kraft black liquor from two Swedish pulp mills. *Chem. Eng. Res. Des.*, **2005**, 83 (A8), 994-999.

36. http://etcpitea.se/blg/document/PBLG_or_RB.pdf

37. http://student.britannica.com

38. http://www.adeq.state.ar.us

39. http://www.britannica.com

40. http://www.buetzer.info

41. http://www.chem.unep.ch

42. http://www.fao.org/forestry

43. http://www.handpapermaking.org

44. http://www.hoganhardwoods.com

45. http://www.lignoboost.com

46. Hu, T. Q. *Chemical modification, properties, and usage of lignin.* Kluwer Academic / Plenum Publishers, New York, **2002**.

47. Hua, D.; Ma, C.; Song, L.; Lin, S.; Zhang, Z.; Deng, Z.; Xu, P. Enhanced vanillin production from ferulic acid using adsorbent resin. *Appl. Microbiol. Biotechnol.*, **2007**, 74, 783-790.

48. Jones, C. W. *Applications of Hydrogen Peroxide and Derivatives.* Royal Society of Chemistry, **1999**.

49. Jones, T.; Finnan, J. L.; Arvizzigno, J. *Process for separation of vanillin by means of azeotropic distillation with dibenzyl ether*. U.S. Patent 5,510,006, **1996**.

50. Kadla, J. F.; Kubo, S. Lignin-based polymer blends: analysis of intermolecular interactions in lignin-synthetic polymer blends. *Composites Part A Appl. Sci. Manufac.*, **2004**, 35, 395-400.

51. Kadla, J. F.; Kubo, S.; Venditti, R. A.; Gilbert, R. D.; Compere, A. L.; Griffith, W. Lignin-based carbon fibers for composite fiber applications. *Carbon*, **2002**, 40, 2913-2920

52. Kantarci, N.; Borak, F.; Ulgen, K. O. Review: Bubble column reactors. *Process Biochem.*, **2005**, 40, 2263-2283.

53. Keshava, C.; Keshava, N.; Whong, W.-Z.; Nath, J.; Ong, T.-M. Inhibition of methotrexate-induced chromosomal damage by vanillin and chlorophyllin in V79 cells. *Teratogenesis, Carcinogenesis, and Mutagenesis*, **1998**, 17, 313–326.

54. Khamadieva, R.; Böhm, U. Mass transfer to the wall of a packed and unpacked bubble column operating with Newtonian and non-Newtonian liquids. *Chem. Eng. J.*, **2006**, 116, 105-113.

55. *Kirk-Othmer Encyclopedia of Chemical Technology*; 5th Edition, John Wiley & Sons, **2005**.

56. Kirwan, M. J. *Paper and Paperboard Packaging Technology.* Blackwell Publishing, **2005**.

57. Klemola, A.; Tuovinen, J. *Method for the production of vanillin*. U.S. Patent 4,847,422, **1989**.

58. Kolppo, K. P. T. *Structural changes of lignin and lignin's interaction with sulphur during Kraft, soda and acid sulfite delignification of Western hemlock*

(Tsuga heterophylla). Ph.D. Dissertation, Michigan Technical University, USA, **1994**.

59. Košíková, B.; Lábaj, J.; Gregorová, A.; Slameňová, D. Lignin antioxidants for preventing oxidation damage of DNA and for stabilizing polymeric composites. *Holzforschung*, **2006**, 60, 166-170.
60. Krings, U.; Berger, R. G. Biotechnological production of flavours and fragrances. *Appl. Microbiol. Biotechnol.*, **1998**, 49, 1-8.
61. Laine, C. *Structures of hemicelluloses and pectins in wood and pulp.* Ph.D. Dissertation, Helsinki University of Technology, Finland, **2005**.
62. Lesage-Meessen, L.; Delattre, M.; Haon, M.; Thibault, J.-F.; Ceccaldi, B. C.; Brunerie, P.; Asther, M. A two-step bioconversion process for vanillin production from ferulic acid combining *Aspergillus niger* and *Pycnoporus cinnabarinus*. *J. Biotechnol.*, **1996a**, 50, 107-113.
63. Lesage-Meessen, L.; Delattre, M.; Haon, M.; Asther, M. *Method for obtaining vanillic acid and vanillin by bioconversion by an association of filamentous microorganisms*. European Patent WO96/08576, **1996b**.
64. Lesage-Meessen, L.; Haon, M.; Delattre, M.; Thibault, J.-F.; Ceccaldi, B. C.; Asther, M. An attempt to channel the transformation of vanillic acid into vanillin by controlling methoxyhydroquinone formation in *Pycnoporus cinnabarinus* with cellobiose. *Appl. Microbiol. Biotechnol.*, **1997**, 47, 393-397.
65. Levenspiel, O. *Chemical Reaction Engineering* (3rd Edition). John Wiley & Sons, USA, **1999**.
66. Li, K.; Frost, J. W. Synthesis of vanillin from glucose. *J. Am. Chem. Soc.*, **1998**, 120, 10545-10546.

67. Li, Z. *Improving the Kraft pulp yield with polysulfide and anthraquinone.* M.Eng Dissertation, McGill University, Canada, **1997**.

68. Liu, G.; Liu, Y.; Ni, J.; Shib, H.; Qian, Y. Treatability of kraft spent liquor by microfiltration and ultrafiltration. *Desalination*, **2004**, 160, 131-141.

69. Llamas, P.; Dominguéz, T.; Vargas, J. M.; Llamas, J.; Franco, J. M.; Llamas, A. A novel viscosity reducer for kraft process black liquors with a high dry solids content. *Chem. Eng. Process.*, **2007**, 46, 193-197.

70. Logan, C. D. *Cyclic process for recovering vanillin and sodium values from lignosulfonic waste liquors by ion exchange*. U.S. Patent 3,197,359, **1965**.

71. López-Malo, A.; Alzamora, S. M.; Argaiz, A. Vanillin and pH synergistic effects on mold growth. *J. Food Sci.*, **1998**, 63(1), 143-146.

72. Lora, J. H.; Glasser, W. G. Recent industrial applications of lignin: A sustainable alternative to non-renewable materials. *J. Polym. Environ.*, **2002**, 10, 39-48.

73. Major, F. W.; Nicolle, M. A. *Vanillin recovery process*. U.S. Patent 4,021,493, **1977**.

74. Mathias, A. L. *Produção de vanilina a partir da lenhina: estudo cinético e do processo.* Ph.D. Dissertation, University of Porto, Portugal, **1993**.

75. Mathias, A. L.; Lopretti, M. I.; Rodrigues, A. E. Chemical and biological oxidation of *Pinus pinaster* lignin for the production of vanillin. *J. Chem. Tech. Biotechnol.*, **1995**, 64, 225-234.

76. Mathias, A. L.; Rodrigues, A. E. Production of vanillin by oxidation of pine Kraft lignins with oxygen. *Holzforschung*, **1995**, 49, 273-278.

77. Mielenz, J. R.; Klasson, K. T.; Adney, W. S.; McMillan, J. D. *Biotechnology for fuels and chemicals – The twenty-eighth symposium.* Springer-Verlag, **2007**.

78. Missen, R. W.; Mims, C. A.; Saville, B. A. *Introduction to chemical reaction engineering and kinetics.* John Wiley & Sons, New York, **1999**.

79. Muheim, A.; Müller, B.; Münch, T.; Wetli, M. *Process for the production of vanillin*. European Patent 0885968, **1998**.

80. Muheim, A.; Lerch, K. Towards a high-yield bioconversion of ferulic acid to vanillin. *Appl. Microbiol. Biotechnol.*, **1999**, 51, 456-461.

81. Nalco Company *The Nalco Water Handbook* (2nd Edition). McGraw Hill, USA, **1988**.

82. Noeres, C.; Hoffmann, A.; Górak, A. Reactive distillation: Non-ideal flow behaviour of the liquid phase in structured catalytic packings. *Chem. Eng. Sci.*, **2002**, 57, 1545-1549.

83. Norgren, M. *On the physical chemistry of Kraft lignin: Fundamental and applications.* Ph.D. Dissertation, Lund University, Sweden, **2001**.

84. Norgren, M.; Edlund, H. Ion specific differences in salt induced precipitation of Kraft lignin. *Nordic Pulp Paper Res. J.*, **2003**, 18 (4), 400-403.

85. Norgren, M.; Edlund, H.; Wågberg, L. Aggregation of lignin derivatives under alkaline conditions. Kinetics and aggregate structure. *Langmuir*, **2002a**, 18 (7), 2859-2865.

86. Norgren, M.; Edlund, H.; Wågberg, L.; Annergren, G. Fundamental physical aspects on lignin dissolution. *Nordic Pulp Paper Res. J.*, **2002b**, 17 (4), 370-373.

87. Oddou, J.; Stentelaire, C.; Lesage-Meessen, L.; Asther, M.; Ceccaldi, B. C. Improvement of ferulic acid bioconversion into vanillin by use of high-density cultures of *Pycnoporus cinnabarinus*. *Appl. Microbiol. Biotechnol.*, **1999**, 53, 1-6.

88. Perry, R. H.; Green, D. W.; Maloney, J. O. *Perry's Chemical Engineers Handbook* (7th Edition), McGraw Hill, New York, **1997**.

89. Petre, C. F.; Larachi, F.; Iliuta, I.; Grandjean, B. P. A. Pressure drop through structured packings: Breakdown into the contributing mechanisms by CFD modeling. *Chem. Eng. Sci.*, **2003**, 58, 163-177.

90. Plaggenborg, R.; Overhage, J.; Loos, A.; Archer, J. A. C.; Lessard, P.; Sinskey, A. J.; Steinbüchel, A.; Priefert, H. Potential of *Rhodococcus* strains for biotechnological vanillin production from ferulic acid and eugenol. *Appl. Microbiol. Biotechnol.*, **2006**, 72, 745-755.

91. Priefert, H.; Rabenhorst, J.; Steinbüchel, A. Biotechnological production of vanillin. *Appl. Microbiol. Biotechnol.*, **2001**, 56, 296-314.

92. Rabenhorst, J.; Hopp, R. *Process for the preparation of vanillin*. U.S. Patent 5,017,388, **1991**.

93. Rao, S. R.; Ravishankar, G. A. Biotransformation of isoeugenol to vanilla flavour metabolites and capsaicin in suspended and immobilized cell cultures of *Capsicum frutescens*: study of the influence of β-cyclodextrin and fungal elicitor. *Process Biochem.*, **1999**, 35, 341-348.

94. Rao, S. R.; Ravishankar, G. A. Review – Vanilla flavour: production by conventional and biotechnological routes. *J. Sci. Food Agric.*, **2000**, 80, 289-304.

95. Rase, H. F. *Chemical reactor design for process plants. Volume One: principles and techniques.* John Wiley & Sons, New York, **1977**.

96. Sandborn, L. T.; Salvesen, J. R.; Howard, G. C. *Process of making vanillin*. U.S. Patent 2,057,117, **1936**.

97. Sales, F. G.; Abreu, C. A. M.; Pereira, J. A. F. R. Catalytic wet-air oxidation of lignin in a three-phase reactor with aromatic aldehyde production. *Brazilian J. Chem. Eng.*, **2004**, 21 (2), 211-218.

98. Sales, F. G.; Maranhão, L. C. A.; Filho, N. M. L.; Abreu, C. A. M.; Pereira, J. A. F. R. Kinetic evaluation and modeling of lignin catalytic wet oxidation to selective production of aromatic aldehydes. *Ind. Eng. Chem. Res.*, **2006**, 45 (20), 6627-6631.

99. Schlüter, S.; Steiff, A., Weinspach, P.-M. Modeling and simulation of bubble column reactors. *Chem. Eng. Process.*, **1992**, 31, 97-117.

100. Schrader, J.; Etschmann, M. M. W.; Sell, D.; Hilmer, J.-M.; Rabenhorst, J. Applied biocatalysis for the synthesis of natural flavour compounds – current industrial processes and future prospects. *Biotechnol. Lett.*, **2004**, 26, 463-472.

101. Schulz, L. *Manufacture of vanillin*. U.S. Patent 2,187,366, **1940**.

102. Sixta, H. *Handbook of pulp*, Wiley-VCH, **2006.**

103. Speight, J. G. *Chemical and Process Design Handbook.* McGraw-Hill, **2002**.

104. Stentelaire, C.; Lesage-Meessen, L.; Delattre, M.; Haon, M.; Sigoillot, J. C.; Ceccaldi, B. C.; Asther, M. Short communication: By-passing of unwanted vanillyl alcohol formation using selective adsorbents to improve vanillin production with *Phanerochaete chrysosporium*. *World J. Microbiol. Biotechnol.*, **1998**, 14, 285-287.

105. Stitt, E. H. Alternative multiphase reactors for fine chemicals. A world beyond stirred tanks? *Chem. Eng. J.*, **2002**, 4025, 1-14.

106. Sun, R.; Tomkinson, J.; Bolton, J. Effects of precipitation pH on the physico-chemical properties of the lignins isolated from the black liquor of oil palm empty fruit bunch fibre pulping. *Polym. Degrad. Stab.*, **1999**, 63, 195-200.

107. Suresh, B.; Ritu, T.; Ravishankar, G. A. Vanilla flavour production through biotransformation using *Capsicum frutescens* root cultures. *Biocatal. Biotransform.*, **2003**, 21 (6), 333-340.

108. Tarabanko, V. E.; Koropatchinskaya, N. V.; Kudryashev, A. V.; Kuznetsov, B. N. Influence of lignin origin on the efficiency of the catalytic oxidation of lignin into vanillin and syringaldehyde. *Russ. Chem. Bull.*, **1995a**, 2, 367-371.

109. Tarabanko, V. E.; Fomova, N. A.; Kuznetsov, B. N.; Ivanchenko, N. M.; Kudryashev, A. V. On the mechanism of vanillin formation in the catalytic oxidation of lignin with oxygen. *React. Kinet. Catal. Lett.*, **1995b**, 55 (1), 161-170.

110. Tarabanko, V. E.; Ivanchenko, N. M.; Selutin, G. E.; Bezrukova, N. P.; Pervishina, E. P.; Kuznetsov, B. N.; Ilyna, I. I. The study of kinetics and mechanism of vanillin formation in the process of catalytic oxidation of lignins. *Khimiya rastitel'nogo syrya*, **1997**, 2, 4-14.

111. Tarabanko, V. E.; Kuznetsov, B. N.; Swistek, M.; Gruber, R.; Chernyak, M. Y.; Pervishina, E. P. Production of the fine chemicals from hardwood. *4th International Symposium "Catalytic and thermochemical conversion of natural organic polymers"*, Krasnoyarsk, Russia, 77-80, June, **2000**.

112. Tarabanko, V. E.; Petukhov, D. V. Study of mechanism and improvement of the process of oxidative cleavage of lignins into the aromatic aldehydes. *Chemistry for Sustainable Development*, **2003**, 11, 655-667.

113. *The Merck Index*; 13th Edition, Merck & Co., New Jersey, USA, **2001**.

114. Thielemans, W.; Can, E.; Morye, S. S.; Wool, R. P. Novel applications of lignin in composite materials. *J. Appl. Polym. Sci.*, **2002**, 83, 323-331.

115. Tilghman, B. *Improved mode of treating vegetable substances for making paper-pulp*. U.S. Patent 70,485, **1867**.

116. Triumph Venture Capital *Part 2-Aroma chemicals derived from effluent from the paper and pulp industry*. In: Study into the establishment of an aroma and fragrance fine chemicals value chain in South Africa (Final Report), FRIDGE, NEDLAC, South Africa, **2004**. (http://www.nedlac.org.za)

117. *Ullmann´s Encyclopedia of Industrial Chemistry*; 7th Edition, Wiley-VCH, Verlag GmbH & Co..KGaA, **2003**.

118. Urseanu, M. I.; Ellenberger, J.; Krishna, R. A structured catalytic bubble column reactor: hydrodynamic and mixing studies. *Catal. Today*, **2001,** 69, 105–113.

119. Van den Heuvel, R. H. H.; Fraaije, M. W.; Laane, C.; Van Berkel, W. J. H. Enzymatic synthesis of vanillin. *J. Agric. Food Chem.*, **2001**, 49 (6), 2954-2958.

120. Villar, J. C.; Caperos, A.; García-Ochoa, F. Oxidation of hardwood kraft-lignin to phenolic derivatives. Nitrobenzene and copper oxide as oxidants. *J. Wood Chem. Technol.*, **1997**, 17 (3), 259-285.

121. Villar, J. C.; Caperos, A.; García-Ochoa, F. Oxidation of hardwood kraft-lignin to phenolic derivatives with oxygen as oxidant. *Wood Sci. Technol.*, **2001**, 35, 245-255.

122. Wallberg, O.; Holmqvist, A.; Jönsson, A.-S. Ultrafiltration of Kraft cooking liquors from a continuous cooking process. *Desalination*, **2005**, 180, 109-118.

123. Wallberg, O.; Jönsson, A.-S.; Wimmerstedt, R. Fractionation and concentration of kraft black liquor lignin with ultrafiltration. *Desalination*, **2003**, 154, 187-199.

124. Wallberg, O.; Linde, M.; Jönsson, A.-S. Extraction of lignin and hemicelluloses from kraft black liquor. *Desalination*, **2006**, 199, 413-414.

125. Walton, N. J.; Mayer, M. J.; Narbad, A. Molecules of interest – Vanillin. *Phytochemistry*, **2003**, 63, 505-515.

126. Washburn, E. W. *International critical tables of numerical data, physics, chemistry and technology* (1st Electronic Edition), Knovel, **2003** (http://www.knovel.com/knovel2/Toc.jsp?BookID=735).

127. Woodings, C. *Regenerated Cellulose Fibres.* Woodhead Publishing, **2001**.

128. Wool, R.; Sun, X. S. *Bio-based polymers and composites.* Elsevier, USA, **2005**.

129. Yang, W.-C. *Fluidization, Solids Handling, and Processing - Industrial Applications.* William Andrew Publishing, **1998**.

130. Yoon, S.-H.; Li, C.; Kim, J.-E.; Lee, S.-H.; Yoon, J.-Y.; Choi, M.-S.; Seo, W.-T.; Yang, J.-K.; Kim, J.-Y.; Kim, S.-W. Production of vanillin by metabolically engineered *Escherichia coli*. *Biotechnol. Lett.*, **2005**, 27, 1829-1832.

131. Zhao, L.-Q.; Sun, Z.-H.; Zheng, P.; Zhu, L. L. Biotransformation of isoeugenol to vanillin by a novel strain of *Bacillus fusiformis*. *Biotechnol. Lett.*, **2005**, 27, 1505-1509.

132. Zhao, L.-Q.; Sun, Z.-H.; Zheng, P.; He, J.-Y. Short communication: Biotransformation of isoeugenol to vanillin by *Bacillus fusiformis* CGMCC1347 with the addition of resin HD-8. *Process Biochem.*, **2006**, 41, 1673-1676.

133. Zheng, L.; Zheng, P.; Sun, Z.; Bai, Y.; Wang, J.; Guo, X. Production of vanillin from waste residue of rice bran oil by *Aspergillus niger* and *Pycnoporus cinnabarinus*. *Bioresour. Technol.*, **2007**, 98, 1115-1119.

3. Batch reactor – experimental and modelling

Lignin oxidation with oxygen in strong alkaline medium was already studied at the LSRE. The work developed by Álvaro Mathias (Mathias, 1993) was related to the effect of operating process parameters (total pressure, temperature, oxygen partial pressure, lignin concentration and sodium hydroxide concentration) applied to the kinetics of the lignin oxidation reaction. The kinetics of vanillin degradation was also investigated by Claire Fargues and a model was developed to account for its degradation rate at various pH 's including an attempt to predict pH variation during the reaction (Fargues et al., 1996a). These works resulted in a kinetic model to simulate the complete process of lignin oxidation to produce vanillin.

In this chapter, batch experiments performed with Kraft lignin supplied by Westvaco Co. (Indulin AT) are presented. Different mathematical models for a batch reactor were also developed for the following systems: isothermal vanillin oxidation; isothermal lignin oxidation and non-isothermal lignin oxidation. These mathematical models were employed to describe batch measurements performed on this thesis and also to other experiments previously reported by Álvaro Mathias (Mathias, 1993). The results obtained in terms of vanillin formation starting from different lignin sources are presented and discussed.

The purpose of this chapter is to determine the vanillin yield of the raw material used (Indulin AT) by comparing the results obtained in batch experiments with the ones obtained with different lignins, but in similar operating conditions. The necessity of this

verification arises from the fact that lignin is a complex biopolymer that does not show a unique chemical structure (Kirk-Othmer Encyclopedia, 2005). Instead, the proportion of its functional groups or building units can differ even when they belong to the same plant source.

3.1. Experimental

3.1.1. Batch reactor setup

The chemical oxidation of lignin with oxygen is a reaction that needs to be carried out on very aggressive *pH* 's conditions (close to 14), temperatures near 150ºC and total pressure of 10 bar. In this work, the batch experiments of lignin oxidation were performed in a Büchi AG laboratory autoclave (model BEP280 type II, Switzerland). This autoclave includes a cylindrical jacketed reactor with a capacity of 1 litre that can handle pressures up to 13 bar, temperatures up to 200ºC and a Planetroll motor (model F63M-2) with maximum rotation speed of 2820 rpm.

The reaction zone is delimited by a borosilicate glass cylindrical tube with 18 cm height, an internal diameter of 8.24 cm and 0.86 cm thickness. This tube is surrounded by a glass jacket, less thick, with a height slightly lower and an external diameter of 12.5 cm. The jacket contains two openings to allow the circulation of a thermo fluid to control the temperature of the reaction medium. Both glass tubes (reaction zone plus glass jacket) are compressed between two stainless steel plates and separated by joints of PTFE and silicon. The upper plate of the reactor has a cooling coil and five screwed holes to place thermocouples, gas feed and sampling lines, admission of the initial liquid phase and a place to fit the agitation shaft.

The heating and control of the reactor temperature is made by a Haake thermostatic bath (model N2-B, Karlsruhe, Germany) with a set point precision of 0.03ºC. This bath has two pumps (one for suction and other for injection) to circulate the thermo fluid through the heating jacket. The thermo fluid is silicon oil (Silicex 322 Siliconas Hispania). The temperatures inside the reactor and in the thermostatic bath were measured using thermocouples type K (nickel-chromium / nickel-aluminum). The combination of these alloys generates a voltage gradient of approximately 43 $\mu V\ ºC^{-1}$ for temperatures between 100 and 500ºC, when the cold junction is maintained at 0ºC.

The total pressure of the reactor was measured by a pressure transducer (Kulite model XYME-190M G, Leonia, USA), placed in the gas feed line. This transducer has a working range of 0 to 17 barg and needs a power supply of 10 V. The output signal is on the interval of 0 to 75 mV and has a linear relation with pressure. It has a sensitivity of 4.46 $mV\ bar^{-1}$ and an output signal of 0.4 mV for atmospheric pressure. This transducer has a high chemical resistance and can be used, without necessity of corrections in very wide conditions (temperature of 27 to 232ºC and pressure up to 34 barg).

The gas feed line has a safety valve (Nupro Swagelook, United Kingdom) regulated to open every time the reactor pressure exceeds 12 bar.

A sampling line to collect liquid samples from the reaction medium was placed on the top stainless steel plate of the reactor and was open and closed by using an electro valve (Asco model HTB262C15T, Scherpenzeel, Netherlands).

A complete view of the experimental set-up of the batch reactor is shown in Figure 3.1.

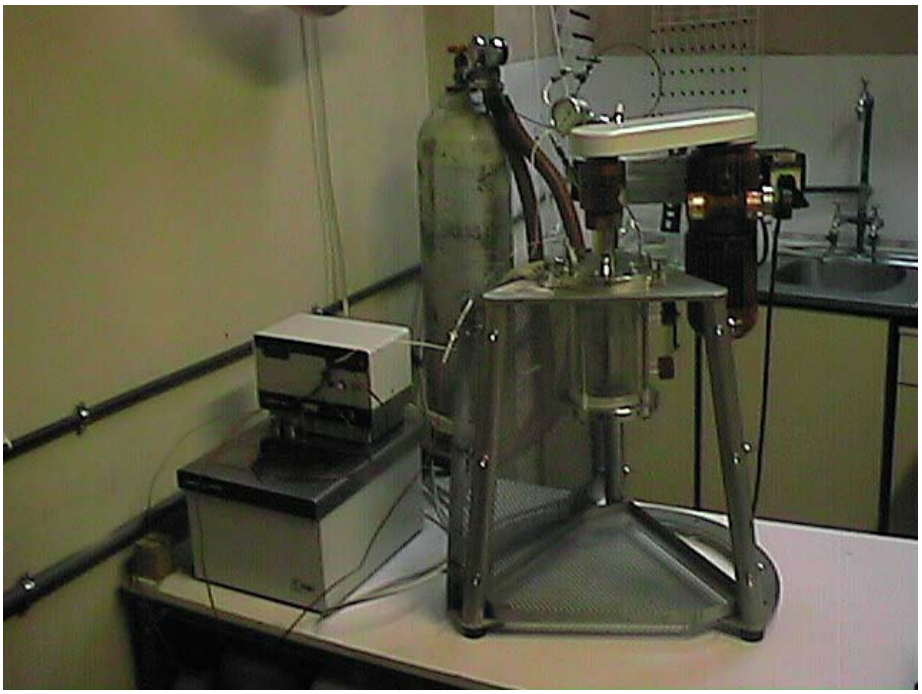

Figure 3.1. View of the batch reactor experimental setup.

A new data acquisition system to store operating conditions during an experiment was also developed within this thesis. The data acquisition system consists in the following parts:

- Advantech (USA) data acquisition board, model 1710 HG.
- Advantech (USA) termination board, model PCLD-8710.
- PC with Pentium III processor at 500 MHz, 128 Mb of RAM memory and hard drive with 8 Gb capacity. The operative system used was Windows 98.

A program for data acquisition was developed in LabView (National Instruments, USA). This program has the purpose of acquiring two voltage signals from thermocouples (temperatures inside the reactor and in the thermostatic bath) and one signal corresponding to a pressure transducer. The user-friendly interface of the data acquisition program can be seen in Figure 3.2.

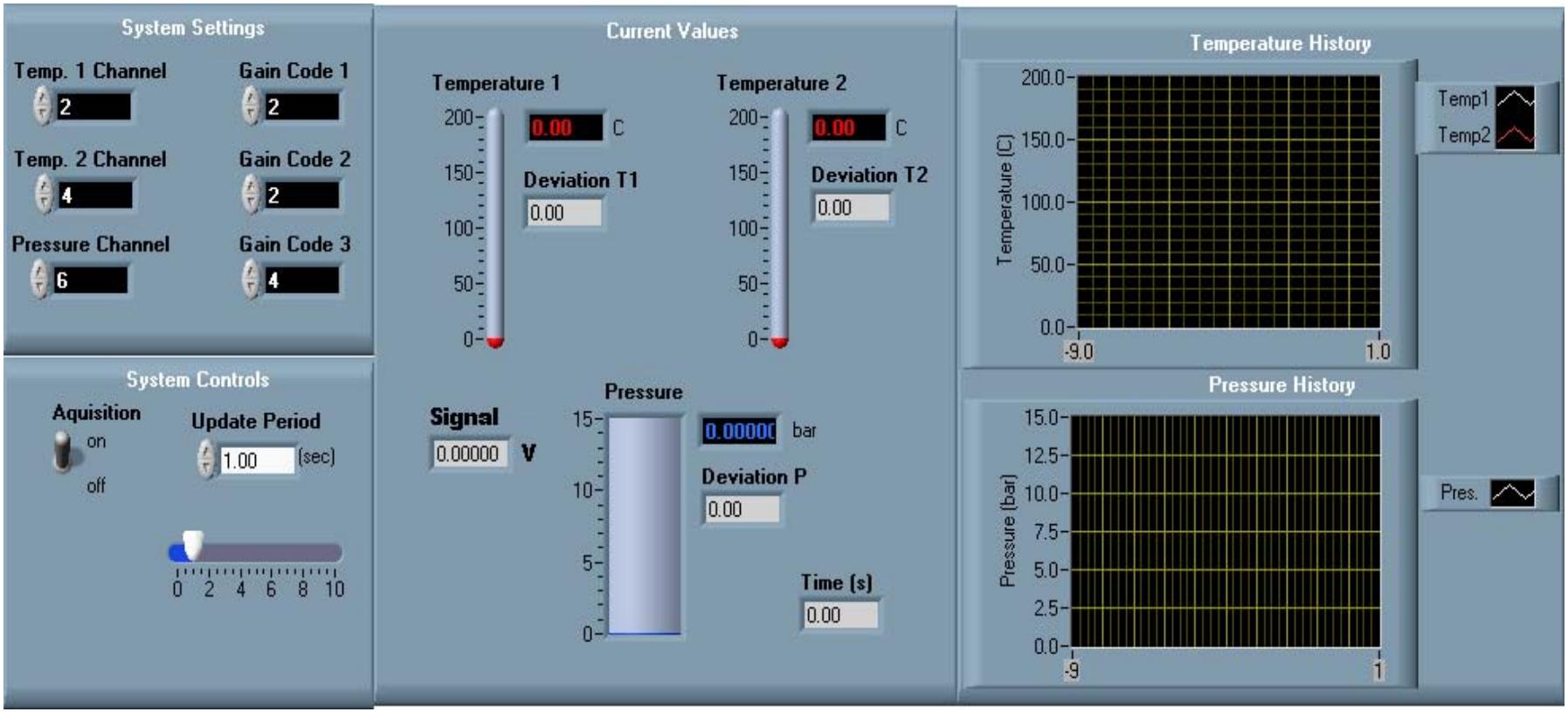

Figure 3.2. Control panel interface of the data acquisition program for the batch reactor installation.

The routines included in the program allow it to perform the following tasks:

- Executes 30 readings on each channel, with time intervals defined by the user.
- Calculates the average and standard deviation of those readings.
- Saves in separate files (a file for each signal) the average values and the correspondent time.

This operation is cyclic and runs until the user stops the program on the control panel interface.

3.1.2. System operation

The first step to start the batch reactor system is to prepare the liquid mixture that consists in a solution of lignin in sodium hydroxide. 40 grams of NaOH were added to approximately 300-350 ml of distilled water. Then 30 grams of lignin (Indulin AT) were solubilised in the sodium hydroxide solution, with the help of a heating plate. To eliminate some of the dissolved oxygen, the resulting mixture is heated during 10-15 minutes, and then the volume of 500 ml was completed with distilled water, previously heated and cooled. The resulting reaction mixture was 500 ml of solution with 60 g/l of lignin and 80 g/l of sodium hydroxide.

The thermostatic bath was previously turned on with a 60ºC set point. The reaction mixture was added to the reactor through one of the holes on the top stainless steel plate, which was then properly closed. Then nitrogen was admitted to the reactor for approximately 5 minutes, with the depressurization valve (valve 2 on Figure 3.3) open to remove air (oxygen) from the gas phase. The feed of nitrogen was then stopped, valve 2 was closed, and the agitation motor was turned on, increasing gradually the speed until it reached 1100 rpm.

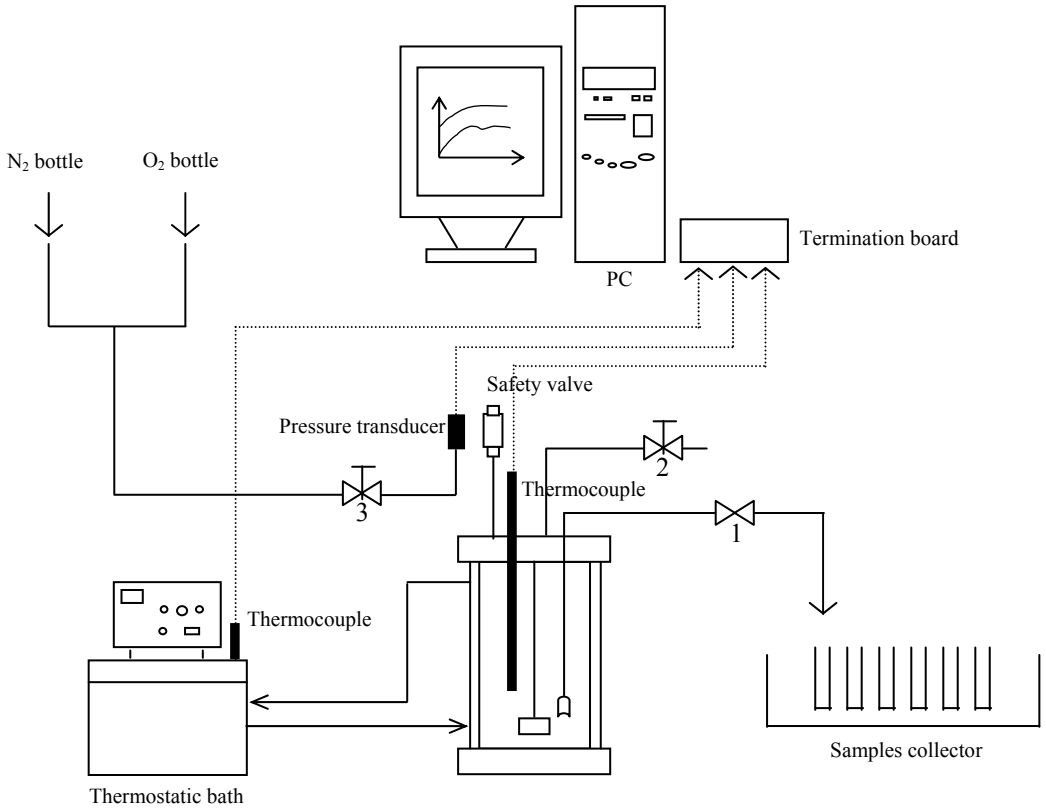

Figure 3.3. Schematic diagram of the batch reactor experimental setup.

The set point of the bath was increased to 160-165ºC to have a steady-state reactor temperature between 120-125ºC. The data acquisition program was then started up. Once achieved the desired value of temperature within the reactor, this acquisition was turned off. This process of heating the system normally took 90 minutes to be completed.

For the pressurization of the reactor the feed of nitrogen and valve 3 were open, starting simultaneously the data acquisition. When the total pressure (nitrogen partial pressure + vapour pressure) of the system reached the desired value, valve 3 was closed as well as the nitrogen bottle, and the acquisition was stopped.

The pressure regulator placed on the oxygen bottle was set to a value approximately 1 bar higher than the desired total pressure in the reactor. This action had

the purpose of guarantee not only that O_2 was always available to be fed to the reactor (in order to maintain the total pressure constant during the reaction phase of the experiment), but also to avoid backflow of liquid mixture to the gas line. Then the valve of the oxygen bottle was opened, and afterwards valve 3 was opened simultaneously with the restart of data acquisition. Only at this point the reaction began and time zero corresponds to the time when initial admission of oxygen was allowed.

Starting at time zero, samples of the liquid mixture were collected at constant time intervals. The collection of samples were performed by opening electro valve 1 to take out a small volume of liquid phase (approximately 2 ml) to a glass tube, in order to clean the liquid exit line. Then valve 1 was opened again to collect around 3 ml of liquid (real sample) into a new tube. This operation was repeated every 5 minutes, until it was reached 130 minutes of reaction. At this time the data acquisition and the admission of oxygen were stopped considering the end of the experimental run. It is also important to note that during the reaction time some small adjustments in the opening position of valve 3 were also made to maintain the total pressure approximately constant.

The final step of the experiment, and not less important, is the shutting down of the equipment. The set point of the thermostatic bath is changed to 35ºC, in order to promote a gradual cooling of the system, with special attention on the glass parts of the reactor. When a reactor temperature around 50ºC was reached, the agitation was stopped and a slow depressurization was promoted.

After complete depressurization of the system, the remaining liquid on the reactor was taken out by its lower stainless steel plate. The PC and the thermostatic bath were shut down. After cooling, the collected samples were placed on PVC vials with pressure cap, previously numbered.

3.1.3. Analytical procedure

The vanillin content on the liquid samples collected during a batch experiment was determined by gas chromatography. The chromatograph used was a DANI GC1000 DPC (Italy) with FID detector, shown in Figure 3.4. The chromatographic column employed was a WCOT Fused Silica, with an internal diameter of 0.53 mm, a length of 50 m, and a stationary phase type CP-WAX 52 CB.

A complete data acquisition system (PC + acquisition board + termination board) was built to collect the output signal of the gas chromatograph. This system is similar to the one used in the batch reactor setup. The corresponding data acquisition program was also made in LabView (National Instruments, USA). This program is prepared to acquire a voltage signal, in the range of 0 to 10 volts, and save it on a file.

Figure 3.4. View of the gas chromatograph DANI GC1000 DPC with FID detector.

The protocol for vanillin analysis is similar to the one used by Mathias (Mathias, 1993) and is described in the following lines:

- Transfer 0.7 ml of liquid sample to a glass tube with cap and add 0.7 ml of HCl 2.5 N. The lignin not completely degraded will precipitate.

- Agitate the mixture during 15 seconds, using a vortex tube agitator at maximum speed.
- Centrifuge the mixture at 5000 rpm, during 15 minutes, having the attention of placing tubes with approximately the same weight (the difference should not exceed 0.05 grams) in diametrically opposed position.
- Transfer 0.5 ml of the supernatant to a new glass tube with cap and add 0.5 ml of ethyl ether. A portion of the low molecular weights compounds present, including vanillin, will be extracted to the organic phase.
- Agitate the mixture during 60 seconds, using a vortex tube agitator at maximum speed.
- Centrifuge the mixture at 1000 rpm, during 5 minutes, in order to define two distinct phases. It should be taken the same care with the positioning of the tubes inside the centrifuge.
- Transfer a part of the upper phase (organic phase) to a vial, protect it with parafilm and place it away of any source of heat, to avoid evaporation of solvent. The refrigerator is not a solution since vanillin will suffer crystallization.
- After the desired operating conditions of the chromatograph are stabilized, turn on its FID detector. At this time the data acquisition program should be ready to start up.
- Inject 1 μl of the liquid placed on the veil and simultaneously start up the temperature program, previously recorded on the chromatograph, and the data acquisition on the PC.
- Clean the syringe with ethyl ether, before and after each injection.

- When the temperature program of the GC is complete, stop the data acquisition and rename the text file created.

Table 3.1. Operation conditions of the gas chromatograph.

T_{oven} (initial)	100ºC	$T_{injector}$	100ºC
t_1	3 min	Q_{N2}	4 ml/min
T_{oven} (final)	215ºC	Q_{H2}	30 ml/min
t_2	40 min	Q_{airK}	300 ml/min
$\alpha_{heating}$	30ºC/min	$V_{injection}$	1 μl
$T_{detector}$	260ºC		

The experimental analysis conditions used in this gas chromatography system are summarized in Table 3.1. The temperature program on the oven starts at 100ºC. This value is constant during 3 minutes (t_1), and then the oven is heated at a rate of 30ºC/min ($\alpha_{heating}$) until it reaches 215ºC where it is maintained during 40 minutes (t_2). At this point the temperature program stops, and the oven temperature returns to 100ºC, ready for a new injection.

The carrier gas employed was nitrogen with a flow rate of 4 ml/min (Q_{N2}), with no makeup gas. Hydrogen and air K (both N50 and supplied by Air Liquide) were fed to the detector at a flow rate ratio of 1:10, respectively: 30 ml/min (Q_{H2}) and 300 ml/min ($Q_{air\,K}$).

In Figure 3.5 a typical representation of the GC output signal resulting from a sample analysis is shown. To identify and calibrate the vanillin concentration a solution of vanillin in ethyl ether was injected in the GC. After the exit of the solvent peak (ethyl ether) another one was observed at 1900 seconds corresponding to the retention time of vanillin in this system.

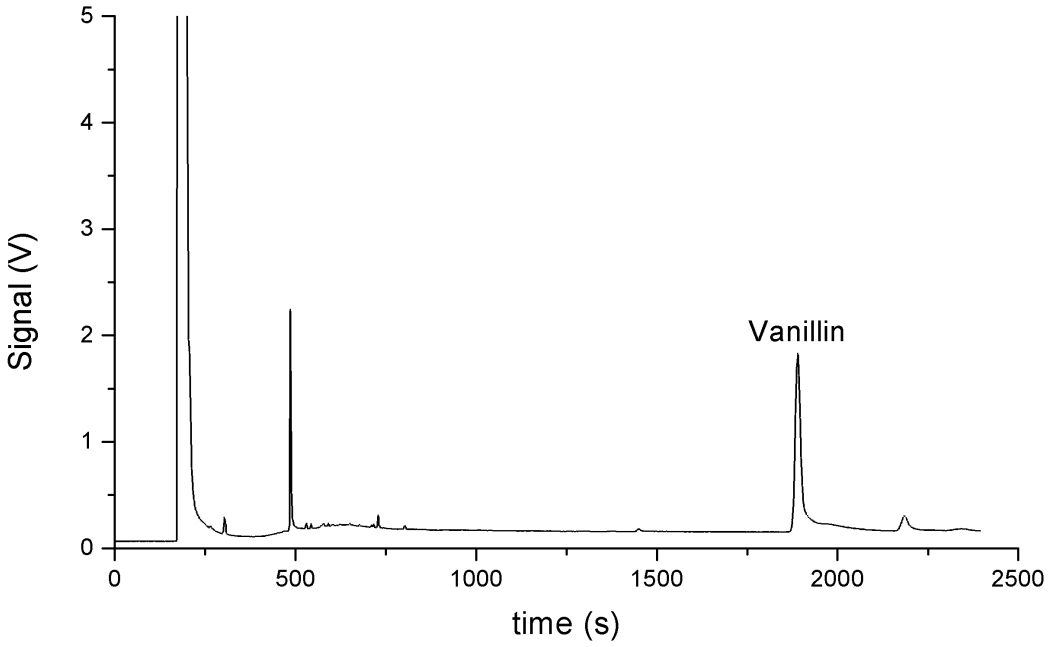

Figure 3.5. Chromatogram obtained in the analysis of a batch experiment sample.

To quantify the desired product it was necessary to relate the areas under the vanillin peaks (retention time of 1900 seconds) with vanillin concentration. For this purpose a calibration curve (presented in Figure 3.6) was build.

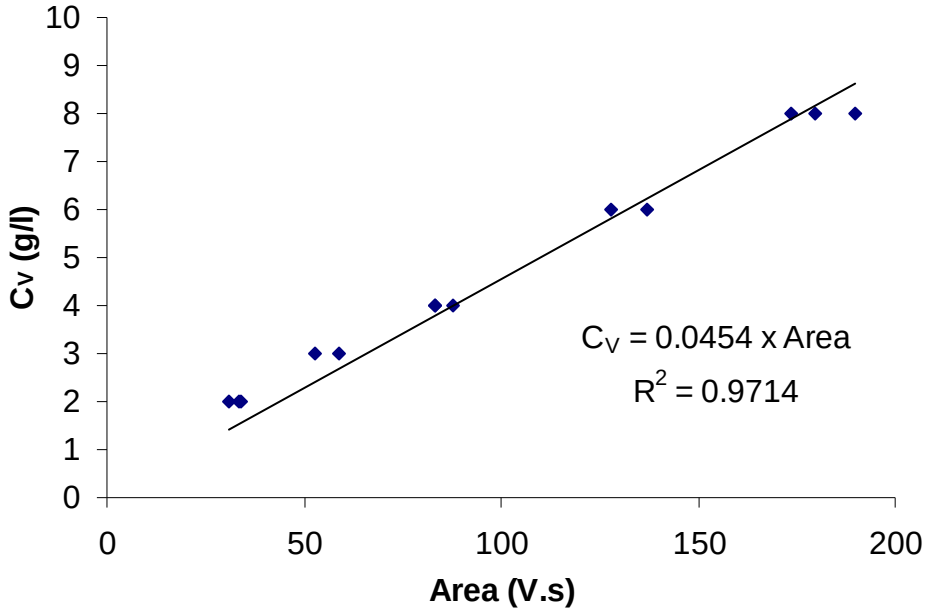

Figure 3.6. Calibration curve for the determination of vanillin concentration.

The calibration curve was prepared employing solutions with 60 g/l of lignin and 80 g/l of NaOH and also with a known concentration of vanillin. These were considered the standard solutions and suffered the same treatment as the ones collected on the batch experiments: acidification; extraction with ethyl ether and injection on the GC. The operating conditions used on the GC are detailed in Table 1. The values of all the areas, referent to standard solutions or batch experiment samples, were determined with Microcal Origin 5.0.

The pH of all samples was measured directly, using a pHmeter CRISON type 2002, previously calibrated.

3.2. Theoretical

In this section different models are presented, describing three different situations on the batch reactor:

1. Isothermal model for vanillin oxidation – this model describes an experiment where a vanillin aqueous solution is oxidized with oxygen. This description assumes no significant temperature change in the system.
2. Isothermal model for lignin oxidation – this model applies to the oxidation of lignin present in an aqueous solution with an initial pH of 14 assuming no significant temperature change in the system.
3. Non isothermal model for lignin oxidation – this model is a more general description of the reaction of lignin oxidation. It describes a batch experiment, considering temporal variations of temperature. The heating phase, before starting the reaction, is also described in order to determine heat transfer parameters necessary in the oxidation simulations.

The complete description of the different mathematical models is given below. All of them were solved using gPROMS (PSA Enterprise, United Kingdom).

3.2.1. Isothermal model for vanillin oxidation

This model was applied to describe the evolution of vanillin concentration in aqueous solution being oxidized by oxygen in a batch reactor. The assumptions of this model are the following:

- isothermal operation: temperature in all the reactor is constant over the entire reaction time
- perfectly mixed reactor: no spatial variations of any variable within the batch reactor
- constant liquid and gas volumes: volumes taken for analysis are negligible compared to the overall volume of the system
- closed system with respect to the liquid phase
- constant total pressure: the oxygen is fed to the system at a rate equal to its consumption in the reactor
- mass transfer resistances are negligible
- oxidation reactions are irreversible

A simple equation to describe the reaction system was assumed:

$$V + \upsilon_2 O_2 \xrightarrow{r_2} D \qquad (3.1)$$

where V is vanillin, O_2 is oxygen, υ_2 is the oxygen stoichiometric coefficient and D is vanillic acid. Vanillic acid was reported to be the main product formed in vanillin oxidation reactions (Bjørsvik and Liguori, 2002; Munavalli et al., 2007).

A generalized material balance on a specified control volume can be written as (Fogler, 1992):

Inlet = Outlet + Accumulated + Consumed by reaction (3.2)

With the previous assumptions the following material balance is defined:

Vanillin

$$\frac{dC_V}{dt} = -r_2 \tag{3.3}$$

where C_V is the vanillin concentration, t is time and r_2 is the rate of disappearance of vanillin.

Since the starting liquid mixture consists in an aqueous solution of vanillin, with known concentration, the initial condition for the balance (3.3) is:

$$t = 0 \qquad C_V = C_V^i \tag{3.4}$$

The rate of disappearance of vanillin was already studied at LSRE (Fargues et al., 1996a). It has two different mathematical expressions, depending on the pH of the medium:

- $pH \geq 11.5$

$$r_2 = k_2 \, C_{O2} \, C_V \tag{3.5}$$

$$k_2 = 3.61 \times 10^{10} \, \exp\left(-\frac{9706.2}{T}\right) \tag{3.6}$$

- $pH < 11.5$

$$r_2 = A \, f(pH) \, C_V^{\,2} \tag{3.7}$$

$$A = 4071 \, \exp\left(-\frac{3103.7}{T}\right) \tag{3.8}$$

$$f(pH) = \left(\frac{B \, C_{H+}}{1 + B \, C_{H+}}\right)^2 \tag{3.9}$$

$$B = 8.88 \times 10^{12} \, \exp\left(-\frac{1936.6}{T}\right) \tag{3.10}$$

where C_{O2} is the concentration of dissolved oxygen on the liquid, T is temperature, k_2, A and B are velocity reaction constants, C_{H+} is the concentration of hydrogen ions in the liquid mixture and $f(pH)$ is a function of C_{H+}.

The original definition of pH, made by Søren Lauritz Sørensen in 1909 (Ullmann's Encyclopedia, 2003), was used to calculate C_{H+}, in mol per litre of liquid:

$$C_{H+} = 10^{-pH} \tag{3.11}$$

The concentration of dissolved oxygen can be obtained with the following empirical correlation (Mathias, 1993):

$$C_{O2} = \left(3.559 - 6.659 \times 10^{-3}\ T - 5.606\ P_{O2} + 1.594 \times 10^{-5}\ P_{O2}\ T^2 + 1.498 \times 10^{3}\ P_{O2}/T\right) \times 10^{-3} \times 10^{-0.144\ I} \tag{3.12}$$

where P_{O2} is the oxygen partial pressure, in bar, and I is the ionic strength of the liquid medium, in mol per litre. In (3.12) C_{O2} is in mol per litre and T in Kelvin.

3.2.2. Isothermal model for lignin oxidation

This model is a simplified description of the oxidation of lignin in an alkaline solution, by the oxygen present in a gas mixture of N_2 and O_2. The reactor system is semi-batch: closed (batch) to the liquid and opened to oxygen. The assumptions made for this model are similar to those in section 3.2.1, for vanillin oxidation.

Since the complete reaction scheme occurring in this system is very difficult to describe with detail, a simplified representation with only two important reaction equations was employed:

Lignin oxidation

$$\alpha\ \mathrm{L} + \upsilon_1 \mathrm{O_2} \xrightarrow{r_1} \mathrm{V} + n\ others \tag{3.13}$$

Vanillin oxidation

$$V + \upsilon_2 O_2 \xrightarrow{r_2} D \qquad (3.1)$$

where L is lignin; α, υ_1 and n are, respectively, lignin, oxygen and "*others*" stoichiometric coefficients on the lignin oxidation reaction; and "*others*" represents the large number of intermediates that can be formed during lignin degradation.

Taking into consideration these assumptions the material balances for the following species are:

Vanillin

$$\frac{dC_V}{dt} = r_1 - r_2 \qquad (3.14)$$

Lignin

$$\frac{dC_L}{dt} = -\alpha\, r_1 \qquad (3.15)$$

Vanillic acid

$$\frac{dC_D}{dt} = r_2 \qquad (3.16)$$

where C_L is the concentration of lignin, and r_1 is the rate of formation of vanillin.

The liquid mixtures prepared to startup the experiments consisted on lignin alkaline solutions, so the initial conditions for (3.14), (3.15) and (3.16) are:

$$t = 0 \qquad C_V = 0 \qquad (3.17)$$

$$t = 0 \qquad C_L = C_L^i \qquad (3.18)$$

$$t = 0 \qquad C_D = 0 \qquad (3.19)$$

The mechanism for rate of formation of vanillin, r_1, is defined by (Mathias, 1993; Fargues et al., 1996a):

$$r_1 = k_1\, C_{O2}^{1.75}\, C_L \qquad (3.20)$$

$$k_1 = 1.376 \times 10^7 \ \exp\left(-\frac{E_a/R}{T}\right) = 1.376 \times 10^7 \ \exp\left(-\frac{3502}{T}\right) \tag{3.21}$$

The variation of *pH*, occurring due to lignin oxidation, can be predicted by the following equation (Fargues et al., 1996a):

$$X = Const \ M_n \left(C_L^i - C_L\right) = 0.03774 \ M_n \left(C_L^i - C_L\right) \tag{3.22}$$

for $X < 1$ N

$$pH = 14 \tag{3.23}$$

for 1 N < X < 1.9955 N

$$pH = 14 + \log_{10}(2 - X) \tag{3.24}$$

for 1.9955 N < X < 2 N

$$pH = pK_a + \log_{10}\left[\frac{x - \left(K_w \ X/K_a\right)^{1/2}}{\left(K_w \ X/K_a\right)^{1/2}}\right]; \ K_a = 10^{-pK_a} \tag{3.25}$$

for $X > 2$ N

$$pH = pK_a + \log_{10}\left(\frac{2}{X - 2}\right) \tag{3.26}$$

where the lignin concentrations are in mol per litre, M_n is the mean molecular weight of lignin, K_w is the water dissociation constant, X is a variable that encloses all possible acid products from lignin oxidation, in equivalents per litre, and K_a is the acid dissociation constant of these oxidation products. Equations (3.22) to (3.26) are valid for a solution containing, initially, two equivalents per litre of hydroxyl ions.

The rate of disappearance of vanillin, r_2, is calculated using the expressions (3.5) to (3.11), except for k_2 which is now defined as (Fargues et al., 1996a):

$$k_2 = 4.356 \times 10^6 \ \exp\left(-\frac{5530}{T}\right) \tag{3.27}$$

The kinetic constant of vanillin oxidation is higher when it occurs in the lignin oxidation medium. This is due to the presence of a greater number of intermediates created on the reactions of lignin degradation.

The concentration of dissolved oxygen, C_{O2}, can be obtained by the correlation (3.12).

3.2.3. Non isothermal model for lignin oxidation

A more general version of the model presented on 3.2.2 can be achieved considering the energy balance of the system: heat production by the oxidation reactions, heat exchanged between the system and the surroundings, liquid and gas volume variations resulting from the collection of samples, and, implicitly temperature and partial pressure variations. In this more complex model, the assumptions are:

- perfectly mixed reactor: constant spatial values of all variables within the batch reactor system
- constant total pressure
- mass transfer resistances are negligible
- irreversible oxidation reactions
- ideal behavior of the gas phase

The description of the reaction system, like in 3.2.2, is made by equations (3.13) and (3.1).

Because of the volume variations, the mass balances were defined in number of moles instead of concentrations. In this case, a molar balance over all the components in the system should be made.

Vanillin

$$\frac{dn_V}{dt} = (r_1 - r_2)\ V_l - \frac{n_V}{V_l}\ \frac{\Delta V_l}{\Delta t} \tag{3.28}$$

Lignin

$$\frac{dn_L}{dt} = -\alpha\ r_1\ V_l - \frac{n_L}{V_l}\ \frac{\Delta V_l}{\Delta t} \tag{3.29}$$

Vanillic acid

$$\frac{dn_D}{dt} = r_2 V_l - \frac{n_D}{V_l} \frac{\Delta V_l}{\Delta t} \tag{3.30}$$

Sodium hydroxide

$$\frac{dn_{NaOH}}{dt} = -\frac{n_{NaOH}}{V_l} \frac{\Delta V_l}{\Delta t} \tag{3.31}$$

Water

$$\frac{dn_{H2O}}{dt} = -\frac{n_{H2O}}{V_l} \frac{\Delta V_l}{\Delta t} \tag{3.32}$$

Oxygen in the liquid phase

$$n_{O2}^l = \left(3.559 - 6.659 \times 10^{-3}\ T - 5.606\ P_{O2} + 1.594 \times 10^{-5}\ P_{O2}\ T^2 + 1.498 \times 10^3\ P_{O2}/T\right) \times 10^{-3} \times 10^{-0.144\ I} \times V_l \tag{3.33}$$

Oxygen in the gas phase

$$n_{O2}^g = \frac{0.987\ P_{O2}\ V_g}{R\ T} \tag{3.34}$$

$$P_{O2} = P - P_{H2O} - P_{N2} \tag{3.35}$$

Liquid volume

$$V_l = V_l^i - \frac{\Delta V_l}{\Delta t}\ t \tag{3.36}$$

Gas volume

$$V_g = V_g^i + \frac{\Delta V_l}{\Delta t}\ t \tag{3.37}$$

where n_V, n_L, n_D, n_{H2O}, n_{NaOH}, n_{O2}^l and n_{O2}^g are, respectively, the number of moles of vanillin, lignin, vanillic acid, water, sodium hydroxide, oxygen dissolved in the liquid phase and oxygen in the gas phase; P, P_{O2}, P_{N2} and P_{H2O} are, respectively, the total pressure of the system, oxygen partial pressure, nitrogen partial pressure and water

vapor pressure, in bar; R is the universal gas constant, in atm l mol^{-1} K^{-1}; V_l is the liquid volume; V_g is the gas volume; ΔV_l is the volume of liquid taken from the system in each sample collection and Δt is the time interval between collection of two consecutive samples. The initial volumes of liquid and gas phase are represented by V_l^i and V_g^i.

The initial conditions for differential equations (3.28) to (3.32) are:

$$t = 0 \qquad n_V = 0 \tag{3.38}$$

$$t = 0 \qquad n_L = m_L^i \,/\, M_n \tag{3.39}$$

$$t = 0 \qquad n_D = 0 \tag{3.40}$$

$$t = 0 \qquad n_{NaOH} = m_{NaOH}^i \,/\, M_{NaOH} \tag{3.41}$$

$$t = 0 \qquad n_{H2O} = n_{H2O}^i \tag{3.42}$$

where M_{NaOH} is the molecular weight of sodium hydroxide; m_L^i and m_{NaOH}^i are the masses of lignin and sodium hydroxide, in grams, used in the preparation of the initial aqueous mixture.

Focusing on the gas phase, first the nitrogen partial pressure can be calculated applying the law of ideal gases:

$$P_{N2} = \frac{n_{N2}\, R\, T}{0.987\, V_g} \tag{3.43}$$

where n_{N2} is the number of moles of nitrogen.

During the reaction phase, n_{N2} is constant and equal to the number of moles of gas present in the system when the heating phase was started plus the number of moles introduced during the pressurization step:

$$n_{N2} = \frac{P_{atm}\, V_g^i}{R\, T_{amb}} + \frac{\Delta P\big|_{press}\, V_g^i}{R\, T^i} \tag{3.44}$$

where P_{atm} is atmospheric pressure, in atm; T_{amb} is the ambient temperature; $\Delta P\big|_{press}$ is the pressure elevation promoted in the pressurization step, in atm; and T^i is the initial temperature of the reaction phase.

The water vapor pressure can be estimated, assuming the gas is always in equilibrium with the liquid, using a temperature dependence of the type (Poling, Prausnitz and O'Connell, 2001):

$$P_{H2O} = \frac{1}{760 \times 0.987}\ \exp\left(A_0 + \frac{B_0}{C_0 + T}\right) \tag{3.45}$$

where P_{H2O} is the water vapor pressure in bar; T is the temperature in Kelvin; A_0, B_0 and C_0 are adjustable parameters depending on the system. Since the values of parameters A_0, B_0 and C_0 corresponding to pure water will lead to large errors and considering that there is no literature available with these parameters for this specific system, they were estimated from experimental data. For that, the temperature and pressure variations data collected during the heating phase of a batch experiment were employed. Considering that the pressure increase during this phase is due to the evaporation of water from the liquid and to the increase of the nitrogen partial pressure, calculated by (3.43) using a n_{N2} equal to the first term of (3.44), a set of experimental data of P_{H2O} vs. T was built. Adjusting (3.45) to this set of data an estimate for the parameters A_0, B_0 and C_0 were obtained:

$$A_0 = 18.8191\ ;\ B_0 = -3818.231\ ;\ C_0 = -87.8474 \tag{3.46}$$

The vapor pressure experimental points and the correspondent P_{H2O} vs. T curve estimated using the parameter values of (3.46) are represented on Figure 3.7.

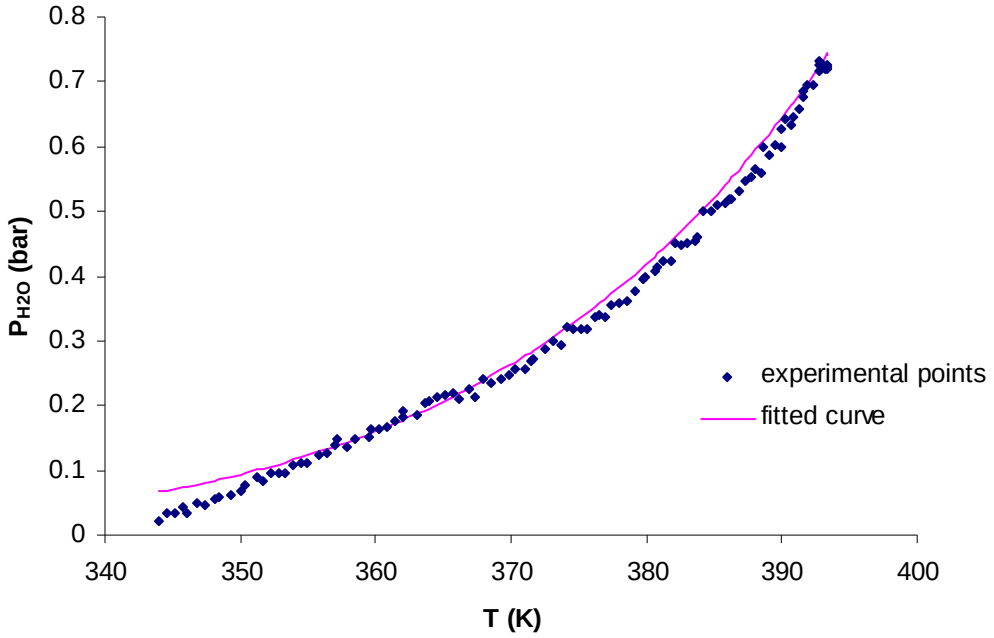

Figure 3.7. Representation of the experimental values (solid points) of vapor pressure versus temperature, obtained during the heating phase of a batch experiment, and the estimated curve (line) using equation (3.45) with parameters values given in (3.46).

The rates of reaction are also expressed in terms of number of moles, and their time unit converted to seconds, to be dimensionally consistent with the energy balance, that will be presented later in this section:

$$r_1 = \frac{k_1}{60} C_{O2}^{1.75} C_L = \frac{k_1}{60} \left(\frac{n'_{O2}}{V_l} \right)^{1.75} \frac{n_L}{V_l} \tag{3.47}$$

where k_1 is defined by (3.21).

<u>for $pH \geq 11.5$</u>

$$r_2 = \frac{k_2}{60} C_{O2} C_V = \frac{k_2}{60} \frac{n'_{O2} n_V}{V_l^2} \tag{3.48}$$

where k_2 is defined by (3.27).

<u>for $pH < 11.5$</u>

$$r_2 = \frac{A}{60} f(pH) C_V^2 = \frac{A}{60} f(pH) \left(\frac{n_V}{V_l} \right)^2 \tag{3.49}$$

The pH prediction is similar to the one described in 3.2.2, except for (3.22) that is substituted by:

$$X = 0.03774\ M_n \left(\frac{m_L^i / M_n - n_L}{V_l} \right) \tag{3.50}$$

The unsteady state energy balance to the system was derived in Appendix A and can be written as:

$$\begin{aligned} & Q - r_1 V_l \Delta H_{R,1} - r_2 V_l \Delta H_{R,2} = \\ & = \lambda_{vap}^{H2O} \left(\left[\frac{-B_0}{(C_0 + T)^2} - \frac{1}{T} \right] \frac{V_g P_{H2O}}{R T} \frac{dT}{dt} + \frac{\Delta V_l}{\Delta t} \frac{P_{H2O}}{R T} \right) + \sum n_i Cp_i \frac{dT}{dt} \end{aligned} \tag{A.13}$$

where $\Delta H_{R,1}$ is the heat of reaction of lignin oxidation; $\Delta H_{R,2}$ is the heat of reaction of vanillin oxidation; λ_{vap}^{H2O} is the heat of vaporization of water and Cp_i is the heat capacity of each species. Expanding the last term of (A.13) to all the species present in the system during lignin oxidation:

$$\begin{aligned} \sum n_i Cp_i \frac{dT}{dt} = & (n_{N2} Cp_{N2} + n_{O2} Cp_{O2} + n_L Cp_L + n_V Cp_V + n_D Cp_D + \\ & + n_{NaOH} Cp_{NaOH} + n_{H2O} Cp_{H2O} + n_{others} Cp_{others} + m_{gl} Cp_{gl}) \frac{dT}{dt} \end{aligned} \tag{3.51}$$

where Cp_{N2}, Cp_{O2}, Cp_L, Cp_V, Cp_D, Cp_{NaOH}, Cp_{H2O} and Cp_{others} are, respectively, the heat capacities of nitrogen, oxygen, lignin, vanillin, products of vanillin oxidation, sodium hydroxide, water and "*others*". The Cp_{gl} represents the heat capacity of the internal glass tube delimiting the reactor, in J kg^{-1} K^{-1}, and m_{gl} is the mass of this tube.

The balance of the heat exchanged between the system and the surroundings can be expressed by:

$$Q = U_1 A_1 (T_F - T) - U_2 A_2 (T - T_{amb}) \tag{3.52}$$

where U_1 is the overall heat transfer coefficient from the thermo fluid in the jacket to the liquid inside the reactor; A_1 is the internal area of the wall of the cylindrical glass limiting the reaction zone; U_2 is the overall heat transfer coefficient of the heat losses from the inside of the reactor to the ambient, through the top and bottom stainless steel plates; A_2 is surface area of one of these steel plates; and T_F is the average temperature of the thermo fluid that circulates inside the jacket.

Using the concept of thermal resistances (Holman, 1989), the overall heat transfer coefficients, U_1 and U_2, are defined as:

$$U_1 = \frac{1}{\frac{1}{h_{gl}} + A_1 \left[\frac{\ln(r_{ext1}/r_{int})}{2\,\pi\,L\,k_{gl}} + \frac{A_1}{A_{ext1}} \frac{1}{h_{fgl}} \right]} \tag{3.53}$$

$$U_2 = \frac{1}{\frac{1}{h_{sg}} + \frac{D_s}{k_s} + \frac{1}{h_{aus}}} + \frac{1}{\frac{1}{h_{sl}} + \frac{D_s}{k_s} + \frac{1}{h_{als}}} \tag{3.54}$$

where h_{gl} is the heat transfer coefficient from the internal glass walls to the liquid inside the reactor; h_{fgl} is the heat transfer coefficient from the thermo fluid to the external glass walls of the reactor; h_{sg} is the heat transfer coefficient from the gas inside the reactor to the internal wall of the upper steel plate; h_{aus} is the heat transfer coefficient from the external wall of the upper steel plate to the ambient; h_{sl} is the heat transfer coefficient from the liquid inside the reactor to the internal wall of the lower steel plate; h_{als} is the heat transfer coefficient from the external wall of the lower steel plate to the ambient; k_{gl} and k_s are, respectively, the thermal conductivities of the glass and the stainless steel; r_{ext1} and A_{ext1} are, respectively, the radius and the area of the external wall of the glass that limits the reaction zone; L is the height of the

cylindrical glass; r_{int} is the radius of the internal wall of the same glass; and D_s is the width of the stainless steel plates on the upper and bottom of the reactor.

Note that in equations (3.53) and (3.54) it was considered that the internal glass wall and the internal wall of the lower steel plate only contact with liquid mixture and the internal wall of the upper steel plate only contact with gas phase.

To calculate h_{gll} a correlation for heat transfer from the agitated liquid of vessels to jacketed walls was used (Perry, Green and Maloney, 1997):

$$\frac{h_{gll}\ D_r}{k_l} = a\left(\frac{D_{imp}^2\ N\ \rho_l}{\mu_l}\right)^b\left(\frac{Cp_l\ \mu_l}{k_l}\right)^{1/3}\left(\frac{\mu_b}{\mu_{lw}}\right)^m \tag{3.55}$$

The term $h_{gll}D_r/k_l$ is the Nusselt number of the liquid, in which the diameter of the reactor is D_r and k_l is the liquid thermal conductivity. The term $D_{imp}^2 N\rho_l/\mu_l$ is the Reynolds number for mixing, where D_{imp} is the impeller diameter, N is the speed of the agitator, ρ_l and μ_l are, respectively, the liquid density and viscosity. The Prandtl number is $Cp_l\mu_l/k_l$, where Cp_l is the liquid heat capacity; μ_b and μ_{lw} are the liquid viscosity at bulk and wall conditions. The recommended values for the correlation constants a, b and m, are 0.54, 2/3 and 0.14 respectively.

The heat transfer coefficient h_{fgl} results from laminar flow inside a concentric annular duct, where the equation of Chen, Hawkins and Solberg was applied (Perry, Green and Maloney, 1997):

$$Nu = \frac{h_{fgl}D_h}{k_f} = 1.02\left(\frac{\rho_f v_f D_h}{\mu_f}\right)^{0.45}\left(\frac{Cp_f\,\mu_f}{k_f}\right)^{0.5}\left(\frac{D_h}{l}\right)^{0.4}\left(\frac{D_2}{D_1}\right)^{0.8}\left(\frac{\mu_f}{\mu_{fw}}\right)^{0.14} Gr^{0.05}$$
$$Gr = \frac{\beta_f \Delta T_f\, g\ D_h^3 \rho_f^2}{\mu_f^2} \tag{3.56}$$

where D_h is the hydraulic diameter; k_f is the thermal conductivity of the thermo fluid; ρ_f is the fluid density; μ_f is the viscosity of the fluid; v_f is the fluid velocity and Cp_f is the fluid heat capacity; D_1 is the diameter of the inner wall and D_2 the diameter of the outer wall. The term $\rho_f v_f D_h / \mu_f$ is the Reynolds number for the flow of the thermo fluid in a hypothetical circular cross sectioned tube, with diameter D_h. The Grashof number is $\beta_f \Delta T\, g\, D_h^3 \rho_f^2 / \mu_f^2$, where β_f is volume coefficient of expansion of the thermo fluid, ΔT_f is the difference between the bulk and wall temperatures, and g is the gravitational constant. All fluid properties were evaluated at the mean bulk temperature, except for μ_{fw}, that is the fluid viscosity at the wall temperature. The hydraulic diameter is defined as (Holman, 1989):

$$D_h = \frac{4A_f}{p_f} = \frac{D_2^2 - D_1^2}{D_2 + D_1} = D_2 - D_1 \tag{3.57}$$

The cross sectional area of the flow is A_f and p_f is the wetted perimeter.

It was assumed that coefficient h_{sl} results from a phenomenon similar to h_{gll}, so the same correlation was used:

$$\frac{h_{sl} D_r}{k_l} = 0.54 \left(\frac{D_{imp}^2 N\ \rho_l}{\mu_l} \right)^{2/3} \left(\frac{Cp_l\ \mu_l}{k_l} \right)^{1/3} \left(\frac{\mu_b}{\mu_{lw}} \right)^{0.14} \tag{3.58}$$

The coefficient h_{als} is expressed as a free convection heat transfer coefficient from the lower surface of a heated horizontal flat plate (Holman, 1989):

$$Nu_a = \frac{h_{als}\ L_s}{k_a} = 0.27\ Ra_a^{1/4} \qquad for\ 10^5 \langle\ Ra_a \langle\ 10^{11} \tag{3.59}$$

$$Ra_a = Gr_a\, Pr_a = \frac{g\ \beta_a\ \Delta T_a L_s^3\ \rho_a^2}{\mu_a^2}\ \frac{Cp_a\ \mu_a}{k_a} \tag{3.60}$$

$$L_s = \frac{A_2}{P_s} = \frac{D_s}{4} \tag{3.61}$$

where A_2, P_s and D_s are, respectively, the surface area, the perimeter and the diameter of the steel plate; L_s is the characteristic dimension of the steel plate; Gr_a and Pr_a are the Grashof and Prandtl numbers of the air, and their product is the Rayleigh number, Ra_a; k_a, ρ_a, μ_a and Cp_a are the thermal conductivity, density, viscosity and heat capacity of the air; β_a is the volume coefficient of expansion of the air, and for ideal gases is the inverse of its absolute temperature; ΔT_a is the temperature difference between the bulk and the steel plate wall; and g is the gravitational constant. All the properties of the air should be determined at the film temperature, which is the arithmetic average between the bulk and the wall temperatures.

As already mentioned before, the upper steel plate has an important difference, with respect to heat losses from the lower steel plate: it has a cooling coil with tap water flowing through. Since this situation appears to represent an important uptake of heat from the system, and is very difficult to quantify theoretically, at least with some degree of accuracy, some alternative way has to be provided to account for it. The approach followed assumes the coefficient h_{aus} is composed of two implicit terms: heat loss from the steel plate to the ambient air and to the water flowing inside the coil.

A proper correlation to predict theoretically the heat transfer coefficient h_{sg} was also not available for this system. For this reason, in equation (3.54) the term $1/h_{sg} + 1/h_{aus}$ is unknown. In order to obtain a value for this sum of thermal resistances, the temperature data from the heating phase of a batch experiment was used to estimate U_1 and U_2. With these values the local heat transfer coefficients obtained

by the empirical correlations described above can be checked and calculate an experimental based $1/h_{sg} + 1/h_{aus}$.

The estimation of the global heat transfer coefficients, using experimental temperature data, obliges to modeling the heating phase of the batch reactor. Inside this reactor are a liquid mixture of lignin, sodium hydroxide and water, and a gas consisting only in nitrogen. This model is described in the following lines.

Heating phase

In this heating experiment there is no flow entering or exiting the system and it is assumed that there is no reaction between the species (no source of heat by reaction). The only variation on the number of moles will be on the water in the liquid and gas phases, since vaporization is promoted by the temperature increase:

$$\frac{dn^{l}_{H2O}}{dt} = -\frac{dn^{g}_{H2O}}{dt} \tag{3.62}$$

Introducing these assumptions in the energy balance (A.4):

$$Q = \left(H^{g}_{H2O} - H^{l}_{H2O}\right) \frac{dn^{g}_{H2O}}{dt} + \sum n_i \frac{dH_i}{dt} = \lambda^{vap}_{H2O} \frac{dn^{g}_{H2O}}{dt} + \sum n_i \frac{dH_i}{dt} \tag{3.63}$$

There is no volume variation in the phases inside the reactor, so (A.11) becomes:

$$\frac{dn^{g}_{H2O}}{dt} = \left[\frac{-B_0}{(C_0 + T)^2} - \frac{1}{T}\right] \frac{V_g \; P_{H2O}}{R \; T} \frac{dT}{dt} \tag{3.64}$$

Substituting into (3.63):

$$Q = \left[\lambda^{vap}_{H2O} \frac{P_{H2O} \, V_g}{R \, T} \left(\frac{-B_0}{(C_0 + T)^2} - \frac{1}{T}\right) + \sum n_i \; Cp_i\right] \frac{dT}{dt} \tag{3.65}$$

The heat exchanges to the system from the surroundings, Q, is expressed by (3.52). The global and local heat transfer coefficients are defined as it was described above.

In the heating experiment, the temperature of the thermo fluid in the heating phase T_F is increasing until it reaches the defined set point. To avoid the development of another energy balance and the necessity to estimate more parameters, T_F was adjusted as a polynomial function of the heating time and used directly into (3.52).

3.3. Vanillin oxidation

3.3.1. Results

The experimental results of oxidation of vanillin obtained at LSRE by Claire Fargues will be analyzed and compared to the mathematical model presented in section 3.2.1 for validation.

The more important reaction conditions on this oxidation, that can be experimentally modified, are P_{O2}, T and pH.

According to equations (3.5) and (3.7) the influence of oxygen partial pressure is important only for pH higher than 11.5. For this reason, the influence of this parameter should be evaluated employing the proper range of pH values. The experimental results of vanillin oxidation for various oxygen partial pressures (with an initial pH of 14) previously obtained at LSRE (Fargues et al., 1996b) are presented in Figure 3.8. The solid lines in Figure 3.8 correspond to the simulation results at different P_{O2} and pH of 14.

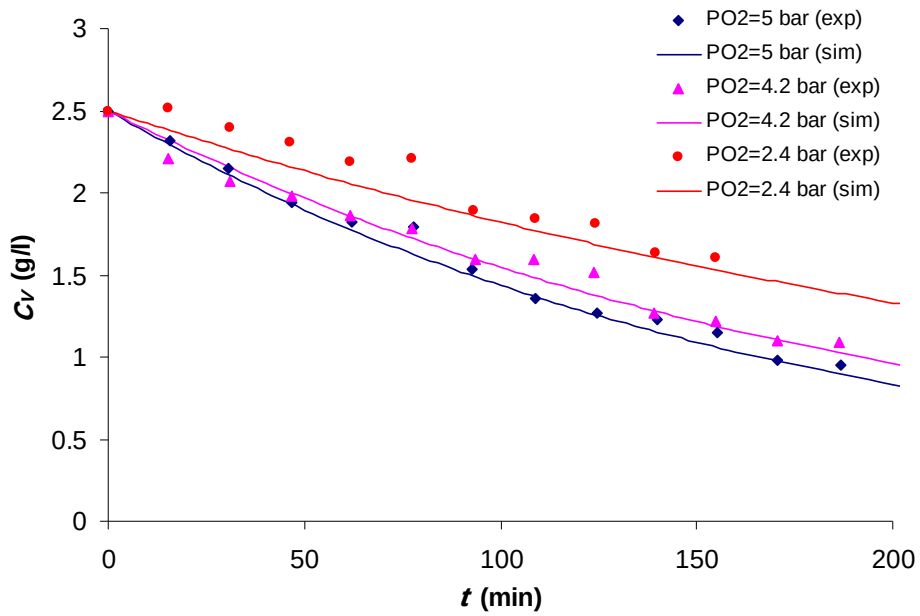

Figure 3.8. Vanillin concentration (C_V) variation in batch experiments of vanillin oxidation at three different oxygen partial pressures (5, 4.2 and 2.4 bar). The initial solution had a vanillin concentration of 2.5 g/l, a *pH* of 14, and the reaction temperature was 141ºC. Solid lines correspond to simulations using the isothermal model for vanillin oxidation presented in section 3.2.1. Data from Fargues et al. (1996b).

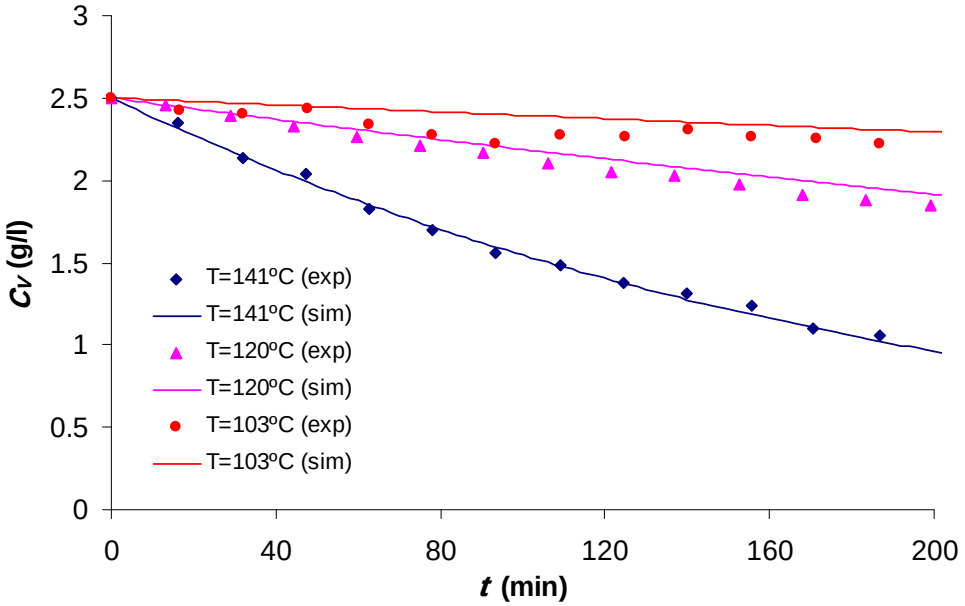

Figure 3.9. Vanillin concentration (C_V) variation in batch experiments of vanillin oxidation at three different temperatures (141, 120 and 103ºC). The initial solution had a vanillin concentration of 2.5 g/l, a *pH* of 14, and the oxygen partial pressure was 4.3 bar. Solid lines correspond to simulations using the isothermal model for vanillin oxidation presented in section 3.2.1. Data from Fargues et al. (1996b).

Other process condition that can be modified is temperature. The effect of temperature in vanillin oxidation in strong alkaline medium is presented in Figure 3.9.

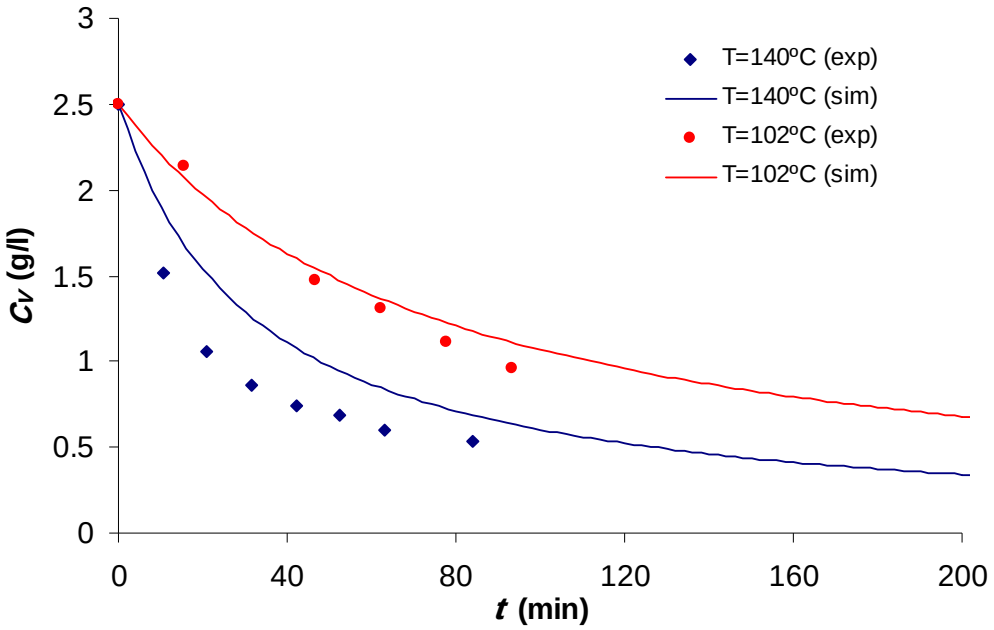

Figure 3.10. Vanillin concentration (C_V) variation in batch experiments of vanillin oxidation at two different temperatures (140 and 102ºC). The initial solution had a vanillin concentration of 2.5 g/l, a *pH* of 9.8, and the oxygen partial pressure was 4 bar. Solid lines correspond to simulations using the isothermal model for vanillin oxidation presented in section 3.2.1. Data from Fargues et al. (1996b).

For a *pH* of 14, the temperature has an important effect on the rate of reaction, and thus, on increasing the vanillin consumption (or degradation). Comparing the results using different temperatures it can be observed that for a reaction time of approximately 186 minutes, at 103ºC 12% of the initial vanillin presented in the solution was degraded while at 141ºC, 58% of the initial lignin was consumed (final concentration of 2.22 and 1.05 g/l for 103 and 141ºC, respectively).

If *pH* 's lower than 11.5 are employed the influence of the process variables is different. The oxidation of vanillin at *pH* = 9.8 is presented in Figure 3.10 for different temperatures. In this image it can be observed that a faster decay is observed at both

temperatures because of the decrease in pH. In this curves, the effect of temperature is less pronounced than at higher pH. Even though, for a reaction time of 186 minutes at 102ºC a consumption of 72% of initial vanillin was observed and this consumption increases to 86% at 140ºC. To observe in more detail the importance of pH in the oxidation of vanillin, several experiments at constant oxygen partial pressure and temperature are presented in Figure 3.11 for different alkaline pH:

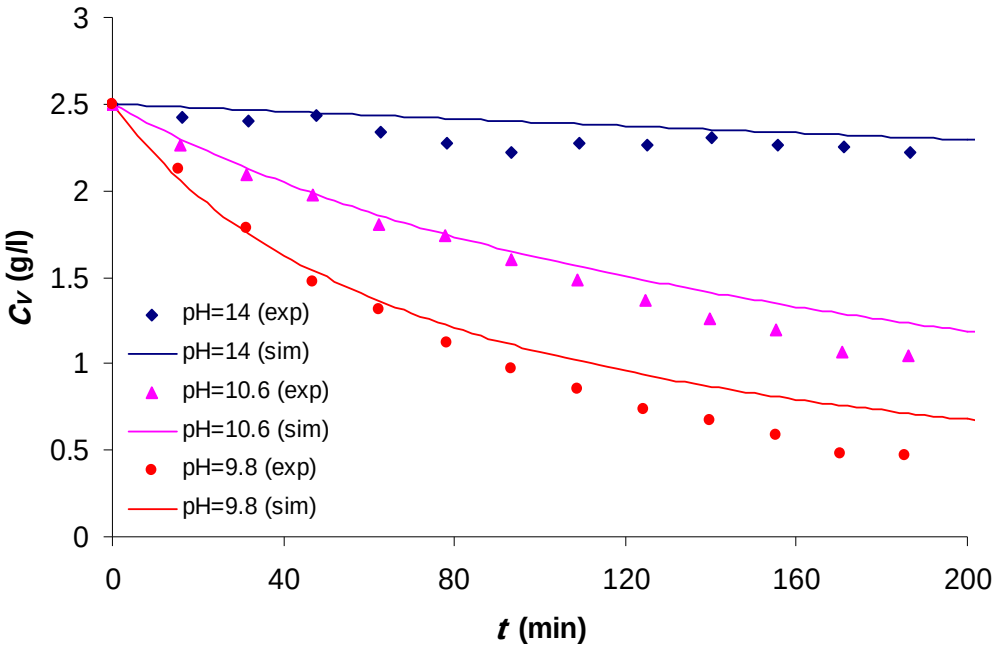

Figure 3.11. Vanillin concentration (C_V) variation in batch experiments of vanillin oxidation at three different pH's (14, 10.6 and 9.8). The initial solution had a vanillin concentration of 2.5 g/l, the temperature was 103ºC, and the oxygen partial pressure was 4.3 bar. Solid lines correspond to simulations using the isothermal model for vanillin oxidation presented in section 3.2.1. Data from Fargues et al. (1996b).

In order to complete the validation of the model for vanillin oxidation, simulations for different initial vanillin concentrations were made, keeping other reaction conditions constant. The simulation results together with the correspondent experimental data (Fargues et al., 1996b) are depicted in Figure 3.12.

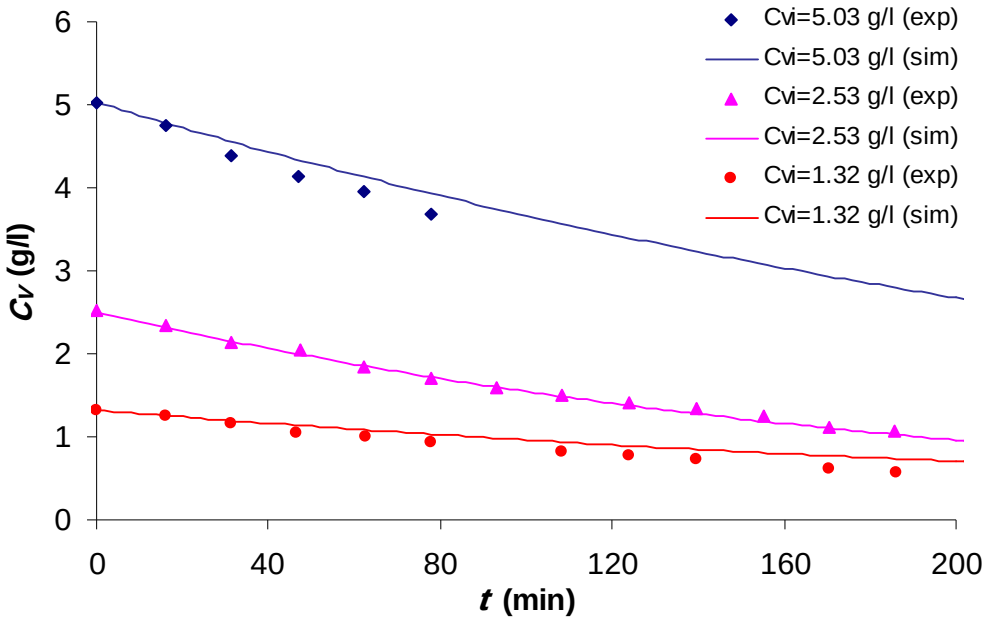

Figure 3.12. Vanillin concentration (C_V) variation in batch experiments of vanillin oxidation at three different initial vanillin concentrations (5.03, 2.53 and 1.32 g/l). The temperature was 141ºC, pH of 14 and the oxygen partial pressure was 4.2 bar. Solid lines correspond to simulations using the isothermal model for vanillin oxidation presented in section 3.2.1. Data from Fargues et al. (1996b).

3.3.2. Discussion

According to the experimental data already available (Fargues et al., 1996b), it was observed that the mathematical model proposed in section 3.2.1 was able to predict the behavior of vanillin oxidation for different operating conditions as shown in Figures 3.8 to 3.12. It is important to validate the model for vanillin degradation separately to ensure that its degradation can be well predicted in the lignin oxidation experiments, where vanillin will unfortunately be also oxidized.

Focusing on the three main variables that can be manipulated on the system, some observations should be pointed out:

- According to the r_2 expressions, the influence of oxygen partial pressure in the vanillin oxidation is important only for very high pH values. This

influence, however, is not as strong as the other process variables evaluated (T and pH).

- Temperature has a very important role on vanillin consumption, since it affects directly the velocity reaction constants. For higher temperatures, the rates of reaction (and consequently the vanillin consumption) get higher as observed in Figure 3.9. However, this influence appears to be more visible at pH > 11.5, because at lower values of pH both the temperature and pH contribute to the C_V decrease.
- When the pH decreases to values below 11.5, the consumptions of vanillin increases in a very pronounced way, as expected from (3.5) to (3.10). The important degradation of vanillin at lower pH and can be observed on Figure 3.11. This change of behavior on the evolution of vanillin concentration is attributed to a switch on the predominant type of mechanism of vanillin degradation, from bimolecular ionic to free radical formation, which reveals to be much faster when pH is very alkaline (Mathias, 1993).

The important role of pH on vanillin oxidation, emphasized above, reveals the necessity to take this variable into special consideration in the subsequent work, when the goal is to produce vanillin from lignin oxidation.

3.4. Lignin oxidation

As the mechanism of vanillin and lignin was previously studied at LSRE, in this work two batch experiments of lignin oxidation were performed, following the procedures described on section 3.1.2 and 3.1.3. These new experiments had the purpose of testing a new raw material available, since lignin composition is not constant

for all sources of lignin. The batch experiments were performed with Kraft lignin Indulin AT kindly supplied by Westvaco Co. The experimental conditions used in the lignin oxidation experiments are summarized on Table 3.2.

Table 3.2. Experimental conditions used in the batch experiments of lignin oxidation.

Experiment 1		**Experiment 2**	
C^{i}_{NaOH} (g/l)	80	C^{i}_{NaOH} (g/l)	80
C^{i}_{L} (g/l)	60	C^{i}_{L} (g/l)	60
T^{i} (ºC)	123	T^{i} (ºC)	123
P(bar)	9	P(bar)	9.5
P^{i}_{O2} (bar)	4	P^{i}_{O2} (bar)	6.5
Agitation (rpm)	1100	Agitation (rpm)	1100

The experimental and simulation results of vanillin concentration, pH and reactor temperature, obtained for both experiments, are presented below.

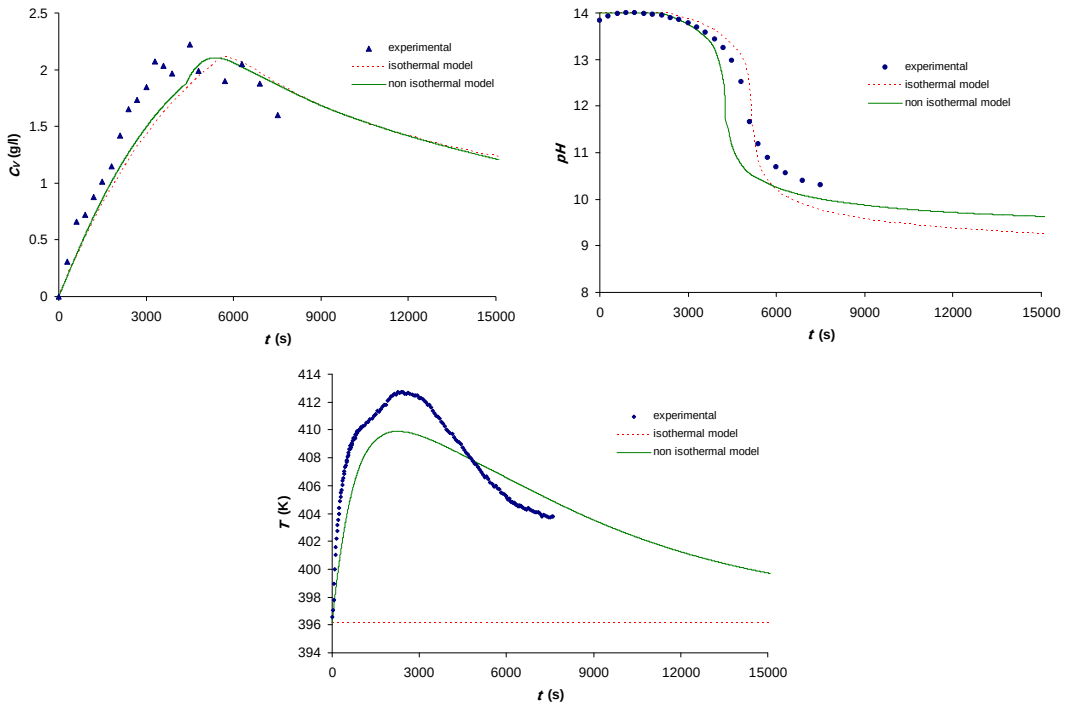

Figure 3.13. Vanillin concentration (C_V), pH and reactor temperature (T) variations in batch experiment 1. The experimental conditions used are in Table 3.2. Red and green solid lines correspond respectively to simulations using the isothermal model (section 3.2.2) and the non isothermal model (section 3.2.3) for lignin oxidation.

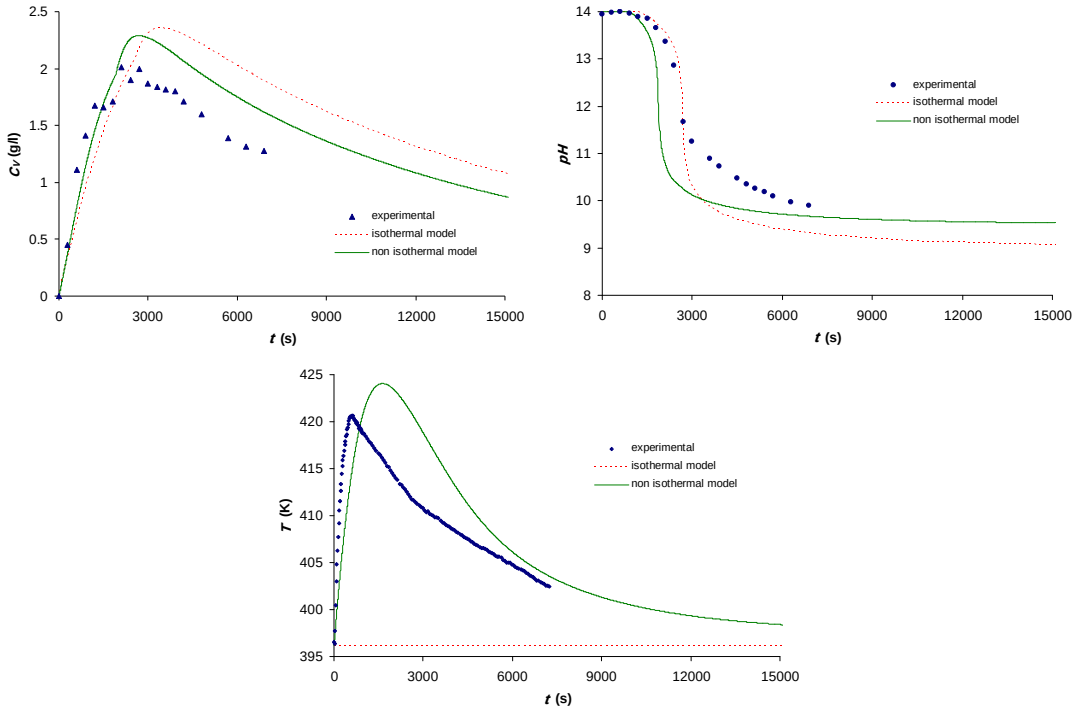

Figure 3.14. Vanillin concentration (C_V), pH and reactor temperature (T) variations in batch experiment 2. The experimental conditions used are in Table 3.2. Red and green solid lines correspond respectively to simulations using the isothermal model (section 3.2.2) and the non isothermal model (section 3.2.3) for lignin oxidation.

Looking at the results above, it can be concluded that the maximum vanillin yield with respect to lignin mass was 3.7 % and 3.4 %, respectively for experiment 1 and 2.

The first step to perform with these experiments was to compare their results with the ones obtained Alvaro Mathias (Mathias, 1993), on similar experimental conditions. The comparison is represented in Figure 3.15, using the C_V obtained in experiment 1 of Table 3.2, and experiment 11 of Mathias's thesis performed at the same operating conditions (Mathias, 1993). Comparing the results, two facts are visible: a maximum C_V approximately two times lower for experiment 1, and the correspondent time of reaction two times higher. These facts revealed that the lignin Indulin AT should be different from the one used by Mathias, requiring the modification of some of the original parameter values on the kinetics and pH prediction expressions, in order to

adjust them to a new reality. To obtain a first estimative of these parameter adjustments it was used the simplified model of section 3.2.2 for isothermal lignin oxidation.

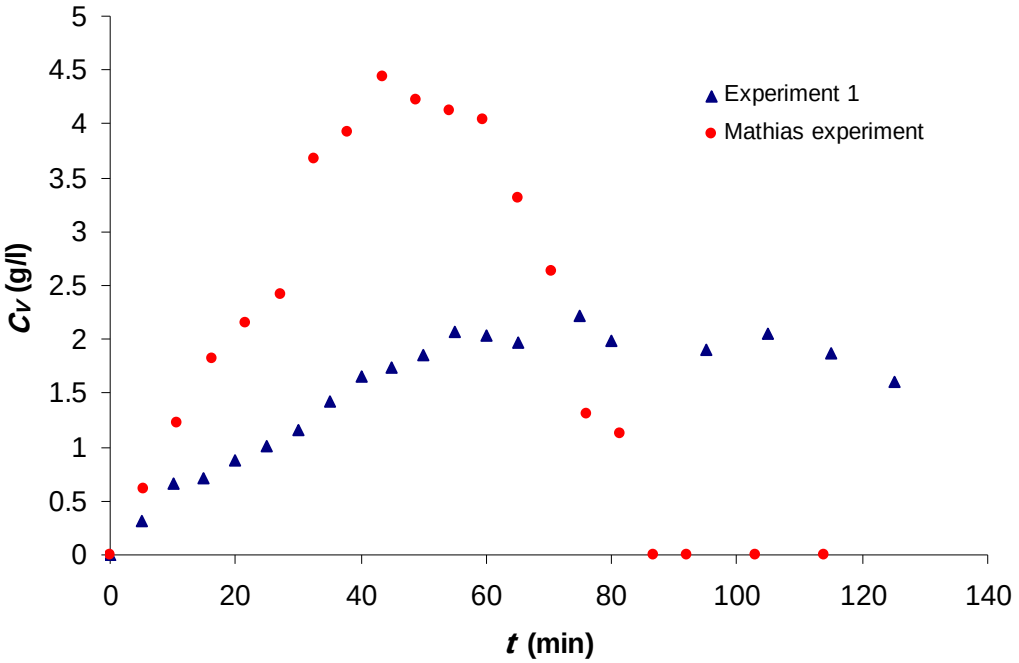

Figure 3.15. Vanillin concentration (C_V) curves for batch experiment 1 and Mathias experiment 11. Data from Mathias (1993).

3.4.1. Isothermal conditions

In order to use the model described in 3.2.2, it was necessary to obtain values for the parameters M_n and α. On the simulations presented in this section and in Figures 3.13 and 3.14, it was used a M_n of 2325 g/mol and a α of 0.5.

The value of M_n was determined experimentally as it is described on Appendix B. To estimate α it was assumed that the maximum possible conversion of lignin in vanillin is 13% in mass basis (Mathias, 1993), value obtained in oxidation with nitrobenzene. Knowing this, it can be written that:

$$\alpha = \frac{n_L}{n_V} = \frac{m_L/M_n}{m_V/M_V} = \frac{m_L/M_n}{0.13\ m_L/M_V} \tag{3.66}$$

Replacing the correspondent values for the raw material (Indulin AT) of this thesis:

$$\alpha = \frac{1/2325}{0.13/152.06} = 0.5$$

The main purpose of the model derived in 3.2.2 was to simplify a first approach on simulating the real system of lignin oxidation on the batch reactor. This approach consisted, essentially, on studying the effects of some parameters that are theoretically dependent on lignin structure, and obtaining new values for them that better describe the experiments performed. However, first it must be known which parameters should have their values adjusted.

Since the results of experiment 1 revealed a slower lignin oxidation and levels of conversion lower than was expected, it means that if it the mass transfer resistances are negligible, which is the case, the degradation of the main reagent (lignin) is more difficult, either by the presence of different structural units on its molecule and/or bonds harder to break or attack. These hypotheses can be mathematically translated by raising the activation energy of the lignin oxidation. So, one of the parameters to adjust was E_a/R, from equation (3.21).

Another parameter that is strictly related to the lignin structure is $Const$ on (3.22). This parameter empirically relates the quantities of oxidized lignin to the correspondent equivalents of acid products formed. It is then obvious that $Const$ will be extremely dependent on the structural units present on the initial polymer molecule.

At this point the effect of parameters E_a/R and $Const$ on the system responses was studied with respect to C_V and pH. For this purpose, some simulations were made with the isothermal model for lignin oxidation, varying the values of E_a/R and $Const$. The results are presented in Figures 3.16 and 3.17.

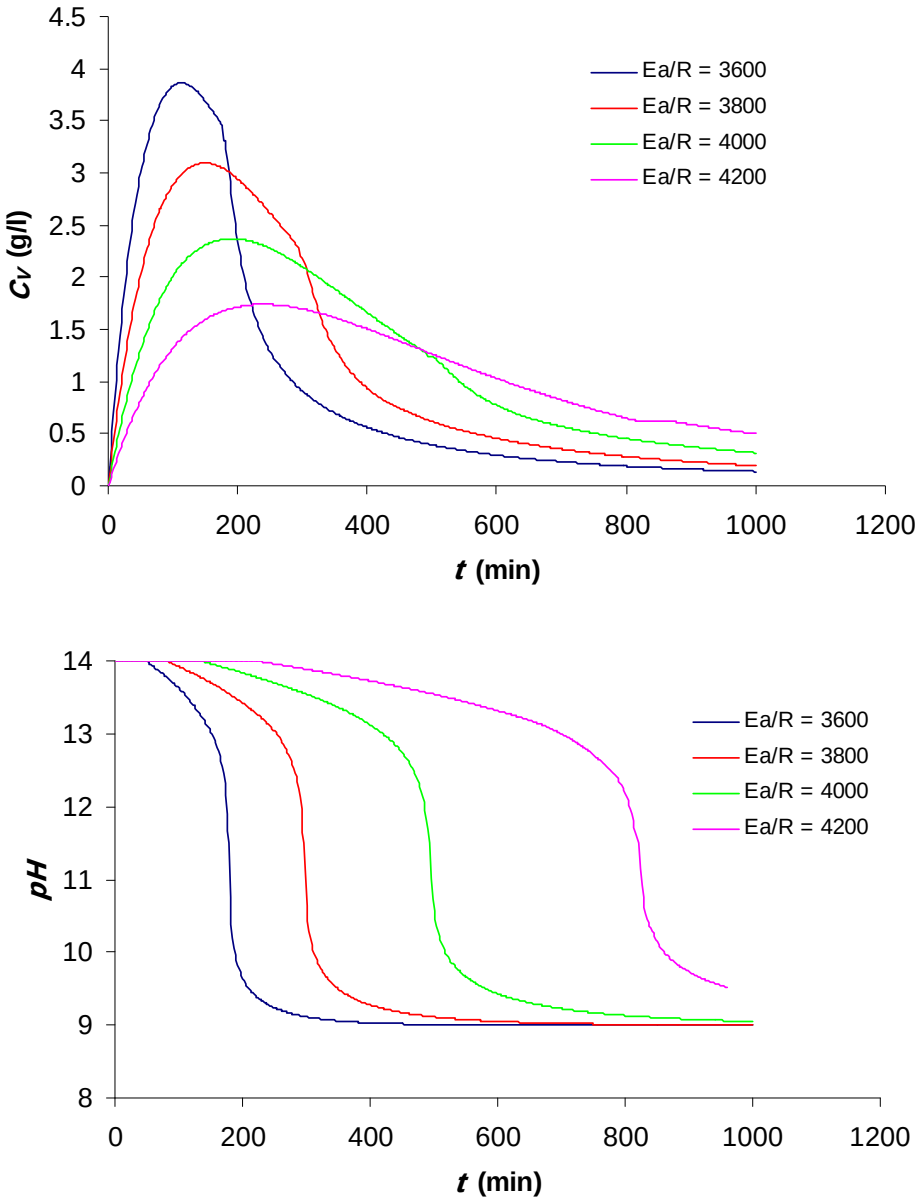

Figure 3.16. Vanillin concentration (C_V) and pH simulation curves, using different values of E_a/R, and $Const$ of 0.03774.

On the C_V curves of Figure 3.16, it can be seen that raising the value of E_a/R results on decreases of the maximum vanillin concentration and increases of the correspondent time of reaction, which goes in the right direction for adjusting the experimental results obtained in this work. However, it is also true that the correspondent pH simulation curves reveal very pronounced increases in the time of their inflection points, which goes in the opposite direction for adjusting the

experimental pH curves. It can be concluded that with higher E_a/R values it is possible to simulate the experimental evolution of vanillin concentration, but the correspondent pH curves will be even farther from the experimental results, than the ones obtained with the original E_a/R. This fact proves that is necessary to adjust both parameters, E_a/R and $Const$, in order to describe the reaction system of this thesis.

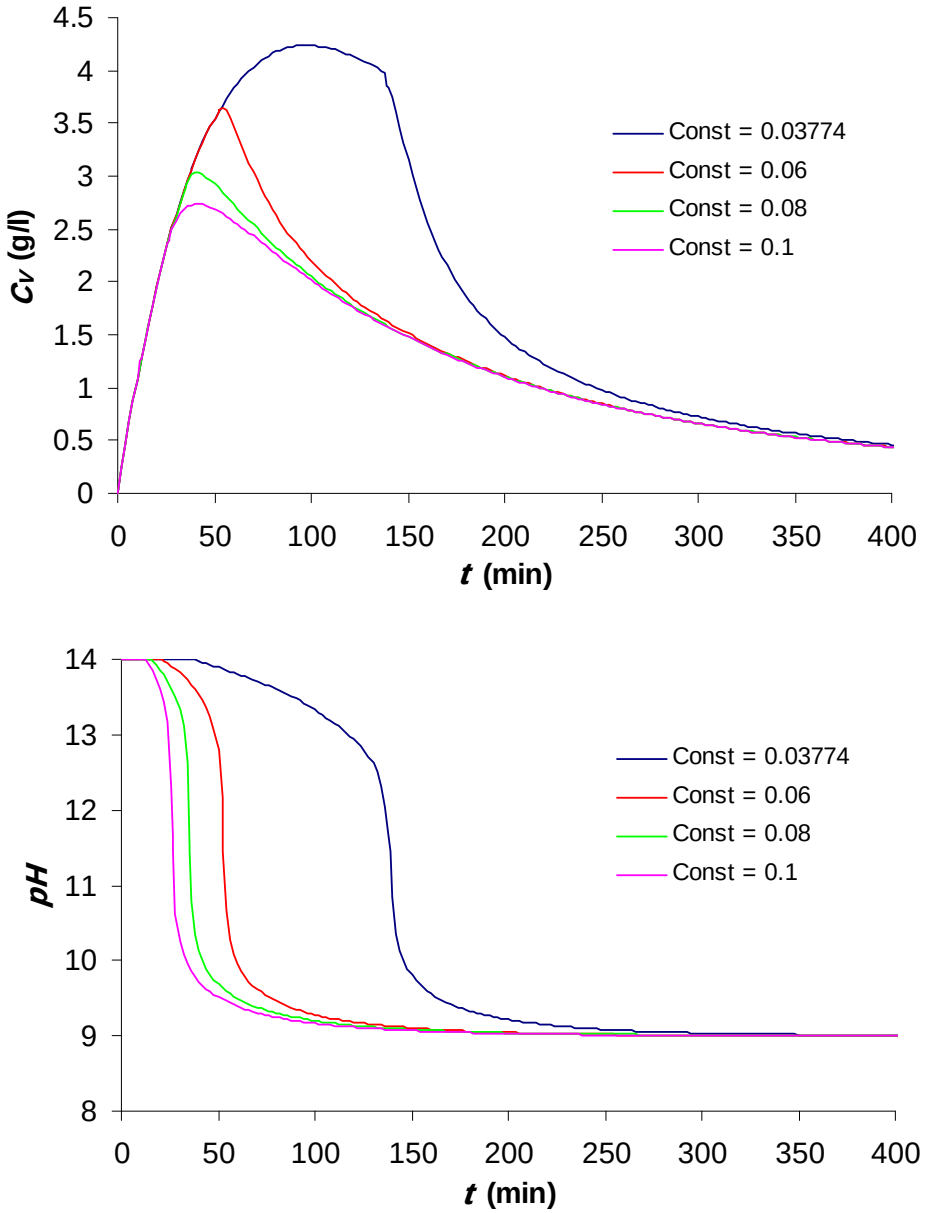

Figure 3.17. Vanillin concentration (C_V) and pH simulation curves, using different values of $Const$, and E_a/R of 3502.

To obtain a starting point of E_a/R for the parameter estimation, it was considered that in the initial moments of reaction there is no vanillin oxidation, so the accumulation of vanillin resumes only to the r_1 term. The initial values of vanillin accumulation can be obtained as the slope of the experimental C_V curve, allowing to calculate an experimental k_1:

$$k_1 = \frac{dC_V/dt\big|_{t=0}}{C_{O2}^{1.75}\, C_L} \tag{3.67}$$

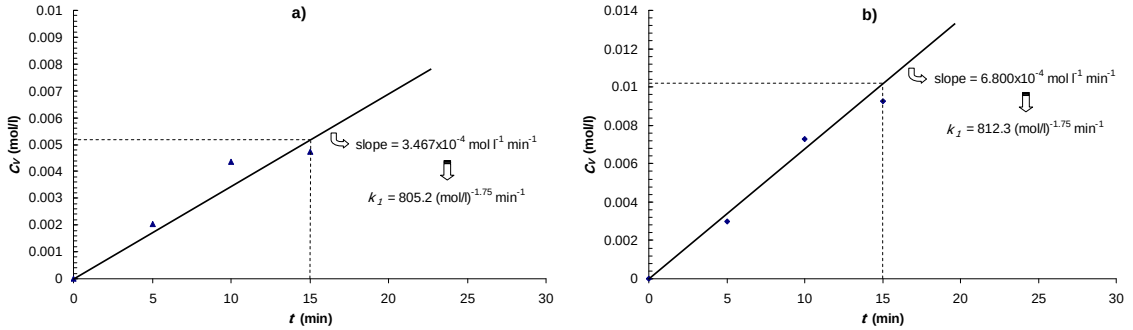

Figure 3.18. Vanillin concentration (C_V) curves for the initial moments of reaction, and determination of $dC_V/dt\big|_{t=0}$ and experimental k_1 values. a) Experiment 1; b) Experiment 2.

Substituting k_1 on (3.21) by the medium value from the two experimental k_1 determined in Figure 3.18, an initial approximation for E_a/R can be calculated and used in a subsequent parameter estimation. The value encountered was 3856. Then it was performed a parameter estimation, using gPROMS software, with an initial estimative of 3856 and 0.03774, respectively for E_a/R and $Const$. The final results obtained were 3960 and 0.098. The correspondent simulations results are present on Figures 3.13 and 3.14.

Observing these two figures it can be said that, with the estimated E_a/R and $Const$, the isothermal model for lignin oxidation describes reasonably well the experimental results. This fact can be also checked calculating a final value of $Const$,

using the inflection point of pH experimental curves and the simulation lignin concentration correspondent to that time of reaction, and comparing it to $Const$ used to run the simulation. Since the inflection point on the pH occurs when the number of equivalents of the acid products formed, X, equals the number of equivalents of sodium hydroxide in the initial liquid mixture, it can be written:

$$Const_{final} = \frac{C^{i}_{NaOH} \cdot 0.5}{M_n \cdot \left(C^{i}_{L} - C_L\right)} \tag{3.68}$$

With (3.68) it was obtained for experiment 1 a $Const_{final}$ of 0.0974, and for experiment 2 a $Const_{final}$ of 0.0937. Comparing to the parameter value used for both simulations, 0.098, it represents deviations of 0.6 % and 4.4 %, respectively.

However this simplified model can describe reasonably well the lignin oxidation on the batch reactor, with respect to the evolution of C_V and pH, it is not a realistic approximation to consider isothermal operation when in fact, during an experiment, the temperature suffers increases in the range of 15-20ºC, due to the high heats of reaction involved. So, for a better description of this system, it was used the general model of section 3.2.3, with a first estimative for E_a/R and $Const$ of 3960 and 0.098 respectively.

3.4.2. Non isothermal conditions - heating phase

Like it was described on section 3.2.3, the data of the heating phase of batch experiment 1 was used to estimate values of the global heat transfer coefficients, U_1 and U_2. The system was defined by the equations (3.62) to (3.65), (3.52) and:

$$T_F = 336.4 + 7.75\times10^{-2}\ t - 2.56\times10^{-5}\ t^2 + 4.23\times10^{-9}\ t^3 - 2.76\times10^{-13}\ t^4 \tag{3.69}$$

where the known parameters and constants are in Table 3.3.

Table 3.3. Constants and parameters used in the system definition during the heating phase.

Cp_L	4586 J mol^{-1} K^{-1}	M_n	2325 g mol^{-1}	ρ_l	1114 kg m^{-3}
Cp_{NaOH}	59.37 J mol^{-1} K^{-1} (*)	n_L	0.0129 mol	V_g	0.5 l
Cp_{H2O}	75.80 J mol^{-1} K^{-1} (**)	n_{NaOH}	1 mol	A_1	4.66x10^{-2} m^2
Cp_{N2}	29.23 J mol^{-1} K^{-1} (**)	n_{H2O}	27.06 mol	A_2	1.77x10^{-2} m^2
λ_{H2O}^{vap}	40626 J mol^{-1} (***)	n_{N2}	0.0202 mol	R	0.082 l atm mol^{-1} K^{-1}
Cp_{gl}	836 J kg^{-1} K^{-1} (+)	m_{gl}	1.007 kg		

(*) – (Yaws, 1999); (**) – (Holman, 1989); (***) – (Smith, Van Ness and Abbott, 1996)
(+) – (Perry, Green and Maloney, 1997)

The number of moles of nitrogen was calculated by the first term of equation (3.44). The number of moles of lignin and sodium hydroxide were obtained by:

$$n_L = \frac{m_L^i}{M_n} = \frac{30}{2325} = 0.0129 \ mol \ ; \ n_{NaOH} = \frac{m_{NaOH}^i}{M_{NaOH}} = \frac{40}{40} = 1 \ mol$$

The liquid density, ρ_l, was experimentally determined as described on Appendix C. With this value it can be calculated the number of moles of water, n_{H2O}:

$$n_{H2O} = \frac{m_{H2O}}{M_{H2O}} = \frac{\rho_l V_l - m_L^i - m_{NaOH}^i}{18} = \frac{487}{18} = 27.06 \ mol$$

The heat transfer areas, A_1 and A_2, were obtained considering them surfaces of a cylinder and a circular plate, respectively. In the case of A_2 the correspondent diameter used is a medium value, since it is not the same on the entire thickness of the steel plates.

$$\begin{aligned} A_1 &= 2 \ \pi \ r_{\text{int}} L \\ A_2 &= \pi \ (r_{med})^2 = \pi \ (0.075)^2 \end{aligned} \qquad (3.70)$$

The heat capacity Cp_L was obtained using the Missenard group additivity method (Poling, Prausnitz and O'Connell, 2001) based on a structural model of Kraft lignin (Knowles, 1998). This estimation procedure is presented on Appendix D. With this procedure it was calculated a lignin heat capacity of 4586 J mol^{-1} K^{-1}, for the medium temperature of the heating process (373.15 K).

The parameter estimation was performed with the software gPROMS for U_1 and U_2, the final results were 73.32 and 77.42 W m^{-2} K^{-1}. The correspondent simulation is presented on Figure 3.19.

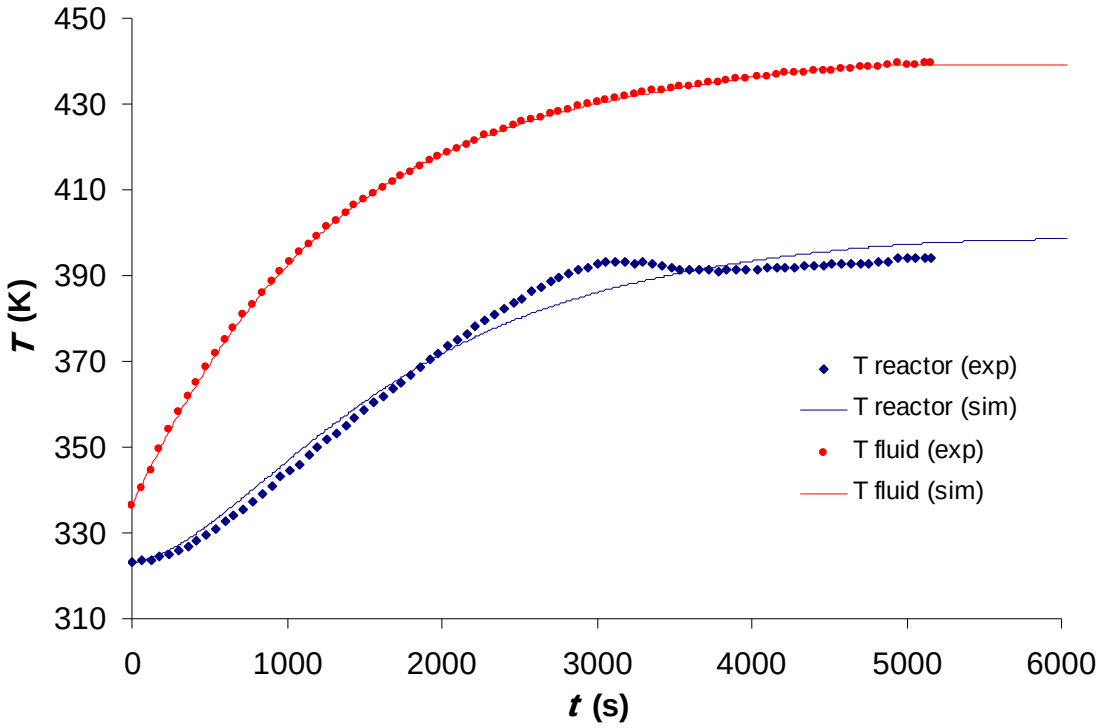

Figure 3.19. Reactor (T) and thermo fluid (T_F) temperature curves for batch experiment 1. Solid lines correspond to the simulations with U_1 of 73.32 W m^{-2} K^{-1} and U_2 of 77.42 W m^{-2} K^{-1}.

The local heat transfer coefficients were estimated with appropriate correlations, as described on section 3.2.3, and the results are in the Table 3.4. These values were obtained using a series of physical and thermodynamic properties of the fluids and materials involved, which are resumed on Table 3.5.

Table 3.4. Values estimated for the local heat transfer coefficients.

h_{sl}	6686 W m^{-2} K^{-1}	h_{gll}	6763 W m^{-2} K^{-1}
h_{als}	4.22 W m^{-2} K^{-1}	h_{fgl}	107.9 W m^{-2} K^{-1}

Table 3.5. Properties used on predicting the local heat transfer coefficients.

Liquid mixture					
k_l	0.682 W m^{-1} K^{-1}	μ_l	2.013x10^{-3} kg m^{-1} s^{-1}	μ_{lw}	G - 1.615x10^{-3} kg m^{-1} s^{-1}
ρ_l	1114 kg m^{-3}	Cp_l	3956 J kg^{-1} K^{-1}		S - 2.184x10^{-3} kg m^{-1} s^{-1}
Thermo fluid					
k_f	0.166 W m^{-1} K^{-1} (*)	μ_f	1.641x10^{-2} kg m^{-1} s^{-1}	μ_{fw}	1.870x10^{-2} kg m^{-1} s^{-1}
ρ_f	1028 kg m^{-3}	Cp_f	1996 J kg^{-1} K^{-1} (*)	β_f	7.8 x10^{-3} K^{-1} (**)
Air					
k_a	0.0282 W m^{-1} K^{-1} (+)	μ_a	1.964x10^{-5} kg m^{-1} s^{-1} (+)	β_a	0.0031 K^{-1}
ρ_a	1.085 kg m^{-3} (+)	Cp_a	1007 J kg^{-1} K^{-1} (+)		
Materials thermal conductivity					
k_{gl}	1.1 W m^{-1} K^{-1} (++)	k_s	16 W m^{-1} K^{-1} (***)		
Dimensions					
D_{imp}	0.0412 m	D_r	0.0824 m	L	0.18 m

G – glass wall; S – steel wall
(*) – (Mathias, 1993); (**) – (Kirk-Othmer Encyclopedia, 2005); (***) – (Mills, 2002)
(+) – (Holman, 1989); (++) – (Perry, Green and Maloney, 1997)

The thermal conductivity of the liquid mixture was estimated using a correlation for black liquor (Järvinen, 2002):

$$k_l = 1.44\times10^{-3}\left(T - 273.15\right) + 0.58 - 0.335\ x_s \tag{3.71}$$

where x_s is the mass fraction of solids in liquor.

In the case of the initial liquid mixture it was considered the alkali and the lignin as the responsible for the mass fraction of solids:

$$x_S = \frac{m_L^i + m_{NaOH}^i}{\rho_l V_l^i} = \frac{30 + 40}{557} = 0.125$$

The viscosity of the liquid mixture was experimentally determined for three different temperatures, as it is described on Appendix C. With this three experimental points we applied the Andrade's equation (Poling, Prausnitz and O'Connell, 2001), resulting an expression for the temperature dependence of μ_l:

$$\ln(\mu_l) = \frac{1105.3}{T} - 9.1703 \tag{3.72}$$

The liquid heat capacity (Cp_l) was estimated recurring also to a correlation made for black liquor (Filho et al., 2000):

$$\begin{aligned} Cp_l = & -0.16972\ x_S(1 - x_S) + 6.19 \times 10^{-4} T + 3.98 + \\ & x_S(-1.6779 - 5.7083 \times 10^{-4} T) \end{aligned} \tag{3.73}$$

These liquid properties were determined for a medium temperature during the heating process, calculated as 373.15 K. The exception was μ_{lw}, where the correspondent temperatures were considered to be approximately 403.15 K for the glass wall, and 363.15 K for the steel wall of the lower plate.

Another issue was to check the values of the lignin heat capacity, obtained by the procedure described in Appendix D, with the correlation (3.73). For that, knowing the mass fraction of each compound in the liquid mixture, and the expression (Poling, Prausnitz and O'Connell, 2001):

$$Cp_l = \sum x_i Cp_i \tag{3.74}$$

it could be estimated a Cp_l based on the individual heat capacities of the substances present. Developing (3.74) for the medium temperature of the heating process (373.15 K), it can be written:

$$Cp_l = x_{H2O} Cp_{H2O} + x_{NaOH} Cp_{NaOH} + x_L Cp_L =$$
$$= 0.874 \ \frac{75.80}{18} + 0.072 \ \frac{59.37}{40} + 0.054 \ \frac{4586}{2325} = 3894 \ J\ kg^{-1} K^{-1}$$

This value is very near the one obtained using the correlation (3.71), which was 3956 J kg^{-1} K^{-1}. In fact it represents a deviation of 1.5 % between them, which gives a higher confidence in the possibility of applying group additivity methods in this work.

The values of viscosity of the thermo fluid, μ_f and μ_{fw}, were also estimated using the Andrade's equation and two points μ vs. T, available on Mathias's thesis (Mathias, 1993):

$$\ln(\mu_f) = \frac{4030.8}{T} - 14.108 \tag{3.75}$$

The variation of ρ_f with the thermo fluid temperature was predicted with the help of the volume coefficient of expansion presented on Table 3.5:

$$\rho_f = \frac{\rho_f^{25°C}}{1 + (T - 298.15)\ \beta_f} \tag{3.76}$$

These thermo fluid properties were determined for a medium temperature inside the jacket, during the heating process, considered to be around 400.15 K, except for the μ_{fw}, where the correspondent temperature used was 395.15 K.

Finally the velocity of the thermo fluid inside the jacket (v_f) was experimentally estimated measuring the correspondent height of the jacket filled per minute, at the start up of the thermostatic bath. It was observed that, per minute, the thermo fluid filled the volume correspondent to a height of 9.1 cm. With this value it was obtained a v_f of 1.52x10^{-3} m s^{-1} and a flow rate of approximately 303 ml min^{-1}.

The medium temperature of the outside wall of the lower steel plate was accepted to be 353.15 K. So, the air properties presented on Table 3.5 were evaluated for a film temperature of 325.65 K.

With the values for the local heat transfer coefficients presented on Table 3.4 and equation (3.53) it was calculated a theoretical value for U_1 of 69.81 W m^{-2} K^{-1}. Comparing with the experimentally determined U_1, it can be said that they are reasonably close (a relative error of 4.8 %), which validates the application of the major part of the estimation processes of physical properties and local heat transfer coefficients developed in this chapter.

The experimental U_2 of 77.42 W m^{-2} K^{-1}, and the coefficients h_{sl} and h_{als} calculated above, allows to obtain through (3.54) a value for the term $1/h_{sg} + 1/h_{aus}$, that represents the sum of the respective thermal resistances. The value obtained for this term was 0.0124 (W m^{-2} K^{-1})$^{-1}$ and will be used later in the reaction phase of the batch experiments.

3.4.3. Non isothermal conditions - reaction phase

Looking to the model presented on section 3.2.3, two important parameters of this process are yet to be defined: the heat of reaction of lignin oxidation, $\Delta H_{R,1}$; and the heat of reaction of vanillin oxidation, $\Delta H_{R,2}$. It was not found any of these values reported on literature, so it was necessary estimate them. These heats of reaction result from very complex mechanisms, specially $\Delta H_{R,1}$, which is almost impossible to predict. The experimental data for the oxidation of the raw material (Indulin AT) was used to estimate a $\Delta H_{R,1}$ value.

Since the vanillin oxidation involves smaller molecules, it was attempted to predict theoretically the $\Delta H_{R,2}$. For that it was assumed a simple reaction equation like (3.1).

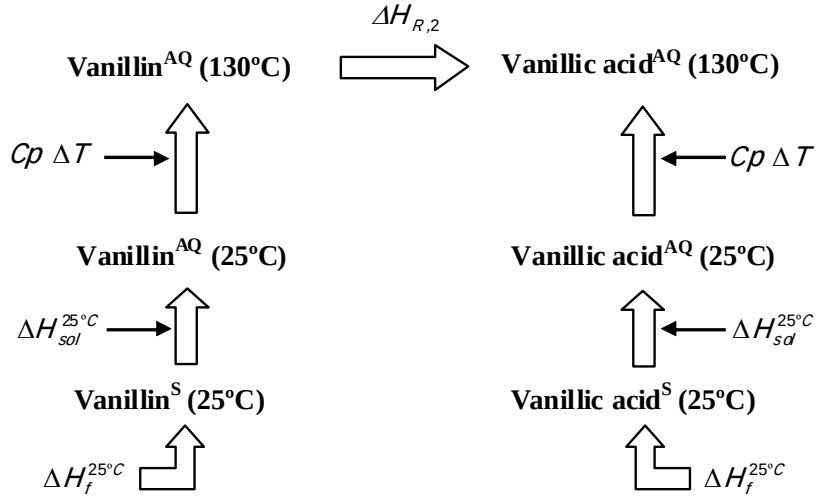

Figure 3.20. Scheme of the thermodynamic path to calculate $\Delta H_{R,2}$.

$$\Delta H_{R,2}(130^{o}C) = \Delta H_f^{130^{o}C}(vanillin) - \Delta H_f^{130^{o}C}(vanillic\ acid) \tag{3.77}$$

The left side of Figure 3.20 represents the calculation of the heat of formation of aqueous vanillin, at 130ºC. It is the sum of the vanillin heat of formation in the solid phase, at 25ºC ($\Delta H_f^{25^{o}C}(vanillin)$), the vanillin heat of solution at 25ºC, ($\Delta H_{sol}^{25^{o}C}(vanillin)$), and the enthalpy change when the temperature of aqueous vanillin is raised from 25ºC to 130ºC:

$$\Delta H_f^{130^{o}C}(vanillin) = \Delta H_f^{25^{o}C}(vanillin) + \Delta H_{sol}^{25^{o}C}(vanillin) + \int_{25^{o}C}^{130^{o}C} Cp_V\, dT \tag{3.78}$$

The right side of Figure 3.20 represents the path to the heat of formation of aqueous vanillic acid, at 130ºC. In this case, it is the sum of the vanillic acid heat of formation in the solid phase, at 25ºC ($\Delta H_f^{25^{o}C}(vanillic\ acid)$), the heat of solution of

vanillic acid at 25ºC, ($\Delta H_{sol}^{25^{\circ}C}(vanillic\ acid)$), and the enthalpy change when the temperature of aqueous vanillin is raised from 25ºC to 130ºC:

$$\Delta H_f^{130^{\circ}C}(vanillic\ acid) = \Delta H_f^{25^{\circ}C}(vanillic\ acid) + \Delta H_{sol}^{25^{\circ}C}(vanillic\ acid) + \int_{25^{\circ}C}^{130^{\circ}C} Cp_D\, dT \tag{3.79}$$

To calculate the heats of formation in the solid phase, at 25ºC, it was used a method based on Benson´s group additivity technique (Salmon and Dalmazzone, 2006), like it is proposed on Appendix E.

For the estimation of Cp_V and Cp_D it was used the Missenard method, the same technique employed for the heat capacity of the Kraft lignin model. The correspondent procedure, equations and values are presented on Appendix D.

In the literature (Washburn, 2003), the heat of solution of vanillin and vanillic acid is -21.8 kJ mol^{-1} and -21.59 kJ mol^{-1}, respectively.

Substituting all the correspondent values on (3.78) and (3.79), it results:

$$\Delta H_f^{130^{\circ}C}(vanillin) = -485.7 - 21.8 + \int_{298.15K}^{403.15K} (0.6996\ T + 52.54)\, dT = -476.23\ kJ/mol$$

$$\Delta H_f^{130^{\circ}C}(vanillic\ acid) = -755.6 - 21.59 + \int_{298.15K}^{403.15K} (0.8218\ T + 36.93)\, dT = -743.06\ kJ/mol$$

Finally, replacing these two values on (3.77), it is obtained the final estimate for the heat of reaction of vanillin oxidation, at 130ºC:

$$\Delta H_{R,2}(130^{o}C) = -743.06 - (-476.23) = -266.83\ kJ/mol$$

In Table 3.6 some of the constants and parameters needed to apply the model of non isothermal lignin oxidation to the reaction phase of the batch experiments are presented.

Table 3.6. Constants and parameters used for the system definition of non isothermal lignin oxidation in batch reactor.

Cp_L	4891 J mol^{-1} K^{-1}	α	0.5	V_l^i	0.5 l
Cp_{NaOH}	60.31 J mol^{-1} K^{-1} (*)	m_L^i	30 g	V_g^i	0.5 l
Cp_{H2O}	76.61 J mol^{-1} K^{-1} (+)	m_{NaOH}^i	40 g	$\Delta V / \Delta t$	$1.67x10^{-5}$ l s^{-1}
Cp_{N2}	29.29 J mol^{-1} K^{-1} (+)	n_{H2O}^i	27.06 mol	A_1	$4.66x10^{-2}$ m^2
Cp_{O2}	30.17 J mol^{-1} K^{-1} (+)	I	2 mol l^{-1}	A_2	$1.77x10^{-2}$ m^2
Cp_V	334.6 J mol^{-1} K^{-1}	T_{amb}	298.15 K	R	0.082 l atm mol^{-1} K^{-1}
Cp_D	368.2 J mol^{-1} K^{-1}	T^i	396.15 K	λ_{H2O}^{vap}	39125 J mol^{-1} (**)
Cp_{gl}	836 J kg^{-1} K^{-1} (***)	M_n	2325 g mol^{-1}	P_{atm}	0.987 atm
m_{gl}	1.007 kg				

(*) – (Yaws, 1999); (**) – (Smith, Van Ness and Abbott, 1996); (+) – (Holman, 1989); (***) – (Perry, Green and Maloney, 1997)

The heat capacities were estimated for 403.15 K, the assumed medium reactor temperature during the oxidation phase. All the values on Table 3.6 are valid to use on simulations of batch experiment 1 and 2. The only experimental condition, present on the model, that differs from both experiments is the $\Delta P\big|_{press}$. This pressure raise assumes the values of 3.8 atm and 0.82 atm, respectively for experiment 1 and 2.

The overall heat transfer coefficients, estimated for the heating phase, had to suffer small adjustments, since the temperature conditions for the reaction phase are different. The local heat transfer coefficients, previously defined by correlations, were recalculated for the medium reaction conditions.

Table 3.7. Values estimated for local heat transfer coefficients.

h_{sl}	7520 W m^{-2} K^{-1}	h_{gll}	7664 W m^{-2} K^{-1}
h_{als}	4.52 W m^{-2} K^{-1}	h_{fgl}	109.7 W m^{-2} K^{-1}

The physical and thermodynamic properties used to achieve the results of Table 3.7 are presented below.

Table 3.8. Properties used on predicting the local heat transfer coefficients.

Liquid mixture					
k_l	0.725 W m^{-1} K^{-1}	μ_l	1.615x10^{-3} kg m^{-1} s^{-1}	μ_{lw}	S - 1.731x10^{-3} kg m^{-1} s^{-1}
ρ_l	1114 kg m^{-3}	Cp_l	3973 J kg^{-1} K^{-1}		G - 1.511x10^{-3} kg m^{-1} s^{-1}
Thermo fluid					
k_f	0.166 W m^{-1} K^{-1} (*)	μ_f	8.188x10^{-3} kg m^{-1} s^{-1}	μ_{fw}	9.168x10^{-3} kg m^{-1} s^{-1}
ρ_f	1005 kg m^{-3}	Cp_f	2019 J kg^{-1} K^{-1} (*)	β_f	7.8 x10^{-3} K^{-1} (**)
Air					
k_a	0.0289 W m^{-1} K^{-1} (+)	μ_a	2.009x10^{-5} kg m^{-1} s^{-1} (+)	β_a	0.0030 K^{-1}
ρ_a	1.050 kg m^{-3} (+)	Cp_a	1008 J kg^{-1} K^{-1} (+)		

(*) – (Mathias, 1993); (**) – (Kirk-Othmer Encyclopedia, 2005); (+) – (Holman, 1989)

The liquid properties were determined for a medium temperature of 403.15 K, during the reaction phase, except μ_{lw}, where the correspondent temperatures were considered to be approximately 413.15 K for the glass wall, and 393.15 K for the steel wall of the lower plate.

The thermo fluid properties were estimated for a medium temperature inside the jacket of 429.15 K, except in the case of μ_{fw}, where that parameter was considered to be 424.15 K.

The air properties presented on Table 3.8 were determined for a film temperature of 335.65 K, since the medium temperature of the outside wall of the lower steel plate was admitted to be 373.15 K.

The values of the materials thermal conductivities and dimensions, presented on Table 3.5 are also applied for the reaction phase.

With the values of the local heat transfer coefficients, presented on Table 3.7, and the term $1/h_{sg} + 1/h_{aus}$ estimated for the heating phase, it was recalculated the overall heat transfer coefficients. The values obtained were 70.52 W m^{-2} K^{-1} and 77.70 W m^{-2} K^{-1}, respectively for U_1 and U_2.

It is also important to notice that on equation (3.51) the term $n_{other}Cp_{others}$ is unknown, since it is very difficult to determine and quantify all the intermediates that can be formed during lignin degradation. However it is possible to have an idea of the order of magnitude of the values associated to this term. Supposing that each lignin molecule cracks into species with only one aromatic ring, similar to vanillin, for each mol of Indulin AT it would result 13 moles of "*others*" and 2 moles of vanillin. Following this supposition, the 30 grams of lignin, initially present on the liquid mixture, could form 0.1677 moles of "*others*". Admitting that the heat capacity of "*others*" and vanillin are similar, the term $n_{other}Cp_{others}$ would be 56 J K^{-1}. Since this value is a rough approximation, it was made a simple study on the importance of $n_{other}Cp_{others}$, varying this term and observing its effects on the resulting simulation curves of C_V, T and pH.

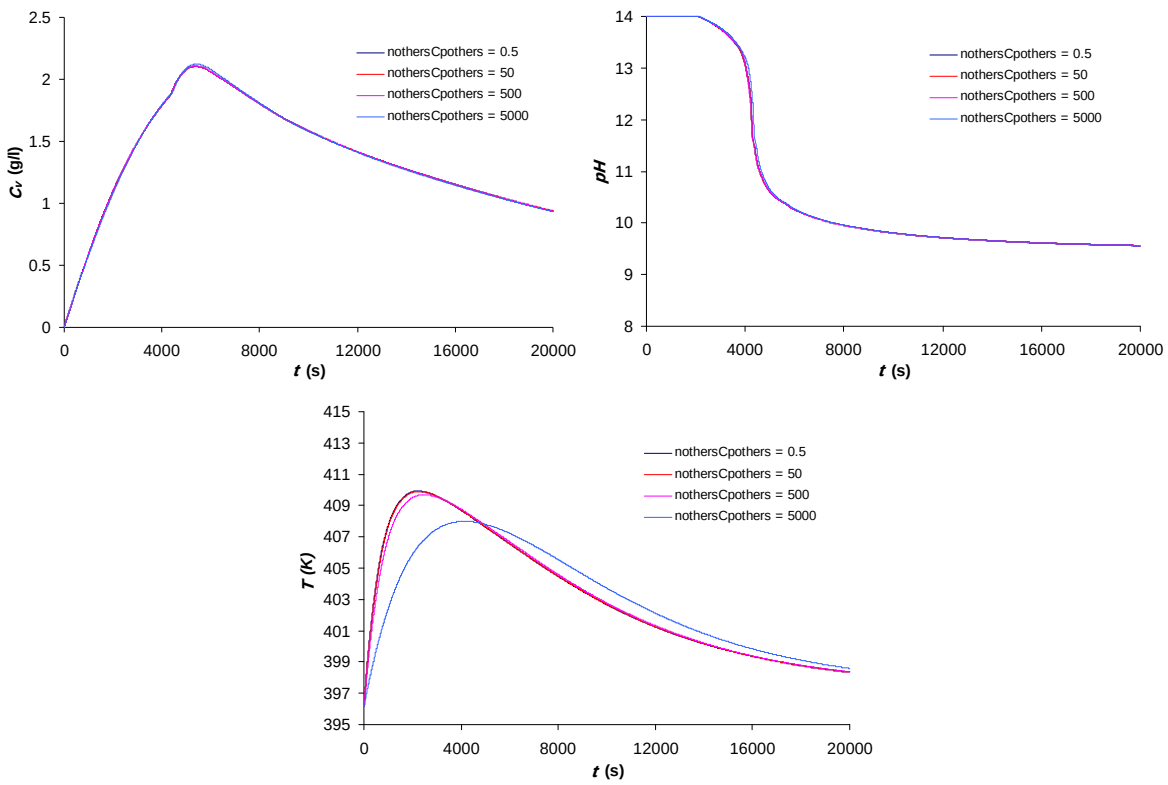

Figure 3.21. Vanillin concentration (C_V), pH and reactor temperature (T) simulation curves for different values of $n_{others}Cp_{others}$. In all of them were used the operating conditions of Experiment 1 (Table 3.2), a $\Delta H_{R,1}$ of -29687 kJ/mol, a E_a/R of 4000 and a $Const$ of 0.098.

The simulation results are almost indifferent to the term $n_{others}Cp_{others}$, as it can be observed by the superposition of the curves in Figure 3.21. The exception is the T curves, because for $n_{others}Cp_{others}$ in the thousands magnitude, they start to flatten as this term grows, showing decreasing temperature maximums and increasing correspondent time delays. However, as it was mentioned above, this term will be around 50, maybe, in an extremist point of view could reach one or two hundred. In this kind of range, the presented mathematical definition of the system is almost insensitive to $n_{others}Cp_{others}$, so the choice of an appropriate value for this term did not imposed any problem. Regarding this, it was used a $n_{other}Cp_{others}$ of 50 J K^{-1}.

The heat of reaction, $\Delta H_{R,1}$, was determined through a similar method to the one exploited on section 3.4.1 for a first estimative of k_1. Considering that in the initial moments of reaction there is no vanillin oxidation, the energy balance equation (A.13) can be reduced to:

$$Q^i - r_1^i V_l^i \Delta H_{R,1} = \lambda_{H2O}^{vap}\left(\left[\frac{-B}{\left(C+T^i\right)^2}-\frac{1}{T^i}\right]\frac{V_g^i P_{H2O}^i}{R\,T^i}\left.\frac{dT}{dt}\right|_{t=0}+\frac{\Delta V_l}{\Delta t}\frac{P_{H2O}^i}{R\,T^i}\right)+ \\ +\left(n_{N2}^i Cp_{N2}+n_{O2}^i Cp_{O2}+n_L^i Cp_L+n_{NaOH}^i Cp_{NaOH}+n_{H2O}^i Cp_{H2O}+m_{gl}Cp_{gl}\right)\left.\frac{dT}{dt}\right|_{t=0} \quad (3.80)$$

All the variables and parameters on (3.80) were known or could be calculated, except $dT/dt|_{t=0}$ and $\Delta H_{R,1}$. The value of $dT/dt|_{t=0}$ can be determined from the temperature data collected in the batch experiments performed in this work.

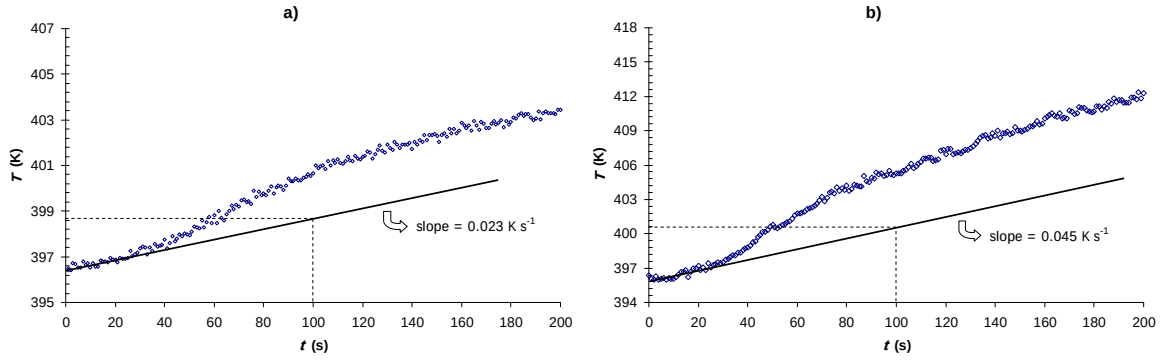

Figure 3.22. Temperature (T) curves for the initial moments of reaction, and determination of $dT/dt|_{t=0}$. a) Experiment 1; b) Experiment 2.

Substituting all the values on (3.80), it is obtained a $\Delta H_{R,1}$ for each temperature data of -29460 kJ mol^{-1} and -29913 kJ mol^{-1}, respectively for experiment 1 and 2. The value of $\Delta H_{R,1}$ used in this work was -29687 kJ/mol or -12769 kJ/kg. The heat released in the total combustion of *pine* wood is 19620 kJ/kg (Berlin, Khalturinskiy, Novikov and Zaikov, 2005), and a heat value of 37143 kJ/kg for a Kraft lignin extracted from *black liquor* was presented by Axegard (Axegard, 2007). These reported values are in the same order of magnitude of the $\Delta H_{R,1}$ determined above.

At this point, it was available all the information needed to apply the non isothermal model for lignin oxidation. Only E_a/R should suffer a small adjustment, since the value obtained from parameter estimation under isothermal conditions regards a temperature lower (123ºC) than the average one during the batch experiments (approximately 130ºC). Because of this fact it was performed a parameter estimation with the model described on 3.2.3, using the software gPROMS, with an initial estimative of 3960 for E_a/R. The final result obtained was 4000.

Finally, the two batch experiments performed were simulated and the results are present on Figures 3.13 and 3.14.

3.4.4. Mathias experiments

Analysing the temperature data of lignin oxidation experiments by Mathias (Mathias, 1993), it can be said that some of them, in the major part of reaction time, were close to be isothermal. This was probably due to manual variation of the set point of the bath, during the reaction phase, with the purpose of steadying the signal of the temperature inside the reactor. Because of this fact, three Mathias's experiments were simulated considering constant reaction temperature. The values of the main operating conditions of these three experiments are listed on Table 3.9.

Table 3.9. Operating conditions of Mathias experiments 12, 29 and 32 (Mathias, 1993).

Experiment	T^{med} (K)	P^{i}_{O2} (bar)	P (bar)	C^{i}_{NaOH} (g/l)	C^{i}_{L} (g/l)
12	407.6	1.41	9.2	80	60
29	399.0	3.90	9.6	80	30
32	402.6	3.23	9.7	80	60

On the second column of Table 3.9 it was placed the average temperature for each experiment, T^{med}, which were considered constant throughout the reaction time.

$$T^{med} = \frac{\int_0^{t_{final}} T\,dt}{t^{final}} \tag{3.81}$$

where t^{final} is the time of the last reactor temperature point collected on each experiment. The oxygen partial pressure at time zero, P_{O2}^{i}, was calculated for the initial volume conditions and average reactor temperature.

The simulation results of Mathias experiments 12, 29 and 32 are shown on Figures 3.23 to 3.25. It was used a model based on section 3.2.3, but without the energy balance and heat transfer equations. This is similar to consider isothermal reaction media with variation on the gas and liquid volumes, and consequently variable partial pressure of the gas components.

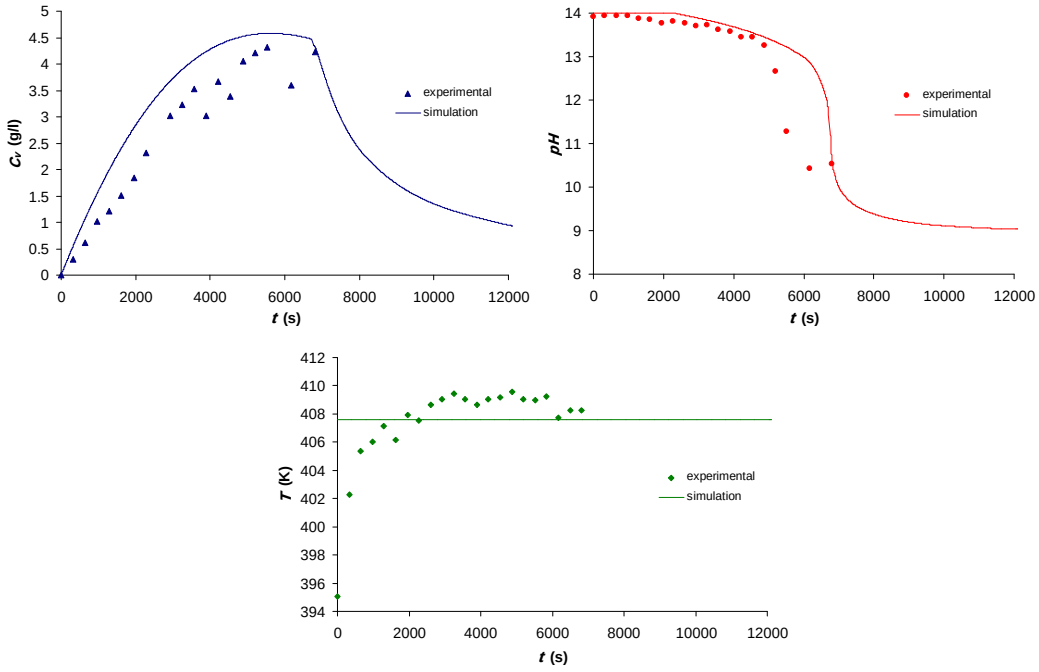

Figure 3.23. Vanillin concentration (C_V), pH and reactor temperature (T) curves for Mathias experiment 12 (Mathias, 1993) and the correspondent simulations considering constant temperature during the reaction and variable phase volumes. The operating conditions are on Table 3.9. The parameters used were E_a/R of 3502, $Const$ of 0.03774, M_n of 1141 g/mol and α equal to 1.

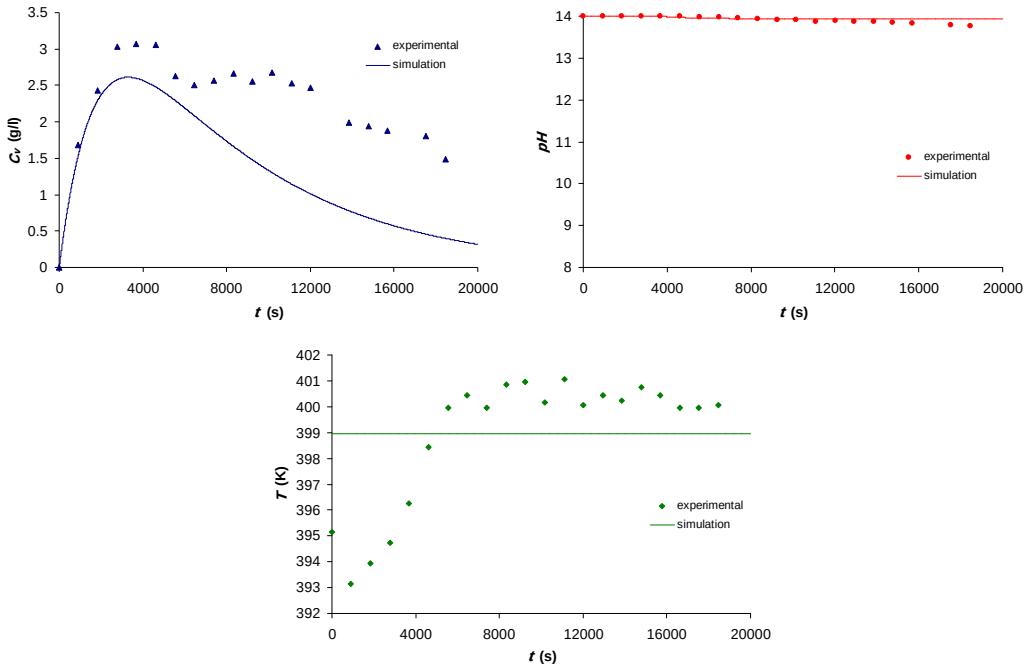

Figure 3.24. Vanillin concentration (C_V), pH and reactor temperature (T) curves for Mathias experiment 29 (Mathias, 1993) and the correspondent simulations considering constant temperature during the reaction and variable phase volumes. The operating conditions are on Table 3.9. The parameters used were E_a/R of 3502, $Const$ of 0.03774, M_n of 1141 g/mol and α equal to 1.

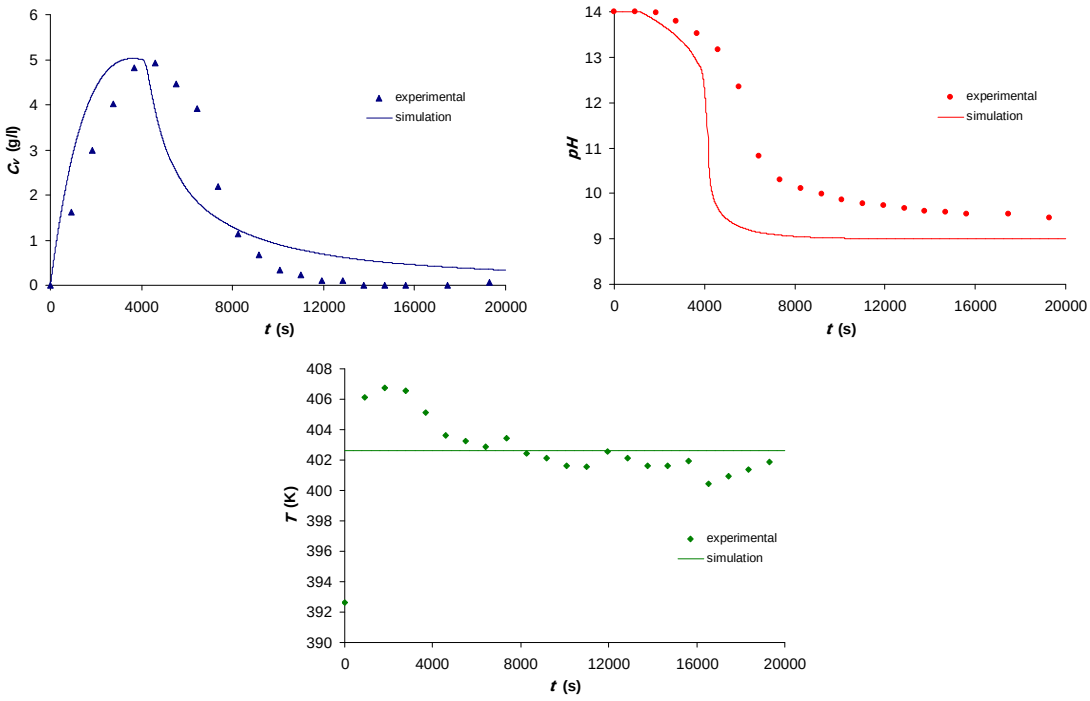

Figure 3.25. Vanillin concentration (C_V), pH and reactor temperature (T) curves for Mathias experiment 32 (Mathias, 1993) and the correspondent simulations considering constant temperature during the reaction and variable phase volumes. The operating conditions are on Table 3.9. The parameters used were E_a/R of 3502, $Const$ of 0.03774, M_n of 1141 g/mol and α equal to 1.

However, not all the Mathias's experiments appeared to have behaviour close to isothermal. In some of them, the temperature data seems proper to be described by the non isothermal model for lignin oxidation. Three of these experiments were simulated by the complete non isothermal model of section 3.2.3, and the results are presented on Figures 3.26 to 3.28. The operating conditions and the parameters used in the correspondent simulations are listed in Table 3.10.

Table 3.10. Operating conditions of Mathias experiments 11, 13 and 28 (Mathias, 1993), and correspondent parameters used in the non isothermal model.

	Experiment 11	**Experiment 13**	**Experiment 28**
C^i_{NaOH} (g/l)	80	80	160
C^i_L (g/l)	60	60	60
T^i (ºC)	121	119	120
P (bar)	9.3	9.5	9.6
P^i_{O2} (bar)	4	6.7	3.5
Agitation (rpm)	1100	1100	1100
$\Delta V / \Delta t$ (l s^{-1})	1.54 x10^{-5}	1.54 x10^{-5}	9.92 x10^{-6}

Constants and parameters					
E_a/R	3502	$Const$	0.03774	ΔH^1_R	-11203 kJ mol^{-1}
ΔH^2_R	-266.83 kJ mol^{-1}	U_1	70.52 W m^{-2} K^{-1}	U_2	77.70 W m^{-2} K^{-1}
V^i_l	0.5 l	V^i_g	0.5 l	M_n	1141 g mol^{-1}
α	1.0	Cp_L	2400 J mol^{-1} K^{-1}	Cp_{NaOH}	60.31 J mol^{-1} K^{-1} (*)
Cp_{H2O}	76.61 Jmol^{-1} K^{-1} (+)	Cp_{N2}	29.29 J mol^{-1} K^{-1} (+)	Cp_{O2}	30.17 J mol^{-1} K^{-1} (+)
Cp_V	334.6 J mol^{-1} K^{-1}	Cp_D	368.2 J mol^{-1} K^{-1}	R	0.082 l atm mol^{-1} K^{-1}
Cp_{gl}	836 J kg^{-1} K^{-1} (**)	m_{gl}	1.007 kg	P_{atm}	0.987 atm
λ^{vap}_{H2O}	39125 J mol^{-1} (***)	I	2 mol l^{-1} for exp. 11 and 13; 4 mol l^{-1} for exp. 28		

(*) – (Yaws, 1999); (**) – (Perry, Green and Maloney, 1997); (+) – (Holman, 1989);
(***) – (Smith, Van Ness and Abbott, 1996)

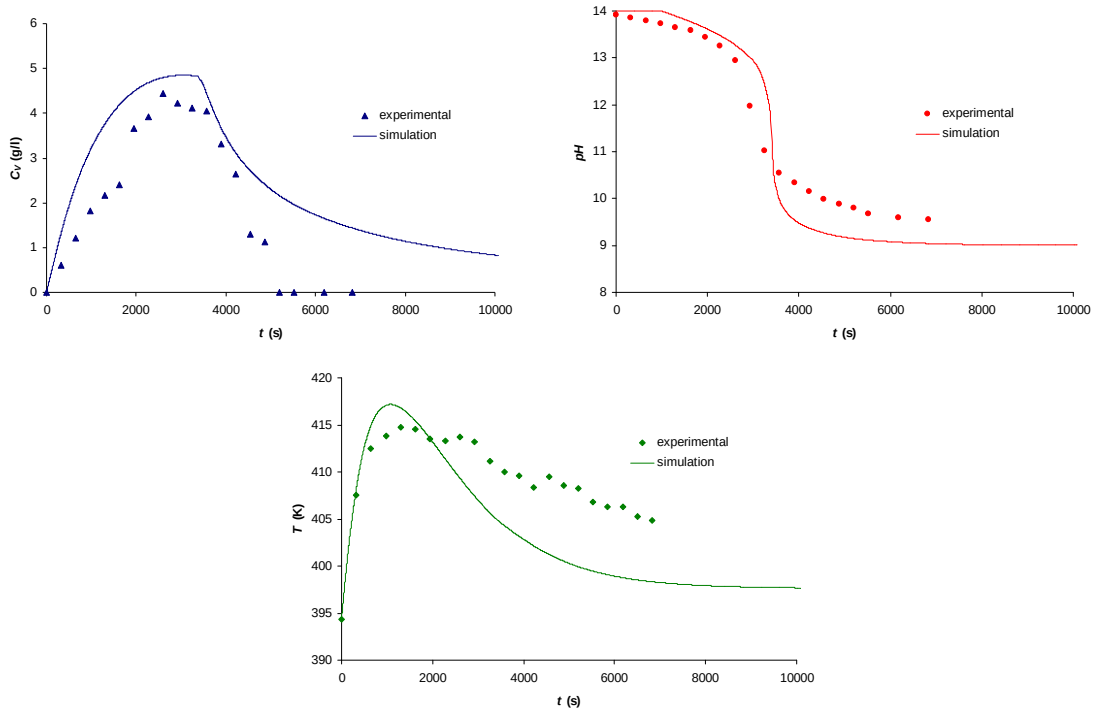

Figure 3.26. Vanillin concentration (C_V), pH and reactor temperature (T) curves for Mathias experiment 11 (Mathias, 1993) and the correspondent simulations considering the model for non isothermal lignin oxidation. The operating conditions and parameters are on Table 3.10. Solid lines correspond to the simulations.

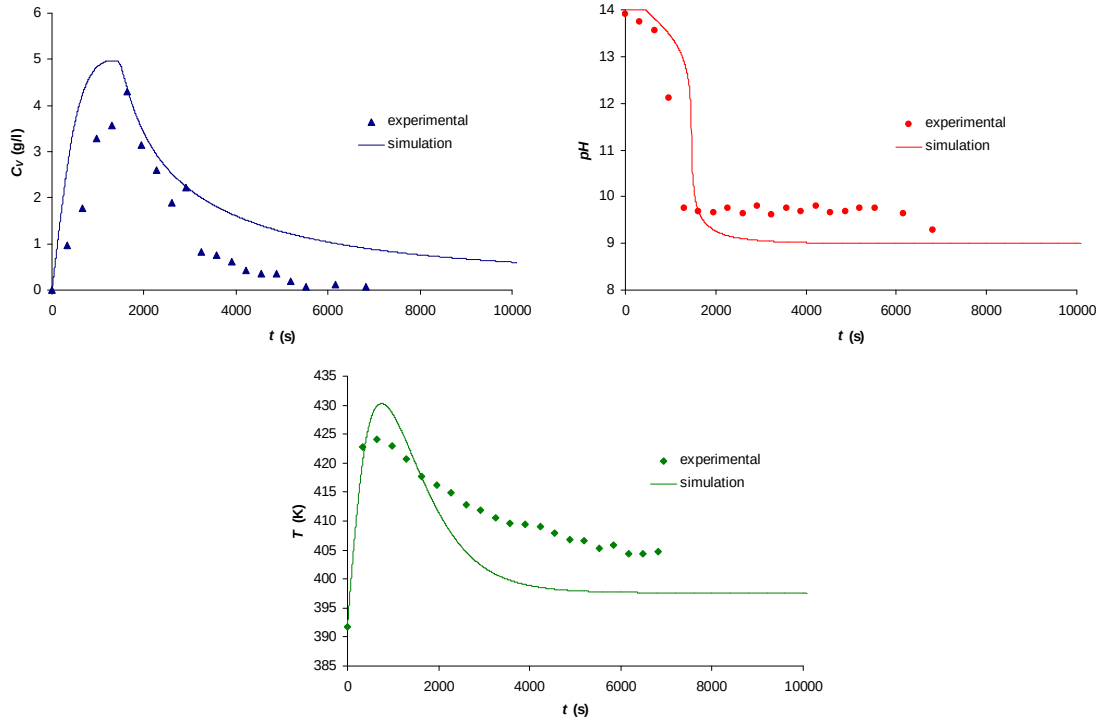

Figure 3.27. Vanillin concentration (C_V), pH and reactor temperature (T) curves for Mathias experiment 13 (Mathias, 1993) and the correspondent simulations considering the model for non isothermal lignin oxidation. The operating conditions and parameters are on Table 3.10. Solid lines correspond to the simulations.

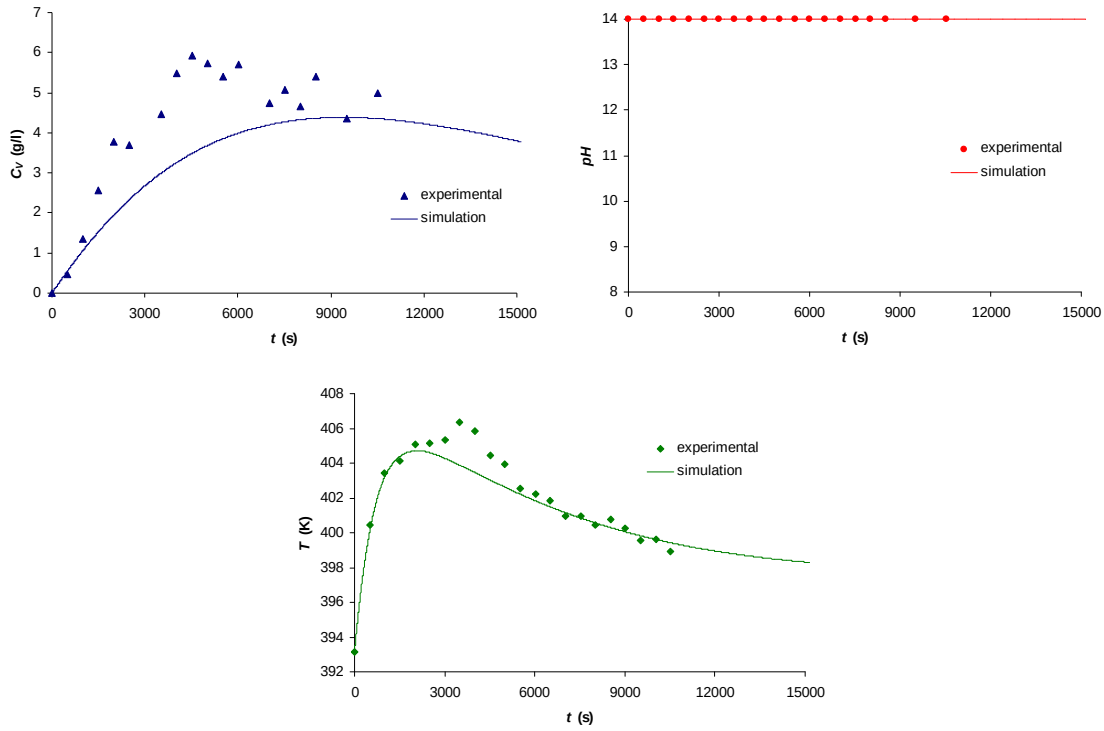

Figure 3.28. Vanillin concentration (C_V), pH and reactor temperature (T) curves for Mathias experiment 28 (Mathias, 1993) and the correspondent simulations considering the model for non isothermal lignin oxidation. The operating conditions and parameters are on Table 3.10. Solid lines correspond to the simulations.

From the observation of Figures 3.23 to 3.28, it can be seen that the experiments presented (Mathias, 1993) are predicted quite well by the correspondent simulations. This fact helps to validate the model elaborated in section 3.2.3, for non isothermal lignin oxidation.

Concerning to the parameters used on the simulations presented on Figures 3.23 to 3.28, it must be said that:

- E_a/R and $Const$ were used with the original values (Mathias, 1993; Fargues et al., 1996a), respectively, 3502 and 0.03774.
- M_n of the lignin used in these experiments was 1141 g/mol (Fargues et al., 1996a), and consequently the α was 1, calculated by (3.66).

- Cp_L was 2400 J mol^{-1} K^{-1}, calculated with the help of Appendix D for a M_n of 1141 g/mol.
- the remaining physical constants and parameters used were the same as the ones presented for the oxidation of Indulin AT. This also includes the overall heat transfer coefficients.

The lignin used by Mathias in his experimental work was different from the raw material of this thesis (Indulin AT). Based on this reality, the heat released in the oxidation of these two lignins, in kJ mol^{-1}, should also be different.

The value of $\Delta H_{R,1}$ for the lignin of Mathias could be obtained with a method similar to the one used for the heat of oxidation of Indulin AT, that was described earlier. However, in this case it is not possible because of the lack of experimental points for the temperature inside the reactor. So, it was made an empirical and simple approach to get an estimate of the $\Delta H_{R,1}$ referent to the lignin used by Mathias, based on an idea of proportionality between the number of equivalents of acid products formed in the lignin oxidation, X, and the heat released in the same reaction. In a base of 1 mol of vanillin formed, it can be said that:

$$X = Const\ \alpha\ M_n \Rightarrow \begin{cases} X^{Mathias} = 0.03774 \times 1 \times 1141 = 43.06\ \ eq/l \\ X^{Indulin} = 0.098 \times 0.5 \times 2325 = 113.93\ \ eq/l \end{cases}$$

Since the heat of oxidation of Indulin AT was already determined, the same parameter for the lignin of Mathias was estimated considering X proportional to $\Delta H_{R,1}$:

$$\Delta H_{R,1}(Mathias) = \Delta H_{R,1}(Indulin)\ \frac{X^{Mathias}}{X^{Indulin}} = \frac{-29687}{2.65} = -11203\ \ kJ\ /\ mol$$

3.5. Conclusions

In this chapter two batch experiments of lignin oxidation were performed to check the vanillin yield of the raw material used (Indulin AT). These experiments were carried out on a semi-batch (closed to the liquid and opened to gas feed) jacketed reactor with agitation, connected to a thermostatic bath for temperature control. The liquid samples collected were analysed by gas chromatography after a pre-treatment with HCl and ethyl ether. The results revealed maximum vanillin yields with respect to lignin mass of 3.7% and 3.4%, for reaction times of 75 min and 35 min, respectively for experiment 1 and 2. This represents approximately half of the maximum yields and the quickness to obtain them, comparing to the results reported by Mathias (Mathias, 1993) in similar operating conditions, which indicates that different lignins have been used.

Three mathematical models were developed for the batch reactor: one describing isothermal vanillin oxidation; other for isothermal lignin oxidation with no phase volume variations; and the last one is a more complex description of lignin oxidation considering non isothermal conditions, volume variations and partial pressure fluctuations.

The isothermal model for vanillin oxidation was used to simulate some experiments reported by Fargues (Fargues et al., 1996b). The simulation results predicted very well the correspondent experimental evolution of vanillin concentration.

Two of the original parameters (E_a/R and $Const$) on the kinetic model description of lignin oxidation already reported (Mathias, 1993; Fargues et al., 1996a) were adjusted for the new raw material used. It was performed a parameter estimation

using the developed model for isothermal lignin oxidation and the values obtained were 3960 and 0.098, respectively for E_a/R and $Const$.

The overall heat transfer coefficients were estimated using the experimental temperature data of the heating step and checked by calculation with local heat transfer coefficients predicted by proper correlations. The final values obtained for the reaction step conditions were 70.52 W m^{-2} K^{-1} and 77.70 W m^{-2} K^{-1}, respectively for U_1 and U_2.

The heats of reaction of lignin and vanillin oxidation were also two important parameters to be estimated. The last one, $\Delta H_{R,2}$, was calculated based on thermodynamic concepts and some reported information. The $\Delta H_{R,1}$ was estimated using experimental data from the initial moments of reaction. The values obtained for $\Delta H_{R,1}$ and $\Delta H_{R,2}$ were -29687 kJ mol^{-1} and -266.83 kJ mol^{-1}, respectively.

With all the needed information compiled, the two performed experiments were simulated using the model for non isothermal lignin oxidation. According to the experimental data it was observed that the mathematical model proposed in section 3.2.3 was able to predict quite acceptably the behavior of lignin oxidation on the batch reactor system.

Finally, some of Mathias experiments (Mathias, 1993) were also simulated using proper values of E_a/R, $Const$, Cp_L and $\Delta H_{R,1}$. The simulation results are quite close to the reported experimental results on the major variables C_V, pH and T, supporting the validation of the developed models.

3.6. Nomenclature

a constant of the correlation for heat transfer from the agitated liquid of vessels to jacketed walls

A velocity reaction constant for vanillin oxidation, l mol^{-1} min^{-1}

A_{ext1} area of the external wall of the cylindrical glass that limits the reaction zone, m^2

A_f cross sectional area of the flow inside the jacket, m^2

A_0 parameter on the equation relating vapor pressure to temperature

A_1 internal area of the cylindrical glass limiting the reaction zone, m^2

A_2 surface area of a steel plate, m^2

b constant of the correlation for heat transfer from the agitated liquid of vessels to jacketed walls

B velocity reaction constant for vanillin oxidation, l/mol

B_0 parameter on the equation relating vapor pressure to temperature

C_i concentration of species i, mol/l

$Const$ parameter of the relation between lignin oxidized and acid products formed

Cp_i heat capacity of species or substance i, J mol^{-1} K^{-1} or J kg^{-1} K^{-1}

C_0 parameter on the equation relating vapor pressure to temperature

D vanillic acid

D_h hydraulic diameter of the jacket, m

D_{imp} impeller diameter, m

D_r internal diameter of the reactor, m

D_s width of the stainless steel plates, m

D_1 diameter of the external wall of the internal cylindrical glass, m

D_2 diameter of the internal wall of the external cylindrical glass, m

E_a activation energy of lignin oxidation, J/mol

E_i total energy of species i, J/mol

$f(pH)$ function of C_{H+}

F_i molar flow rate of species i, mol/s

F_{O2}^{in} molar flow rate of oxygen entering the system, mol/s

g gravitational constant, m s^{-2}

Gr_a Grashof number of the air

h_{als} heat transfer coefficient from the external wall of the lower steel plate to the ambient, W m^{-2} K^{-1}

h_{aus} heat transfer coefficient from the external wall of the upper steel plate to the ambient, W m^{-2} K^{-1}

h_{fgl} heat transfer coefficient from the thermo fluid to the external glass walls of the reactor, W m^{-2} K^{-1}

h_{gll} heat transfer coefficient from the internal glass walls to the liquid inside the reactor, W m^{-2} K^{-1}

h_{sg} heat transfer coefficient from the gas inside the reactor to the internal wall of the upper steel plate, W m^{-2} K^{-1}

h_{sl} heat transfer coefficient from the liquid inside the reactor to the internal wall of the lower steel plate, W m^{-2} K^{-1}

H_i enthalpy of formation of species i, J/mol

H_{O2}^{in} enthalpy of formation of the oxygen at the system inlet conditions, J/mol

I ionic strength of the liquid medium, mol/l

k_i thermal conductivity of material i, W m^{-1} K^{-1}

k_1 velocity reaction constant for vanillin formation, $(l/mol)^{1.75}$ min^{-1}

k_2 velocity reaction constant for vanillin oxidation, l mol^{-1} min^{-1}

K_a acid dissociation product of all the acid species formed during lignin oxidation

K_w water ionic product

L height of the cylindrical glass, m

l_s characteristic dimension of the steel plate, m

L lignin

m constant of the correlation for heat transfer from the agitated liquid of vessels to jacketed walls

m_{gl} mass of the internal glass tube delimiting the reactor, kg

m_i mass of species i, g

M_{H2O} molecular weight of water, g/mol

M_n lignin mean molecular weight, g/mol

M_{NaOH} molecular weight of sodium hydroxide, g/mol

M_V molecular weight of vanillin, g/mol

n "*others*" stoichiometric coefficient on the lignin oxidation reaction

n_i number of moles of species i, mol

N speed of the agitator, rotations per second

Nu_a Nusselt number of the air

P total pressure, bar

P_{atm} atmospheric pressure, bar

P_i partial pressure of species i, bar

P_f wetted perimeter of the jacket, m

P_s perimeter of a steel plate, m

Q heat received by the system from the surroundings, W

Q_{airK} flow rate of air K to the detector of the GC, ml/min

Q_{H2} flow rate of hydrogen to the detector of the GC, ml/min

Q_{N2} flow rate of carrier gas to the GC, ml/min

r_{ext1} radius of the external wall of the glass that limits the reaction zone, m

r_{int} radius of the internal wall of the internal cylindrical glass, m

r_{med} medium radius of the steel plates, m

r_1 rate of formation of vanillin, mol m^{-3} s^{-1} or mol m^{-3} min^{-1}

r_2 rate of oxidation of vanillin, mol m^{-3} s^{-1} or mol m^{-3} min^{-1}

R universal gas constant, l atm mol^{-1} K^{-1}

Ra_a Rayleigh number of the air

t_1, t_2 periods of constant oven temperature on the GC temperature program, min

T reactor temperature, K

T_{amb} ambient temperature, K

$T_{\text{det}ector}$ detector temperature on the gas chromatograph, ºC

T_F thermo fluid temperature inside the jacket, K

$T_{injector}$ injector temperature on the gas chromatograph, ºC

T_{oven} oven temperature on the gas chromatograph, ºC

U_1 overall heat transfer coefficient from the thermo fluid in the jacket to the liquid inside the reactor, W m^{-2} K^{-1}

U_2 overall heat transfer coefficient from inside of the reactor to the ambient through the top and bottom stainless steel plates, W m^{-2} K^{-1}

v_f thermo fluid velocity inside the jacket, m/s

V vanillin

V_i specific volume of species i, m^3/mol

$V_{injection}$ sample volume injected on the GC, μl

V_l volume of the liquid phase inside the reactor, m^3

V_g volume of the gas phase inside the reactor, m^3

W_S shaft work, W

x_i mass fraction of species i in the liquid mixture

x_S mass fraction of solids in the liquid mixture

X variable that encloses all possible acid products from lignin oxidation, eq/l

Greek letters

$\Delta H_{R,1}$ heat of reaction of lignin oxidation, J/mol

$\Delta H_{R,2}$ heat of reaction of vanillin oxidation, J/mol

$\Delta P|_{press}$ pressure elevation promoted in the pressurization step, atm

Δt time interval between collection of two consecutive liquid samples, s

ΔT_a temperature difference between the bulk of the ambient air and the steel plate wall, K

ΔT_f temperature difference between the bulk of the thermo fluid and the internal jacket wall, K

ΔV_l volume of liquid taken from the system in each sample collection, m^3

α lignin stoichiometric coefficient on the lignin oxidation reaction

$\alpha_{heating}$ rate of the oven temperature rising on the GC temperature program, ºC/min

υ_1 oxygen stoichiometric coefficient on the lignin oxidation reaction

υ_2 oxygen stoichiometric coefficient on the vanillin oxidation reaction

λ_{vap}^{H2O} heat of vaporization of water, J/mol

ρ_i density of substance i, kg/m^3

μ_i viscosity of substance i, kg m^{-1} s^{-1}

β_i volume coefficient of expansion of substance i, K^{-1}

Subscripts

a ambient air

b bulk conditions

D vanillic acid

f thermo fluid

fw thermo fluid at wall conditions

g gas phase

gl glass

H^+ hydrogen ions

H2O water

l liquid phase

lw liquid at wall conditions

L lignin

NaOH sodium hydroxide

N2 nitrogen

others intermediates that can be formed during lignin degradation

$O2$ oxygen

V vanillin

Superscripts

g gas phase

i initial value

l liquid phase

3.7. References

1. Axegard, P. *The Kraft pulp mill as a biorefinery.* ICEP4 Conference, Belo Horizonte, Brazil, March 5-8, **2007**.
2. Berlin, A. A.; Khalturinskiy, N. A.; Novikov, I. A.; Zaikov, G. E. *Chemical physics of pyrolysis, combustion, and oxidation*, Nova Publishers, **2005**.
3. Bjørsvik, H.-R.; Liguori, L. Organic processes to pharmaceutical chemicals based on fine chemicals from lignosulfonates. *Org. Process Res. Dev.*, **2002**, 6 (3), 279-290.
4. Fargues, C.; Mathias, A.; Rodrigues, A. Kinetics of vanillin production from Kraft lignin oxidation. *Ind. Eng. Chem. Res.*, **1996a**, 35, 28-36.
5. Fargues, C.; Mathias, A.; Silva, J.; Rodrigues, A. Kinetics of vanillin oxidation. *Chem. Eng. Technol.*, **1996b**, 19 (2), 127-136.
6. Filho, L. C.; Simões, M. R.; Wolff, F. *Propriedades térmicas do licor negro de processo Kraft.* Congreso Iberoamericano de Investigación en Celulosa y Papel (CIADICYP), Argentina, **2000**.

7. Fogler, H. S. *Elements of Chemical Reaction Engineering* (2nd Edition), Prentice Hall International, USA, **1992**.
8. Holman, J. P. *Heat transfer* (SI Metric Edition), McGraw Hill, Singapore, **1989**.
9. Järvinen, M. P. *Numerical modeling of the drying, devolatilization and char conversion processes of black liquor droplets.* Ph.D. Dissertation, Helsinki University of Technology, Finland, **2002**.
10. *Kirk-Othmer Encyclopedia of Chemical Technology*; 5th Edition, John Wiley & Sons, **2005**.
11. Knowles, D. A. *Chemistry and Technology of Agrochemical Formulations*, Kluwer Academic Publishers, United Kingdom, **1998**.
12. Mathias, A. L. *Produção de vanilina a partir da lenhina: estudo cinético e do processo.* Ph.D. Dissertation, University of Porto, Portugal, **1993**.
13. Mills, K. C. *Recommended values of thermophysical properties for selected commercial alloys*, Woodhead Publishing, United Kingdom, **2002**.
14. Munavalli, D. S.; Shimatadar, S. A.; Nandibewoor, S. T. Oxidation of vanillin by a new oxidant diperiodatoargentate(III) in aqueous alkaline medium. *Ind. Eng. Chem. Res.*, **2007**, 46 (5), 1459-1464.
15. Perry, R. H.; Green, D. W.; Maloney, J. O. *Perry's Chemical Engineers Handbook* (7th Edition), McGraw Hill, New York, **1997**.
16. Poling, B. E.; Prausnitz, J. M.; O'Connell, J. P. *The properties of gases and liquids* (5th Edition), McGraw Hill, USA, **2001**.
17. Salmon, A.; Dalmazzone, D. Prediction of enthalpy of formation in the solid state (at 298.15 K) using second-order group contributions. Part 1. Carbon-hydrogen and carbon-hydrogen-oxygen compounds. *J. Phys. Chem. Ref. Data*, **2006**, 35 (3), 1443-1457.

18. Smith, J. M.; Van Ness, H. C.; Abbott, M. M. *Introduction to Chemical Engineering Thermodynamics* (5th Edition), McGraw Hill, Singapore, **1996**.

19. *Ullmann´s Encyclopedia of Industrial Chemistry*; 7th Edition, Wiley-VCH, Verlag GmbH & Co..KGaA, **2003**.

20. Washburn, E. W. *International critical tables of numerical data, physics, chemistry and technology* (1st Electronic Edition), Knovel, **2003** (http://www.knovel.com/knovel2/Toc.jsp?BookID=735).

21. Yaws, C. L. *Chemical properties handbook*, McGraw Hill, USA, **1999**.

4. Continuous Reactor Setup for vanillin production

The main objective of this work is the continuous production of vanillin using lignin as raw material. To fulfil this goal, the first and most important step was the design and construction of a complete and operational pilot installation. This chapter describes the experimental setup developed with the main objective of studying the effect of reaction and hydrodynamic parameters on the continuous lignin oxidation to produce vanillin. However its versatility allows an operation with different chemical systems and flow conditions, for example in semi-batch mode (closed to gas or liquid). It is also prepared to work with temperatures up to 170ºC and pressures up to 15 bar, in very strong alkaline medium (pH =14).

The heart of this equipment is a bubble column reactor where the chemical oxidation takes place. Bubble columns are mass transfer and reaction devices, which in its simpler form are a vertical cylinder where the gas enters at the bottom through a gas distributor that may vary in design, and the liquid phase may be fed in batch form or it may move with or against the flow of the gas phase (Deckwer, 1992). The top of the bubble column is usually widened to promote the separation of phases.

Two main advantages of bubble column reactors are its simple construction and the absence mechanically operated parts (Deckwer, 1992). The decision to use a bubble column reactor on this work is supported on these two factors plus some advantages pointed out next:

- No shaft sealing is required, which enables the operation of aggressive substances even at high temperatures and pressures. This feature is important

because the liquid phase normally used (black liquor) had a concentration of 2 M in sodium hydroxide.

- Adaptable type of reactor, reasonable in price and can be built in large sizes. It can be a decisive point on a possible future application to industrial scale.
- It features high heat transfer coefficients, providing uniform temperature throughout even with strong exothermal reactions, which is the case of chemical oxidations involved in this study.

In this chapter a description of the bubble column reactor and ancillary equipment is provided. The procedures used to perform the continuous reactor experiments on vanillin oxidation, lignin oxidation and tracer tests along with the correspondent analytical protocols are also described.

4.1. General description of the installation

The apparatus built in this work was conceived to promote gas-liquid reactions in a continuous operating mode. Its layout is schematically presented in Figure 4.1, and two pictures of this setup are shown in Figure 4.2.

The main piece of equipment is a bubble column reactor with a working capacity of around 8 liters, which structure can be physically divided into four parts:

- Liquid stabilization chamber;
- Gas distributor to disperse the gas entering into the column;
- Cylindrical main body filled with structured packing where the gas-liquid reactions take place. This section is fully jacketed together with the liquid stabilization chamber;
- Head to separate the dispersed gas from the liquid phase.

A thermostatic bath (Haake, model N2-B, Germany), with 12 litters capacity, circulates a heating fluid through the jacket of the liquid stabilization chamber and the cylindrical main body of the reactor for retaining constant temperature. The temperature employed in this work goes up to 140ºC. The heating fluid used for this purpose was a high temperature resistant silicone oil (Silicex 322, Siliconas Hispania, Spain).

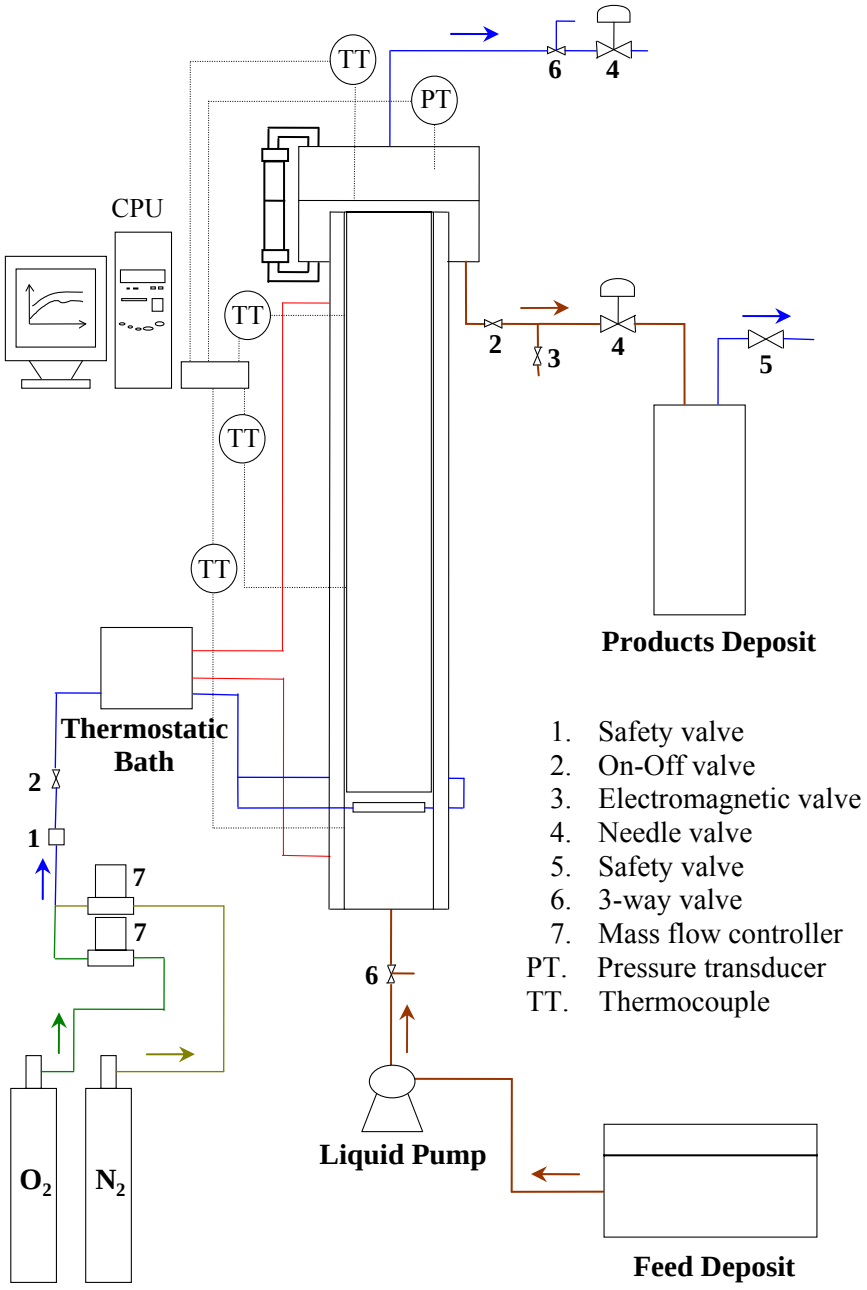

Figure 4.1. Layout of the installation for the production of vanillin from lignin.

Figure 4.2. Pictures of the laboratory setup for the continuous production of vanillin. On the left is the apparatus when its construction was finished, and on the right is a photo during a lignin oxidation experiment.

The fluid flow of the liquid and gas streams through the system is described as follows:

- Liquid stream – the liquid solution is stored in a stainless steel reservoir and is fed to the base of the reactor by a piston pump (Dosapro Milton Roy, Milroyal, USA) developed to work in strongly alkaline media, in the range of 1.3 – 13 l/h. Then, the liquid phase passes through the stabilization chamber to stabilize its flow conditions and increase its temperature, and continues to move upward through the packed column where it reacts with the oxygen transferred from the gas phase. The final liquid product is collected on the lower part of the separation head of the reactor. Since this product stream has a temperature and pressure reasonably higher than the atmospheric conditions (around 130ºC and 10 bar), and a very high *pH* (above 12), it requires special care, and cannot be driven directly to the sewer. After the separation head, in the liquid exit line there is an on-off valve (security) followed by a needle valve in order to promote

a pressure drop, and manually control the discharge flow rate on the products deposit. This valve is adjusted to keep a constant liquid level in the separation head. The deposit is also made on 316L stainless steel, and has a safety valve to avoid the increase of pressure to values higher than a specified set point. Between this deposit and the exit of the reactor there is a derivation on the pipeline with a manual electromagnetic valve. This valve allows the operator to collect liquid samples whenever it is desired. The entire liquid line is made of 1/4" tube on stainless steel. All the valves and fittings are Swagelok (Ohio, USA) except for the electromagnetic valve used for sampling (Asco model HTB262C15T, Scherpenzeel, Netherlands).

- Gas line – the gas line starts on nitrogen (N45) and oxygen (N50) cylinders supplied by Air Liquide, allowing mixtures of these two components to be fed to the reactor. Flows are controlled by two mass flow controllers (Bronkhorst, Netherlands): 0 – 1 SLPM and 0 – 2 SLPM calibrated for O_2 and N_2, respectively. The gas flow rates employed ensures that one gas cylinder can be used for at least five experiments (considering that the experiment may take up to 12 hours). The mixture stream passes through a coil, placed inside the thermostatic bath, heating up to values near the desired reaction temperature before entering the gas distributor. The entrance line of the gas is divided into four streams made in 1/8" tube of equal length that are connected to the gas sparger in equidistant positions to provide homogeneous gas distribution. The gas is bubbled into the liquid phase and flows upward through the packed column. When it reaches the column head, it is separated from the liquid due to gravitational forces, building up a bulk gas phase in the top of the equipment. Then, the gas phase leaves the reactor through the top of the separation head,

where it is connected an exit line containing a needle valve to control the correspondent flow rate. The opening of this valve will indirectly control the operation pressure.

4.2. Structured packed bubble column reactor

As already mentioned, the main piece of equipment of this work is a structured packed bubble column reactor made in 316L stainless steel, designed in LSRE and built by Neves & Neves (Trofa, Portugal). One of the initial targets of this work was to design a reactor with a volume of at least five liters. The dimensions of the reactor are also limited by the structured packing employed. In Figure 4.3 is presented a picture of the bubble column reactor where are indicated the main parts of its structure. In the following sections the main parts of this reactor are described with more detail.

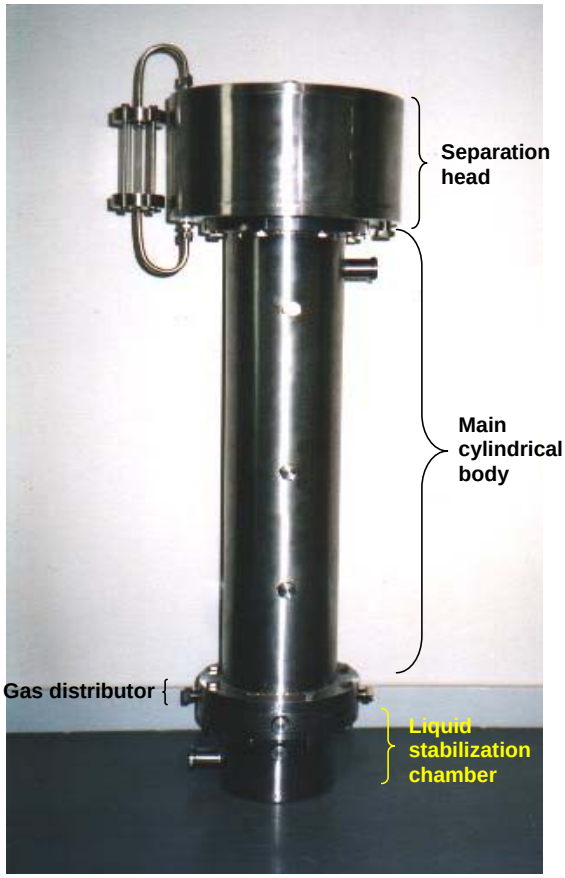

Figure 4.3. Picture of the bubble column reactor and identification of its main parts.

4.2.1. Liquid stabilization chamber

The liquid stabilization chamber is the lower piece of the column with a height of 10 cm and same internal diameter. This column is surrounded by a jacket with 1.5 cm of width. The main functions of the liquid stabilization chamber are to smooth the flow conditions of the liquid phase after it enters the reactor, and promote a pre-heating of this phase before contacting with the gas reagent. In Figure 4.4 two pictures of this reactor section and the correspondent schematic draws are shown.

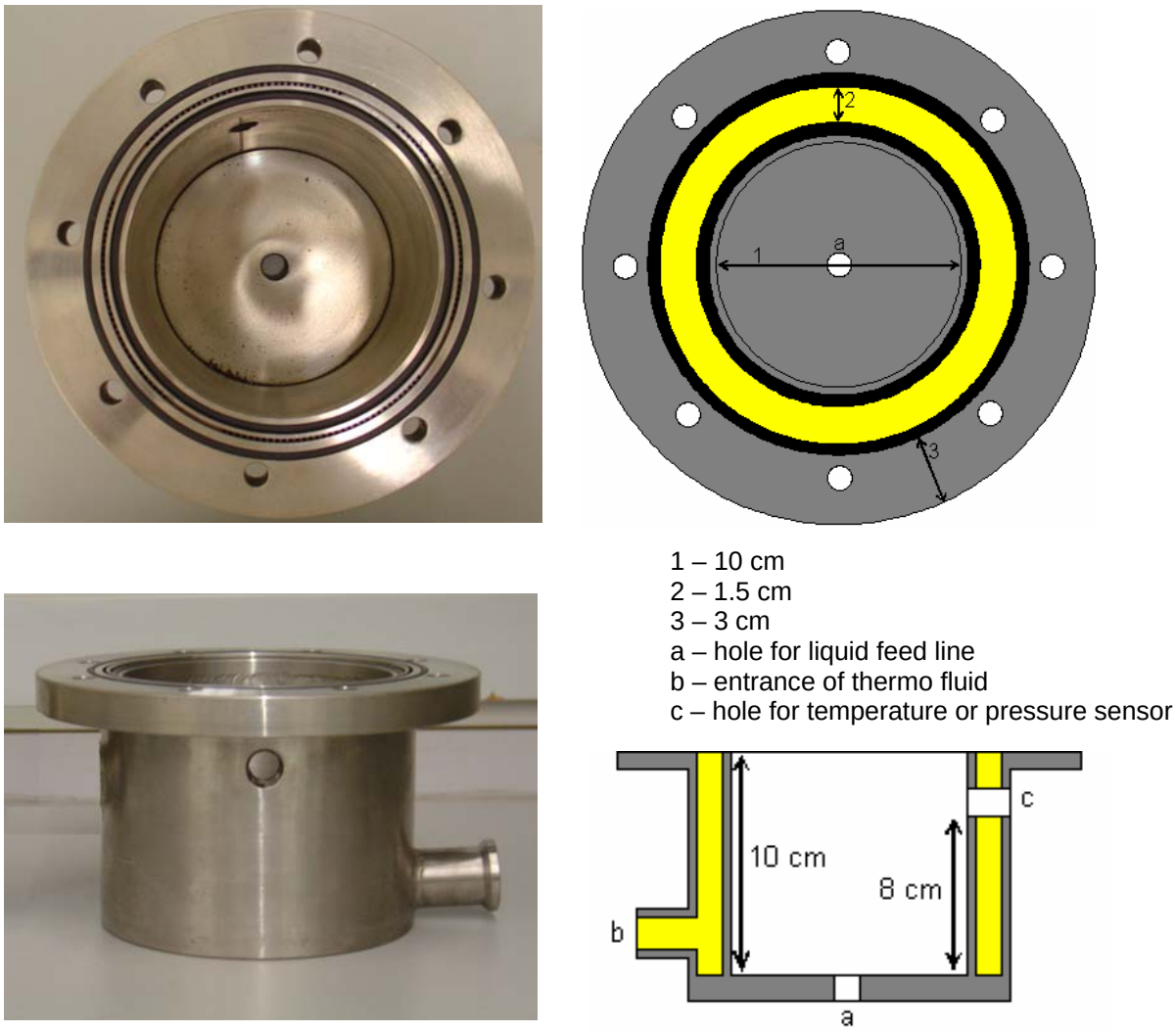

Figure 4.4. Images of the liquid stabilization chamber (upper and front view on the top left and bottom left of the figure, respectively). On the right side of this figure, a draw scheme of the upper view from this reactor section is presented at the top, and at the bottom is a representation of a longitudinal cut from the front view of the same section. The most relevant dimensions and holes of this piece are also identified.

The liquid feed line is connected to the reactor through a 1/4" NPT threaded hole placed at the bottom centre of the liquid stabilization chamber (hole a in Figure 4.4). Near the bottom of this section, the thermo fluid enters the jacket by opening b. There is another 1/4" NPT threaded hole at 8 cm height where it can be connected a temperature or pressure sensor (hole c in Figure 4.4). The possible internal leak points are prevented by using proper Teflon O-rings. These rings can be seen in the upper photo of Figure 4.4 and are represented in black colour in the correspondent draw.

4.2.2. Gas distributor

The gas distributor has an important influence on hold-up, interfacial area and the level of mass transfer in all bubble columns. Gas may be dispersed through pores or holes – static gas distributors, in contrast to the dynamic twin jet variety that takes advantage of the kinetic energy generated by the liquid force. Perforated plates, normally made of metal, with holes between 1 and 5 mm in diameter are simple gas distributors which are the most commonly used.

The distributor used on this work is a hollow piece with 1 cm of internal width and a shape shown in Figure 4.5. The gas comes out from upper surface of the distributor, bubbling on the reaction medium, through holes with a diameter of 1 mm. These holes are placed on the upper surface of the distributor in such a way to be distanced 2 cm from each other (like vertices of equilateral triangles). The idea is to promote the formation of small bubbles, with a uniform distribution in the liquid (state of homogeneous flow), and avoid the aggregation in larger ones throughout the column.

The gas feed line is divided into four isolated tubes that are connected to the distributor, in perpendicular directions to each other, through 1/4" NPT threaded holes (holes d in Figure 4.5).

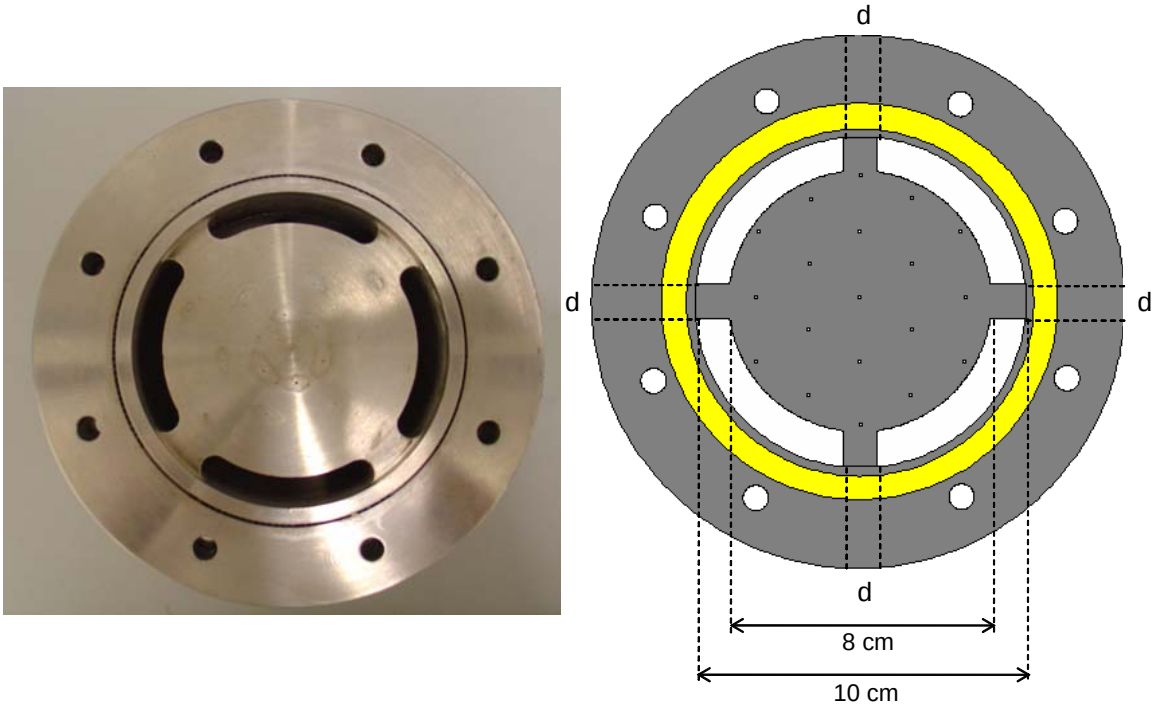

Figure 4.5. Top view picture of the gas distributor and the correspondent design draw. The box of the distributor has an external diameter of 8 cm and openings d are for the entrance of the gas phase.

4.2.3. Main cylindrical body

The main cylindrical body of the reactor is the section where the gas-liquid reactions take place. This section was designed to have a minimum volume of five liters. It has an internal diameter of 10 cm and 70 cm height, as it can be seen in Figure 4.6, and is fully jacketed to provide the media with proper reaction temperatures. As it was already mentioned, this jacket is shared with the liquid stabilization chamber and has a width of 1.5 cm. After circulating in the jacket, the thermo fluid exits to the thermostatic bath through opening f (Figure 4.6).

This section of the column has three 1/4" NPT threaded holes to connect thermocouples (holes e in Figure 4.6), respectively at heights of 15, 30 and 55 cm above the gas distributor. The connection between the main cylindrical body and the

liquid stabilization chamber is provided with Teflon O-rings to avoid fluid leakage. These rings are visible in the pictures of top and bottom views presented in Figure 4.6.

The end of the main cylindrical body is placed 5 cm inside of the separation head, at a higher relative position than the exit line of the liquid phase, to guarantee the almost absence of dispersed gas in the liquid collected from the reactor.

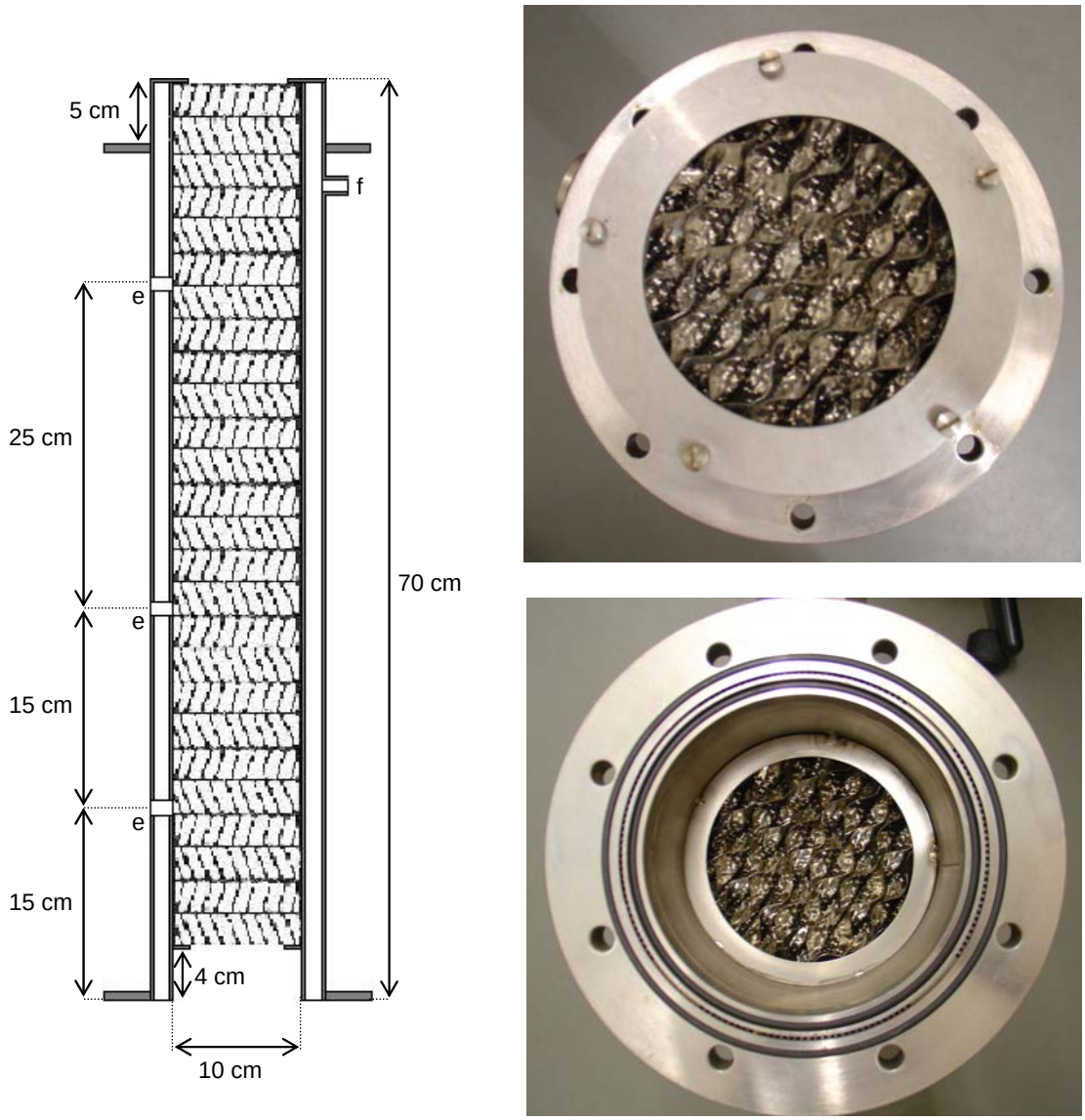

Figure 4.6. Schematic draw of a longitudinal cut of the main cylindrical body containing its major dimensions and openings. On the right top of the figure there is a picture of a view from above of this reactor section, and on the right bottom is presented a picture viewing from below.

The main cylindrical body of the reactor is filled with three modules of Mellapak 750.Y structured packing from Sulzer Chemtech (Switzerland) made in 316L stainless steel. The diameter of the reactor was selected to fit tightly the structured packings avoiding lateral gas by-passing. The goal is to enhance the overall mass transfer performance of the system. Each of the modules is rotated 90º with respect to the adjacent one to promote radial mixing of the fluids in the transition between packing elements. The column has a disk-shape welded knocker at a height of 4 cm to avoid the obstruction of the gas distributor holes by the packing metal sheets. The packing elements are stacked between this knocker and other one placed at the end of the column. This last knocker is also disk-shaped but instead of being welded it is attached to the column by screws, allowing an easy charge and discharge of the packing modules whenever is the desire of the operators. The two referred knockers are visible in the photographs of Figure 4.6.

In Figure 4.7 two pictures of a Mellapak 750.Y packing element are presented. This type of packing is characterized by a geometric specific area of 750 m^2/m^3 and a void fraction of 0.95 (Siminiceanu et al., 2007). The corrugated metal sheets that make up these packings are inclined by an angle of 45º with respect to the vertical axis.

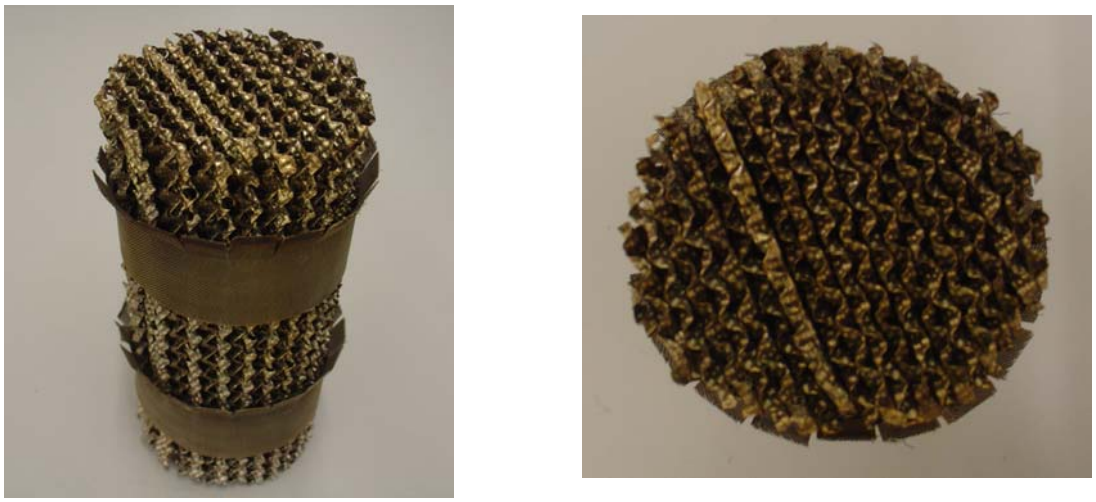

Figure 4.7. Lateral and top view photographs of a Mellapak 750.Y packing module from Sulzer Chemtech (Switzerland).

4.2.4. Separation head

The objective of having a separation head at the top of the reactor is to separate gas and liquid streams, obtaining a final liquid stream with no dispersed gas, taking advantage of the impulsion forces on the gas bubbles. This section of the reactor is shown in the photographs and draws of Figure 4.8. Basically, it has a cylindrical shape with an internal diameter of 23 cm and height of 12 cm.

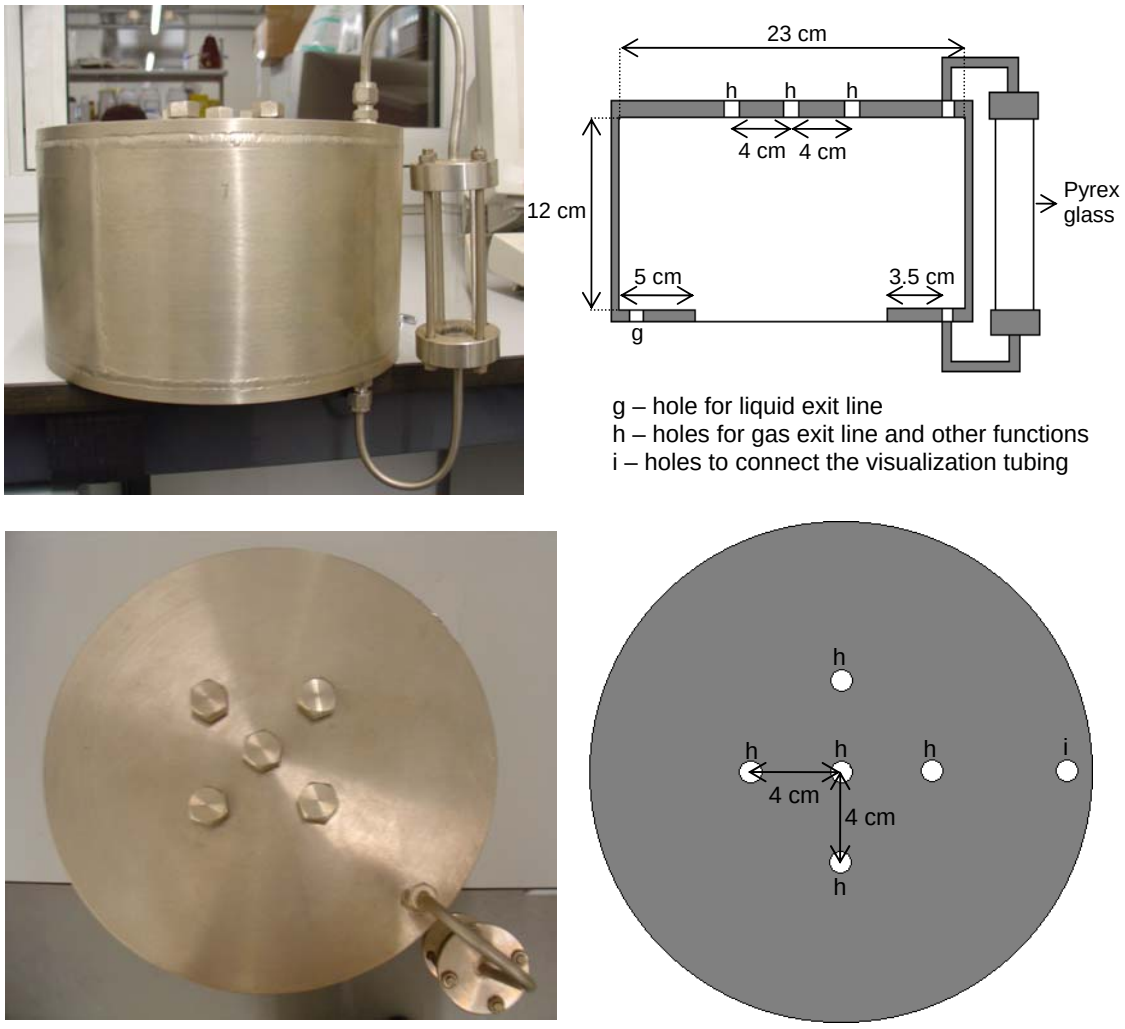

Figure 4.8. Images of the separation head (side and upper view, on the top left and bottom left of the figure, respectively). On the right side of the figure two schematic draws are presented: at the top is a longitudinal cut from the side view of the separation head, and at bottom is the upper view of this reactor section. The most relevant dimensions and holes of this piece are also presented.

During the operation of the reactor is very important to control the height of the liquid surface inside the separation head. This height should not reach levels too high, to provide a sufficient volume of bulk gas in the top of the head that allows a safer control of the pressure vessel. On the other hand, it is not advisable that the liquid height lowers too much, to avoid the collection of gas in the liquid exit stream and the consequent high instabilities in the flow rate of this stream. The liquid exit stream is connected to the bottom of the separation head through a 1/4" NPT threaded hole, identified as opening g in Figure 4.8.

In the top plate of the separation head are placed five 1/4" NPT threaded holes (holes h in Figure 4.8). At the centre hole was connected a thermocouple to measure the temperature of the media at the exit of the main cylindrical body of the reactor. The other four openings were used to connect different functions, such as the gas exit line, a pressure transducer, and a U-tube with a manometer in one side and a safety valve in the other side.

4.3. Sensors and data acquisition

The pressure at the separation head and the temperature in three different positions of the main cylindrical body were followed continuously during the experimental runs performed on the structured packed bubble column reactor. The pressure was read by a pressure transducer (Lucas Schaevitz, U. K.) placed in contact with the gas bulk phase at the top of the separation head. The temperatures inside the reactor were measured on three different locations distanced of 15, 30 and 70 cm from the gas distributor. For this purpose three thermocouples type K (Omega, U.K.) were

used, measuring the temperature of the media near the column wall, since the main cylindrical body of the reactor was filled with the structured packing.

The electric signals of the thermocouples and the pressure transducer are acquired by a system composed by a terminal board PCLD-8710 (Advantech, USA), an acquisition board PCI-1710HG (Advantech, USA) and a PC Pentium III 500 MHz. This data acquisition system is the same that was used in experimental runs described on Chapter 3 of this thesis.

The program for data acquisition was developed in LabView (National Instruments, USA) and has equal functionalities to the one used in the batch reactor, with the difference that it acquired three instead of two voltage signals from thermocouples. It performed cyclically the tasks of making 30 readings of each signal with time intervals defined by the user, averaging and saving the average values from each sensor in separate files along with the correspondent time.

The used-friendly interface of this data acquisition program is similar to the one presented in Figure 3.2 of Chapter 3, with the exception of adding one more temperature to the system settings, visualization of current values and temperature history.

4.4. System operation

4.4.1. Tracer experiments

The residence time distribution (RTD) is a very useful tool for characterizing the basic hydrodynamics of a vessel, helping to analyze the reactor performance and estimating parameters for non-ideal reactor models (Fogler, 1992; Levenspiel, 1999; Missen, Mims and Saville, 1999).

The experimental determination of the RTD is usually made by the stimulus-response method. This method consists on injecting a tracer material of known concentration at the inlet of the vessel and then measuring its concentration in the effluent stream as a function of time.

For achieving RTD results that are meaningful and representative of the liquid flow in a system, the tracer should be a non-reactive species, physically similar to those in the reaction medium, non-volatile, and completely soluble in the mixture used for the RTD experiments. The tracer must not be adsorbed on the surfaces of the vessel and should be a stable compound to allow the application of simple material balances relating the input to the output of the reactor. It should also be easily detected in the outlet stream by a reproducible analytical procedure.

The RTD experiments performed in this work used water as the flowing liquid phase and N_2 as the gas phase. The operating temperature and pressure were 50ºC and 10 bar, respectively, and the maximum inlet concentration of the tracer was around 45 mg/l. Vanillin was used as the tracer material since in these experimental conditions it presents complete solubility in water and it does not suffer oxidation (no oxygen employed). It is also a model compound, since is one of the products formed in the reaction mixture of lignin oxidation and can be easily and linearly quantified by spectrophotometric analysis. The description of a generic RTD experiment is detailed below.

The first step was to prepare a vanillin aqueous solution of known concentration that would be used for a tracer pulse. Distilled water was placed in the feed reservoir and all the valves of the liquid and gas exit lines were closed. The piston pump was turned on to fill the reactor with water, and shut off when it reached the desired liquid height by visualization of the Pyrex glass tube of the separation head. The nitrogen

bottle was opened, the correspondent mass flow controller was turned on and N_2 was fed to the system until the total pressure was 10 bar (also removing oxygen from the reactor).

Afterwards, the piston pump was turned on again and the valves of the liquid exit line were opened. The needle valve placed in this line was regulated to a position that allowed a flow rate of liquid exit stream equal to the one entering the reactor. This was attained by certifying that there was no variation in the liquid height inside the separation head neither in the total pressure of the system. Once the liquid circulation in the reactor was stabilized, the same procedure to equalize the inlet and outlet flow rates was applied to the gas phase (N_2).

After the stabilization of the operating conditions the system was ready to start the tracer experiment. The data acquisition was started and, simultaneously, the feed of the piston pump was changed to the vanillin solution. When the desired volume of tracer solution was inserted in the reactor the liquid feed was directed again to the water reservoir.

Samples of the liquid phase were taken for approximately nine hours, starting at the injection of the tracer. This sampling was made in two different points of the reactor: liquid stream exiting the separation head and at the end of the main cylindrical body filled with structured packing. At the end of the experiment, the data acquisition was stopped, the piston pump was turned off and the valves in the gas feed line were closed. The reactor was depressurized and the water inside of it was discharged using the 3 way valve placed in liquid feed line.

4.4.2. Experiments of lignin oxidation

A complete experimental run of lignin oxidation can be divided in three main parts. The first part consisted on passing water through the system to clean the residues left in the reactor and the liquid lines by a former experiment.

The second part of the experiment started with the preparation of 40 litres of an aqueous solution with 60 g/l of lignin and 80 g/l of sodium hydroxide. This liquid mixture was placed in the feed reservoir and the piston pump was turned on to fill the reactor. The gas exit line was opened and nitrogen was admitted to the system, during approximately 15 minutes, to replace the air in the gas bulk phase by inert N_2. The set point of the thermostatic bath was placed at 170ºC and the thermo fluid started to circulate through the jacket with the purpose of achieving a steady-state temperature inside the reactor around 130ºC. Nitrogen was again admitted to the reactor, but now with the exit gas line closed to pressurize the system to the desired operating value. The liquid and gas outlet flow rates were regulated using a similar method to the one described for the tracer experiments. Once that operating temperature, pressure and flow rates were stabilized and the oxidation of lignin could be initiated. This phase of the experiment comprised:

- Close the valve of the gas feed line and establish the desired N_2 and O_2 flow rates in the mass flow controllers.
- Start the data acquisition and reopen the valve of the gas feed line (the oxidation initiates in this moment).
- Collect samples of the liquid stream exiting the separation head during 8 to 9 hours.
- Stop the data acquisition, turn off the piston pump and close the gas feed.

- Depressurize and discharge the liquid mixture inside the reactor using the 3 way valve of the liquid feed line.
- Analyze the liquid samples to determine its vanillin concentration.

The third and final part concerns the treatment of the residues. The liquid phase collected during the experiment and at the discharge of the reactor is very alkaline and needs to be neutralized before its disposal. This liquid (around 40 litres) was treated with hydrochloric acid (HCl) until it reached a *pH* around 7 and only then could be disposed into the sewer.

It is important to notice that a lignin oxidation experiment in the continuous reactor is complex, difficult to execute and very time consuming. A complete experiment in this system, including the liquid sample analysis, takes 10 to 12 days to be performed.

4.4.3. Experiments of vanillin oxidation

The procedure for the vanillin oxidation experiments performed in the structured packed bubble column reactor is similar to the one presented in section 4.4.2 for lignin oxidation. The only difference is in the liquid mixture prepared that consisted in aqueous solutions of 5 g/l and 4 g/l of vanillin with a *pH* of 14 and 9.8, respectively.

4.5. Analytical procedure

4.5.1. Tracer experiments

The samples collected in the tracer experiments were analyzed in a spectrophotometer model 7800 from Jasco (USA). The absorbance of the samples was

measured at the wavelength of 348 nm and converted to vanillin content using the calibration curve in Figure 4.9.

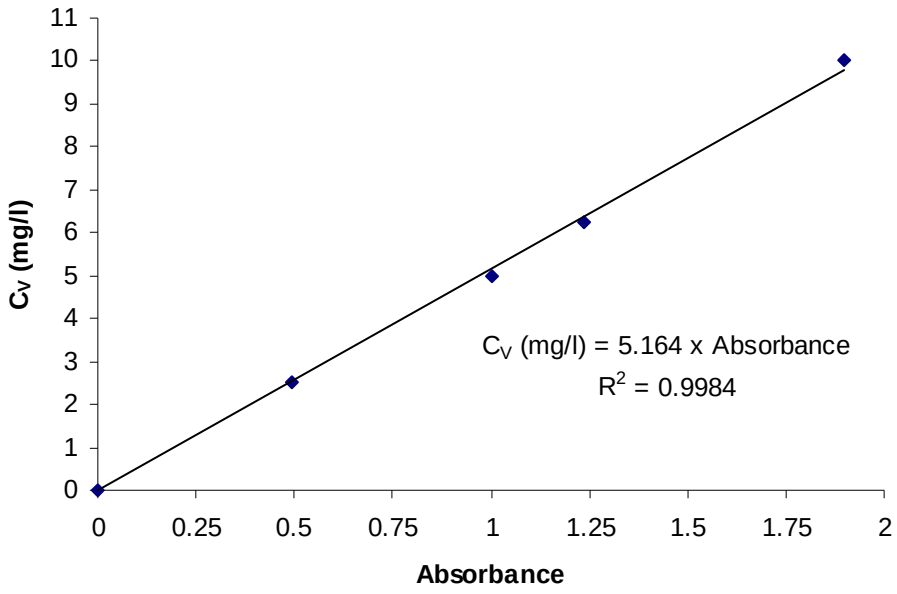

Figure 4.9. Calibration curve relating the vanillin concentration of aqueous solution to its absorbance at 348 nm.

4.5.2. Experiments of lignin oxidation

The vanillin content of the samples obtained in the lignin oxidation experiments was determined by a gas chromatographic method. The analytical procedure is the same as the one used for the batch reactor experiments and described in section 3.1.3 of Chapter 3.

4.5.3. Experiments of vanillin oxidation

The samples of the vanillin oxidation experiments suffered 1:800 dilutions in aqueous solutions with 0.1 mol/l of NaOH. The diluted samples were analyzed in the same spectrophotometer used for the samples of the tracer experiments. The vanillin content was determined with the help of the calibration curve in Figure 4.9.

4.6. Tracer experiments

RTD can be determined with the help of all sorts of input techniques. In this work pulse input experiments were chosen, since they are easier to perform and to analyze (Levenspiel, 1999).

A perfect pulse input experiment, represented in Figure 4.10, consists in the measurement of the system response to an instantaneous injection of a known quantity of tracer (M_T) into the fluid feed of the vessel to characterize. This response is the transient tracer concentration curve (C_T^{out}) in the outlet stream of the reactor.

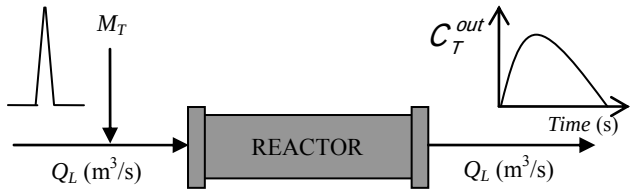

Figure 4.10. Schematic representation of a pulse input experiment (based on Alvaré and Al-Dahhan (2006)).

The $E(t)$ curve can be obtained with a simple normalization of the output tracer concentration as follows:

$$E(t) = \frac{C_T^{out}(t)}{\int_0^{\infty} C_T^{out}(t)dt} \tag{4.1}$$

This equation is valid for closed boundary conditions, i.e. the tracer molecules cross the inlet and the outlet of the vessel only once.

From the tracer mass balance equation around the vessel, for constant liquid flow rate, it can be written that:

$$M_T = Q_L \int_0^{\infty} C_T^{out}(t)dt \tag{4.2}$$

Knowing the experimental values of M_T and the volumetric flow rate of the inlet stream (Q_L), the equation (4.2) can be used to test the quality of an experiment, since it checks if the amount of tracer leaving the system is equal to the amount of tracer injected.

Once the $E(t)$ curve has been obtained, it is also fundamental to calculate its first and second moments:

$$\mu_1 = \bar{t}_R = \int_0^\infty t\ E(t)dt \tag{4.3}$$

$$\sigma^2 = \int_0^\infty \left(t - \bar{t}_R\right)^2 E(t)dt \tag{4.4}$$

The first moment of the $E(t)$ physically represents the mean residence time ($\bar{t}_R$) of the tracer inside the reactor. This important system parameter allows the experimental determination of the active volume inside the vessel:

$$V_{act} = \bar{t}_R \cdot Q_L \tag{4.5}$$

The second moment is equal to the variance (σ^2) and quantifies the spread of the RTD curve.

4.6.1. Reactor flow model

Tracer experiments on the liquid phase were performed in two distinct reactor systems: structured packed bubble column reactor and simple bubble column reactor. In both cases a model with compartments in series representing two physical sections was considered: column section (liquid stabilization chamber + main cylindrical body) and the separation head. A schematic diagram of this compartment model is made on Figure 4.11.

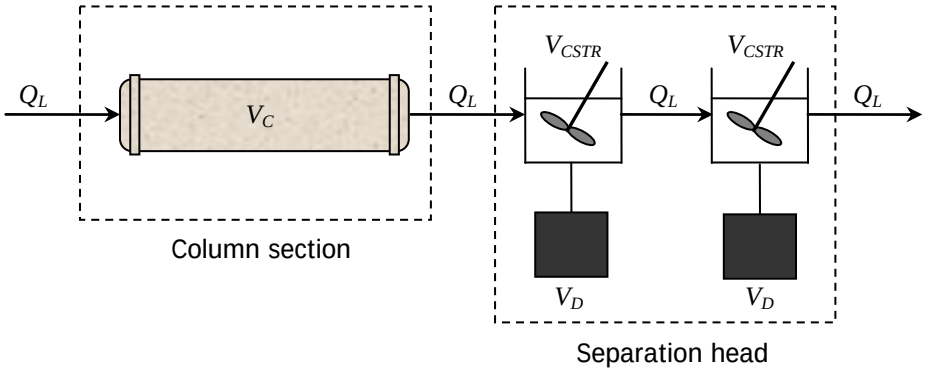

Figure 4.11. Schematic representation of the compartment model selected to describe the liquid phase flow in the structured packed bubble column reactor and simple bubble column reactor.

For both packed and simple bubble columns, the most widely used model to characterize the flowing of liquid phase is the axial dispersion model (Belfares et al., 2001; Lakota et al., 2001; Levenspiel, 1999; Missen, Mims and Saville, 1999). A one-dimensional model was assumed to represent the liquid hydrodynamics in the column section. According to this RTD flow model, the tracer spreads in the axial direction when it passes through the column as a result of a dispersive process superimposed on ideal plug flow. This phenomena is generally quantified by a parameter called axial dispersion coefficient (D_{ax}).

The liquid inside the separation head flows through an annular volume, as it can be seen in Figure 4.12.

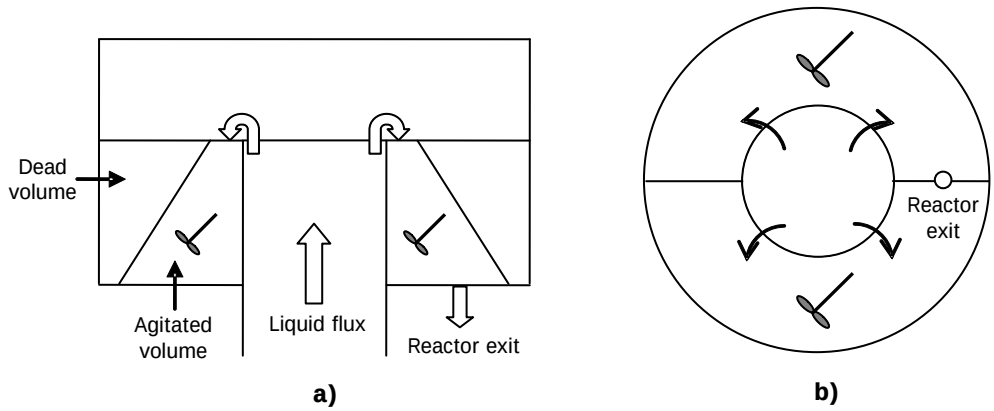

Figure 4.12. Sketch of the liquid flow configuration assumed for the separation head.

Since there is no gas bubbling in the annular volume of the separation head, the corresponding liquid will be far from perfect mixing. In fact, the degree of agitation that this amount of liquid suffers is probably the result of the suction promoted by the pressure gradient between the liquid exit and the contents of the separation head. Admitting that this kind of agitation is more effective at distances closer to the reactor exit, the annular volume of liquid can be divided into two sections with different behaviours (Figure 4.12a). In the top section, it is assumed that the liquid volume present is approximately inert to the flow process (dead volume), and so the tracer molecules will travel directly to the agitated section.

Taking a symmetry axis that passes through the reactor exit, the annular volume of the separation head can be hypothetically divided in two identical slices as it is shown in Figure 4.12b), each of them comprising a fraction of dead volume and a fraction of agitated volume. If it is accepted that the liquid flow rate entering the separation head is equally divided into the two slices, then it is most probably true that a tracer molecule travels through both agitated fractions before exiting the reactor.

The conceptual assumptions made for the liquid phase flow model are mathematically described below and will be validated in the results section of this chapter.

Based on axial dispersion flow, an unsteady state material balance for the tracer in the column section can be expressed as:

Column section

$$\varepsilon_L D_{ax} \frac{\partial^2 C_T}{\partial z^2} = u_{LS} \frac{\partial C_T}{\partial z} + \varepsilon_L \frac{\partial C_T}{\partial t} \tag{4.6}$$

where t is time; z is axial position relative to the liquid entrance; C_T is the tracer concentration; u_{LS} is the superficial liquid velocity and ε_L is the liquid hold-up.

The superficial liquid velocity is obtained from the volumetric flow rate of liquid (Q_L) and the total cross section area of the column (A_C):

$$u_{LS} = \frac{Q_L}{A_C} \tag{4.7}$$

The liquid hold-up represents the fraction of the liquid volume (V_L) in the total volume of the column (V_C):

$$\varepsilon_L = \frac{V_L}{V_C} \tag{4.8}$$

Considering the active volume in the separation head as two equal continuous stirred tank reactors, an unsteady state mass balance for the tracer leads to:

Separation head

Tank 1: $$C_T^{out} Q_L = C_{T1} Q_L + V_{CSTR} \frac{dC_{T1}}{dt} \tag{4.9}$$

Tank 2: $$C_{T1} Q_L = C_{T2} Q_L + V_{CSTR} \frac{dC_{T2}}{dt} \tag{4.10}$$

where C_T^{out}, C_{T1} and C_{T2} are, respectively, the tracer concentration in the exit of the column section, inside the first stirred tank and in the outlet stream of the reactor. The volume of each stirred tank is represented by V_{CSTR}.

The boundary conditions used for equation (4.6) are the ones stated by Danckwerts for a closed-closed vessel (Fogler, 1992; Levenspiel, 1999; Missen, Mims and Saville, 1999):

At $z = 0$: $$u_{LS} C_T^{input} = u_{LS} C_T\big|_{0,t} - \varepsilon_L D_{ax} \left.\frac{\partial C_T}{\partial z}\right|_{0,t} \tag{4.11}$$

At $z = L$: $$\left.\frac{\partial C_T}{\partial z}\right|_{L,t} = 0 \tag{4.12}$$

where L is the length of the column section, and C_T^{input} is the disturbance on the tracer concentration promoted in the inlet stream of the column.

The initial conditions for the equations (4.6), (4.9) and (4.10) are:

$$t = 0 \qquad C_T\big|_{z,0} = 0 \tag{4.13}$$

$$t = 0 \qquad C_{T1} = 0 \tag{4.14}$$

$$t = 0 \qquad C_{T2} = 0 \tag{4.15}$$

4.6.2. Results

4.6.2.1. Structured packed bubble column reactor (SPBCR)

As the main goal of this work is to operate a SPBCR for lignin oxidation, four tracer experiments were performed in this unit to obtain some hydrodynamic data necessary for its characterization. These experiments followed the procedure described in section 4.4.1, and the correspondent operating conditions are presented in Table 4.1.

Table 4.1. Experimental conditions used in the tracer experiments of the SPBCR. All experiments were performed at a temperature of 50ºC and 10 bar of total pressure.

	Experiment 1	**Experiment 2**	**Experiment 3**	**Experiment 4**
M_T (mg)	13.7	12.9	14.5	13.8
Q_L (l/h)	4.33	4.51	4.68	4.70
Q_G (ml_N/min)	1000	625	250	0

The experimental and simulation results for tracer concentration, obtained for the experiments of Table 4.1, are presented below. Two sampling points of liquid phase were placed in the SPBCR unit: one at the end of the column section (samples B) and the other in the exit of the separation head (samples A). The objective was to gather

experimental information that allowed the validation of the flow model for each reactor section and a source of estimation of the correspondent model parameters: ε_L and D_{ax} for the column, and V_{CSTR} for the separation head.

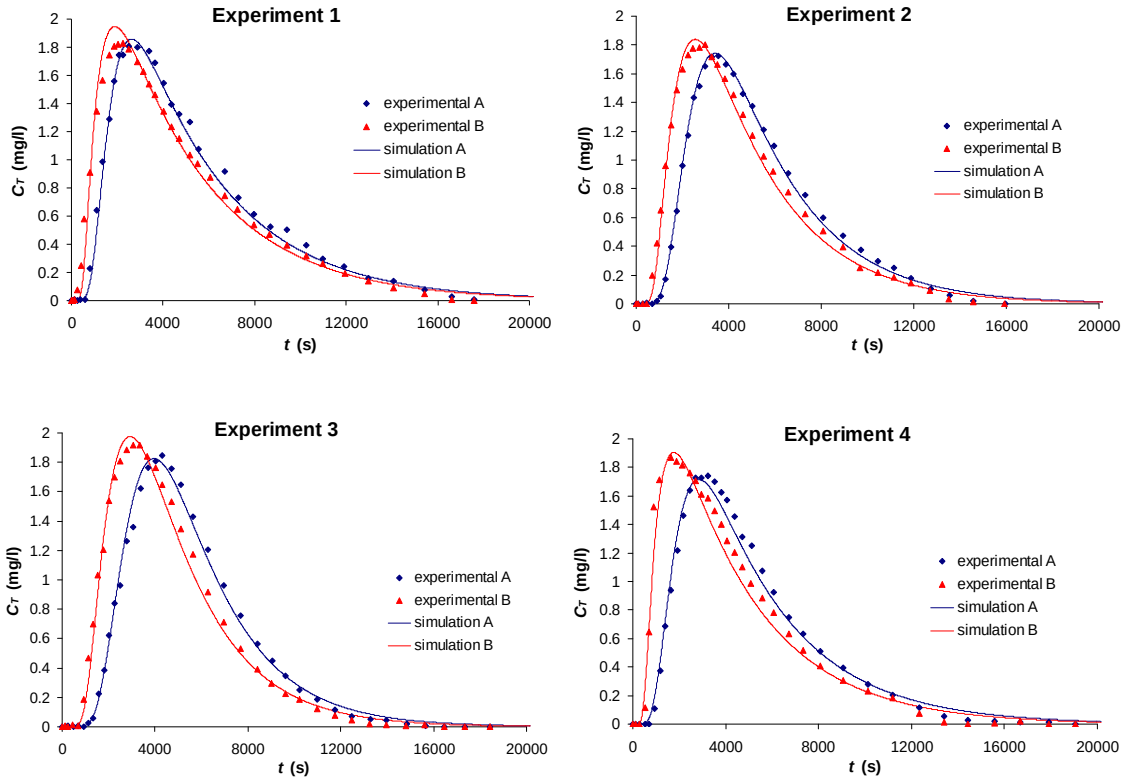

Figure 4.13. Variation of the tracer concentration for the experiments performed in the SPBCR unit. The experimental conditions are in Table 4.1. Blue points represent the liquid samples collected at the exit of the reactor (samples A), and the red points correspond to the samples collected at the end of the column section (samples B). Red and blue solid lines correspond respectively to simulations using the flow model for the column section (axial dispersion model), and the flow model for the entire reactor (axial dispersion model + 2 CSTR's). The parameters used in the simulations (ε_L, D_{ax} and V_{CSTR}) are in Tables 4.3, 4.4 and 4.5.

The first step on the analysis of the tracer experiments was the determination of the mean residence times ($\bar{t}_R$), in the column and in the separation head, and the correspondent active volumes of liquid. All the tracer concentration curves were normalized to obtain $E(t)$, and the first and second moments of these distribution curves were calculated according to equations (4.3) and (4.4).

Since the liquid flow rate (Q_L) is a known operating condition, the active volumes of liquid (V_{act}) could be determined from the mean residence times. These values are presented in Table 4.2.

Table 4.2. Results of the $\bar{t}_R$, σ and V_{act} obtained in the SPBCR tracer experiments.

		Experiment 1	**Experiment 2**	**Experiment 3**	**Experiment 4**
Samples A	$\bar{t}_R^A$ (s)	5397	5429	5505	5114
	σ_A (s)	3272	2687	2416	2838
	V_{act}^A (ml)	6491	6801	7156	6676
Samples B	$\bar{t}_R^B$ (s)	4822	4719	4622	4281
	σ_B (s)	3219	2700	2376	2781
	V_{act}^B (ml)	5800	5912	6008	5590

The values of liquid hold-up (ε_L) in the column section are divided in two zones. In the liquid stabilization chamber the system consists only on liquid phase, so the ε_L is assumed as 1. Above the gas distributor, the liquid hold-up can be calculated from the experimental V_{act}^B as follows:

$$\varepsilon_L = \frac{V_{act}^B - V_{LC}}{V_C - V_{LC}} \tag{4.16}$$

where V_{LC} and V_C are respectively the volume of the liquid stabilization chamber and the total volume of the column. This expression is based on the assumption that the liquid stabilization chamber is absent of dead volumes.

Gas phase is present only above the distributor (ε_G is 0 in the liquid stabilization chamber), and its hold-up can be obtained from:

$$\varepsilon_G = 1 - \varepsilon_L - \varepsilon_S \tag{4.17}$$

where ε_S is the volumetric fraction occupied by the packing, based on the empty volume of the main cylindrical body and considering that the packing is placed 4 cm above the gas distributor, and the packing elements have a 3 mm gap between them and the reactor wall. The void fraction of the material is 0.95 (Siminiceanu et al., 2007) so $\varepsilon_S = 0.0417$.

The values obtained from the tracer experiments for the volumetric fractions described above are gathered in Table 4.3.

Table 4.3. Experimental volumetric data for the column section of the reactor.

	V_{LC} (ml)	V_C (ml)	**Main cylindrical body**		
			ε_L	ε_G	ε_S
Experiment 1	785	6283	0.912	0.0463	0.0417
Experiment 2	785	6283	0.932	0.0263	0.0417
Experiment 3	785	6283	0.950	0.0083	0.0417
Experiment 4	785	6283	0.874	-----	0.0417

Since experiment 4 was carried out in the absence of gas, the liquid hold-up should be around 0.958, according to equation (4.17). However, the corresponding result shown in Table 4.3 is smaller, which reveals a possible physical inconsistency. This observation could be explained by the development of dead volumes in the main cylindrical body when there is no gas to promote some degree of agitation.

These dead volumes in experiment 4 are estimated to be 464 ml. The major fraction of them are probably in a region immediately above the gas distributor since the tracer molecules that pass between the reactor wall and the distributor are no longer agitated before entering the packing channels. Instead, the tracer can take a more direct path to the packing leading also to a mal-distribution of its molecules between the

channels and the possible development of dead zones inside the packed bed. These hydrodynamic problems in the column are neglected in all the experiments that contain gas flow.

The axial dispersion coefficient (D_{ax}) in the column was extracted, for each experiment, by matching the experimental concentration curves for samples B with simulations using the flow model established for this reactor section. This parameter estimation was performed with the software gPROMS (PSE, United Kingdom) and the final results are presented in Table 4.4.

Table 4.4. Values of the experimental D_{ax} for the column section of the reactor.

	Experiment 1	**Experiment 2**	**Experiment 3**	**Experiment 4**
D_{ax} (m^2/s)	9.245×10^{-5}	4.737×10^{-5}	3.234×10^{-5}	9.678×10^{-5}
Pe	1.45	2.89	4.31	1.43

From Table 4.4 it can be verified that the experimental D_{ax} increase with the gas flow rate, with the exception of experiment 4. As it was already explained, this exception probably results from dead volumes and preferential paths of the liquid inside the packed bed, especially through the 3 mm space between the packing and reactor cylindrical wall.

The tendency of increasing dispersion in the column with the gas flow rate can be better visualized in Figure 4.14, and corroborated by a similar behaviour of the standard deviation values (σ_A) in Table 4.2. Although the liquid flow rates of the experiments represented in Figure 4.14 are not equal, as it can be seen in Table 4.1, their maximum difference is only 8 %, which lead to the assumption that the variations in D_{ax} mainly resulted from the quantities of gas supplied to the column. Theoretically,

the higher the gas content, more liquid is entrained in the rising bubbles, which promotes larger amounts of spreading of the tracer molecules throughout the column.

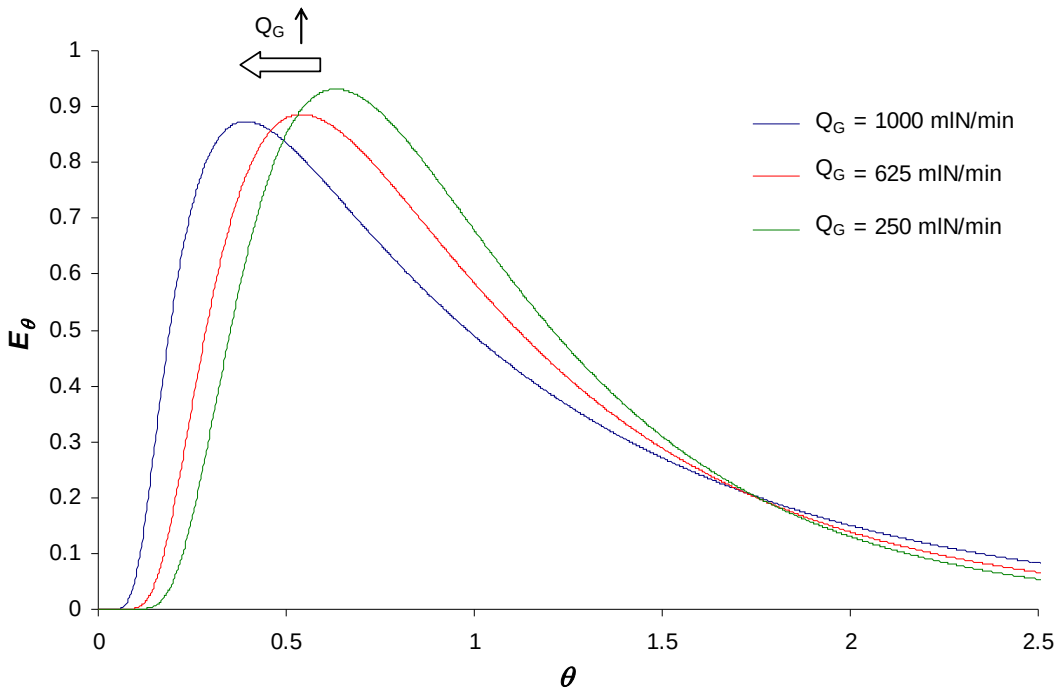

Figure 4.14. Simulation curves of the normalized residence time distributions of samples B for experiments 1, 2 and 3. The experimental conditions are in Table 4.1. The y-axis correspond to $E_\theta = E \cdot \bar{t}_R$ and in the x-axis is the dimensionless time ($\theta = t/\bar{t}_R$).

The annular volume of the separation head is admitted to confine only liquid divided into active and dead volume. Since the flow model of the separation head includes two ideal stirred tanks of equal size, the value of V_{CSTR} is considered to be half of the experimental volume of active liquid in this reactor section. The volume of active liquid in the separation head, and the corresponding dead volume, are calculated from V_{act}^{A} and V_{act}^{B}:

$$V_{CSTR} = \frac{V_{act}^{A} - V_{act}^{B}}{2} \tag{4.18}$$

$$V_D = V_{SH} - V_{act}^{A} - V_{act}^{B} \tag{4.19}$$

where V_D and V_{SH} are respectively the dead volume and the total liquid volume inside the separation head.

The experimental results for the model parameters V_{CSTR} and V_D of the separation head are shown in Table 4.5.

Table 4.5. Experimental values of the model parameters for the separation head.

	Experiment 1	**Experiment 2**	**Experiment 3**	**Experiment 4**
$V_{CSTR} \times 2$ (ml)	691	889	1148	1087
V_{SH} (ml)	1800	1800	1800	1800
V_D (ml)	1109	911	652	713

The total volume of liquid inside the separation head (V_{SH}) is based on the external diameter of the outside jacket tube, on the internal diameter of the separation head, and assuming throughout the experiments a constant liquid height inside the head of 5 cm.

The results of V_{CSTR} and V_D varied considerably between experiments with some sort of relationship with the gas flow rate. When the gas flow rate increased the total active volume of the head seems to decrease. However, there is no apparent reason for that behaviour since there should be no gas bubbling in the annular volume of the head, and if that possibility was true, the increase of the gas flow rate should lead to a higher agitation and consequently to lower dead volumes, which is opposite to the results obtained.

The most plausible explanation is connected to the fact that the liquid height inside the head is a difficult operating condition to stabilize during the experiments, and a simple deviation of 1 cm promotes a variation of 360 ml. This could promote

experimental errors with an order of magnitude close to the differences observed in the V_{CSTR} and V_D between experiments.

4.6.2.2. Bubble column reactor (BCR)

In order to set a reference for the performance of the structured packing, the reactor unit was also studied in the simple bubble column configuration (with no internals).

Two tracer experiments were performed in the BCR: one with gas-liquid flow at operating conditions similar to SPBCR tracer experiment 1, and the other in the complete absence of gas flow. In both of them, the tracer injection was assumed to be a pulse input and the liquid samples were collected only at the exit of the separation head. The operating conditions are resumed in Table 4.6.

Table 4.6. Experimental conditions used in the tracer experiments of the BCR. The experiments were performed at a temperature of 50ºC and 10 bar of total pressure.

	Experiment 1	**Experiment 2**
M_T (mg)	17.3	16.5
Q_L (l/h)	4.10	4.04
Q_G (ml_N/min)	1000	0

The experimental and simulation curves of the BCR experiment 1 are presented in Figure 4.15. The flow model assumed to describe this system is the same as the one applied for the complete SPBCR, i.e. a column with axial dispersion followed by two continuous stirred tank reactors with dead volume. The values of the model parameters are shown in Table 4.7.

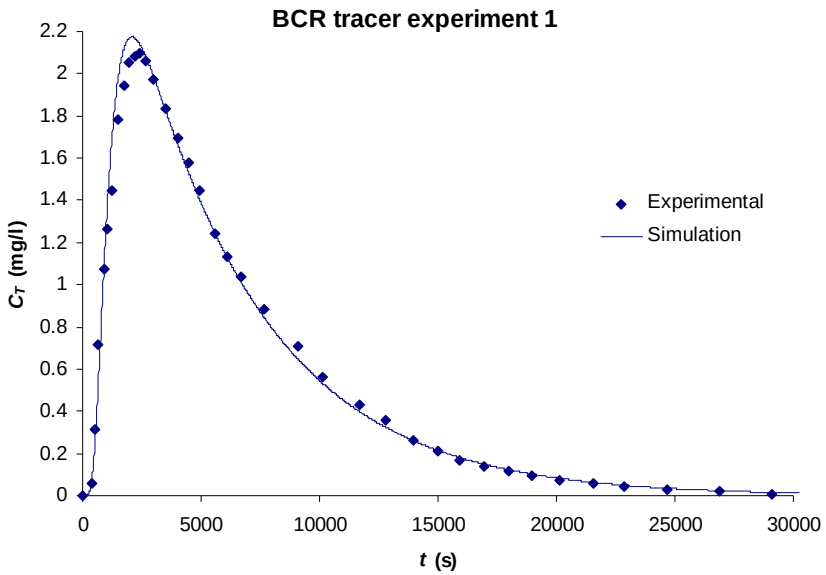

Figure 4.15. Variation of the tracer concentration for experiment 1 performed in the BCR unit. The experimental conditions are in Table 4.6. The points represent the tracer concentration of the liquid samples collected at the exit of the reactor. Solid line corresponds to the simulation using the flow model for the entire BCR (axial dispersion model + 2 CSTR's) with the parameter values of Table 4.7.

Table 4.7. Values of the model parameters for the BCR in the tracer experiment 1.

Main cylindrical body			**Separation head**		
ε_L	ε_G	D_{ax} (m^2/s)	$V_{CSTR} \times 2$ (ml)	V_D (ml)	V_{SH} (ml)
0.974	0.0262	6.923×10^{-4}	900	900	1800

The liquid flow in the separation head is considered to be independent from the presence of internal in the column section, so the $V_{CSTR} \times 2$ was taken as the arithmetic media of the correspondent values for the tracer experiments in the SPBCR (Table 4.5).

The volumetric fraction of liquid (ε_L) in the column is divided in two zones:

- $\varepsilon_L = 1$ for the first 10 cm of the column (liquid stabilization chamber).
- for the main cylindrical body the ε_L was extracted from the RTD data.

The experimental results of the tracer concentration were normalized into $E(t)$ and the mean residence time of this distribution curve was calculated from equation (4.3). The value obtained for $\bar{t}_R$ was 6181 s.

Once that $\bar{t}_R$ is known, the experimental values of the volumetric fractions inside the main cylindrical body are determined from:

$$\varepsilon_L = \frac{Q_L \cdot \bar{t}_R - V_{CSTR} \times 2 - V_{LC}}{V_C - V_{LC}} \tag{4.20}$$

$$\varepsilon_G = 1 - \varepsilon_L \tag{4.21}$$

The axial dispersion coefficient (D_{ax}) in the column was determined in a similar fashion to the SPBCR unit. The experimental concentration curve was matched to a simulation using the flow model that describes the complete reactor. This parameter estimation was performed with the software gPROMS (PSE, United Kingdom).

The results for the BCR tracer experiment 2 (absence of gas) are presented in Figure 4.16. The purpose of this experiment is only to validate the experimental techniques applied in limit ranges of one of the most relevant operating variables (Q_G).

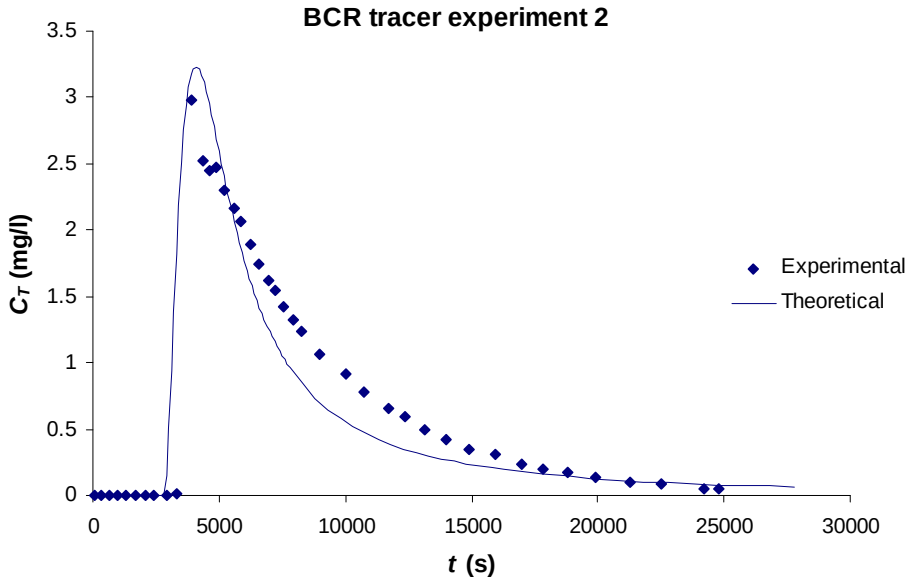

Figure 4.16. Variation of the tracer concentration for experiment 2 performed in the BCR unit. The experimental conditions are in Table 4.6. The points represent the tracer concentration of the liquid samples collected at the exit of the reactor. Solid line corresponds to the expected evolution of the tracer concentration.

The model for the separation head is again composed of two equal stirred tank reactors with a total volume of 900 ml and a dead volume of 900 ml.

The situation in the column section is analogue to a single fluid flowing inside a tube or a pipe. According to a chart from Ananthakrishnan et al. (1965), it can be chosen the appropriate model to use. The Bodenstein number ($u_L d_C / D_M$) around 1.4×10^4 and the vessel geometry factor (L/d_C) of 8, locates the corresponding point of BCR experiment 2 in the region of the pure convection model. The molecular diffusion (D_M) was considered to be in the range of 1×10^{-9} m^2/s.

The information taken from the chart of Ananthakrishnan et al. (1965), the shape of the experimental $C_T(t)$ curve, and the fact that the Reynolds number ($\rho_L u_L d_C / \mu_L$) is around 26 supports that the column section should be described by a convection model for laminar flow.

The development of the theoretical curve of Figure 4.16 was based on the independence between the regions that compose the BCR flow unit. The meaning of this independence is that a tracer molecule "loses its memory" as it passes from the column to the separation head (Levenspiel, 1999).

The $E(t)$ curve for laminar flow in pipes, assuming a planar introduction of the tracer in the system, is defined as follows (Levenspiel, 1999):

$$\begin{cases} E_L(t) = 0 & \text{if} \quad t < \dfrac{\bar{t}_R}{2} \\ E_L(t) = \dfrac{\bar{t}_R}{2t^2} & \text{if} \quad t \geq \dfrac{\bar{t}_R}{2} \end{cases} \tag{4.22}$$

The mean residence time ($\bar{t}_R$) of the column is 5599 s, and was determined from (4.5) using its total volume of 6283 ml and the liquid flow rate of 4.04 l/h.

Considering that the tracer injection was a pulse input, the tracer concentration exiting the column (C_T^{out}) can be obtained from:

$$C_T^{out} = E_L(t) \cdot \frac{M_T}{Q_L} \tag{4.23}$$

The concentration of the outlet stream of the reactor (C_{T2}) is finally obtained applying a convolution integral to C_T^{out} with the residence time distribution characteristic of the separation head (E_{SH}):

$$C_{T2} = \int_0^{t'} C_T^{out}(t - t') \cdot E_{SH}(t')dt' \tag{4.24}$$

Since the flow model of the separation head consists on two equally sized CSTR in series with a dead volume, the E_{SH} is defined as:

$$E_{SH}(t) = \frac{t}{(V_{CSTR}/Q_L)^2} \cdot \exp\left(-\frac{t}{(V_{CSTR}/Q_L)}\right) \tag{4.25}$$

4.7. Conclusions

In this chapter, the design, construction and operation of a pilot bubble column reactor installation was summarized. The main piece of equipment is a jacketed column reactor working in co-current gas-liquid up flow and the reactor could be filled with structured packing or used empty.

Tracer experiments were performed in the two configurations: structured packed bubble column reactor and simple bubble column reactor. These experiments had the purpose of supporting the development of a model to characterize the liquid flow inside the reactor. This flow model consisted on a piston diffusion model for the column section, followed by two stirred tanks with dead volume for the separation head. The parameter values of the model (ε_L, D_{ax}, V_{CSTR} and V_D) were extracted from the tracer experiments and presented on Tables 4.3, 4.4 and 4.5, for the SPBCR, and on Table 4.7 for the bubble column reactor.

The simulation results using the developed flow model predicted very well the experimental tracer concentration curves for gas-liquid flow in the structured packed configuration (see Figure 4.13). The exception in this unit was the situation without gas flow where it was concluded the existence of dead volumes and preferential paths inside the column section. These hydrodynamic anomalies eliminate, for this particular operational case, the physical meaning of the application of the pure axial dispersion model. Instead, it was probably more correct to use a piston diffusion exchange (PDE) model (Belfares et al., 2001), but this feature was not explored since the study of the system without gas flow was not a priority.

The tracer experiment 1 in the bubble column reactor was also very well predicted by the correspondent simulation results (Figure 4.15). The axial dispersion coefficient (D_{ax}) estimated in this case is approximately seven times higher than the one obtained in the SPBCR unit for similar operating conditions. This fact reveals a significant decrease in the back-mixing when applying structured packing as a column internal, which normally causes an improvement in the reactor performance in terms of conversion.

The complete flow model for the bubble column reactor without gas flow was assumed as a tube with convection model for laminar flow followed by two stirred tanks with dead volume. The theoretical prediction shows a considerable discrepancy from the experimental tracer concentration curve (see Figure 4.16). Since there is no particular reason to admit any change in the flow inside the separation head, the problem should be in the model prediction of the column section. The fact the column diameter is relatively large, and the number of perturbations (contractions and expansions) suffered by the liquid flow when it enters and leaves the stabilization chamber could be contributing to a certain level of tracer spreading inside the column, and avoiding the

development of a perfect parabolic liquid velocity profile characteristic of pure laminar flow.

4.8. Nomenclature

A_C	cross sectional area of the column, m^2
C_T	tracer concentration inside the column section, g/m^3
C_T^{input}	tracer concentration in the inlet liquid stream of the column section, g/m^3
C_T^{out}	tracer concentration in the end of the column section, g/m^3
C_{T1}	tracer concentration inside the first stirred tank of the separation head model, g/m^3
C_{T2}	tracer concentration in the outlet liquid stream of the reactor, g/m^3
d_C	internal diameter of the column section, m
D_{ax}	axial dispersion coefficient of the liquid in the column section, m^2/s
D_M	molecular diffusion of the tracer in water, m^2/s
E_L	residence time distribution for laminar flow in pipes, s^{-1}
E_{SH}	residence time distribution for the separation head, s^{-1}
L	column length, m
M_T	tracer mass injected into the reactor, g or mg
NPT	National pipe thread
Pe	liquid Peclet number ($= u_{LS} L / \varepsilon_L D_{ax}$)
Q_G	gas flow rate, ml_N/min
Q_L	liquid flow rate, m^3/s or l/h

t time, s

$\bar{t}_R$ mean residence time, s

T temperature, ºC

V_{act} active volume of liquid, m^3 or ml

V_C total volume of the column section, m^3 or ml

V_{CSTR} volume of each ideal stirred tank in the separation head model, m^3 or ml

V_D liquid dead volume inside the separation head, m^3 or ml

V_L liquid volume inside the column, m^3 or ml

V_{LC} total volume of the liquid stabilization chamber, m^3 or ml

V_{SH} total liquid volume inside the separation head, m^3 or ml

u_{LS} superficial liquid velocity inside the column, m/s

z axial position relative to the liquid entrance, m

Greek letters

ε_G gas hold-up inside the column

ε_L liquid hold-up inside the column

ε_S volumetric fraction occupied by the packing

μ_L liquid phase dynamic viscosity, kg m^{-1} s^{-1}

μ_1 first moment of the residence time distribution, s

ρ_L liquid phase density, kg/m^3

σ standard deviation of the residence time distribution, s

θ dimensionless time unit

Superscripts

A referent to the liquid samples collected at reactor outlet

B referent to the liquid samples collected at the end of the column section

4.9. References

1. Ananthakrishnan, V.; Gill, W. N.; Barduhn, A. J. Laminar dispersion in capillaries: Part 1. Mathematical analysis. *AIChE J.*, **1965**, 11, 1063-1072.
2. Belfares, L.; Cassanello, M.; Grandjean, B. P. A.; Larachi F. Liquid back-mixing in packed bubble column reactors: a state-of-the-art correlation. *Catal. Today*, **2001,** 64, 321–332.
3. Deckwer, W.-D., *Bubble column reactors.* John Wiley & Sons, England, **1992**.
4. Fogler, H. S. *Elements of Chemical Reaction Engineering* (2nd Edition), Prentice Hall International, USA, **1992**.
5. Lakota, A.; Jazbec, M.; Levec, J. Impacto f structured packing on bubble column mass transfer characteristics. Part 1. Backmixing in the liquid phase. *Acta Chim. Slov.*, **2001**, 48, 453-468.
6. Levenspiel, O. *Chemical Reaction Engineering* (3rd Edition). John Wiley & Sons, USA, **1999**.
7. Missen, R. W.; Mims, C. A.; Saville, B. A. *Introduction to chemical reaction engineering and kinetics.* John Wiley & Sons, New York, **1999**.
8. Siminiceanu, I.; Friedl, A.; Drăgan, M. A simple equation for the effective mass transfer area of the Mellapak 750Y structured packing (Available online in 30/11/07 at: http://www.upg-ploiesti.ro/sescom/pdf/s09/s09-l21-is.pdf).

5. Continuous reactor – experimental and modelling

A continuous gas-liquid reactor setup was already described and characterized in the previous chapter. The use of this installation to continuously produce vanillin from lignin oxidation is the main goal of this thesis.

In the present chapter, experiments of Kraft lignin oxidation and vanillin oxidation are presented. The main purpose of this chapter is to determine the reactor performance for the lignin oxidation in terms of vanillin formation. This experimental work was performed in two different reactor configurations: structured packed bubble column reactor (SPBCR) and bubble column reactor (BCR). The idea was to compare the performance of the SPBCR and BCR configurations, and the correspondent vanillin yield increase due to the use of structured packing internals.

A mathematical model for the continuous reactor was developed that can be applied to SPBCR and BCR configurations. The mathematical model was employed to understand the reaction and transport phenomena for different sets of operating variables employed in the experiments.

5.1. Experimental

The experimental work of this chapter consisted on a set of lignin oxidation and vanillin oxidation experiments performed for each reactor configuration (SPBCR and

BCR). The operating conditions used on these experiments are summarized in Table 5.1 and 5.2.

Table 5.1. Operating conditions of the experiments performed in the BCR.

Vanillin oxidation experiments							
	C_V^{in} (g/l)	pH^{in}	Q_L (l/h)	Q_{O2} * (ml_{NTP}/min)	Q_{N2} * (ml_{NTP}/min)	P (bar)	T_F^{set} (K)
BCR 1	5	14	2.08	1000	1000	10	436
Lignin oxidation experiments							
	C_L^{in} (g/l)	pH^{in}	Q_L (l/h)	Q_{O2} (ml_{NTP}/min)	Q_{N2} (ml_{NTP}/min)	P (bar)	T_F^{set} (K)
BCR 2	60	14	2.41	1000	1000	10	443 (t < 1900 s) 436 (t > 1900 s)
BCR 3	60	14	2.12	1000	1000	10	443 (t < 2410 s) 440 (t > 2410 s)
BCR 4	60	14	2.50	2000	1000	10	436 (t < 3990 s) 432 (t > 3990 s)

* NTP: normal temperature and pressure: 273K and 1 atmosphere.

Table 5.2. Operating conditions of the experiments performed in the SPBCR.

Vanillin oxidation experiments							
	C_V^{in} (g/l)	pH^{in}	Q_L (l/h)	Q_{O2} (ml_{NTP}/min)	Q_{N2} (ml_{NTP}/min)	P (bar)	T_F^{set} (K)
SPBCR 1	5	14	4.90	250	375	10	443
SPBCR 2	4	9.8	2.16	1000	1000	10	443
Lignin oxidation experiments							
	C_L^{in} (g/l)	pH^{in}	Q_L (l/h)	Q_{O2} (ml_{NTP}/min)	Q_{N2} (ml_{NTP}/min)	P (bar)	T_F^{set} (K)
SPBCR 3	60	14	4.20	250	375	10	443
SPBCR 4	60	14	4.22	100	150	10	443
SPBCR 5	60	14	4.70	1000	1000	10	443
SPBCR 6	60	14	2.12	1000	1000	10	443
SPBCR 7	60	14	0.99	1000	1000	10	433 (t < 3990 s) 428 (t > 3990 s)

Other experimental conditions to be taken into account are:

- All the experiments were performed with a liquid feed containing 2 mol/l of sodium hydroxide with the exception of SPBCR 2 experiment. In this case, the *pH* of the reaction media was controlled by using a carbonate buffer system in the liquid feed, with a composition of 0.1 mol/l of NaOH, 0.5 mol/l of Na_2CO_3 and 0.5 mol/l of $NaHCO_3$.
- The set point of the thermostatic bath (T_F^{set}) was decreased during the reaction phase of some experiments. This was done whenever the observed increase of the reactor temperature was considered excessive for the purposes of the respective experiments.

The experimental procedures employed to operate the reactor and protocols to analyze the inlet and effluent concentrations were already described in Chapter 4.

5.2. Theoretical

In this section a complete description of a single mathematical model for the dynamic state of both SPBCR and BCR is presented. In the one-dimensional model, the liquid flows through two different compartments in series accounting for two physical sections of the reactor: column section (liquid stabilization chamber + main cylindrical body) and the separation head. The assumptions of the mathematical model are the following:

- In the column section the process variables depend on the axial position (z) and time (radial variations are neglected).
- In the separation head the process variables only present temporal dependence.

- Liquid superficial velocity in the column ($u_{LS} = Q_L / A_R$) is constant for all z and t.
- The physical properties and the hydrodynamic parameters of the system are constant for all z and t.
- Plug flow in the gas phase;
- Mass transfer resistance in the gas side is negligible.
- The dissolved oxygen in the liquid is in equilibrium with the gas at the interface of the two phases.
- Neglect dissolution of nitrogen in the liquid phase.
- Ideal behaviour of the gas phase.
- For the same axial position, the temperatures of the packing, gas and liquid phases are equal (pseudo-homogeneous model for the energy balance).
- The external tube of the reactor jacket is thermally insulated from the surroundings.
- No heat losses in the thermo fluid between the exit of the bath and the entrance of the reactor jacket.

5.2.1. Complete model

Column section

A generic material balance can be expressed as:

Inlet + generation (consumption) = Outlet + accumulation – mass transfer (5.1)

In agreement with the model assumptions presented above, it can be written the following set of equations for compound *i* in a differential volume of the liquid phase:

$$\text{Inlet (mol/s)} = F_{i,L}\Big|_z = A_R u_{LS} C_{i,L}\Big|_z - \varepsilon_L D_{ax} A_R \frac{\partial C_{i,L}}{\partial z}\Bigg|_z \quad (5.2)$$

$$\text{Outlet (mol/s)} = F_{i,L}\Big|_{z+dz} = A_R u_{LS} C_{i,L}\Big|_{z+dz} - \varepsilon_L D_{ax} A_R \frac{\partial C_{i,L}}{\partial z}\Big|_{z+dz} \tag{5.3}$$

$$\text{Formed by reaction (mol/s)} = \varepsilon_L A_R dz \sum_k \nu_{i,k} r_k \tag{5.4}$$

$$\text{Accumulation (mol/s)} = \varepsilon_L A_R dz \frac{\partial C_{i,L}}{\partial t} \tag{5.5}$$

$$\text{Mass transfer (mol/s)} = k_L a\left(C^*_{i,L} - C_{i,L}\right) A_R dz \tag{5.6}$$

where A_R is the internal cross section area of the column; u_{LS} is the liquid superficial velocity; D_{ax} is the axial dispersion coefficient; ε_L is the liquid hold-up; k_L is liquid side mass transfer coefficient, in m/s; a is the gas-liquid interfacial area per unit of reactor volume; $C^*_{i,L}$ is the concentration of compound i in the liquid side at the gas-liquid interface; $C_{i,L}$ and $F_{i,L}$ are, respectively, the concentration and the molar flow rate of compound i on the liquid phase; r_k is the rate of reaction k; and $\nu_{i,k}$ is the stoichiometric coefficient of compound i in the reaction k.

Substituting (5.2) to (5.6) into the general mass balance equation (5.1) and considering $dz \to 0$:

$$\varepsilon_L D_{ax} \frac{\partial^2 C_{i,L}}{\partial z^2} = u_{LS} \frac{\partial C_{i,L}}{\partial z} - \varepsilon_L \sum_k \nu_{i,k} r_k + \varepsilon_L \frac{\partial C_{i,L}}{\partial t} - k_L a\left(C^*_{i,L} - C_{i,L}\right) \tag{5.7}$$

Focusing now in a differential control volume of the gas phase, a mass balance for compound i is:

$$\text{Inlet (mol/s)} = F_{i,G}\Big|_z = A_R u_{GS}\Big|_z C_{i,G}\Big|_z \tag{5.8}$$

$$\text{Outlet (mol/s)} = F_{i,G}\Big|_{z+dz} = A_R u_{GS}\Big|_{z+dz} C_{i,G}\Big|_{z+dz} \tag{5.9}$$

$$\text{Accumulation (mol/s)} = \varepsilon_G A_R dz \frac{\partial C_{i,G}}{\partial t} \tag{5.10}$$

$$\text{Mass transfer (mol/s)} = -k_L a\left(C_{i,L}^{*} - C_{i,L}\right) A_R dz \tag{5.11}$$

where u_{GS} is the gas superficial velocity; ε_G is the gas hold-up; $C_{i,G}$ is the concentration of compound i in the gas bubbles; and $F_{i,G}$ is the molar flow rate of compound i in the gas phase.

Replacing (5.8) to (5.11) in the mass balance equation (5.1), rearranging and making $dz \to 0$:

$$C_{i,G}\frac{\partial u_{GS}}{\partial z} + u_{GS}\frac{\partial C_{i,G}}{\partial z} + \varepsilon_G \frac{\partial C_{i,G}}{\partial t} + k_L a\left(C_{i,L}^{*} - C_{i,L}\right) = 0 \tag{5.12}$$

Applying the concept of ideal gas behaviour:

$$P_i = C_{i,G} RT \tag{5.13}$$

where P_i is the partial pressure of compound i; and R is the universal gas constant.

For the overall gas phase, the set of equations (5.8) to (5.11) becomes:

$$\text{Inlet (mol/s)} = F_G\big|_z = A_R u_{GS}\big|_z \frac{P\big|_z}{RT\big|_z} \tag{5.14}$$

$$\text{Outlet (mol/s)} = F_G\big|_{z+dz} = A_R u_{GS}\big|_{z+dz} \frac{P\big|_{z+dz}}{RT\big|_{z+dz}} \tag{5.15}$$

$$\text{Accumulation (mol/s)} = \varepsilon_G A_R dz \frac{\partial}{\partial t}\left(\frac{P}{RT}\right) \tag{5.16}$$

$$\text{Mass transfer (mol/s)} = -\sum_i k_L a\left(C_{i,L}^{*} - C_{i,L}\right) A_R dz \tag{5.17}$$

where F_G is the total molar flow rate of the gas phase; P is the total pressure; and T is the reactor temperature.

Replacing (5.14) to (5.17) into equation (5.1), rearranging and making $dz \to 0$:

$$u_{GS}\left(\frac{1}{T}\frac{\partial T}{\partial z} - \frac{1}{P}\frac{\partial P}{\partial z}\right) = \frac{\partial u_{GS}}{\partial z} + \frac{\varepsilon_G}{P}\frac{\partial P}{\partial t} - \frac{\varepsilon_G}{T}\frac{\partial T}{\partial t} + \frac{RT}{P}\sum_i k_L a\left(C_{i,L}^{*} - C_{i,L}\right) \tag{5.18}$$

The energy balance in a differential volume inside the column section of the reactor can be expressed by the equations:

Inlet = Outlet + accumulation – generation (consumption) – heat transfer (5.19)

$$\text{Inlet (J/s)} = E\big|_z = \left(\rho_L u_{LS} C_{P,L} + \rho_G u_{GS}\big|_z C_{P,G}\right) A_R T\big|_z - \lambda_{ef} A_R \left.\frac{\partial T}{\partial z}\right|_z \quad (5.20)$$

$$\text{Outlet (J/s)} = E\big|_{z+dz} = \left(\rho_L u_{LS} C_{P,L} + \rho_G u_{GS}\big|_{z+dz} C_{P,G}\right) A_R T\big|_{z+dz} - \lambda_{ef} A_R \left.\frac{\partial T}{\partial z}\right|_{z+dz} \quad (5.21)$$

$$\text{Accumulation} = \left(\rho_L \varepsilon_L C_{P,L} + \rho_G \varepsilon_G C_{P,G} + \rho_S \varepsilon_S C_{P,S} + \rho_W \frac{A_W}{A_R} C_{P,W}\right) A_R dz \frac{\partial T}{\partial t} \quad (5.22)$$

$$\text{Generated in reactions} = \varepsilon_L A_R dz \sum_k \left(-\Delta H_{R,k}\right) r_k \quad (5.23)$$

$$\text{Heat transfer} = 2\pi R_2 U \left(T_F - T\right) dz \quad (5.24)$$

$$A_W = \pi\left(R_2 - R_1\right)^2 \quad (5.25)$$

where E is the energy flow rate; ρ_L, ρ_G, ρ_S and ρ_W are, respectively, the liquid phase, gas phase, structured packing, and reactor wall densities; λ_{ef} is the effective thermal dispersion coefficient inside the reactor; A_W is the difference between the external and the internal cross section area of the column; $C_{P,L}$, $C_{P,G}$, $C_{P,S}$ and $C_{P,W}$ are, respectively, the heat capacities of the liquid phase, gas phase, structured packing and the reactor wall; $\Delta H_{R,k}$ is the heat of reaction k; R_1 and R_2 are, respectively, the radius of the internal and the external wall of the reactor column; U is the overall heat transfer coefficient between the reaction media and the thermo fluid inside the jacket; and T_F is the thermo fluid temperature.

Combining (5.19) to (5.24), the energy balance inside the column section of the reactor becomes:

$$\lambda_{ef}\frac{\partial^2 T}{\partial z^2}=\left(u_{LS}\rho_L C_{P,L}+u_{GS}\rho_G C_{P,G}\right)\frac{\partial T}{\partial z}+\rho_G C_{P,G}T\frac{\partial u_{GS}}{\partial z}+$$
$$\left(\varepsilon_L\rho_L C_{P,L}+\varepsilon_G\rho_G C_{P,G}+\varepsilon_S\rho_S C_{P,S}+\rho_W\frac{A_W}{A_R}C_{P,W}\right)\frac{\partial T}{\partial t} \qquad (5.26)$$
$$-\varepsilon_L\sum\left(-\Delta H_{R,k}\right)r_k-{}^{2\pi R_2}\!/_{A_R}\,U\left(T_F-T\right)$$

Performing an energy balance on the thermo fluid inside the jacket and on the insulated outer tube of the jacket leads, respectively, to (5.27) and (5.28):

$$\rho_F u_F C_{P,F}\frac{\partial T_F}{\partial z}+\frac{2R_1}{R_3^2-R_2^2}U\left(T_F-T\right)+\frac{2R_3}{R_3^2-R_2^2}h_1\left(T_F-T_{IT}\right)+$$
$$\rho_F C_{P,F}\frac{\partial T_F}{\partial t}=0 \qquad (5.27)$$

$$k_W\frac{\partial^2 T_{IT}}{\partial z^2}=\rho_W C_{P,W}\frac{\partial T_{IT}}{\partial t}-\frac{2R_3}{R_4^2-R_3^2}h_1\left(T_F-T_{IT}\right) \qquad (5.28)$$

where ρ_F is the density of the thermo fluid; u_F is the velocity of the thermo fluid inside the jacket; $C_{P,F}$ is the heat capacity of the thermo fluid; R_3 and R_4 are, respectively, the radius of the internal and the external wall of the outer jacket tube; T_{IT} is the temperature of the outer jacket tube; k_W is the thermal conductivity of the reactor wall; and h_1 is heat transfer coefficient between the thermo fluid and the internal wall of the tube that delimits the jacket.

The total pressure variation across the bed length is assumed to be comprised by two contributions (frictional pressure drop and hydrostatic head) and it can be expressed as:

$$\frac{\partial P}{\partial z}=\left(\frac{\partial P}{\partial z}\right)_{frict}-g\left(\varepsilon_G\rho_G+\varepsilon_L\rho_L\right) \qquad (5.29)$$

where g is the acceleration of gravity.

Separation head

The liquid flow in the separation head was modelled as two continuous stirred tanks in series and a dead volume (Chapter 4). A complete absence of gas bubbles in the liquid is assumed. With these assumptions, the material balance on a generic compound *i*, it is obtained:

$$\text{Tank 1 - } Q_L C_{i,L}\Big|_{z=L} = Q_L C_i^1 + V_{CSTR}\sum_k \nu_{i,k} r_k + V_{CSTR}\frac{dC_i^1}{dt} \tag{5.30}$$

$$\text{Tank 2 - } Q_L C_i^1 = Q_L C_i^2 + V_{CSTR}\sum_k \nu_{i,k} r_k + V_{CSTR}\frac{dC_i^2}{dt} \tag{5.31}$$

where $C_{i,L}\Big|_{z=L}$ is the molar concentration of compound *i* at the end of the column section; V_{CSTR} is the volume of each stirred tank considered in the flow model of the separation head; C_i^1 is the molar concentration of compound *i* in the stirred tank 1; and C_i^2 is the molar concentration of compound *i* in the stirred tank 2.

The temperature is considered to be same in the entire separation head and equal to the temperature of the reaction media at the end of the column section:

$$T_{SH} = T\Big|_{z=L} \tag{5.32}$$

5.2.2. Simplifications

Following, four important simplifications to the complete reactor model developed on the previous section are presented.

1. Isobaric reactor

The first simplification is made by assuming constant pressure throughout the reactor. In the case of the BCR it is only considered the contribution of the hydrostatic head in equation 5.29. This contribution as values around 0.1 bar, which is 1% of the

operation pressure of BCR experiments (10 bar). Because of this, in the range of operating conditions applied in this work, it is possible to assume the BCR configuration as isobaric.

The presence of internals in the SPBCR configuration leads to initially considering the two contributions in the equation (5.29). The operating total pressure and the static pressure are similar to the BCR case, so the hydrostatic head is again neglected. The contribution of the frictional pressure drop to the total pressure variation was also estimated.

Packed beds for gas-liquid systems can be operated in counter-current flow, downward co-current flow and upward co-current flow. The studies found on structured packings refers almost exclusively to their application as internals of distillation or absorption columns operated in counter-current flow – liquid flowing down as a falling film in the packing walls and upward annular flow of gas (Billet and Schultes, 1992; Fair et al., 2000; Gualito et al., 1997; Henriques de Brito et al., 1992; Henriques de Brito et al., 1994; Laso et al., 1995; Macías-Salinas and Fair, 1999; Macías-Salinas and Fair, 2000; Olujić et al.; 1999; Olujić and Behrens, 2006; Urseanu et al., 2001; Wang et al., 2006). These configurations imply a hydrodynamic environment completely different from the present reactor system, so the correlations encountered for the prediction of parameters are not useful to the case study. The option taken was to estimate the hydrodynamic parameters for the SPBCR model, on studies about gas-liquid upward co-current flow through beds filled with random packings, also called flooded bed reactors.

The frictional pressure drop was one of the parameters for which a set of correlations were compiled from literature (Khan et al., 1997; Khan et al., 2002; Larachi et al., 1994; Turpin and Huntington, 1967). From these correlations, the higher values of

frictional pressure drop were obtained with the equations proposed by Khan et al. (1997):

$$G_M^T = 0.1 + \frac{e^{0.2L_M}}{200 + e^{0.2L_M}} \tag{5.33}$$

$$f = 3 \times 10^7 \, Re_G^{0.18} \, Re_L^{-1.7} \left(D_P / D_C \right) \tag{5.34}$$

$$\Delta P_{frict} = \frac{L_M^2 \cdot f \cdot L_{ef}}{2 \cdot \rho_L \cdot D_P} \tag{5.35}$$

where G_M^T is the gas mass flux of transition from bubble flow to pulse flow; L_M is the liquid mass flux; f is the friction factor; Re_G and Re_L are, respectively, the gas and the liquid Reynolds number; D_P is a characteristic dimension of the packing channels; D_C is the column diameter; ΔP_{frict} is the frictional pressure drop on the packed section of the column; and L_{ef} is an effective channel length of the packed bed. Three flow regimes were identified: bubble flow, pulse flow and spray flow. The system in study is assumed to be in the bubble flow region (low flow rates of gas and liquid), since the gas mass flux (G_M) is always smaller than the correspondent transition value (G_M^T).

The definition of average hydraulic diameter was used as the characteristic dimension of the packing channels (Kolev, 2006):

$$D_P = 4 \, \varepsilon / a_P \tag{5.36}$$

where ε is the void fraction of the packing, and a_P is the specific surface area of the packing.

The effective length of the column section filled with structured packing (L_{ef}) is estimated from (Woerlee et al., 2001):

$$L_{ef} = \left(\frac{(2/\pi) D_C}{\sin \alpha} + 0.4 \cdot D_P \cdot \theta \right) \left(\frac{H_P \tan \theta}{(2/\pi) D_C} \right) \tag{5.37}$$

where H_P is the height of the column packed section; and θ is the inclination angle of the packing channels with the horizontal axis (45º for Mellapak 750Y).

Combining (5.33) to (5.37) for the prediction of the frictional pressure drop (ΔP_{frict}), on the experiments performed in the SPBCR, the maximum value obtained was 0.053 bar (Experiment SPBCR 3). Comparing this value to the total operation pressure (10 bar) it can be concluded that the influence of ΔP_{frict} in P is also negligible. Knowing this, with the experimental conditions used in the present work, the total pressure can be considered as constant throughout the SPBCR and equation (5.29) is removed from the model.

2. Constant gas composition

The stationary rise velocity of an individual bubble in a BCR can be calculated as described by Mendelson (1967):

$$u_t = \sqrt{\left(\frac{2\sigma_L}{D_B \rho_L} + 0.5 D_B g\right)} \tag{5.38}$$

where u_t is the stationary rise velocity of the bubble; σ_L is the surface tension; and D_B is gas bubble diameter. This equation is proper for D_B between 0.2 cm and 8 cm.

The Sauter diameter (D_S) was assumed as an approximation to the bubble diameter. Correlations presented by Kumar et al. (1976) were used to estimate D_S:

$$D_S = 0.32\, Re_O^{0.425}\left(\frac{\sigma_L D_O}{(\rho_L - \rho_G)g}\right)^{1/4} \quad \text{when } 10 < Re_O < 2100 \tag{5.39}$$

$$Re_O = \frac{D_O u_{GO} \rho_G}{\mu_G} \tag{5.40}$$

where Re_O is the gas Reynolds number based on the D_O and u_{GO}; D_O is the diameter of the holes in the distributor; and u_{GO} is the gas velocity through each distributor hole.

The values of u_t estimated for the BCR experiments are around 0.22 m/s, with a respective Sauter diameter of 3.7 mm and Re_O of 116. This means that an individual bubble takes 3.2 s to pass through the 70 cm of column above the gas distributor.

In the case of the SPBCR experiments, the stationary rise velocity of the bubble is in the range of 0.22 to 0.28 m/s, with a D_S between 2.0 and 3.7 mm. Since the channels of the structured packing have a 45º inclination with the horizontal axis, the path for the gas bubble is increased by a factor of sin(45º) comparing to the BCR. Taking this into account, a bubble with u_t of 0.22 m/s needs 4.5 s to travel from the gas distributor to the end of the column filled with three modules of Mellapak 750Y.

With the bubble residence times presented above (3.2 s for BCR and 4.5 s for SPBCR), it is admitted that the contact time with the liquid is too short to transfer a significant amount of water to the gas phase. Because of this, the gas phase is considered to be free of water vapour ($P_{H2O} = 0$).

Focusing on the reacting gas (O_2), the assumption of constant oxygen partial pressure in the gas phase is dependent on the respective mass transfer parameters ($k_L a$) and the driving force ($C^*_{O2,L} - C_{O2,L}$). The low range of the operation flow rates used in the experimental work and the consequent low gas hold-ups, most likely limit the $k_L a$ to small values.

The driving force mainly depends on the gas solubility and the rate of consumption in the liquid. Since oxygen is a gas with low solubility in aqueous systems and the studied reactions are slow, the driving force will not achieve large values.

As the dissolution of the inert gas compound (N_2) can be neglected, it can be assumed that the oxygen and nitrogen composition of a gas bubble is approximately constant throughout the reactor. In the mathematical model this reflects by substituting equations (5.12) and (5.13) by:

$$P_i = \frac{Q_{i,G}}{Q_G} \cdot P \tag{5.41}$$

where $Q_{i,G}$ is the volumetric gas flow rate of compound *i*.

3. Constant gas velocity

The assumption of constant gas velocity (u_{GS}) is almost a consequence of the approximation to isobaric reactor with constant gas hold-up. Equation (5.18) is removed from the model.

4. Temperature of the outer tube equal to the thermo fluid

Considering the reactor well insulated, in steady state the heat flux, from the thermo fluid, should only occur in the direction of the reaction medium.

Assuming an instantaneous thermal equilibrium between the thermo fluid and the outer jacket tube, in every z, the temperature gradient between these two sections will be zero ($T_F = T_{IT}$). This implies the elimination of equation (5.28) from the original model, and equation (5.27) becomes:

$$\rho_F u_F C_{P,F} \frac{\partial T_F}{\partial z} + \frac{2R_1}{R_3^2 - R_2^2} U\left(T_F - T\right) + \rho_F C_{P,F} \frac{\partial T_F}{\partial t} = 0 \tag{5.42}$$

5.2.3. Vanillin oxidation

Applying the simplified version of the model, for the column section of the reactor, to the vanillin oxidation system it is obtained the following set of equations with the correspondent boundary and initial conditions:

Vanillin mass balance

$$\varepsilon_L D_{ax} \frac{\partial^2 C_{V,L}}{\partial z^2} = u_{LS} \frac{\partial C_{V,L}}{\partial z} + \varepsilon_L r_2 + \varepsilon_L \frac{\partial C_{V,L}}{\partial t} \tag{5.43}$$

$$Q_L C_{V,L}^{in} = A_R u_{LS} C_{V,L}\Big|_{0,t} - \varepsilon_L A_R D_{ax} \frac{\partial C_{V,L}}{\partial z}\Big|_{0,t} \tag{5.44}$$

$$\frac{\partial C_{V,L}}{\partial z}\Big|_{L,t} = 0 \tag{5.45}$$

$$C_{V,L}\Big|_{z,0} = C_{V,L}^{in} \tag{5.46}$$

Dissolved oxygen mass balance

$$\varepsilon_L D_{ax} \frac{\partial^2 C_{O2,L}}{\partial z^2} = u_{LS} \frac{\partial C_{O2,L}}{\partial z} + \varepsilon_L r_2 + \varepsilon_L \frac{\partial C_{O2,L}}{\partial t} - k_L a\left(C_{O2,L}^{*} - C_{O2,L}\right) \tag{5.47}$$

$$Q_L C_{O2,L}^{in} = 0 = A_R u_{LS} C_{O2,L}\Big|_{0,t} - \varepsilon_L A_R D_{ax} \frac{\partial C_{O2,L}}{\partial z}\Big|_{0,t} \tag{5.48}$$

$$\frac{\partial C_{O2,L}}{\partial z}\Big|_{L,t} = 0 \tag{5.49}$$

$$C_{O2,L}\Big|_{z,0} = 0 \tag{5.50}$$

Energy balance on the thermo fluid inside the jacket – equation (5.42)

$$T_F\Big|_{0,t} = T_F^{in} \tag{5.51}$$

$$T_F\Big|_{z,0} = f(z) \tag{5.52}$$

Energy balance on the reactor medium

$$\lambda_{ef}\frac{\partial^2 T}{\partial z^2} = \left(u_{LS}\rho_L C_{P,L} + u_{GS}\rho_G C_{P,G}\right)\frac{\partial T}{\partial z} + \left(\varepsilon_L\rho_L C_{P,L} + \varepsilon_G\rho_G C_{P,G} + \varepsilon_S\rho_S C_{P,S} + \rho_W\frac{A_W}{A_R}C_{P,W}\right)\frac{\partial T}{\partial t} - \varepsilon_L\left(-\Delta H_{R,2}\right)r_2 - {2\pi R_2}\Big/{A_R}\,U\left(T_F - T\right) \tag{5.53}$$

$$\rho_L u_{LS} C_{P,L} T^i = \rho_L u_{LS} C_{P,L} T\Big|_{0,t} - \lambda_{ef}\frac{\partial T}{\partial z}\Big|_{0,t} \tag{5.54}$$

$$\frac{\partial T}{\partial z}\Big|_{L,t} = 0 \tag{5.55}$$

$$T\Big|_{z,0} = f'(z) \tag{5.56}$$

where $C_{V,L}$ and $C_{O2,L}$ are, respectively, the concentration of vanillin and dissolved oxygen in the liquid phase; r_2 is the reaction rate of vanillin oxidation; $\Delta H_{R,2}$ is the heat of reaction of vanillin oxidation, with an estimated value of -267 kJ/mol (section 3.4.3 of Chapter 3); $C^i_{V,L}$ and $C^i_{O2,L}$ are, respectively, the concentration of vanillin and dissolved oxygen in the liquid feed; T^i_F is the temperature of the thermo fluid entering the jacket; and T^i is the temperature of the liquid feed. The initial temperatures inside the reactor and thermo fluid are functions of the axial position and can be taken from the steady state of the previous heating phase.

In the separation head, the vanillin oxidation system is described by:

Tank 1 - $$Q_L C_{V,L}\Big|_{L,t} = Q_L C^1_V + V_{CSTR}\,r_2 + V_{CSTR}\frac{dC^1_V}{dt}\quad ;\ C^1_V\Big|_{t=0} = C^{in}_{V,L} \tag{5.57}$$

$$Q_L C_{O2,L}\Big|_{L,t} = Q_L C^1_{O2} + V_{CSTR}\,r_2 + V_{CSTR}\frac{dC^1_{O2}}{dt}\quad ;\ C^1_{O2}\Big|_{t=0} = 0 \tag{5.58}$$

Tank 2 - $$Q_L C^1_V = Q_L C^2_V + V_{CSTR}\,r_2 + V_{CSTR}\frac{dC^2_V}{dt}\quad ;\ C^2_V\Big|_{t=0} = C^{in}_{V,L} \tag{5.59}$$

$$Q_L C^1_{O2} = Q_L C^2_{O2} + V_{CSTR}\,r_2 + V_{CSTR}\frac{dC^2_{O2}}{dt}\quad ;\ C^2_{O2}\Big|_{t=0} = 0 \tag{5.60}$$

where C_V^1 and C_{O2}^1 are, respectively, the concentration of vanillin and dissolved oxygen in the stirred tank 1; C_V^2 and C_{O2}^2 are, respectively, the concentration of vanillin and dissolved oxygen in the stirred tank 2.

It is assumed in this system that 1 mol of vanillin reacts with 1 mol of dissolved oxygen, just like represented in equation (3.1). The rate of disappearance of vanillin was already defined in Chapter 3, and is converted to SI units in the following lines:

- $pH \geq 11.5$

$$r_2 = k_2 \, C_{O2,L} C_{V,L} \quad \text{mol m}^{-3}\,\text{s}^{-1} \tag{5.61}$$

$$k_2 = 6.017 \times 10^5 \, \exp\left(-\frac{9706.2}{T}\right) \quad \text{m}^3\,\text{mol}^{-1}\,\text{s}^{-1} \tag{5.62}$$

- $pH < 11.5$

$$r_2 = A \; f(pH) \; C_{V,L}{}^2 \quad \text{mol m}^{-3}\,\text{s}^{-1} \tag{5.63}$$

$$A = 4071 \, \exp\left(-\frac{3103.7}{T}\right) \quad \text{m}^3\,\text{mol}^{-1}\,\text{s}^{-1} \tag{5.64}$$

$$f(pH) = \left(\frac{B \, C_{H+} \times 10^3}{1 + B \, C_{H+} \times 10^3}\right)^2 \tag{5.65}$$

$$B = 8.88 \times 10^9 \, \exp\left(-\frac{1936.6}{T}\right) \quad \text{m}^3/\text{mol} \tag{5.66}$$

where k_2, A and B are velocity reaction constants; C_{H+} is the concentration of hydrogen ions in the liquid mixture, in mol/l; $f(pH)$ is a function of C_{H+}.

The concentration of dissolved oxygen was estimated by the same correlation referred in Chapter 3 (Mathias, 1993):

$$C_{O2,L} = \left(3.559 - 6.659 \times 10^{-3} \; T - 5.606 \; P_{O2} + 1.594 \times 10^{-5} \; P_{O2} \; T^2 + 1.498 \times 10^3 \; P_{O2}/T\right) \times 10^{-0.144\,I} \tag{5.67}$$

where P_{O2} is the oxygen partial pressure, in bar, I is the ionic strength of the liquid medium, in mol per litre; $C_{O2,L}$ is in mol per m^3 and T in Kelvin.

5.2.4. Lignin oxidation

The simplified model for the column section of the reactor is applied to the lignin oxidation system and the resulting set of equations is presented below. The reaction scheme is again represented by (3.1) and (3.13).

Lignin mass balance

$$\varepsilon_L D_{ax} \frac{\partial^2 C_{L,L}}{\partial z^2} = u_{LS} \frac{\partial C_{L,L}}{\partial z} + \alpha \varepsilon_L r_1 + \varepsilon_L \frac{\partial C_{L,L}}{\partial t} \tag{5.68}$$

$$Q_L C_{L,L}^{in} = A_R u_{LS} C_{L,L}\Big|_{0,t} - \varepsilon_L A_R D_{ax} \frac{\partial C_{L,L}}{\partial z}\Big|_{0,t} \tag{5.69}$$

$$\frac{\partial C_{L,L}}{\partial z}\Big|_{L,t} = 0 \tag{5.70}$$

$$C_{L,L}\Big|_{z,0} = C_{L,L}^{in} \tag{5.71}$$

Vanillin mass balance

$$\varepsilon_L D_{ax} \frac{\partial^2 C_{V,L}}{\partial z^2} = u_{LS} \frac{\partial C_{V,L}}{\partial z} + \varepsilon_L (r_2 - r_1) + \varepsilon_L \frac{\partial C_{V,L}}{\partial t} \tag{5.72}$$

$$Q_L C_{V,L}^{in} = 0 = A_R u_{LS} C_{V,L}\Big|_{0,t} - \varepsilon_L A_R D_{ax} \frac{\partial C_{V,L}}{\partial z}\Big|_{0,t} \tag{5.73}$$

$$\frac{\partial C_{V,L}}{\partial z}\Big|_{L,t} = 0 \tag{5.74}$$

$$C_{V,L}\Big|_{z,0} = 0 \tag{5.75}$$

Dissolved oxygen mass balance

$$\varepsilon_L D_{ax} \frac{\partial^2 C_{O2,L}}{\partial z^2} = u_{LS} \frac{\partial C_{O2,L}}{\partial z} + \varepsilon_L (r_2 + \upsilon_1 r_1) + \varepsilon_L \frac{\partial C_{O2,L}}{\partial t} - k_L a\left(C_{O2,L}^{*} - C_{O2,L}\right) \tag{5.76}$$

$$Q_L C_{O2,L}^{in} = 0 = A_R u_{LS} C_{O2,L}\Big|_{0,t} - \varepsilon_L A_R D_{ax} \frac{\partial C_{O2,L}}{\partial z}\Big|_{0,t} \tag{5.77}$$

$$\frac{\partial C_{O2,L}}{\partial z}\Big|_{L,t} = 0 \tag{5.78}$$

$$C_{O2,L}\big|_{z,0} = 0 \tag{5.79}$$

Energy balance on the thermo fluid inside the jacket – equation (5.42)

$$T_F\big|_{0,t} = T_F^{in} \tag{5.80}$$

$$T_F\big|_{z,0} = f(z) \tag{5.81}$$

Energy balance on the reactor medium

$$\lambda_{ef}\frac{\partial^2 T}{\partial z^2} = \left(u_{LS}\rho_L C_{P,L} + u_{GS}\rho_G C_{P,G}\right)\frac{\partial T}{\partial z} + \left(\varepsilon_L\rho_L C_{P,L} + \varepsilon_G\rho_G C_{P,G} + \varepsilon_S\rho_S C_{P,S} + \rho_W\frac{A_W}{A_R}C_{P,W}\right)\frac{\partial T}{\partial t} - \varepsilon_L\left[\left(-\Delta H_{R,1}\right)r_1 + \left(-\Delta H_{R,2}\right)r_2\right] - {2\pi R_2}\Big/{A_R}\,U\left(T_F - T\right) \tag{5.82}$$

$$\rho_L u_{LS} C_{P,L} T^{i} = \rho_L u_{LS} C_{P,L} T\big|_{0,t} - \lambda_{ef}\left.\frac{\partial T}{\partial z}\right|_{0,t} \tag{5.83}$$

$$\left.\frac{\partial T}{\partial z}\right|_{L,t} = 0 \tag{5.84}$$

$$T\big|_{z,0} = f'(z) \tag{5.85}$$

where $C_{L,L}$ is the concentration of lignin; r_1 is the reaction rate of lignin oxidation; $\Delta H_{R,1}$ is the heat of reaction of lignin oxidation, with a value of -29687 kJ/mol (section 3.4.3 of Chapter 3); and $C_{L,L}^{i}$ is the concentration of lignin in the liquid feed. The initial temperatures inside the reactor and thermo fluid are again taken from the steady state of the correspondent heating phase.

In the separation head, the lignin oxidation system is described by:

Tank 1 - $$Q_L C_{L,L}\big|_{L,t} = Q_L C_L^1 + V_{CSTR}\,\alpha r_1 + V_{CSTR}\frac{dC_L^1}{dt} \;\; ; \;\; C_L^1\big|_{t=0} = C_{L,L}^{in} \tag{5.86}$$

$$Q_L C_{V,L}\big|_{L,t} = Q_L C_V^1 + V_{CSTR}\left(r_2 - r_1\right) + V_{CSTR}\frac{dC_V^1}{dt} \;\; ; \;\; C_V^1\big|_{t=0} = 0 \tag{5.87}$$

$$Q_L C_{O2,L}\big|_{L,t} = Q_L C_{O2}^1 + V_{CSTR}\left(r_2 + \upsilon_1 r_1\right) + V_{CSTR}\frac{dC_{O2}^1}{dt} \;\; ; \;\; C_{O2}^1\big|_{t=0} = 0 \tag{5.88}$$

Tank 2 - $$Q_L C_L^1 = Q_L C_L^2 + V_{CSTR}\ \alpha r_1 + V_{CSTR}\ \frac{dC_L^2}{dt} \quad ;\quad C_L^2\Big|_{t=0} = C_{L,L}^{in} \tag{5.89}$$

$$Q_L C_V^1 = Q_L C_V^2 + V_{CSTR}(r_2 - r_1) + V_{CSTR}\ \frac{dC_V^2}{dt} \quad ;\quad C_V^2\Big|_{t=0} = 0 \tag{5.90}$$

$$Q_L C_{O2}^1 = Q_L C_{O2}^2 + V_{CSTR}(r_2 + \upsilon_1 r_1) + V_{CSTR}\ \frac{dC_{O2}^2}{dt} \quad ;\quad C_{O2}^2\Big|_{t=0} = 0 \tag{5.91}$$

where C_L^1 and C_L^2 are, respectively, the concentration of lignin in the stirred tank 1 and in the stirred tank 2.

The rate of formation of vanillin, in SI units, is defined by (Mathias, 1993; Fargues et al., 1996a):

$$r_1 = k_1\ C_{O2,L}{}^{1.75}\ C_{L,L} \ \text{ mol m}^{-3}\ \text{s}^{-1} \tag{5.92}$$

$$k_1 = 1.289\ \exp\left(-\frac{E_a/R}{T}\right) = 1.289\ \exp\left(-\frac{4000}{T}\right) \ (\text{m}^3/\text{mol})^{1.75}/\text{s} \tag{5.93}$$

The rate of vanillin oxidation, r_2, is calculated using the expressions (5.61) to (5.66), except for k_2 which is now defined as (in SI units):

$$k_2 = 72.6\ \exp\left(-\frac{5530}{T}\right) \ \text{mol m}^{-3}\ \text{s}^{-1} \tag{5.94}$$

The concentration of dissolved oxygen, $C_{O2,L}$, is again estimated by the correlation (5.67).

The variation of pH that occurs during the lignin oxidation is estimated by the variable, X, that encloses all the acid products that are formed. Based on the information already provided in Chapter 3, the respective balances on X, in equivalents per litre, are defined as:

Column section

$$\varepsilon_L D_{ax}\ \frac{\partial^2 X}{\partial z^2} = u_{LS}\ \frac{\partial X}{\partial z} + \varepsilon_L\ \frac{\partial X}{\partial t} - 0.098\left(\frac{M_n}{1000}\right)\ \varepsilon_L \alpha\ r_1 \tag{5.95}$$

$$Q_L X^{in} = 0 = A_R u_{LS} X\big|_{0,t} - \varepsilon_L A_R D_{ax} \left.\frac{\partial X}{\partial z}\right|_{0,t} \tag{5.96}$$

$$\left.\frac{\partial X}{\partial z}\right|_{L,t} = 0 \tag{5.97}$$

$$X\big|_{z,0} = 0 \tag{5.98}$$

Separation head

$$\text{Tank 1 - } Q_L X\big|_{L,t} = Q_L X^1 - 0.098\left(\frac{M_n}{1000}\right) V_{CSTR}\ \alpha\ r_1 + V_{CSTR}\ \frac{dX^1}{dt} \tag{5.99}$$

$$\text{Tank 2 - } Q_L X^1 = Q_L X^2 - 0.098\left(\frac{M_n}{1000}\right) V_{CSTR}\ \alpha\ r_1 + V_{CSTR}\ \frac{dX^2}{dt} \tag{5.100}$$

where X^1 and X^2 are, respectively, the quantification of acid products, formed by lignin oxidation, in the stirred tank 1 and 2; X^{in} is the liquid feed concentration of the acid products liberated by the lignin oxidation; and M_n is the mean molecular weight of lignin.

Knowing the dependence of X with the axial position and time, the respective values of pH are obtained by the application of equations (3.23) to (3.26).

5.3. Experimental results

5.3.1. Bubble column reactor experiments

Bubble column reactors are equipments of simple construction that provide an environment of complex interactions between chemical and physical phenomena. The mathematical model chosen for this work reveals a considerable degree of simplicity to avoid some of the mathematical resolution problems typically encountered when modelling this kind of systems, and also a lack of experimental data taken from the installation (particularly hydrodynamic parameters and gas phase composition).

However, it is impossible to completely avoid the incorporation of several uncertain hydrodynamic parameters that must be known before advancing to the solution of the model. These parameters include the dispersion coefficients, phase hold-ups and heat and mass transfer coefficients.

5.3.1.1. Gas hold-up and axial dispersion coefficient

A large number of studies are published about phase hold-ups and D_{ax} in bubble column reactors and several correlations were developed in these fields. Some of these studies were analysed to evaluate their degree of success on predicting the parameters of the systems used in this work.

Gas hold-up depends mainly on the gas flow velocity, but also on the size of the column, type of gas distributor and properties of the materials (Deckwer, 1992). Although the experimental determination of this parameter encloses large relative errors, due to the small percentages of gas expected in the working system, the values of the phase hold-ups were based on the predictions of ε_G to globally minimize the magnitude of absolute errors. The correlations selected for the estimation of gas hold-up are:

Anabtawi et al. (2003) - $$\varepsilon_G = 0.60\ u_{GS}^{0.60} H_P^{-0.38} \rho_L^{0.02} \mu_L^{-0.24} \sigma_L^{0.22} \quad (5.101)$$

Kelkar et al. (1983) - $$\varepsilon_G = 0.475\ u_{GS}^{0.37} \quad (5.102)$$

Kumar et al. (1976) - $$\varepsilon_G = 0.728\ u_G - 0.485\ u_G^2 + 0.0975\ u_G^3 \quad (5.103)$$

$$u_G = u_{GS}\left(\sigma_L\left(\rho_L - \rho_G\right)g/\rho_L^2\right)^{1/4} \quad (5.104)$$

Reilly et al. (1986) - $$\varepsilon_G = \left(296\ u_{GS}^{0.44} \sigma_L^{-0.16} \rho_L^{-0.98} \rho_G^{0.19}\right) + 0.009 \quad (5.105)$$

Urseanu et al. (2003) - $$\varepsilon_G = 0.21\ u_{GS}^{0.58} D_C^{-0.18} \mu_L^{-0.12} \rho_G^{[0.3\exp(-9\mu_L)]} \quad (5.106)$$

Zahradnik et al. (1995) - $$\varepsilon_G = 0.87\ u_{GS}^{0.62} \quad (5.107)$$

In the following table, the gas hold-up measured from the BCR tracer experiment (Chapter 4) is presented together with the predictions from the selected correlations, for the same operation conditions.

Table 5.3. Measured and predicted values of ε_G for the BCR tracer experiment.

Experimental	Anabtawi et al.	Kelkar et al.	Kumar et al.
0.0262	0.0177	0.0216	0.0011
Reilly et al.	**Urseanu et al.**	**Zahradnik et al.**	
0.0300	0.0124	0.0049	

The correlations on ε_G presented above are the result of studies performed with fluid velocity ranges higher than those used in this work, especially for the gas velocity, different gas-liquid systems and much lower pressures. The combination of such specific features in the reaction experiments of the system in study – low flow rates; complex reaction media; high pressures and temperatures – obliges to an extrapolation of the correlations found in literature from the original ranges of applications in which they were developed. This necessity was common for the hydrodynamic parameters based on correlation predictions either for BCR or SPBCR configurations.

Comparing the result obtained by the BCR tracer experiment with the estimated values, for the same operation conditions, it can be seen that the predictions from the correlations of Kelkar et al. (1983) and Reilly et al. (1986) have a smaller deviation from the experimental gas hold-up. Since the work of Kelkar et al. (1983) includes the use of electrolytes, and the experiments on vanillin and lignin oxidation are performed in a reaction media with an ionic strength of 2 mol per litter, this correlation was chosen to predict the ε_G values needed for the BCR model.

The gas hold-up estimations for the reaction experiments in the BCR configuration, based on Kelkar et al. (1983), are presented in Table 5.4.

Table 5.4. Estimation of ε_G for the BCR experiments using Kelkar et al. (1983).

Experiment	BCR 1	BCR 2	BCR 3	BCR 4
ε_G	0.0305	0.0306	0.0307	0.0355

The liquid phase dispersion coefficient, D_{ax}, in a simple bubble column is normally a function of the gas velocity and the column diameter, and remains unaffected by the liquid velocity up to values around 0.03 m/s (Ullman's Encyclopedia, 2003). From the literature about bubble column reactors, it was gathered the following set of correlations for the prediction of the axial dispersion coefficient (Deckwer, 1992):

Ohki and Inoue - $$D_{ax} = 0.30\ D_C^2 u_{GS}^{1.2} + 170 D_O \quad (5.108)$$

Towell and Ackermann - $$D_{ax} = 1.23\ D_C^{1.5} u_{GS}^{0.5} \quad (5.109)$$

Badura - $$D_{ax} = 2.7 D_C^{1.4} u_{GS}^{0.3} \quad (5.110)$$

Baird and Rice - $$Bo_L^* = 2.83 Fr^{0.34} \quad (5.111)$$

Akita - $$Bo_L^* = \frac{Fr^{0.5}}{0.06 + 0.55 Fr^{0.35}} \quad (5.112)$$

where Bo_L^* is the modified Bodenstein number ($u_{GS} D_C / D_{ax}$), and Fr is the Froude number ($u_{GS}^2 / g D_C$). In equations (5.108) to (5.110), D_C and D_O are in cm, D_{ax} is in cm^2/s, and u_{GS} is in cm/s.

The values of the axial dispersion coefficient estimated with the previous correlations (5.108) to (5.112), for the gas velocity conditions used in the BCR tracer experiment (Chapter 4), are presented in Table 5.5. Comparing with the experimental D_{ax} it can be easily verified that all the investigated correlations have the tendency to overestimate this parameter value, with the exception of Towell and Ackermann. This

overestimation is very high in three of them: Badura; Baird and Rice; and especially in the Akita equation where the difference reaches one order of magnitude. With Ohki and Inoue correlation the overestimation is not so severe, and is the only case that incorporates a distributor effect on the axial dispersion coefficient.

Table 5.5. Measured and estimated values of D_{ax}, in cm^2/s, for the BCR tracer experiment.

Experimental	**Ohki and Inoue**	**Towell and Ackermann**
6.9	8.8	6.0
Badura	**Baird and Rice**	**Akita**
22.1	24.3	61.0

Since the equation developed by Towell and Ackermann presents the smaller deviation from the experimental D_{ax}, it was selected to predict the axial dispersion coefficient in the BCR reaction experiments. The predictions of the D_{ax} for the reaction experiments in the BCR configuration, based on the correlation of Towell and Ackermann, are presented in Table 5.6.

Table 5.6. Estimated values of D_{ax}, in cm^2/s, for the BCR reaction experiments using the Towell and Ackermann correlation.

Experiment	BCR 1	BCR 2	BCR 3	BCR 4
D_{ax} (cm^2/s)	9.5	9.6	9.6	11.7

5.3.1.2. Heat transfer parameters

The mathematical model derived in section 5.2 contains two heat transfer parameters: the effective heat dispersion coefficient (λ_{ef}) in the column section, and the overall heat transfer coefficient between the reaction media and the thermo fluid flowing inside the jacket (U).

For a bubble column reactor, the Lewis's analogy is generally applied, which consists on assuming the liquid mass Peclet number equal to the liquid thermal Peclet number. Expressing this into a mathematical equation and solving for λ_{ef} :

$$\lambda_{ef} = \varepsilon_L \, D_{ax} \, \rho_L \, C_{P,L} \tag{5.113}$$

Using equation (5.113) the values of the effective heat dispersion coefficient were calculated for each BCR reaction experiment. The results obtained are presented in Table 5.7.

Table 5.7. Effective heat dispersion coefficient (λ_{ef}) for the BCR reaction experiments.

Experiment	BCR 1	BCR 2	BCR 3	BCR 4
λ_{ef} (W m^{-1} K^{-1})	3689	4100	4110	4979

Physically, the overall heat transfer coefficient (U) results from the contribution of three terms: heat transfer between the reaction media and the interior side of the inner jacket wall, the thermal conductivity of the stainless steel, and the heat transfer from the exterior side of the inner jacket wall to the bulk of the flowing thermo fluid.

During the heating phase and the subsequent pressurization phase of the BCR, the data from the temperature inside the column was collected at three different axial positions. These phases would last until it was observed a stationary state in the temperature, flow rates and total pressure, like it was described in section 4.4.2.

The thermostatic bath and the liquid pump were turned on at the same time, so the initial part of the heating phase was performed simultaneously to the filling of the reactor with the liquid media. Since the operation liquid flow rates were low, to accelerate the process of filling, the debit position of the pump was placed higher until the liquid reached the separation head. This was done in all the experiments presented in

this chapter, with the exception of SPBCR 3. The variation of the thermo fluid temperature inside the bath was also registered during the heating phase of the reactor.

The steady state data collected at the end of the heating and pressurization could be used to estimate an experimental value of U, together with the proper equations of the reactor model. In this phase, the model comprises the energy balance equations (5.42) and (5.82), with the elimination of the heat reaction term from the last one. These parameter estimations were performed for each BCR experiment with the help of software gPROMS (PSE, United Kingdom) and the final results are presented in Table 5.8.

Table 5.8. Experimental and predicted steady state temperatures inside the reactor and the respective estimated values of U.

Experiment	**Reactor temperature**			**U (W m^{-2} K^{-1})**
BCR 1	Experimental T (K)			50.5
	z = 0.25 m	z = 0.4 m	z = 0.8 m	
	407.2	408.0	408.6	
	Predicted T (K)			
	z = 0.25 m	z = 0.4 m	z = 0.8 m	
	407.3	408.0	408.5	
BCR 2	Experimental T (K)			52.4
	z = 0.25 m	z = 0.4 m	z = 0.8 m	
	401.9	402.9	403.3	
	Predicted T (K)			
	z = 0.25 m	z = 0.4 m	z = 0.8 m	
	402.1	402.7	403.4	
BCR 3	Experimental T (K)			60.0
	z = 0.25 m	z = 0.4 m	z = 0.8 m	
	413.5	414.7	415.1	
	Predicted T (K)			
	z = 0.25 m	z = 0.4 m	z = 0.8 m	
	413.9	414.5	415.1	
BCR 4	Experimental T (K)			56.9
	z = 0.25 m	z = 0.4 m	z = 0.8 m	
	402.7	403.1	403.4	
	Predicted T (K)			
	z = 0.25 m	z = 0.4 m	z = 0.8 m	
	402.5	403.1	403.6	

The overall heat transfer coefficients presented above are almost similar, which is a result of the utilization of very close operating conditions within these BCR experiments. The small variations observed between the values of U can be explained by the differences in the liquid and gas flow rates and in the temperatures ranges of stabilization.

5.3.1.3. Vanillin oxidation

The BCR experiments were performed to determine the specific effects of the structured packing and will be employed as reference values. To model the lignin oxidation in the reactor, there are two unknown parameters: the volumetric mass transfer coefficient ($k_L a$) and the stoichiometric coefficient of the dissolved oxygen (υ_1) in the liquid, as it is represented in equation (3.13). The experiments in the BCR can be employed to determine the value of υ_1.

Since the BCR is a reactor configuration extensively investigated and the description of the vanillin oxidation system does not include υ_1, the strategy followed to estimate this coefficient started with the C_V^2 results obtained in a BCR vanillin oxidation experiment. With these results, it was chosen a proper $k_L a$ correlation that could also be applied to predict this mass transfer coefficient in the BCR lignin oxidation systems.

Experiment BCR 1

The first experiment done was the oxidation of a solution of vanillin in water and sodium hydroxide (to adjust pH in 14). The physical properties and the parameters used to characterize the system of experiment BCR 1 are presented in Tables 5.9 and

5.10. The liquid heat capacity, $C_{P,L}$, was considered constant and calculated for the feed stream composition. The velocity of the thermo fluid, u_F, is 1.99 x 10^{-3} m/s (assumed to be linearly proportional to its viscosity).

The experimental and simulation results of the vanillin concentration in the exit stream of the separation head, C_V^2, are presented in Figure 5.1. The measured operating pressure is shown in Figure 5.2, together with the simulation and experimental temperatures collected by the three thermocouples placed along the column.

Table 5.9. Physical properties of the vanillin oxidation experiment BCR 1.

$C_{P,L}$ (J/kg K)	4171 (*)	ρ_L (kg/m^3)	963 (*)	μ_L (kg/m s)	2.03x10^{-4}
$C_{P,G}$ (J/kg K)	995 (+)	ρ_G (kg/m^3)	8.99 (+)	μ_G (kg/m s)	2.41x10^{-5} (+)
$C_{P,S}$ (J/kg K)	500 (**)	ρ_S (kg/m^3)	7912 (**)	σ_L (N/m)	0.054 (*)
$C_{P,F}$ (J/kg K)	1996	ρ_F (kg/m^3)	1028		

(*) - (Kirk-Othmer Encyclopedia, 2005); (+) - (Holman, 1989); (**) - (Mills, 2002)

Table 5.10. Model parameters for the of the vanillin oxidation experiment BCR 1.

Column section				
ε_L	$z < 0.1$ m	1	D_{ax} (m^2/s)	9.540 x 10^{-4}
	$z \geq 0.1$ m	0.969	λ_{ef} (W/m K)	3689
ε_G	$z < 0.1$ m	0	U (W/m^2 K)	50.5
	$z \geq 0.1$ m	0.0305	α	0.5
Separation head				
V_{CSTR} (ml)		900	α	0.5

Two different simulation curves are shown in Figure 5.1. The solid line is the simulation curve using a value of k_La extracted from fitting the model to the experimental results. The dashed line results from a simulation performed with a k_La

predicted by a proper correlation for bubble column reactors. The parameter estimations and simulations were performed in the software gPROMS (PSE, United Kingdom).

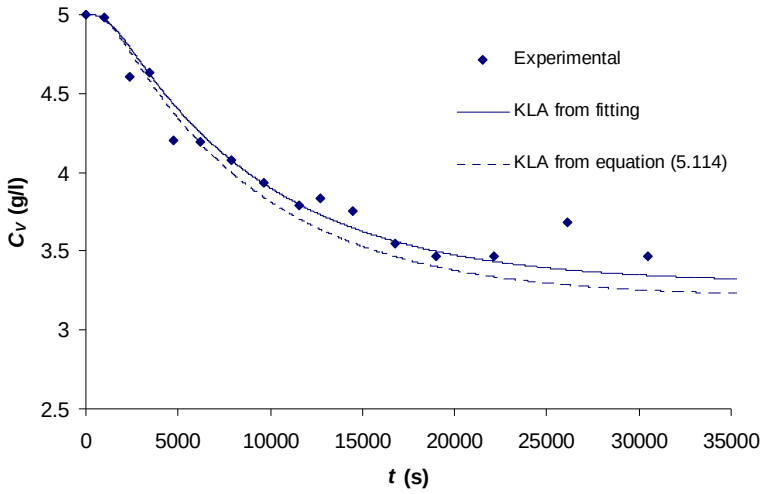

Figure 5.1. Vanillin concentration history at the exit stream of the reactor, C_V^2, for the experiment BCR 1. Blue points represent the measured C_V^2 collected at the exit of the reactor. The solid line corresponds to the simulation results using the reactor model for vanillin oxidation with a $k_L a$ of 1.57×10^{-3} s^{-1}, extracted from a fitting to the experimental results of C_V^2. The dashed line represents the simulation results using the model for vanillin oxidation, with a $k_L a$ of 1.95×10^{-3} s^{-1}, estimated from equations (5.114) and (5.115). The experimental conditions are in Table 5.1 and physical properties and model parameters used in the simulations are in Tables 5.9 and 5.10.

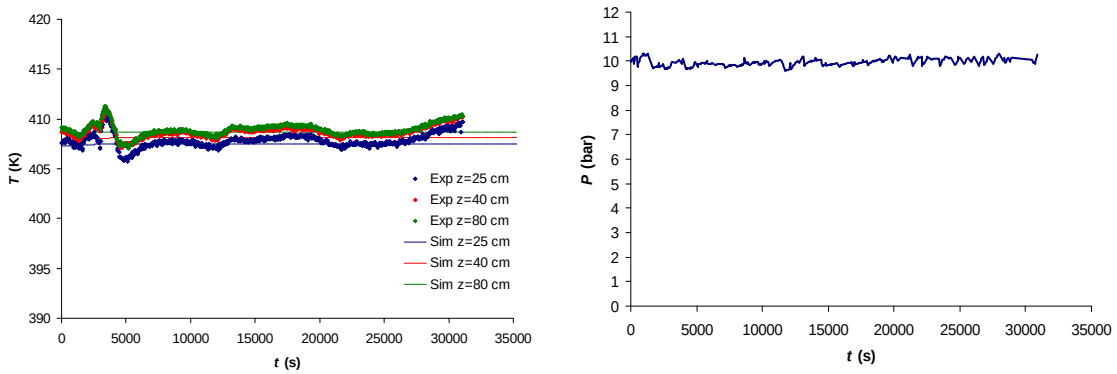

Figure 5.2. Temperature history at three different axial positions of the column, and measured operating pressure for experiment BCR 1. In the graph of the left side are represented the temperature measurements (points) and the correspondent simulation results (solid lines) using the reactor model for vanillin oxidation with a $k_L a$ of 1.95×10^{-3} s^{-1}. In the right is the total pressure values collected during the experiment. The experimental conditions are in Table 5.1 and physical properties and model parameters used in the simulations are in Tables 5.9 and 5.10.

From Figure 5.1 it can be seen that the C_V^2 experimental results could be well fitted with a single parameter ($k_L a$). The steady state is apparently reached with an exit vanillin concentration around 3.5 g/l for experiment times above the 20000 s.

Knowing the operating liquid flow rate, and considering a total volume of liquid inside the reactor around 6.8 litres, it can be concluded that it took approximately 3.3 hours for reaching a decay of 30% in the vanillin concentration fed to the reactor. A decay of 40% of vanillin concentration was observed in the batch reactor for similar reaction times and operating conditions. This fact clearly reveals the existence of mass transfer limitations in this BCR unit when compared to the batch operation where oxygen was continuously supplied and with intense stirring to enhance mass transfer.

The reactor temperature was also well predicted by the employed reactor model, as it is shown in Figure 5.2. During the experiment, the temperature values are almost constant due to the low heat of reaction of vanillin oxidation. They only show small variations caused by fluctuations in the operating liquid flow rate.

Several studies on mass transfer coefficients in bubble columns were analysed to determine a proper correlation to predict $k_L a$ in the case study (Akita and Yoshida, 1973; Hikita et al., 1981; Jordan et al., 2002; Kojima et al., 1997; Lau et al., 2004; Letzel et al., 1999; Shimizu et al., 2000; Wilkinson et al., 1994; Zlokarnik, 1979). A large dispersion of values were observed with the diffenent correlations, differing in some cases in one or two orders of magnitude.

The estimation of $k_L a$ from the work of Zlokarnik (1979) was the closest one to the value of the mass transfer coefficient obtained by fitting the model to the C_V^2 in experiment BCR 1. The value of the correlation-based $k_L a$ was 1.95×10^{-3} s^{-1} and the experimental $k_L a$ was 1.57×10^{-3} s^{-1}, which represents a deviation of 19%. In

experiment BCR 1, the effect of this deviation into the simulation curves of C_V^2 is very acceptable, as it can be seen from the proximity of the lines in Figure 5.1.

The work developed by Zlokarnik (1979) consisted on a mass transfer equation for industrial gas distributors based on a sorption number, Y:

$$Y = \frac{k_L a}{u_{GS}} \left(\frac{\mu_L^2}{\rho_L^2 g} \right)^{1/3} \tag{5.114}$$

$$Y = 3.9 \times 10^{-5} \left[\frac{u_{GS} \rho_L^{1/3}}{(\mu_L g)^{1/3}} \right]^{-0.1} \tag{5.115}$$

5.3.1.4. Lignin oxidation

The three experiments of lignin oxidation performed in the BCR configuration, with different temperatures and/or gas flow rates, were used to fit a single value of υ_1. Applying equations (5.114) and (5.115) in the BCR-lignin oxidation system to predict $k_L a$, it leaves the reactor model with only one unknown parameter (υ_1) to extract from a set of three experiments.

Experiment BCR 2

The physical properties and the parameters used to characterize the first lignin oxidation experiment (BCR 2) are presented in Tables 5.11 and 5.12.

Table 5.11. Physical properties of the lignin oxidation experiment BCR 2.

$C_{P,L}$ (J/kg K)	3972	ρ_L (kg/m^3)	1114	M_n (g/mol)	2325
$C_{P,G}$ (J/kg K)	995 (+)	ρ_G (kg/m^3)	8.99 (+)	μ_L (kg/m s)	1.54x10^{-3}
$C_{P,S}$ (J/kg K)	500 (**)	ρ_S (kg/m^3)	7912 (**)	μ_G (kg/m s)	2.41x10^{-5} (+)
$C_{P,F}$ (J/kg K)	1996	ρ_F (kg/m^3)	1028	σ_L (N/m)	0.061 (++)

(*) - (Kirk-Othmer Encyclopedia, 2005); (+) - (Holman, 1989); (**) - (Mills, 2002); (++) – (Ferreira et al., 2005)

Table 5.12. Model parameters for the lignin oxidation experiment BCR 2.

Column section				
ε_L	$z < 0.1$ m	1	D_{ax} (m^2/s)	9.576 x 10^{-4}
	$z \geq 0.1$ m	0.969	λ_{ef} (W/m K)	4100
ε_G	$z < 0.1$ m	0	U (W/m^2 K)	52.4
	$z \geq 0.1$ m	0.0306	α	0.5
			$k_L a$ (s^{-1})	5.88 x 10^{-4}
Separation head				
V_{CSTR} (ml)		900	α	0.5

The liquid heat capacity, $C_{P,L}$, was considered constant and calculated for the initial lignin oxidation media using equation (3.73). The velocity of the thermo fluid, u_F, was assumed equal to the one of experiment BCR 1, since in most of the time the set point of the thermostatic bath was similar (436 K).

The experimental C_V^2 and pH are presented in Figure 5.3. In the same Figure were also placed the respective simulation results using υ_1 as a fitting parameter for the three BCR lignin oxidation experiments. The simulated and measured temperatures are shown in Figure 5.4, together with the experimental evolution of the total pressure.

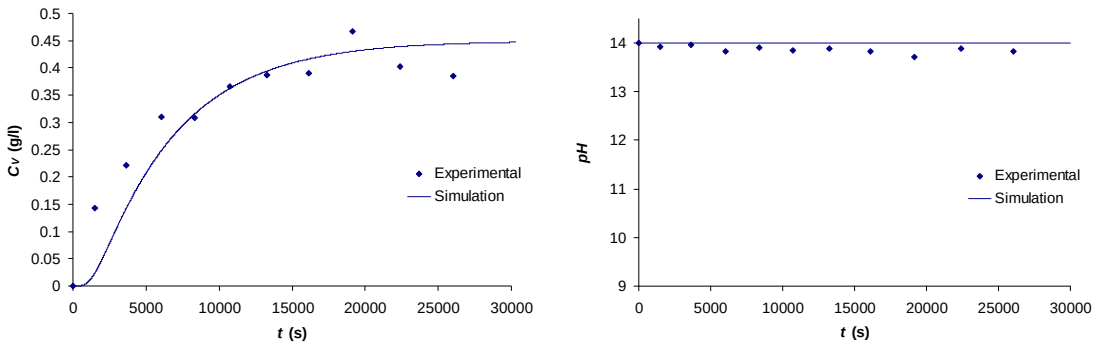

Figure 5.3. Variation of the vanillin concentration and pH, at the exit stream of the reactor, for the experiment BCR 2. Blue points represent experimental values, and the solid lines corresponds to the simulation results using the model for lignin oxidation with a υ_1 of 1.56. The experimental conditions are in Table 5.1 while physical properties and parameters used in the simulations are in Tables 5.11 and 5.12.

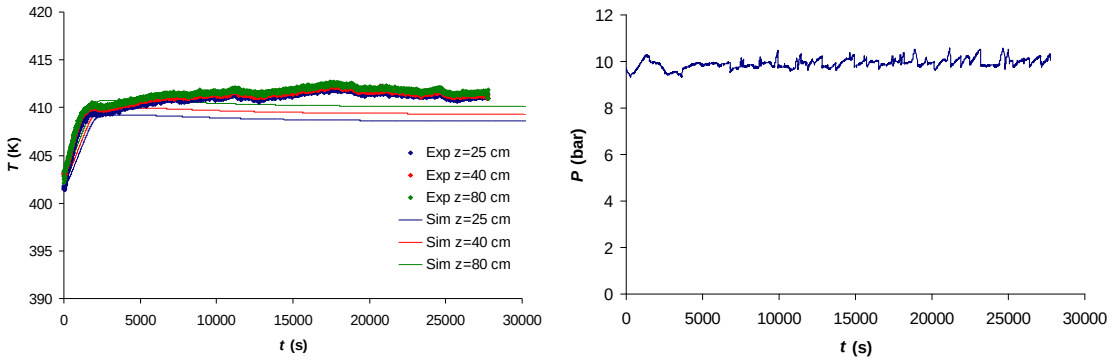

Figure 5.4. Temperature variation at three different axial positions of the column, and measured operating pressure for experiment BCR 2. In the graph on the left side are represented the temperature measurements (points) and the correspondent simulation results (solid lines) using the reactor model for lignin oxidation with a υ_1 of 1.56. In the right side is the total pressure values collected during the experiment. The experimental conditions are in Table 5.1 while physical properties and parameters used in the simulations are in Tables 5.11 and 5.12.

The steady state of experiment BCR 2 is reached with a medium C_V^2 of 0.41 g/l, which represents 0.68% of conversion of the lignin mass into vanillin. From Figures 5.3 and 5.4, it can also be seen that the experimental profiles of the temperatures and C_V^2 were well adjusted by the simulation results, using the reactor model with a υ_1 of 1.56.

In this experiment, the set point of the thermostatic bath was 436 K during the heating and pressurization. However, at the start-up of the reaction phase, this set point was raised to 443 K for a small period of time (1900 s) and then placed again in 436 K.

Experiment BCR 3

The physical properties and the parameters used to characterize the second lignin oxidation experiment (BCR 3) are presented in Tables 5.13 and 5.14. The purpose of this experiment was to verify the effect of increasing 10 K the initial temperature range, comparing to experiment BCR 2.

The liquid heat capacity, $C_{P,L}$, was assumed constant and calculated for the liquid feed composition using equation (3.73). The velocity of the thermo fluid, u_F,

was assumed equal to 2.30 x 10^{-3} m/s, corresponding to a set point of the thermostatic bath of 443 K.

Table 5.13. Physical properties of the lignin oxidation experiment BCR 3.

$C_{P,L}$ (J/kg K)	3978	ρ_L (kg/m^3)	1114	M_n (g/mol)	2325
$C_{P,G}$ (J/kg K)	997 (+)	ρ_G (kg/m^3)	8.80 (+)	μ_L (kg/m s)	1.51x10^{-3}
$C_{P,S}$ (J/kg K)	500 (**)	ρ_S (kg/m^3)	7912 (**)	μ_G (kg/m s)	2.45x10^{-5} (+)
$C_{P,F}$ (J/kg K)	1996	ρ_F (kg/m^3)	1028	σ_L (N/m)	0.061 (++)

(*) - (Kirk-Othmer Encyclopedia, 2005); (+) - (Holman, 1989); (**) - (Mills, 2002); (++) – (Ferreira et al., 2005)

Table 5.14. Model parameters for the lignin oxidation experiment BCR 3.

Column section				
ε_L	$z < 0.1$ m	1	D_{ax} (m^2/s)	9.599 x 10^{-4}
	$z \geq 0.1$ m	0.969	λ_{ef} (W/m K)	4110
ε_G	$z < 0.1$ m	0	U (W/m^2 K)	60.0
	$z \geq 0.1$ m	0.0307	α	0.5
			$k_L a$ (s^{-1})	5.98 x 10^{-4}
Separation head				
V_{CSTR} (ml)		900	α	0.5

The experimental and simulation values of vanillin concentration and pH in the exit stream are presented in Figure 5.5. The measured and predicted temperatures are shown in Figure 5.6, as well as the total reactor pressure.

From Figures 5.5 and 5.6, it can be concluded that the experimental profiles of the temperatures and C_V^2 were predicted with good accuracy using the model for lignin oxidation with a υ_1 of 1.56. In this experiment, the steady state was achieved with a medium vanillin concentration in the exit stream of 0.56 g/l, which represents a conversion of 0.93% of the lignin mass into vanillin. Comparing this result with the one

of experiment BCR 2, it reveals a small improvement that was expected, particularly due to the effect of higher temperatures on the reaction rates of lignin oxidation. However, the value of lignin conversion is still far from the desirable levels.

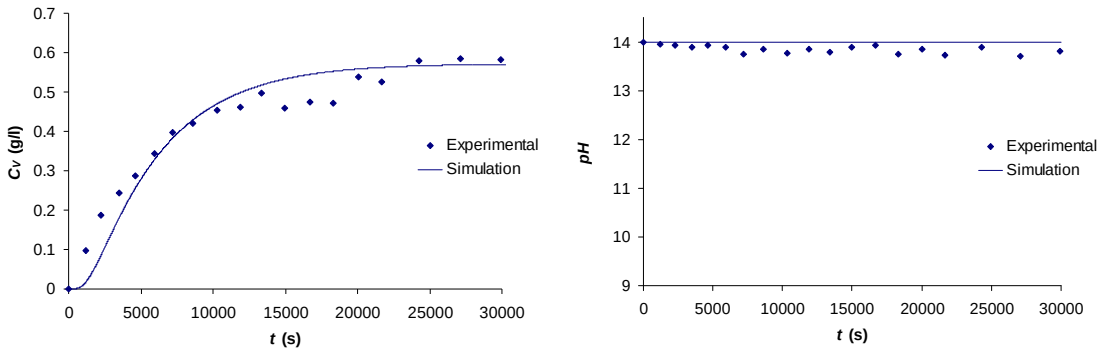

Figure 5.5. Variation of the vanillin concentration and pH, at the exit stream of the reactor, for the experiment BCR 3. Blue points represent experimental values, and the solid lines corresponds to the simulation results using the model for lignin oxidation with a υ_1 of 1.56. The experimental conditions are in Table 5.1. The physical properties and remaining parameters used in the simulations are in Tables 5.13 and 5.14.

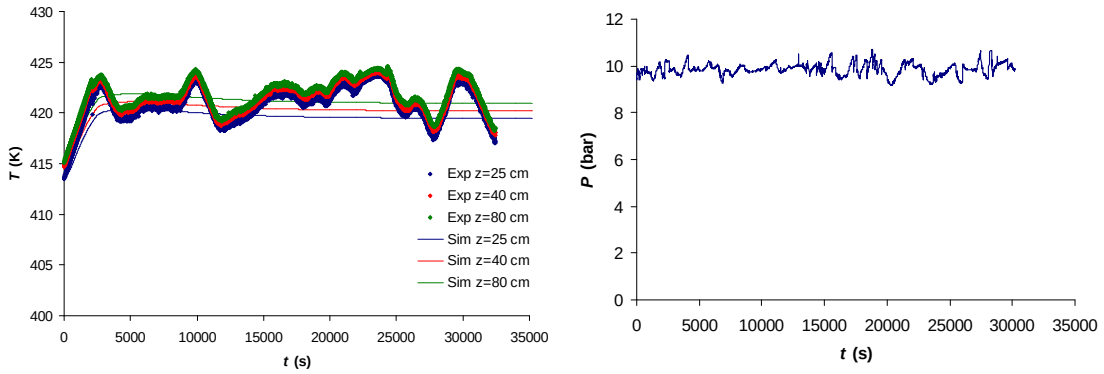

Figure 5.6. Temperature variation at three different axial positions of the column, and measured operating pressure for experiment BCR 3. In the graph of the left side are presented the experimental temperatures (points) and the correspondent simulation results (solid lines) using the model for lignin oxidation with a υ_1 of 1.56. In the right side is the total pressure values collected during the experiment. The experimental conditions are in Table 5.1. The physical properties and remaining parameters used in the simulations are in Tables 5.13 and 5.14.

The temperature profiles show an increase of approximately 7 K due to the heat liberated by the reactions, until the system reaches a state of apparent stabilization. This state presented some pronounced temperature fluctuations, as a result of the difficulties to control the liquid flow rate of the exit stream. The increase of 7 K is similar to what was observed in experiment BCR 2 (Figure 5.4), which is consistent to the proximity of the lignin conversion levels.

Experiment BCR 4

The physical properties and the parameters used in the reactor model for the third lignin oxidation experiment (BCR 4) are presented in Tables 5.15 and 5.16. This experiment was made to check the effects on the system performance of increases in the total gas flow rate and, particularly the oxygen partial pressure.

Table 5.15. Physical properties of the lignin oxidation experiment BCR 4.

$C_{P,L}$ (J/kg K)	3978	ρ_L (kg/m^3)	1114	M_n (g/mol)	2325
$C_{P,G}$ (J/kg K)	979 (+)	ρ_G (kg/m^3)	9.09 (+)	μ_L (kg/m s)	1.54×10^{-3}
$C_{P,S}$ (J/kg K)	500 (**)	ρ_S (kg/m^3)	7912 (**)	μ_G (kg/m s)	2.49×10^{-5} (+)
$C_{P,F}$ (J/kg K)	1996	ρ_F (kg/m^3)	1028	σ_L (N/m)	0.061 (++)

(*) - (Kirk-Othmer Encyclopedia, 2005); (+) - (Holman, 1989); (**) - (Mills, 2002);
(++) – (Ferreira et al., 2005)

The liquid heat capacity, $C_{P,L}$, was obtained from equation (3.73) using the liquid feed composition. The velocity of the thermo fluid, u_F, was assumed equal to 1.99×10^{-3} m/s, corresponding to a set point of the thermostatic bath of 436 K.

The experimental and simulation results of C_V^2 and pH are presented in Figure 5.7. The measured and predicted temperature profiles are shown in Figure 5.8, as well as the total reactor pressure.

Table 5.16. Model parameters for the lignin oxidation experiment BCR 4.

Column section				
ε_L	$z < 0.1$ m	1	D_{ax} (m^2/s)	11.69 x 10^{-4}
	$z \geq 0.1$ m	0.965	λ_{ef} (W/m K)	4979
ε_G	$z < 0.1$ m	0	U (W/m^2 K)	56.95
	$z \geq 0.1$ m	0.0355	α	0.5
			$k_L a$ (s^{-1})	8.42 x 10^{-4}
Separation head				
V_{CSTR} (ml)		900	α	0.5

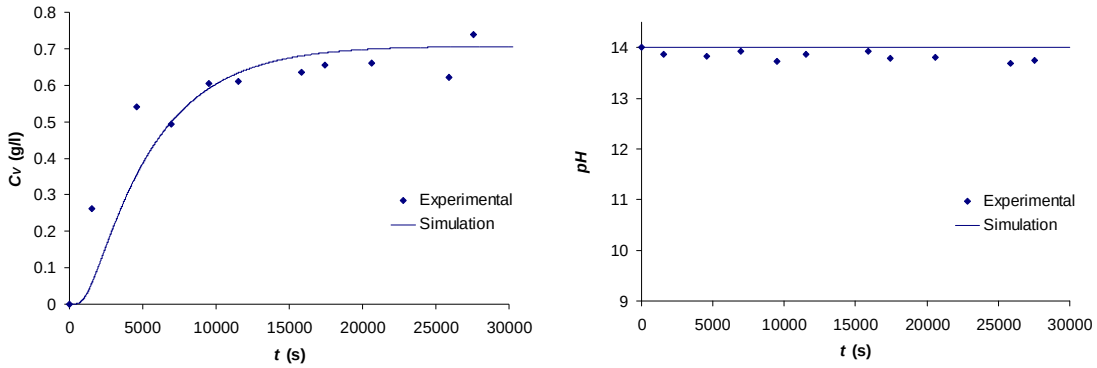

Figure 5.7. Variation of the vanillin concentration and pH, at the exit stream of the reactor, for the experiment BCR 4. Blue points represent experimental values, and the solid lines corresponds to the simulation results using the model for lignin oxidation with a υ_1 of 1.56. The experimental conditions are in Table 5.1. The physical properties and remaining parameters used in the simulations are in Tables 5.15 and 5.16.

The vanillin concentration in the reactor exit stream reached a steady state value around 0.67 g/l (lignin mass conversion of 1.12%). This value is a further improvement to experiments BCR 2 and BCR 3, but not good enough comparing to the values obtained in the batch reactor. This increase is the result of a higher P_{O2} in the oxygen solubility in the liquid phase, and also a higher mass transfer coefficient, due to the increase in gas flow rate.

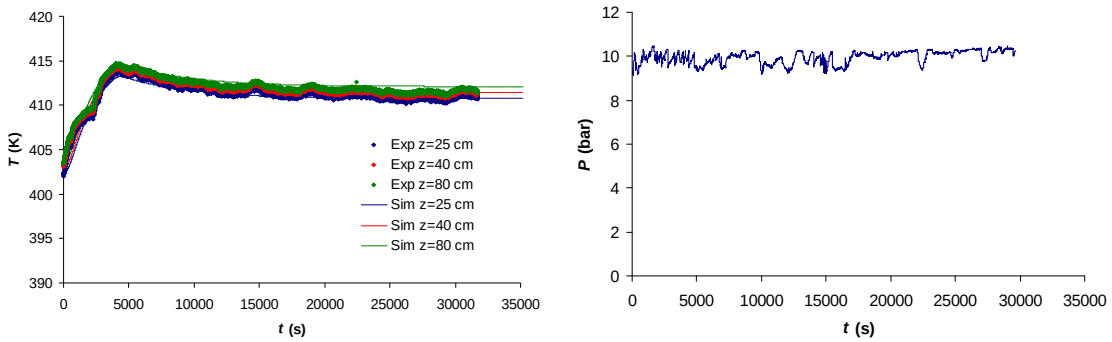

Figure 5.8. Temperature variation at three different axial positions of the column, and measured operating pressure for experiment BCR 4. In the graph of the left side are presented the experimental temperatures (points) and the correspondent simulation results (solid lines) using the model for lignin oxidation with a υ_1 of 1.56. In the right side is the total pressure values collected during the experiment. The experimental conditions are in Table 5.1. The physical properties and remaining parameters used in the simulations are in Tables 5.15 and 5.16.

In an initial part of the experiment, the temperature profiles showed an increase of approximately 10-11 K, but then they suffered a small decrease, stabilizing in values 7-8 K higher than the start-up temperatures. The faster reaction rates due to the higher amounts of available oxygen, liberates more heat that tends to promote larger increases in the reactor temperature. For that reason, when this tendency was observed during the experiment, the set point of the thermostatic bath suffered an adjustment.

From Figures 5.7 and 5.8, it can be concluded that the experimental profiles of the temperatures and C_V^2 were well predicted using the model for lignin oxidation with a υ_1 of 1.56.

5.3.2. SPBCR experiments

The results presented earlier, for the BCR unit, revealed limitations regarding the gas-liquid mass transfer. In order to enhance gas-liquid mass transfer, and thus achieve higher product yields, three structured packing (Mellapak 750Y) were introduced in the column section above the gas distributor.

The performance of this SPBCR configuration was evaluated with seven experiments: two vanillin oxidation experiments at different pH values (14 and 9.8); and five lignin oxidation experiments at different liquid and gas flow rates.

The models used to simulate these experiments are described, respectively, in sections 5.2.3 and 5.2.4, and were applied with one fitting parameter - $k_L a$. Since the hydrodynamic environment is completely different, the values of the parameters used for the BCR are not valid in the SPBCR configuration. New values for the same kind of parameters (dispersion coefficients, phase hold-ups and heat transfer coefficients) were estimated or taken from the available experimental data.

5.3.2.1. Gas hold-up and axial dispersion coefficient

As already explained in section 5.2.2, there is a great lack of research focused on the application of structured packings in upflow flooded gas-liquid reactors. To circumvent the lack of data, particularly for phase hold-ups and D_{ax} analogies with gas-liquid upflow co-current reactors filled with random packings were employed.

The gas hold-up in co-current packed bubble column reactors depends mainly on the gas velocity, especially for low ranges of liquid velocity (u_{LS} < 1.5 cm/s). It also increases with liquid viscosity and decreases for higher surface tensions (Gianetto and Silveston, 1986). At low gas flow rates, packed columns generally present higher gas hold ups (ε_G) than empty bubble columns, operating in the same conditions.

Recent studies on the phase hold-ups of upflow packed bed bubble column reactors are mainly focused on the liquid phase (Bensetiti et al., 1997; Cassanello et al., 1998; Dudukovic et al., 2002; Iliuta and Thyrion, 1997; Larachi et al., 1991; Saroha and Khera, 2006; Yang et al., 1993). Some correlations were found in literature to estimate the gas hold-up in packed columns:

Achwal and Stepanek (1976) - $$\varepsilon_G = \varepsilon \Big/ \left[1 + 0.59\ u_{LS}^{-0.433} \left(\frac{u_{LS}}{u_{GS}} \right)^{0.563} \right] \quad (5.116)$$

Larachi et al. (1991) - $$\varepsilon_G = \varepsilon \left(\frac{u_{GS} - J_{DF}}{u_{GS} + u_{LS}} \right) \ ; \ J_{DF} = a\, u_{GS}^{b} \quad (5.117)$$

$$0.4 < a_{DF} < 0.54; \ 0.91 < b_{DF} < 1.07$$

Weber (1961) - $$\varepsilon_G = 0.454 u_{GS}^{0.3} \quad (5.118)$$

Yang et al. (1990) - $$\varepsilon_G = 0.16 \frac{u_{GS}}{u_{GS} + u_{LS}} \quad (5.119)$$

where J_{DF} is the drift flux, which is a unique function of the gas velocity; a_{DF} and b_{DF} are constants that depend on the system, distributor and reactor type.

The values of the gas hold-up determined in the first three SPBCR tracer experiments (Chapter 4) are presented In Table 5.17, together with the respective ε_G estimated from equations (5.116) to (5.119).

Table 5.17. Measured and predicted values of ε_G for the first three SPBCR tracer experiments presented in Chapter 4.

	Experiment 1	**Experiment 2**	**Experiment 3**
Q_L (l/h)	4.33	4.51	4.68
Q_G (ml_{NTP}/min)	1000	625	250
Experimental ε_G	0.0463	0.0263	0.0083
Achwal and Stepanek (1976)	0.0438	0.0338	0.0204
Larachi et al. (1991)	0.0699	0.0419	0.0079
Weber (1961)	0.0371	0.0322	0.0170
Yang et al. (1990)	0.0972	0.0770	0.0422

Comparing the experimental and estimated values of ε_G for the SPBCR tracer experiments, large deviations can be observed, particularly for Larachi et al. (1991) and Yang et al. (1992). Based on this comparison presented in Table 5.17, the equation from Achwal and Stepanek (1976) was selected, since it presented smaller deviations at

higher gas flow rates; most of the experimental work on the SPBCR was performed with gas flow rates (Q_G) in the range of 625 to 2000 ml_{NTP}/min.

The experimental conditions used in this work are again out of the range for which equations (5.116) to (5.119) were developed: low gas and liquid velocity. To employ these equations, it was necessary to make some extrapolations, not only because of the experimental conditions but also due to the different characteristic of the packing applied; very high void fraction (0.95).

The gas hold-up estimations for the reaction experiments in the SPBCR configuration, based on Achwal and Stepanek (1976), are presented in Table 5.18.

Table 5.18. Values of gas hold-up (ε_G) for the SPBCR experiments estimated with the work of Achwal and Stepanek (1976).

	SPBCR 1	SPBCR 2	SPBCR 3	SPBCR 4	SPBCR 5	SPBCR 6	SPBCR 7
ε_G	0.0377	0.0780	0.0382	0.0233	0.0704	0.0784	0.0858

The liquid phase dispersion coefficient, D_{ax}, in a packed bubble column is generally known to increase with increasing gas velocities, particularly in low ranges of gas velocity (u_{GS}), and to decrease with increasing liquid velocities (Belfares et al., 2001; Gianetto and Silveston, 1986). From the scarce literature available about D_{ax} in packed bubble column reactors, initial calculations were performed with several correlations, to check the applicability to this system (Achwal and Stepanek, 1979; Belfares et al., 2001; Heilmann and Hofmann, 1969; Stiegel and Shah, 1977; van Gelder and Westerterp, 1990; Weber, 1961). Their predictions of D_{ax} were compared with the axial dispersion coefficients determined in the SPBCR tracer experiments (presented in Chapter 4). However, the estimated values with all of these correlations are quite far

from the experimental D_{ax} (one or two orders of magnitude lower), which makes impossible to apply them in the SPBCR configuration of this work.

To solve this problem, a different of approach was taken. The tracer experiments on the SPBCR were performed with similar liquid flow rates and different gas flow rates, allowing a comparison of the effect of gas velocity (u_{GS}) in the experimental D_{ax}. A correlation that obeys a ratio of the axial dispersion coefficients obtained in the experiments for different gas velocities as expressed in equation (5.120) was selected.

$$\left.\frac{D_{ax}^2}{D_{ax}^1}\right|_{experimental} \approx \left.\frac{D_{ax}^2}{D_{ax}^1}\right|_{estimated} \tag{5.120}$$

where D_{ax}^1 and D_{ax}^2 are the axial dispersion coefficients based on different gas velocity conditions.

The correlation developed by Heilmann and Hofmann (1969) predicted a closer ratio of the evolution of D_{ax} with gas velocity closer to the one verified by the experimental values presented in Chapter 4. The original correlation and the expression used to calculate D_{ax}, for different operating conditions, is presented below:

$$Bo_L = \frac{u_{LS} D_P}{\varepsilon_L D_{ax}} = \frac{\varepsilon_L}{470}\left[\frac{Re_L/\varepsilon_L}{\varepsilon_G D_P^{3.3}}\right]^{0.735} \tag{5.121}$$

$$D_{ax}^2 = D_{ax}^1 \left(\frac{\rho_L^1 \mu_L^2}{\rho_L^2 \mu_L^1}\right)^{0.736} \left(\frac{\varepsilon_G^2}{\varepsilon_G^1}\right)^{0.736} \left(\frac{\varepsilon_L^1}{\varepsilon_L^2}\right)^{0.264} \left(\frac{u_{LS}^2}{u_{LS}^1}\right)^{0.264} \tag{5.122}$$

where Bo_L is the liquid Bodenstein number; and the superscripts 1 and 2 refers to different operating conditions and/or materials (one of them must be known).

In Table 5.19 the predictions of the D_{ax} for the reaction experiments in the SPBCR configuration are presented, based on the D_{ax} values obtained in the tracer experiments and in expression (5.122).

Table 5.19. Estimated values of D_{ax}, in cm^2/s, for the SPBCR reaction experiments using the experimental values of the tracer runs and equation (5.122).

	SPBCR 1	SPBCR 2	SPBCR 3	SPBCR 4	SPBCR 5	SPBCR 6	SPBCR 7
D_{ax} (cm^2/s)	0.319	0.551	1.241	0.638	2.630	2.203	1.929

5.3.2.2. Heat transfer parameters

The heat transfer parameters contained in the mathematical model are: the effective axial heat dispersion coefficient (λ_{ef}) in the column section, and the overall heat transfer coefficient between the reaction media and the thermo fluid flowing inside the jacket (U). The effective axial thermal conductivity (λ_{ef}) in the column section of the SPBCR was assumed to be a result of two contributions:

$$\lambda_{ef} = \lambda_L + \lambda_S \tag{5.123}$$

where λ_L is the contribution of the mass dispersion in the packed bed effective conductivity; and λ_S is the effective axial thermal conductivity of the packed bed at zero flow.

The contribution of the mass dispersion in the λ_{ef} is obtained by using the Lewis's analogy, as in the bubble column reactor:

$$\lambda_L = \varepsilon_L \, D_{ax} \, \rho_L \, C_{P,L} \tag{5.124}$$

The estimation of a value for λ_S was based on the steady state temperature data at the end of the heating + pressurization phase of experiments as explained in section 5.3.1.2.The energy balance equations (5.42) and (5.82), with the elimination of the heat reaction term from the last one, were fitted by two unknown parameters (λ_{ef} and U) to the steady state temperature data collected at the end of the heating + pressurization. These two parameter estimations were performed with gPROMS software (PSE, United Kingdom). Knowing λ_L from equation (5.124) and λ_{ef}, an average value of 719 $W\ m^{-1}$

K^{-1} for λ_S in the two referred experiments was obtained. Assuming λ_S constant in the two studied reaction media (vanillin oxidation and lignin oxidation), it could be use to predict the effective axial thermal conductivity of the remaining experiments from equation (5.124). The results obtained are presented in Table 5.20.

Table 5.20. Effective heat dispersion coefficient (λ_{ef}) for the SPBCR reaction experiments.

	SPBCR 1	SPBCR 2	SPBCR 3	SPBCR 4	SPBCR 5	SPBCR 6	SPBCR 7
λ_{ef} ($Wm^{-1}K^{-1}$)	950	915	1173	833	1705	1531	1418

With the values of λ_{ef} presented in Table 5.20, the heat transfer coefficient U, was estimated in a similar way to what was done in the BCR experiments. The steady state data collected at the end of the heating + pressurization could be fitted with the proper energy balance equations with only one unknown parameter (U).These parameter estimations were performed with the software gPROMS (PSE, United Kingdom) and the final results are presented in Table 5.21.

The variation of the U values presented above with the operating conditions is consistent with the following criteria:

- Decrease in the heat transfer coefficient with decreasing liquid flow rates due to higher convection in the gap between the reactor wall and the structured packing (SPBCR 5, SPBCR 6 and SPBCR 7).
- Increase of U with increasing gas flow rate also by higher convection (SPBCR2, SPBCR 3 and SPBCR 4). The effect of the gas flow rate is much less pronounced than the effect of the liquid flow rate.
- The vanillin oxidation media presents heat transfer coefficients slightly higher than the ones obtained with lignin oxidation media, in similar flow rate

conditions. The lower viscosity of aqueous vanillin solution seems to have some positive effect on the heat transfer convection between the reaction media and the wall.

Table 5.21. Experimental state temperatures inside the reactor and the respective estimated values of U.

Experiment	**Reactor temperature**			**U (W m^{-2} K^{-1})**
SPBCR 1	Experimental T (K) *			113.2
	z = 0.25 m	z = 0.4 m	z = 0.8 m	
	400.6	403.2	406.3	
SPBCR 2	Experimental T (K)			42.5
	z = 0.25 m	z = 0.4 m	z = 0.8 m	
	409.7	410.9	411.8	
SPBCR 3	Experimental T (K)			77.2
	z = 0.25 m	z = 0.4 m	z = 0.8 m	
	395.8	400.2	403.4	
SPBCR 4	Experimental T (K)			72.5
	z = 0.25 m	z = 0.4 m	z = 0.8 m	
	395.6	399.1	401.8	
SPBCR 5	Experimental T (K)			97.3
	z = 0.25 m	z = 0.4 m	z = 0.8 m	
	399.3	400.5	401.5	
SPBCR 6	Experimental T (K)			36.8
	z = 0.25 m	z = 0.4 m	z = 0.8 m	
	404.3	405.8	406.9	
SPBCR 7	Experimental T (K)			24.0
	z = 0.25 m	z = 0.4 m	z = 0.8 m	
	405.4	406.8	408.2	

* – extrapolated from the steady state of the reaction phase.

Comparing U values of the SPBCR and BCR, for similar conditions, it can be verified that the BCR configuration presented higher heat transfer coefficients. Since one of the functions of the structured packing is to minimize the liquid circulation flow that characterizes bubble column reactors, it also seems to diminish the heat transfer at the reactor wall by limiting the fluid convection.

5.3.2.3. Vanillin oxidation

Two experiments of vanillin oxidation were performed in the SPBCR configuration with different pH media. The reactor model for the SPBCR contains the volumetric mass transfer coefficient ($k_L a$) as the only unknown parameter. Besides the main purpose of checking the effect of the operating variables in the degradation of the desired product (vanillin) of this study, the vanillin oxidation experiments were also performed to verify the order of magnitude of the $k_L a$ values found in the SPBCR.

Experiment SPBCR 1

The physical properties and the parameters used to characterize the system of experiment SPBCR 1 are presented in Tables 5.22 and 5.23. The liquid heat capacity, $C_{P,L}$, was considered constant and calculated for the feed stream composition. The velocity of the thermo fluid, u_F was 2.30 x 10^{-3} m/s.

Table 5.22. Physical properties of the vanillin oxidation experiment SPBCR 1.

$C_{P,L}$ (J/kg K)	4109 (*)	ρ_L (kg/m^3)	963 (*)	μ_L (kg/m s)	2.03x10^{-4}
$C_{P,G}$ (J/kg K)	1005 (+)	ρ_G (kg/m^3)	8.97 (+)	μ_G (kg/m s)	2.35x10^{-5} (+)
$C_{P,S}$ (J/kg K)	500 (**)	ρ_S (kg/m^3)	7912 (**)	σ_L (N/m)	0.054 (*)
$C_{P,F}$ (J/kg K)	1996	ρ_F (kg/m^3)	1028		

(*) - (Kirk-Othmer Encyclopedia, 2005); (+) - (Holman, 1989); (**) - (Mills, 2002)

The experimental and simulation results of the vanillin concentration at the exit of the separation head, C_V^2, are presented in Figure 5.9. The total pressure is shown in Figure 5.10, together with the simulation and experimental temperatures collected by the three thermocouples placed along the column.

Table 5.23. Model parameters for the vanillin oxidation experiment SPBCR 1.

Column section				
ε_L	$z < 0.1$ m	1	D_{ax} (m^2/s)	9.540 x 10^{-4}
	$z \geq 0.1$ m	0.969	λ_{ef} (W/m K)	3689
ε_G	$z < 0.1$ m	0	U (W/m^2 K)	50.5
	$z \geq 0.1$ m	0.0305	α	0.5
ε_S	$z < 0.1$ m	0		
	$z \geq 0.1$ m	0.0417		
Separation head				
V_{CSTR} (ml)		900	α	0.5

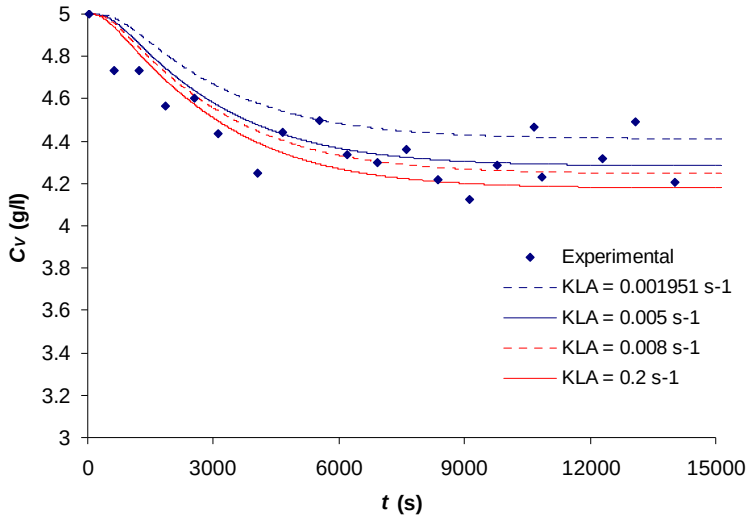

Figure 5.9. Vanillin concentration history at the exit stream of the reactor, C_V^2, for the experiment SPBCR 1. Blue points represent the measured C_V^2 on the liquid samples collected at the exit of the reactor. The solid and dashed lines correspond to the simulation results using the reactor model for vanillin oxidation with different values of $k_L a$. The experimental conditions are in Table 5.1 and the physical properties and remaining parameters used in the simulations are in Tables 5.22 and 5.23.

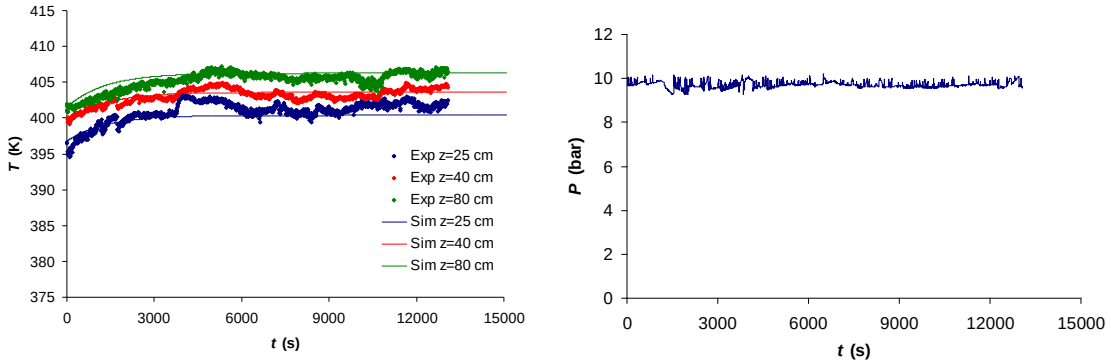

Figure 5.10. Temperature history at three different axial positions of the column and measured operating pressure for experiment SPBCR 1. In the graph of the left side are represented the temperature measurements (points) and the correspondent simulation results (solid lines) using the model for vanillin oxidation with a $k_L a$ of 5×10^{-3} s^{-1}. In the right side is the total pressure measured during the experiment. The experimental conditions are in Table 5.1 and the physical properties and remaining parameters used in the simulations are in Tables 5.22 and 5.23.

Four different simulation curves (referent to four different values of $k_L a$) are presented in Figure 5.9. It can be observed that for values higher than 10^{-1} s^{-1} the value of the mass transfer parameter has no influence in the results. In fact, if the mass transfer coefficient increases 40 times, (from 5×10^{-3} to 2×10^{-1} s^{-1}), the concentration of vanillin in steady state only decreases around 0.1 g/l. Since the vanillin oxidation rate is expected to be low at a pH of 14, for values above the referred order of magnitude of $k_L a$, the reaction should start to be the step that controls the process.

The temperature profiles of the experiment showed an initial increase 4-5 K. This was not caused by the heat of reaction of vanillin oxidation, since it was already focused that it does not affect the reactor temperature. Instead, the reactive phase of the experiment was started-up before the stabilization of the temperature was achieved leading that anomaly in the temperature curves. This fact was properly introduced into the reactor model by adapting the initial temperature conditions.

Experiment SPBCR 2

The physical properties and the parameters used simulations of the experiment SPBCR 2 are presented in Tables 5.24 and 5.25. The liquid heat capacity, $C_{P,L}$, was assumed constant and calculated for the initial liquid composition. The velocity of the thermo fluid, u_F, was equal to the one of SPBCR 1 (2.30×10^{-3} m/s).

Table 5.24. Physical properties of the vanillin oxidation experiment SPBCR 2.

$C_{P,L}$ (J/kg K)	4178 (*)	ρ_L (kg/m^3)	960 (*)	μ_L (kg/m s)	2.03×10^{-4}
$C_{P,G}$ (J/kg K)	996 (+)	ρ_G (kg/m^3)	8.93 (+)	μ_G (kg/m s)	2.42×10^{-5} (+)
$C_{P,S}$ (J/kg K)	500 (**)	ρ_S (kg/m^3)	7912 (**)	σ_L (N/m)	0.054 (*)
$C_{P,F}$ (J/kg K)	1996	ρ_F (kg/m^3)	1028		

(*) - (Kirk-Othmer Encyclopedia, 2005); (+) - (Holman, 1989); (**) - (Mills, 2002)

Table 5.25. Model parameters for the vanillin oxidation experiment SPBCR 2.

Column section				
ε_L	$z < 0.1$ m	1	D_{ax} (m^2/s)	0.551×10^{-4}
	$z \geq 0.1$ m	0.880	λ_{ef} (W/m K)	915
ε_G	$z < 0.1$ m	0	U (W/m^2 K)	42.5
	$z \geq 0.1$ m	0.0780	α	0.5
ε_S	$z < 0.1$ m	0		
	$z \geq 0.1$ m	0.0417		
Separation head				
V_{CSTR} (ml)		900	α	0.5

The experimental and simulated values at the exit of the reactor (C_V^2) are presented in Figure 5.11. The simulation results have one fitting parameter - $k_L a$. The experimental and simulated temperature curves are presented in Figure 5.12, as well as the measured total pressure.

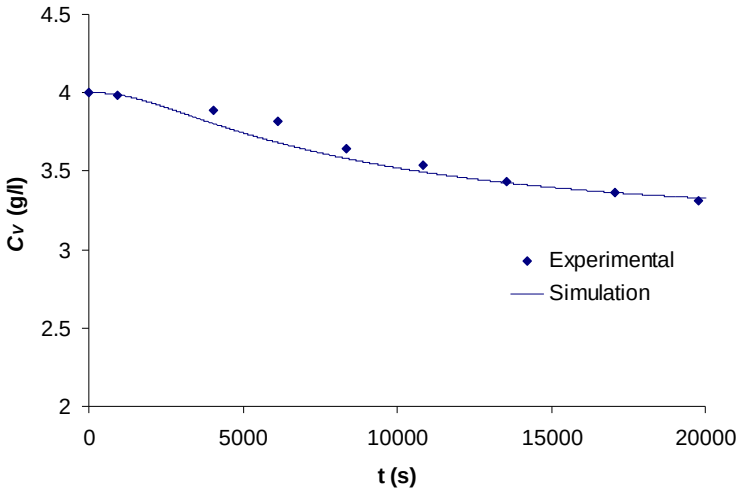

Figure 5.11. Vanillin concentration history at the exit stream of the reactor, C_V^2, for the experiment SPBCR 2. Blue points represent the measured C_V^2 on the liquid samples collected at the exit of the reactor. The solid line correspond to the simulation results using the reactor model for vanillin oxidation with a $k_L a$ of 2.2×10^{-4} s^{-1}. The experimental conditions are in Table 5.1, while the physical properties and remaining parameters used in the simulations are in Tables 5.24 and 5.25.

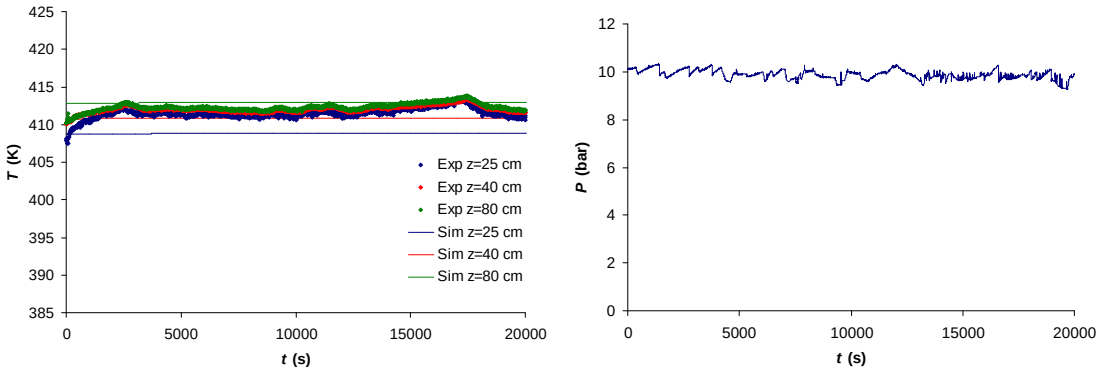

Figure 5.12. Temperature history in three different axial positions of the column, and measured operating pressure for experiment SPBCR 2. In the graph of the left side are represented the temperature measurements (points) and the correspondent simulation results (solid lines) using the model for vanillin oxidation with a $k_L a$ of 2.2×10^{-3} s^{-1}. In the right side is the total pressure measured during the experiment. The experimental conditions are in Table 5.1, while the physical properties and remaining parameters used in the simulations are in Tables 5.24 and 5.25.

According to the reaction mechanism proposed by (Fargues et al., 1996b) in a media with pH of 9.8, the reaction rate of vanillin oxidation only depends on vanillin concentration (equation 5.63). This kinetic law was developed in a batch reactor with no

or little mass transfer limitations, and consequently, with an excess of dissolved oxygen available to promote the oxidation. Since the current SPBCR and BCR configurations presents important mass transfer limitations, and the reaction rate is very fast at pH below 11.5, it was assumed that the rate of vanillin consumption was controlled by the oxygen mass transfer rate:

$$r_2 = \frac{k_L a}{\varepsilon_L} \left(C^*_{O2,L} - C_{O2,L} \right) \tag{5.125}$$

The value obtained for the fitting parameter $k_L a$ was 2.2×10^{-4} s^{-1}, considering that 1 mol of oxygen is consumed per each mol of vanillin oxidised. However, when the pH is lower than 11.5, the mechanism of reaction gets much more complex (Fargues et al., 1996b). This can probably cause an increase in the oxygen stoichiometric coefficient in the global vanillin oxidation reaction. For example, using a stoichiometric coefficient of 3 the experimental results were fitted by a $k_L a$ of 1.3×10^{-3} s^{-1}, which is much closer to the expected range for this parameter.

5.3.2.4. Lignin oxidation

Five experiments of lignin oxidation were performed in the SPBCR configuration, with different liquid and gas flow rates. The model described in section 5.2.4 was used with one fitting parameter for each experiment ($k_L a$). A value of the stoichiometric coefficient of oxygen in lignin oxidation reaction of υ_1= 1.56 was employed, which was estimated in the BCR lignin oxidation experiments.

Experiment SPBCR 3

The physical properties and parameters used to characterize the system of experiment SPBCR 3 are presented in Tables 5.26 and 5.27.

Table 5.26. Physical properties of the lignin oxidation experiment SPBCR 3.

$C_{P,L}$ (J/kg K)	3970	ρ_L (kg/m^3)	1114	M_n (g/mol)	2325
$C_{P,G}$ (J/kg K)	1004 (+)	ρ_G (kg/m^3)	8.97 (+)	μ_L (kg/m s)	1.54x10^{-3}
$C_{P,S}$ (J/kg K)	500 (**)	ρ_S (kg/m^3)	7912 (**)	μ_G (kg/m s)	2.33x10^{-5} (+)
$C_{P,F}$ (J/kg K)	1996	ρ_F (kg/m^3)	1028	σ_L (N/m)	0.061 (++)

(*) - (Kirk-Othmer Encyclopedia, 2005); (+) - (Holman, 1989); (**) - (Mills, 2002);
(++) – (Ferreira et al., 2005)

Table 5.27. Model parameters for the lignin oxidation experiment SPBCR 3.

Column section				
ε_L	$z < 0.1$ m	1	D_{ax} (m^2/s)	1.241 x 10^{-4}
	$z \geq 0.1$ m	0.920	λ_{ef} (W/m K)	1173
ε_G	$z < 0.1$ m	0	U (W/m^2 K)	72.5
	$z \geq 0.1$ m	0.0382	α	0.5
ε_S	$z < 0.1$ m	0	υ_1	1.56
	$z \geq 0.1$ m	0.0417		
Separation head				
V_{CSTR} (ml)		900	α	0.5

The liquid heat capacity, $C_{P,L}$, was considered constant and calculated for the initial lignin oxidation media using equation (3.73). The velocity of the thermo fluid, u_F, was equal to the one of experiment SBCR 2.

The experimental C_V^2 and pH are presented in Figure 5.13. The simulation results using $k_L a$ as a fitting parameter are also placed in the same figure. The simulated and measured temperatures are shown in Figure 5.14, together with the experimental data of the total pressure.

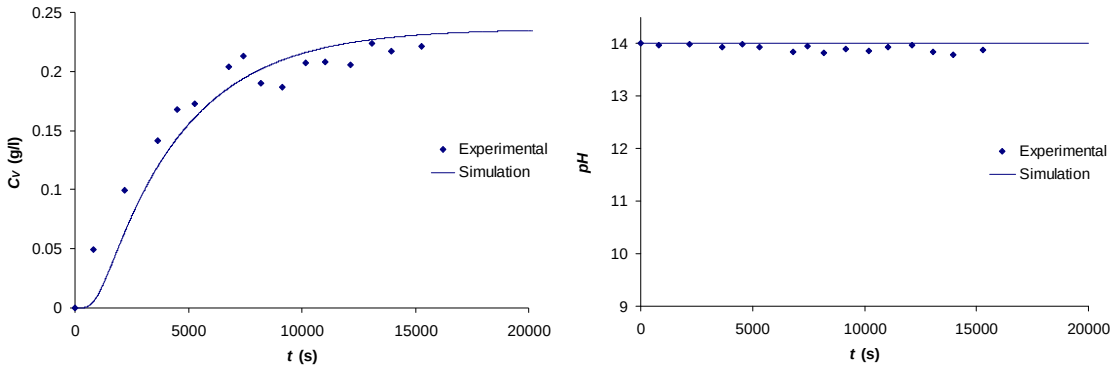

Figure 5.13. Variation of the vanillin concentration and pH, at the exit stream of the reactor, for the experiment SBCR 3. Blue points represent experimental values, and the solid lines corresponds to the simulation results using the model for lignin oxidation with a $k_L a$ of 4.5×10^{-4} s^{-1}. The experimental conditions are in Table 5.1. The physical properties and remaining parameters used in the simulations are in Tables 5.26 and 5.27.

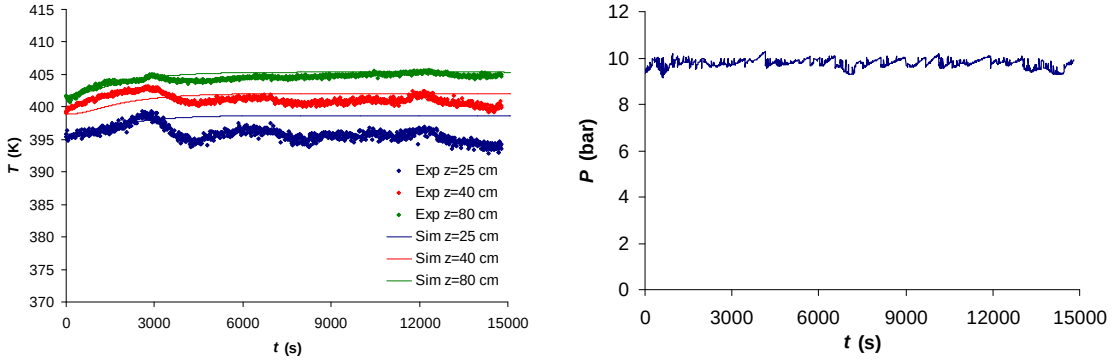

Figure 5.14. Temperature variation at three different axial positions of the column and operating pressure for experiment SPBCR 3. In the graph of the left side are presented the experimental temperatures (points) and the correspondent simulation results (solid lines) using the model for lignin oxidation with a $k_L a$ of 4.5×10^{-4} s^{-1}. In the right side is the total pressure values collected during the experiment. The experimental conditions are in Table 5.1. The physical properties and remaining parameters used in the simulations are in Tables 5.26 and 5.27.

The steady state is achieved with a vanillin concentration in the exit stream of 0.22 g/l, which represents a conversion of 0.37% of the lignin mass into vanillin. This value of lignin conversion is very low, which is also corroborated by the slight increase of the temperature during the experiment.

Experiment SPBCR 4

The physical properties and parameters used to characterize the system of experiment SPBCR 4 are presented in Tables 5.28 and 5.29.

Table 5.28. Physical properties of the lignin oxidation experiment SPBCR 4.

$C_{P,L}$ (J/kg K)	3970	ρ_L (kg/m^3)	1114	M_n (g/mol)	2325
$C_{P,G}$ (J/kg K)	1005 (+)	ρ_G (kg/m^3)	8.97 (+)	μ_L (kg/m s)	1.54×10^{-3}
$C_{P,S}$ (J/kg K)	500 (**)	ρ_S (kg/m^3)	7912 (**)	μ_G (kg/m s)	2.35×10^{-5} (+)
$C_{P,F}$ (J/kg K)	1996	ρ_F (kg/m^3)	1028	σ_L (N/m)	0.061 (++)

(*) - (Kirk-Othmer Encyclopedia, 2005); (+) - (Holman, 1989); (**) - (Mills, 2002);
(++) – (Ferreira et al., 2005)

Table 5.29. Model parameters for lignin oxidation experiment SPBCR 4.

Column section				
ε_L	$z < 0.1$ m	1	D_{ax} (m^2/s)	0.638×10^{-4}
	$z \geq 0.1$ m	0.935	λ_{ef} (W/m K)	833
ε_G	$z < 0.1$ m	0	U (W/m^2 K)	77.2
	$z \geq 0.1$ m	0.0233	α	0.5
ε_S	$z < 0.1$ m	0	υ_1	1.56
	$z \geq 0.1$ m	0.0417		
Separation head				
V_{CSTR} (ml)		900	α	0.5

The liquid heat capacity, $C_{P,L}$, was considered constant and calculated for the liquid feed composition. The velocity of the thermo fluid, u_F, was equal to the one of experiment SBCR 3.

The experimental and simulated C_V^2 and pH are presented in Figure 5.15. The respective simulations were performed by using $k_L a$ as a fitting parameter. The

simulated and experimental temperatures are shown in Figure 5.16, together with the collected data of the total pressure.

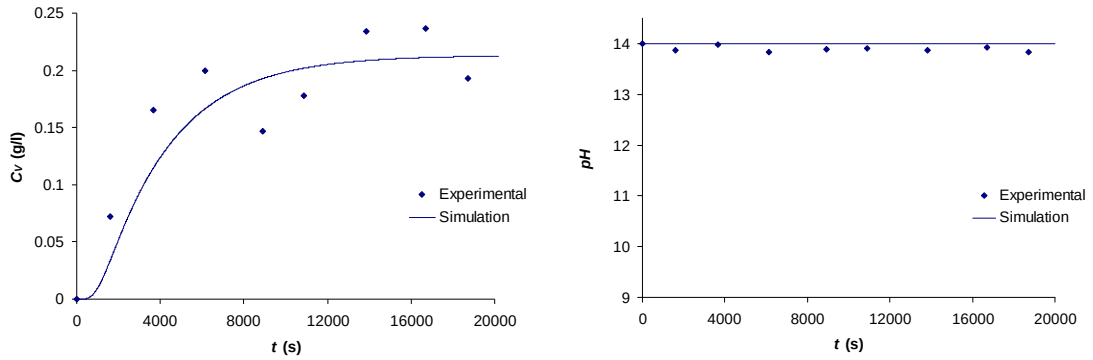

Figure 5.15. Variation of the vanillin concentration and pH, at the exit stream of the reactor, for the experiment SBCR 4. Blue points represent experimental values, and the solid lines corresponds to the simulation results using the model for lignin oxidation with a $k_L a$ of 3.8×10^{-4} s^{-1}. The experimental conditions are in Table 5.1. The physical properties and parameters used in the simulation are in Tables 5.28 and 5.29.

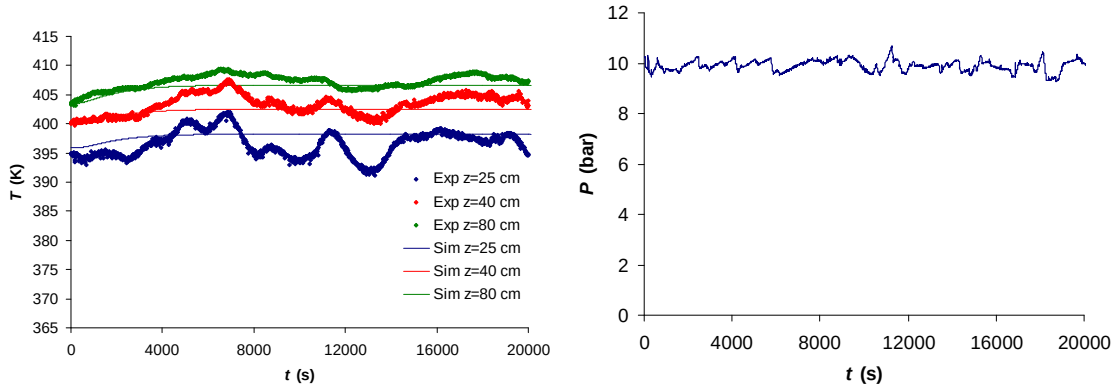

Figure 5.16. Temperature variation at three different axial positions of the column and operating pressure for experiment SPBCR 4. In the graph of the left side are presented the experimental temperatures (points) and the correspondent simulation results (solid lines) using the model for lignin oxidation with a $k_L a$ of 3.8×10^{-4} s^{-1}. In the right side are presented the pressure values collected during the experiment. The experimental conditions are in Table 5.1. The physical properties and remaining parameters used in the simulation are in Tables 5.28 and 5.29.

The average value of C_V^2 obtained at steady state was around 0.20 g/l, which represents almost the same lignin conversion than the one obtained in experiment SPBCR 3. Besides some variations due to fluctuations in the liquid flow rate, the temperature curves also show a low global increase, due to the small levels of

conversion achieved and consequent low quantities of heat liberated by the oxidation. Since the range of the gas flow rate used in the two previous experiments seemed to be completely insufficient, the following experiment was performed with the higher gas flow rate allowed by the equipment for an oxygen partial pressure of 5 bar.

Experiment SPBCR 5

The physical properties and parameters used to characterize the system of experiment SPBCR 5 are presented in Tables 5.30 and 5.31.

Table 5.30. Physical properties of the lignin oxidation experiment SPBCR 5.

$C_{P,L}$ (J/kg K)	3970	ρ_L (kg/m^3)	1114	M_n (g/mol)	2325
$C_{P,G}$ (J/kg K)	994 (+)	ρ_G (kg/m^3)	9.09 (+)	μ_L (kg/m s)	1.54×10^{-3}
$C_{P,S}$ (J/kg K)	500 (**)	ρ_S (kg/m^3)	7912 (**)	μ_G (kg/m s)	2.39×10^{-5} (+)
$C_{P,F}$ (J/kg K)	1996	ρ_F (kg/m^3)	1028	σ_L (N/m)	0.061 (++)

(*) - (Kirk-Othmer Encyclopedia, 2005); (+) - (Holman, 1989); (**) - (Mills, 2002);
(++) – (Ferreira et al., 2005)

Table 5.31. Model parameters for lignin oxidation experiment SPBCR 5.

Column section				
ε_L	$z < 0.1$ m	1	D_{ax} (m^2/s)	2.630×10^{-4}
	$z \geq 0.1$ m	0.888	λ_{ef} (W/m K)	1705
ε_G	$z < 0.1$ m	0	U (W/m^2 K)	97.3
	$z \geq 0.1$ m	0.0704	α	0.5
ε_S	$z < 0.1$ m	0	υ_1	1.56
	$z \geq 0.1$ m	0.0417		
Separation head				
V_{CSTR} (ml)		900	α	0.5

The liquid heat capacity, $C_{P,L}$, was considered constant and calculated for the liquid feed composition. The velocity of the thermo fluid, u_F, was equal to the one of

experiment SBCR 3. The experimental C_V^2 and pH are presented in Figure 5.17. The simulation results using $k_L a$ as a fitting parameter are also placed in the same figure. The simulated and measured temperatures are shown in Figure 5.18, together with the experimental data of the total pressure.

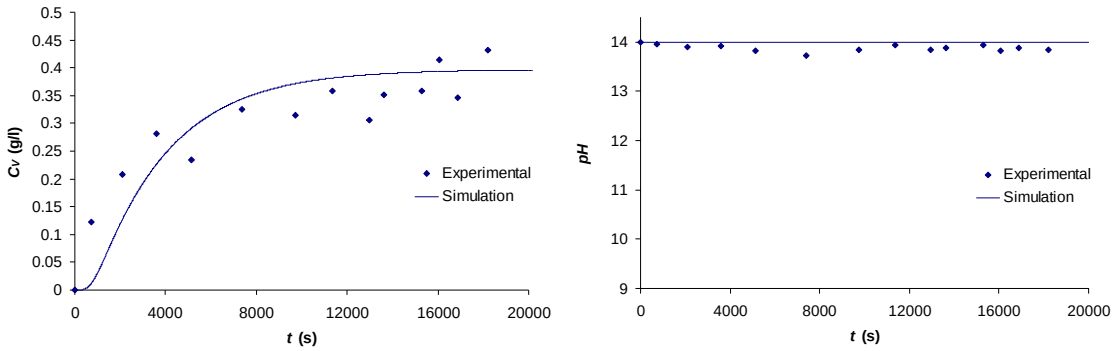

Figure 5.17. Variation of the vanillin concentration and pH, at the exit stream of the reactor, for the experiment SBCR 5. Blue points represent experimental values, and the solid lines corresponds to the simulation results using the model for lignin oxidation with a $k_L a$ of 7.35×10^{-4} s^{-1}. The experimental conditions are in Table 5.1. The physical properties and parameters used in the simulation are in Tables 5.30 and 5.31.

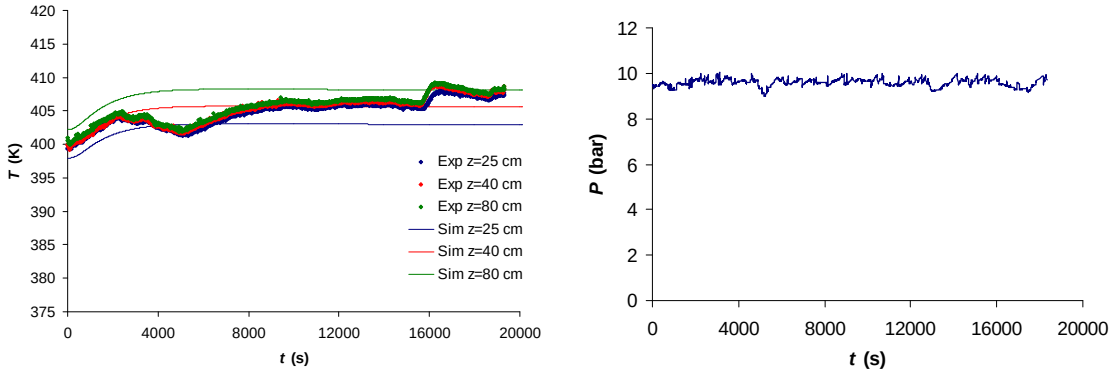

Figure 5.18. Temperature variation at three different axial positions of the column and operating pressure for experiment SPBCR 5. In the graph of the left side are presented the experimental temperatures (points) and the correspondent simulation results (solid lines) using the model for lignin oxidation with a $k_L a$ of 7.35×10^{-4} s^{-1}. In the right side are presented the pressure values collected during the experiment. The experimental conditions are in Table 5.1. The physical properties and remaining parameters used in the simulations are in Tables 5.30 and 5.31.

From Figure 5.15, it can be seen that the steady state vanillin concentration reaches a value of 0.43 g/l (0.72% lignin mass conversion into vanillin). The

temperature curves show a higher increase than in the two previous experiments (more heat of reaction liberated), and are closer to each other due to the higher dispersion in the reactor promoted by the increase in the gas flow rate.

Since the yield obtained is still far from the values obtained in the batch reactor, the next step was to increase the liquid residence time, by lowering the liquid flow rate, and maintaining the gas flow rates of the experiment SPBCR 5.

Experiment SPBCR 6

The physical properties and parameters used to characterize the system of experiment SPBCR 6 are presented in Tables 5.32 and 5.33. The velocity of the thermo fluid, u_F, was equal to the one used in experiment SBCR 2.

The experimental C_V^2 and pH are presented in Figure 5.19. The simulation results using $k_L a$ as a fitting parameter are also placed in the same figure. The simulated and measured temperatures are shown in Figure 5.20, together with the experimental data of the total pressure.

Table 5.32. Physical properties of the lignin oxidation experiment SPBCR 6.

$C_{P,L}$ (J/kg K)	3978	ρ_L (kg/m^3)	1114	M_n (g/mol)	2325
$C_{P,G}$ (J/kg K)	996 (+)	ρ_G (kg/m^3)	8.90 (+)	μ_L (kg/m s)	1.54x10^{-3}
$C_{P,S}$ (J/kg K)	500 (**)	ρ_S (kg/m^3)	7912 (**)	μ_G (kg/m s)	2.43x10^{-5} (+)
$C_{P,F}$ (J/kg K)	1996	ρ_F (kg/m^3)	1028	σ_L (N/m)	0.061 (++)

(*) - (Kirk-Othmer Encyclopedia, 2005); (+) - (Holman, 1989); (**) - (Mills, 2002); (++) – (Ferreira et al., 2005)

The maximum vanillin concentration obtained in this experiment was 0.73 g/l, which is a lignin mass conversion into vanillin of 1.22%. These values are three times higher comparing to the first lignin oxidation experiment (SPBCR 3), and are almost the

double of the yield achieved in the previous one (SPBCR 5), indicating a significant improvement once liquid flow rate decreases.

Table 5.33. Model parameters for lignin oxidation experiment SPBCR 6.

Column section				
ε_L	$z < 0.1$ m	1	D_{ax} (m^2/s)	2.203 x 10^{-4}
	$z \geq 0.1$ m	0.880	λ_{ef} (W/m K)	1531
ε_G	$z < 0.1$ m	0	U (W/m^2 K)	36.8
	$z \geq 0.1$ m	0.0784	α	0.5
ε_S	$z < 0.1$ m	0	υ_1	1.56
	$z \geq 0.1$ m	0.0417		
Separation head				
V_{CSTR} (ml)		900	α	0.5

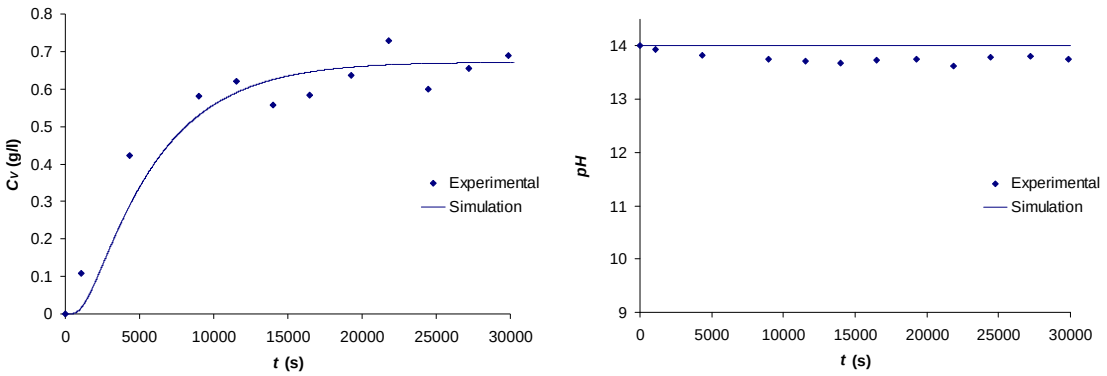

Figure 5.19. Variation of the vanillin concentration and pH, at the exit stream of the reactor, for the experiment SBCR 6. Blue points represent experimental values, and the solid lines corresponds to the simulation results using the model for lignin oxidation with a $k_L a$ of 8.05×10^{-4} s^{-1}. The experimental conditions are in Table 5.1. The physical properties and parameters used in the simulation are in Tables 5.32 and 5.33.

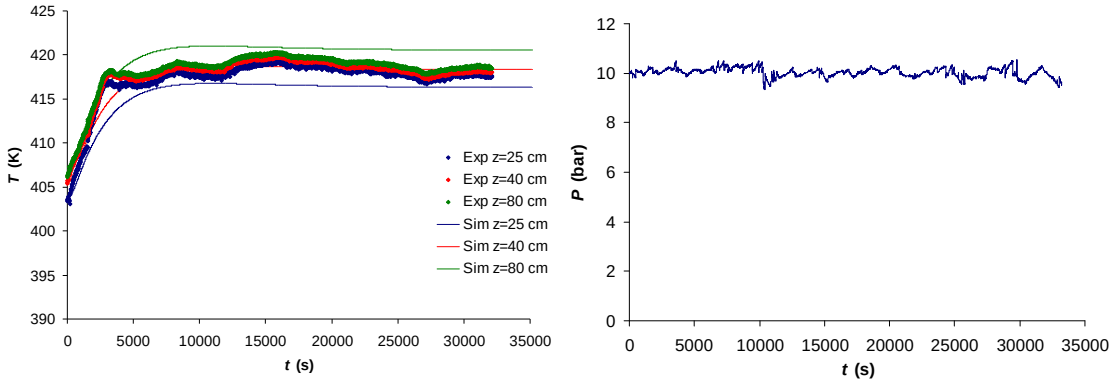

Figure 5.20. Temperature variation at three different axial positions of the column and operating pressure for experiment SPBCR 6. In the graph of the left side are presented the experimental temperatures (points) and the correspondent simulation results (solid lines) using the model for lignin oxidation with a $k_L a$ of 8.05×10^{-4} s^{-1}. In the right side are presented the pressure values collected during the experiment. The experimental conditions are in Table 5.1. The physical properties and remaining parameters used in the simulations are in Tables 5.32 and 5.33.

The temperature histories inside the reactor show a considerable increase (around 11 K) due to a higher lignin degradation and consequent heat formation. The thermal dispersion is also high, similarly to experiment SPBCR 5, as it can be observed by the proximity of the experimental temperature curves for different column heights.

Experiment SPBCR 7

The last experiment of lignin oxidation in the SPBCR unit was performed at the minimum value of liquid flow rate allowed by the safe operating range of the piston pump. The gas flow rates and partial pressures were similar to experiment SPBCR 6.

The physical properties and parameters used to characterize the system of experiment SPBCR 3 are presented in Tables 5.34 and 5.35. The liquid heat capacity, $C_{P,L}$, was assumed constant and obtained for the liquid feed composition. The velocity of the thermo fluid, u_F, was equal to 1.83 x 10^{-3} m/s.

Table 5.34. Physical properties of the lignin oxidation experiment SPBCR 7.

$C_{P,L}$ (J/kg K)	3978	ρ_L (kg/m^3)	1114	M_n (g/mol)	2325
$C_{P,G}$ (J/kg K)	996 (+)	ρ_G (kg/m^3)	8.90 (+)	μ_L (kg/m s)	1.54×10^{-3}
$C_{P,S}$ (J/kg K)	500 (**)	ρ_S (kg/m^3)	7912 (**)	μ_G (kg/m s)	2.43×10^{-5} (+)
$C_{P,F}$ (J/kg K)	1996	ρ_F (kg/m^3)	1028	σ_L (N/m)	0.061 (++)

(*) - (Kirk-Othmer Encyclopedia, 2005); (+) - (Holman, 1989); (**) - (Mills, 2002); (++) – (Ferreira et al., 2005)

Table 5.35. Model parameters for lignin oxidation experiment SPBCR 7.

Column section				
ε_L	$z < 0.1$ m	1	D_{ax} (m^2/s)	1.929×10^{-4}
	$z \geq 0.1$ m	0.873	λ_{ef} (W/m K)	1418
ε_G	$z < 0.1$ m	0	U (W/m^2 K)	24.0
	$z \geq 0.1$ m	0.0858	α	0.5
ε_S	$z < 0.1$ m	0	υ_1	1.56
	$z \geq 0.1$ m	0.0417		
Separation head				
V_{CSTR} (ml)		900	α	0.5

The experimental and simulation results of C_V^2 and pH are presented in Figure 5.21. The measured and predicted temperature profiles are shown in Figure 5.22, as well as the total reactor pressure.

The maximum lignin mass conversion obtained in this experiment was 1.48%, which corresponds to a vanillin concentration of 0.89 g/l. This result is 11.4% of the maximum obtainable vanillin concentration, considering that in complete lignin degradation, using nitrobenzene, only 13% of the lignin mass can be transformed into vanillin (which corresponds to 7.80 g/l of vanillin). There is an improvement comparing to the experiment SPBCR 6, but the liquid flow rate employed in this experiment is the smaller one that can be employed with the piston pump of the equipment.

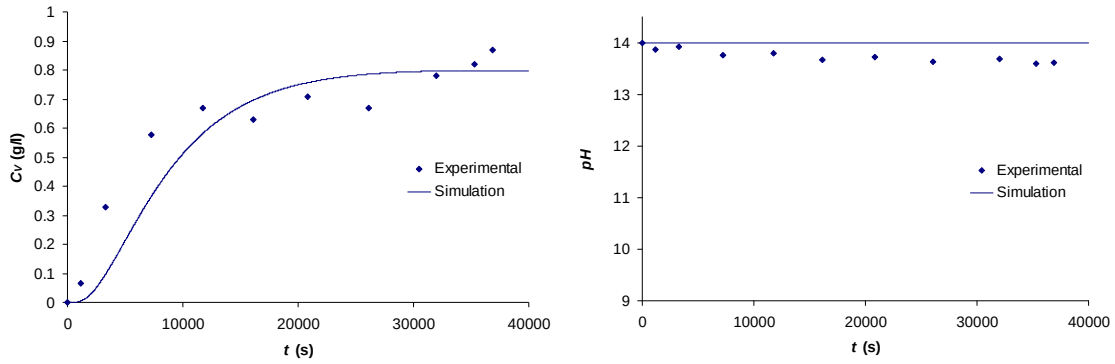

Figure 5.21. Variation of the vanillin concentration and pH, at the exit stream of the reactor, for the experiment SBCR 7. Blue points represent experimental values, and the solid lines corresponds to the simulation results using the model for lignin oxidation with a $k_L a$ of 7.06×10^{-4} s^{-1}. The experimental conditions are in Table 5.1. The physical properties and parameters used in the simulation are in Tables 5.34 and 5.35.

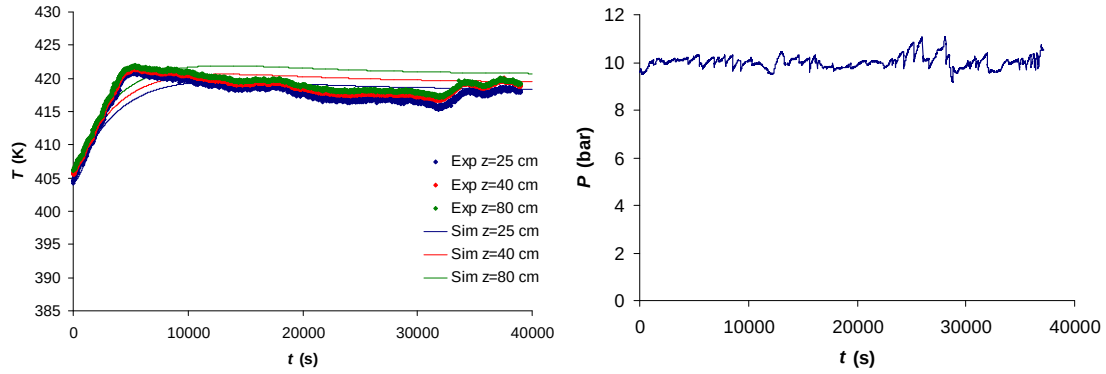

Figure 5.22. Temperature history at three different axial positions of the column and operating pressure for experiment SPBCR 7. In the graph of the left side are presented the experimental temperatures (points) and the correspondent simulation results (solid lines) using the model for lignin oxidation with a $k_L a$ of 7.06×10^{-4} s^{-1}. In the right side are presented the pressure values collected during the experiment. The experimental conditions are in Table 5.1. The physical properties and remaining parameters used in the simulations are in Tables 5.34 and 5.35.

The values of $k_L a$ obtained for the SPBCR experiments on lignin oxidation are compiled in Table 5.36.

Table 5.36. Values of $k_L a$ obtained as a fitting parameter of the experimental results.

	SPBCR 3	SPBCR 4	SPBCR 5	SPBCR 6	SPBCR 7
$k_L a$ (s^{-1})	4.50×10^{-4}	3.80×10^{-4}	7.35×10^{-4}	8.05×10^{-4}	7.06×10^{-4}

The mass transfer coefficient for the SPBCR configuration is slightly affected by the u_{LS} in the low range of liquid flow rates used in this work, as it can be concluded by comparing the values for experiments SPBCR 5, SPBCR 6 and SPBCR 7.

On the other side, the values of $k_L a$ for experiments SPBCR 3, SPBCR 4 and SPBCR 5, show that the gas flow rate has an important effect in the mass transfer coefficient. The properties of the liquid media seems to also have a decisive influence in $k_L a$. Since the predicted order of magnitude for this parameter (10^{-3}) in experiment SPBCR 1, concerning the vanillin oxidation media, is significant higher comparing the analogous experiment on lignin oxidation (SPBCR 1).

5.3.3. Discussion of results

The comparison between the SPBCR and BCR performances are made by focusing in three points: back-mixing, mass transfer coefficient ($k_L a$) and lignin conversion into vanillin. Starting by the last point, the experimental C_V^2 results for experiments SPBCR 6 and BCR 3 are presented in Figure 5.23.

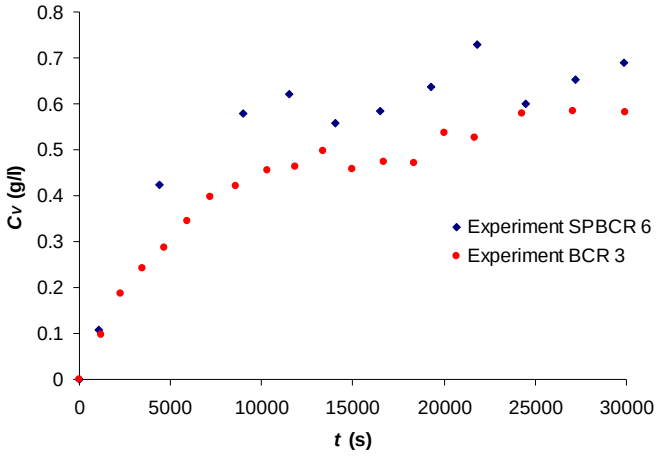

Figure 5.23. Variation of the vanillin concentration at the exit stream of the reactor, for the experiments SBCR 6 and BCR 3. Blue points represent experimental values for the experiment SPBCR 6 and the red points are referred to the experiment BCR 3.

From the predicted values of D_{ax} and λ_{ef}, presented in earlier sections, it could be concluded that the SPBCR configuration enclosed lower levels of dispersion. To better visualize this lowering effect on the back-mixing by the structured packing, the simulation axial profiles of C_V and T, in steady state, are presented in Figure 5.24.

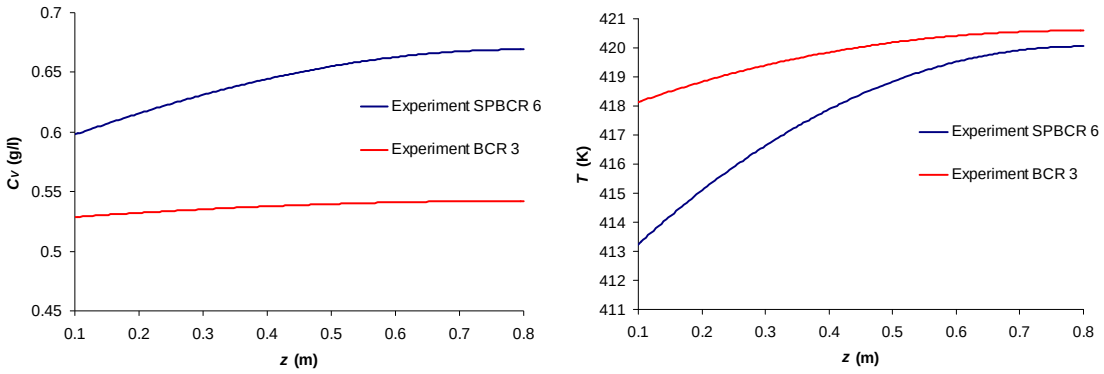

Figure 5.24. Simulated C_V and T axial profiles in steady state (reaction of time of 30000 s). Blue lines represent values for the experiment SPBCR 6 and the red lines are referred to the experiment BCR 3.

The predicted gradients of the vanillin concentration and temperature, throughout the column, are much larger for the SPBCR configuration, which reflects lower dispersion characteristics. These gradients for the SPBCR configuration, particularly with respect to C_V, still show the presence of a considerable degree of dispersion due to the low range of the operating liquid flow rate.

According to the results obtained, it is possible to observe that the conversion in all the experiments performed, was substantially smaller than the conversion obtained in the batch reactor. The main reason of this difference is the poor mass transfer of oxygen from gas phase to the liquid phase. The packings should improve mass transfer when compared to a bubble column reactor, but the mass transfer coefficient ($k_L a$) only improves mass transfer constant 1.35 times (8.05×10^{-4} using packings against 5.98×10^{-4} s^{-1} without packings).

In order to improve the reaction rate, a higher mass transfer coefficient (one order of magnitude) is desirable so that a high conversion of lignin to vanillin is obtained. In fact, the amount of oxygen transfer to the liquid should be such that the pH value is higher than 11.5. Another way to improve the mass transfer to the liquid phase is to increase the gas flow rate: increasing gas flow rate directly increases the gas hold-up and consequently the mass transfer coefficient, but as negative effects it increases the axial dispersion. In terms of unit performance, increasing the gas flow rate enhance the costs of power consumption and also reduces the liquid hold-up, decreasing productivity.

A very important operating condition that should be also considered is the temperature inside the reactor. Increasing temperature, all the reaction rates increases and also the solubility of oxygen in the liquid phase is reduced. Correct operating temperature should satisfy a trade-off situation between high vanillin conversion with small (or none) oxidation of vanillin but keeping as high as possible the solubility of oxygen in the liquid.

5.4. Improving the reactor performance

In the SPBCR experiments performed the production of vanillin was small compared to the results obtained in batch experiments. To improve the performance of the continuous reactor and approach it to the production levels obtained in the batch reactor, the influence of some operating conditions was studied. These variables were the liquid feed flow rate (Q_L), gas feed flow rate (Q_G), set point of the thermostatic bath (T_F^{set}), and the oxygen partial pressure (P_{O2}). The effect of the mass transfer parameter, $k_L a$, was also added to this study. The inclusion of the total pressure was

considered to be redundant, since it was admitted to influence only the density and superficial gas velocity which can also be expressed by changing the gas flow rate.

The simulation results of the steady state vanillin concentration in the SPBCR reactor for different operating conditions are presented in Figure 5.25. Values are presented for different Q_G, T_F^{set}, P_{O2} and k_La, in three different ranges of liquid flow rate.

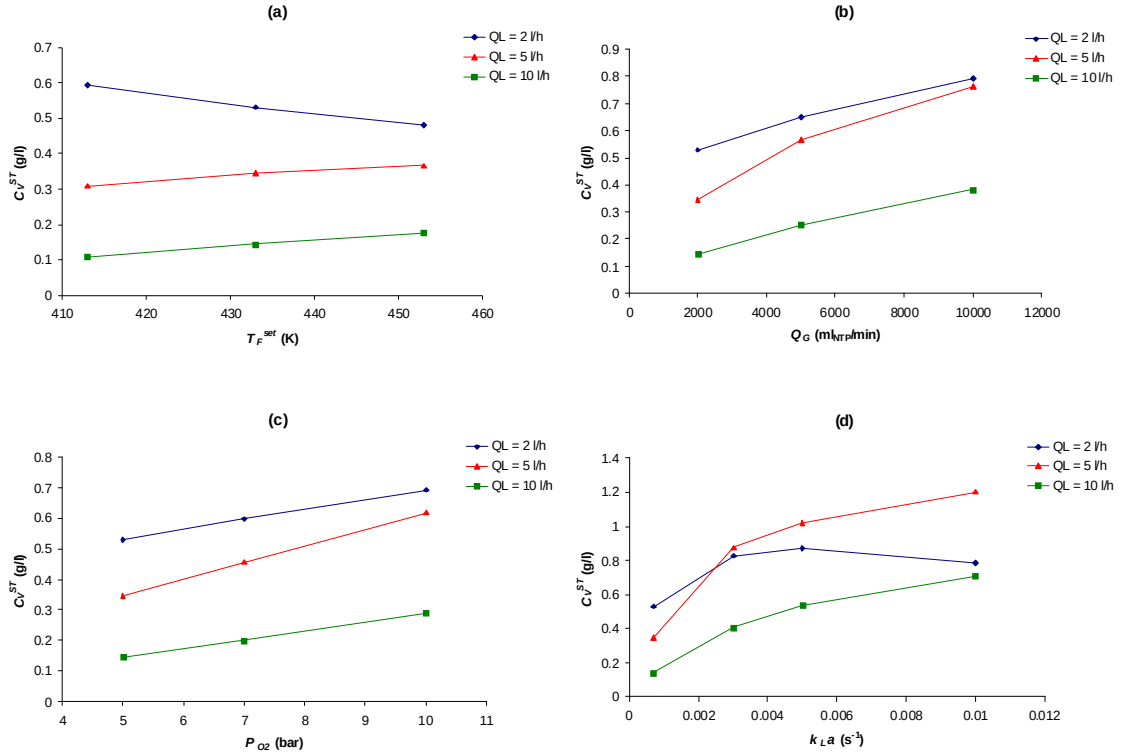

Figure 5.25. Predicted values of the steady state vanillin concentration in the exit stream (C_V^{ST}) for different T_F^{set} (a), Q_G (b), P_{O2} (c) and k_La (d). The fixed values for each case where: (a) - Q_G of 2000 ml$_{NTP}$/min, P_{O2} of 5 bar and k_La of 7.06×10^{-4} s^{-1}; (b) - T_F^{set} of 433 K, P_{O2} of 5 bar and k_La of 7.06×10^{-4} s^{-1} (Q_G of 2000 ml$_{NTP}$/min), 1.36×10^{-3} s^{-1} (Q_G of 5000 ml$_{NTP}$/min) and 2.42×10^{-3} s^{-1} (Q_G of 10000 ml$_{NTP}$/min); (c) - T_F^{set} of 433 K, Q_G of 2000 ml$_{NTP}$/min and k_La of 7.06×10^{-4} s^{-1}; (d) - T_F^{set} of 433 K; Q_G of 2000 ml$_{NTP}$/min and P_{O2} of 5 bar. The total pressure was 10 bar for all simulations.

It can be observed from Figure 5.25(a) that for the higher liquid flow rates (5 and 10 l/h), increasing the set point of the thermostatic bath (T_F^{set}) in the range of 413

to 453 K leads to an increase in the vanillin amounts obtained in the exit stream. This behaviour is opposed to the one predicted for the lower liquid flow rate (2 l/h) in the same set point range. The value of T_F^{set} has a direct influence in the reactor temperature. At higher pH values, when the temperature of the media increases, it leads to an increase of all the kinetic constants of the reactions involved in the system, but also to a decrease in the ratio between the kinetic constants for lignin and for vanillin oxidation, respectively. The most important result of increasing the temperature of the media is to increase the difference between the reaction rates ($r_1 - r_2$), enhancing the levels of lignin degradation. The case of the higher liquid flow rates fits into this kind of scenario, since the low residence time together with the low oxygen transfer rates from the gas leads to low levels of lignin consumption. When the liquid residence time is increased, the lignin degrades more and the pH starts to decrease into values where the growing tendency of the difference between the reaction rates with temperature inverts, and this can explain what it observed in Figure 5.25(a) for a liquid flow rate of 2 l/h.

An increase in the gas flow rate results in a higher gas superficial velocity. It was verified that in the experimental range of the Q_G, the k_La increased almost linearly with the gas superficial velocity. This linear dependency was extrapolated to the values of gas flow rates (up to 10000 ml_{NTP}/min) used in Figure 5.25(b). Higher steady state vanillin concentrations in the exit stream were obtained for higher gas flow rates, due to the linear increase of k_La. For the lower liquid residence times (higher liquid flow rates) the degree of vanillin formation is poorer, since the oxygen mass transfer rate is still not good enough.

It can be observed in Figure 5.25(c) that an increase in the partial pressure of oxygen (P_{O2}) results in an increase in vanillin yield. The explanation is again related to

the oxygen transfer rate to the liquid. The oxygen mass transfer rate depends not only on the $k_L a$ but also on the concentration driving force between the gas-liquid interface and the liquid bulk. The oxygen partial pressure has a major influence in the oxygen solubility in the liquid and thus in the mass transfer driving force. When the P_{O2} is increased, the oxygen solubility is higher promoting a media with a higher oxidative capacity.

Other situation tested was kept all operating conditions constant and change the values of the volumetric mass transfer coefficient ($k_L a$). The results are presented in Figure 5.25(d) and reveal an increase in the vanillin production with $k_L a$, with the exception of the results for Q_L of 2 l/h. In this case, it seems that there is a maximum level of vanillin formation with $k_L a$, and then the productivity starts to decrease (undesired vanillin oxidation). For a high liquid flow rate of 10 l/h, it was still necessary to further increase the oxygen transfer levels in order to achieve more satisfactory vanillin concentration results.

Once the influence of some important variables was determined, it is worthy to find a set of operating conditions to increase the vanillin yield. The first step was to increase the gas flow rate to obtain higher levels of oxygen mass transfer. A selected set of conditions was: Q_L of 4 l/h; T_F^{set} of 433 K for the heating + pressurization and 423 K for the reaction phase; P_{O2} of 5 bar; P of 10 bar and Q_G of 40000 ml_{NTP}/min (u_{GS} of 1.3 cm/s). The respective value of $k_L a$ for this range of gas flow rate is admitted to be 1×10^{-2} s^{-1}. The simulation results of C_V^2, pH and temperature profiles are shown in Figure 5.26.

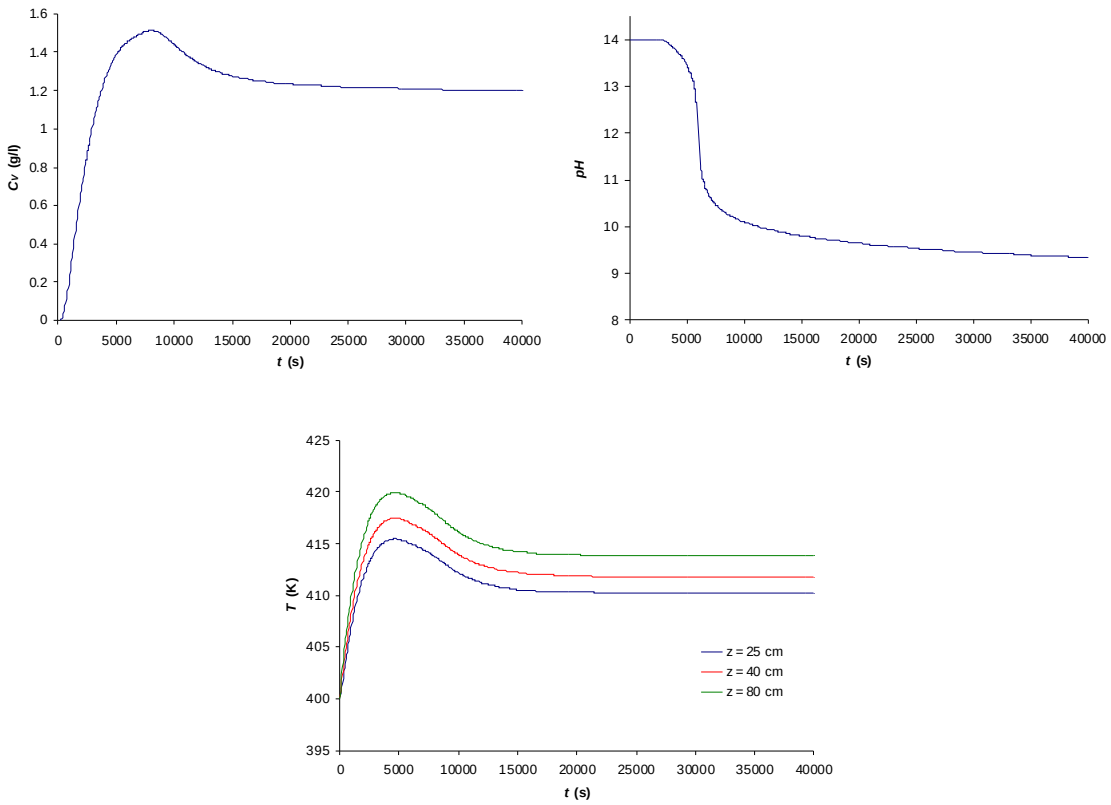

Figure 5.26. Simulation results for the vanillin concentration and pH, at the exit stream of the reactor, and temperature history at three different axial positions of the column. The conditions used were Q_L of 4 l/h; T_F^{set} of 423 K; P_{O2} of 5 bar; P of 10 bar; Q_G of 40000 ml_{NTP}/min and k_La of 1×10^{-2} s^{-1}.

The vanillin concentration (Figure 5.26) shows a maximum before achieving its steady state value. This maximum results from the change in the reaction rate equation for vanillin oxidation that occurs when the pH gets lower than 11.5. This change leads to higher values for the reaction rate of vanillin oxidation, forcing the system to a lower steady state than the one that was originally being developed before the pH reached 11.5.

The final C_V^{ST} value is around 1.2 g/l, which represents 15% of the maximum obtainable lignin conversion, considering that in complete lignin degradation conditions (using nitrobenzene) only 13% of its mass can be transformed into vanillin. This result

is approximately 55% of the maximum levels of vanillin concentration obtained in the batch reactor, which is still not satisfactory.

A new set of operating conditions was chosen: Q_L of 10 l/h; T_F^{set} of 433 K; P_{O2} of 10 bar; P of 10 bar; Q_G of 40000 ml_{NTP}/min; and k_La of 1.5×10^{-2} s^{-1}. The simulation results of C_V^2, pH and temperature profiles are shown in Figure 5.27. The axial concentration profiles of vanillin for different reaction times were also added to Figure 5.27.

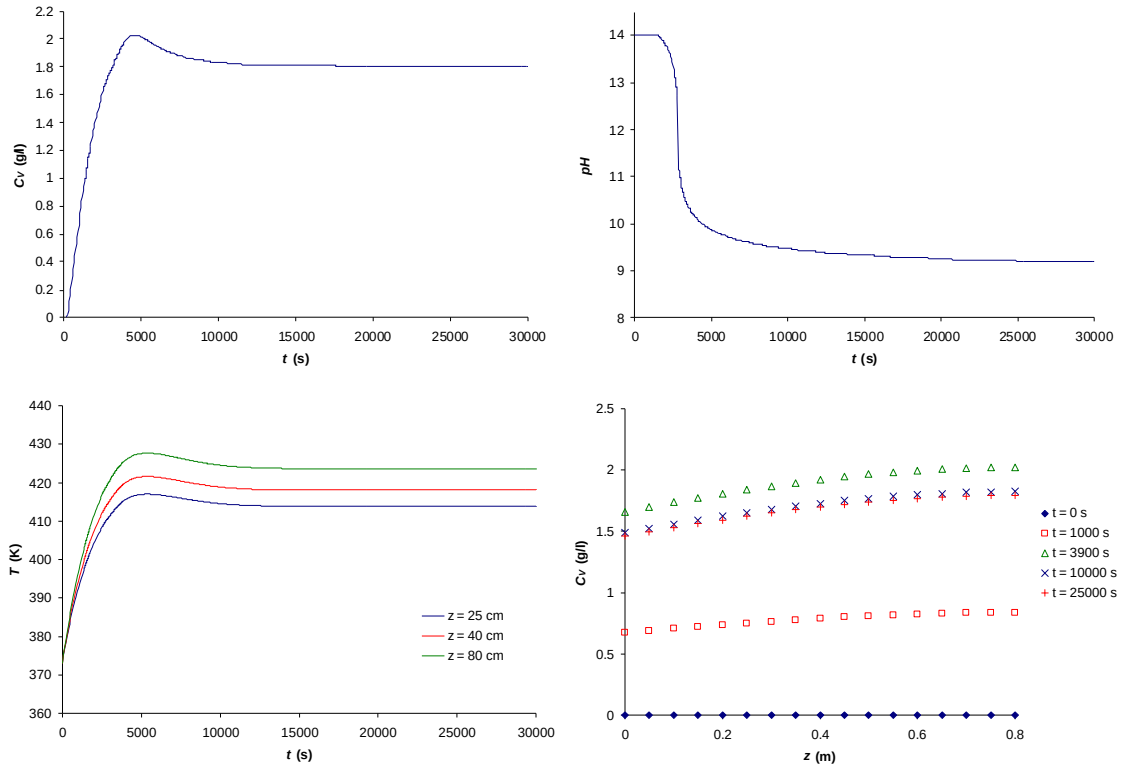

Figure 5.27. Simulation results for the vanillin concentration and pH, at the exit stream of the reactor, and temperature history at three different axial positions of the column. In the bottom right of the figure are represented the axial concentration profiles of vanillin for different reaction times. The conditions used were Q_L of 10 l/h; T_F^{set} of 423 K; P_{O2} of 10 bar; P of 10 bar; Q_G of 40000 ml_{NTP}/min and k_La of 1.5×10^{-2} s^{-1}.

This new set of operating conditions were used to improve the yield of the system by testing the limit situation of pure oxygen in the gas feed, maintaining the gas

flow rate and increasing the liquid flow rate. The idea was to increase the oxygen mass transfer rates taking into account that the liquid residence time should be decreased to avoid excessive vanillin oxidation. The steady state value of the vanillin concentration in the exit stream is around 1.8 g/l (3% of mass lignin conversion into vanillin), which is 23% of the maximum level of vanillin that can be achieved. This result is approximately 85% of the maximum levels of vanillin concentration obtained in the batch reactor.

5.5. Conclusions

A continuous bubble column reactor was tested for both vanillin and lignin oxidation. A limited number of experiments were performed since each experiment took one day to be performed and around ten days to analyze the vanillin concentration of all samples taken. The effect of structured packings (Mellapak 750Y) in the bubble column was also tested. The structured packings should increase the mass transfer of the oxygen from gas phase to the liquid phase.

A mathematical model to describe the reaction media in the bubble column reactor (with and without structured packings) was proposed and tested using the available experimental data. The model includes: mass balances for lignin, vanillin and dissolved oxygen in the reaction media, energy balances for the reactor and the thermo fluid inside the jacket and different reaction rate expressions for vanillin according to three pH ranges.

According to the properties of the reactor and gas and liquid velocities employed, a significant effect of axial dispersion was observed indicating that the

bubble column reactor operates closely to a continuous stirred tank reactor (Peclet number based on column length smaller than 1).

From all the lignin oxidation experiments performed, the oxygen mass transfer was the limiting step to vanillin formation. The structured packings inside the reactor only resulted in an improvement of 1.35 times the mass transfer coefficient, but an improvement of one order of magnitude may be necessary to achieve high lignin conversion to vanillin.

5.6. Nomenclature

a	gas-liquid interfacial area, m^{-1} (interfacial area per unit of reactor volume)
a_{DF}	constant of the drift flux equation
a_P	specific surface area of the packing, m^{-1}
A	velocity reaction constant for vanillin oxidation, $m^3\ mol^{-1}\ s^{-1}$
A_R	internal cross section area of the column, m^2
A_W	difference between the external and the internal cross section area of the column, m^2
b_{DF}	constant of the drift flux equation
B	velocity reaction constant for vanillin oxidation, m^3/mol
Bo_L	Bodenstein number ($u_{LS} D_P / \varepsilon_L D_{ax}$)
Bo_L^*	modified Bodenstein number ($u_{GS} D_C / D_{ax}$)
C_i^1	concentration of species i in the stirred tank 1 of the separation head, mol/m^3

C_i^2 concentration of species i in the stirred tank 2 of the separation head, mol/m^3

$C_{i,L}$ concentration of species i in the liquid phase, mol/m^3 (based on liquid volume)

$C_{i,L}^*$ concentration of compound i in the liquid side at the gas-liquid interface, mol/m^3 (based on liquid volume)

$C_{i,G}$ concentration of compound i in the gas phase, mol/m^3 (based on gas volume)

$Const$ parameter of the relation between lignin oxidized and acid products formed

$C_{P,F}$ heat capacity of the thermo fluid, J kg^{-1} K^{-1}

$C_{P,G}$ heat capacity of the gas phase, J kg^{-1} K^{-1}

$C_{P,L}$ heat capacity of the liquid phase, J kg^{-1} K^{-1}

$C_{P,S}$ heat capacity of the structured packing, J kg^{-1} K^{-1}

$C_{P,W}$ heat capacity of the reactor wall, J kg^{-1} K^{-1}

C_V^{ST} steady state vanillin concentration in the liquid exit stream, mol/m^3

D_{ax} axial dispersion coefficient, m^2/s

D_B gas bubble diameter, m

D_C internal diameter of the reactor, m

D_O diameter of the holes in the distributor, m

D_P characteristic dimension of the packing, m

D_S Sauter diameter, m

E energy flow rate, J/s

f	friction factor
$f(pH)$	function of C_{H+}
$F_{i,L}$	molar flow rate of species i in the liquid phase, mol/s
$F_{i,G}$	molar flow rate of compound i in the gas phase, mol/s
F_G	total molar flow rate of the gas phase, mol/s
Fr	Froude number (u_{GS}^2 / gD_C)
g	gravitational constant, m s^{-2}
G_M	gas mass flux, kg m^{-2} s^{-1}
G_M^T	gas mass flux of transition from bubble flow to pulse flow, kg m^{-2} s^{-1}
H_P	height of the column packed section, m
I	ionic strength of the liquid medium, mol/l
J_{DF}	drift flux equation
k_L	liquid side mass transfer coefficient, m/s (based on liquid film length)
k_S	thermal conductivity of the structured packing, W m^{-1} K^{-1}
k_W	thermal conductivity of the reactor wall, W m^{-1} K^{-1}
k_1	velocity reaction constant for vanillin formation, $(m^3/mol)^{1.75}$ s^{-1}
k_2	velocity reaction constant for vanillin oxidation, m^3 mol^{-1} s^{-1}
K_a	acid dissociation product of all the acid species formed during lignin oxidation
K_w	water ionic product
L	lignin
L_{ef}	effective channel length of the packed bed, m
L_M	liquid mass flux, kg m^{-2} s^{-1}

M_n	lignin mean molecular weight, g/mol
P	total pressure, bar
P_i	partial pressure of species i, bar
Q_G	gas flow rate, l/h
$Q_{i,G}$	volumetric gas flow rate of compound i, l/h
Q_L	liquid flow rate, l/h
Q_{N2}	nitrogen flow rate, ml_{NTP}/min
Q_{O2}	oxygen flow rate, ml_{NTP}/min
r_1	rate of formation of vanillin, mol m^{-3} s^{-1} or mol m^{-3} min^{-1}
r_2	rate of oxidation of vanillin, mol m^{-3} s^{-1} or mol m^{-3} min^{-1}
r_k	rate of a generic reaction k, mol m^{-3} s^{-1} or mol m^{-3} min^{-1}
R	universal gas constant, m^3 bar mol^{-1} K^{-1}
R_1	radius of the internal wall of the reactor column, m
R_2	radius of the external wall of the reactor column, m
R_3	radius of the internal wall of the outer jacket tube, m
R_4	radius of the external wall of the outer jacket tube, m
Re_G	gas Reynolds number
Re_L	liquid Reynolds number
Re_O	gas Reynolds number for the conditions in the distributor holes
t	time, s
T	reactor temperature, K
T_F	thermo fluid temperature inside the jacket, K
T_F^{set}	set point of the thermostatic bath, K

T_{IT} temperature of outer jacket tube, K

T_{SH} temperature of the separation head, K

u_F thermo fluid velocity inside the jacket, m/s

u_{GO} gas velocity through each distributor hole, m/s

u_{GS} superficial gas velocity, m/s

u_{LS} superficial liquid velocity, m/s

u_t stationary rise velocity of the bubble, m/s

U overall heat transfer coefficient from the thermo fluid in the jacket to the liquid inside the reactor, W m^{-2} K^{-1}

V_{CSTR} volume of each stirred tank considered in the flow model of the separation head, m^3

X variable that encloses all possible acid products from lignin oxidation, eq/l

X^1 acid products in the stirred tank 1 of the separation head, eq/l

X^2 acid products in the stirred tank 2 of the separation head, eq/l, eq/l

Y sorption number from Zlokarnik equation

z axial position, m

Greek letters

α lignin stoichiometric coefficient on the lignin oxidation reaction

ΔP_{frict} total frictional pressure drop on the packed section of the column, bar

$\Delta H_{R,1}$ heat of reaction of lignin oxidation, J/mol

$\Delta H_{R,2}$ heat of reaction of vanillin oxidation, J/mol

$\Delta H_{R,k}$ heat of a generic reaction k, J/mol

ε	void fraction of the packing (based on the total column volume)
ε_G	gas hold-up (based on the total column volume)
ε_L	liquid hold-up (based on the total column volume)
λ_{ef}	effective thermal dispersion coefficient, W m^{-1} K^{-1}
λ_L	contribution of the mass dispersion to the effective thermal dispersion coefficient, W m^{-1} K^{-1}
λ_S	effective axial thermal conductivity of the packed bed at zero flow, W m^{-1} K^{-1}
υ_1	oxygen stoichiometric coefficient on the lignin oxidation reaction
υ_2	oxygen stoichiometric coefficient on the vanillin oxidation reaction
$\nu_{i,k}$	stoichiometric coefficient of compound *i* in the reaction *k*
μ_L	liquid viscosity, kg m^{-1} s^{-1}
ρ_F	thermo fluid density, kg/m^3
ρ_G	gas density, kg/m^3
ρ_L	liquid density, kg/m^3
ρ_S	structured packing density, kg/m^3
ρ_W	reactor wall density, kg/m^3
θ	inclination angle of the packing channels with the horizontal axis
σ_L	surface tension, N m^{-1}

Subscripts

H2O	water
L	lignin or liquid

$O2$	oxygen
V	vanillin

Superscripts

in	value in the respective feed stream

5.7. References

1. Achwal, S. K.; Stepanek, J. B. Holdup profiles in packed beds. *Chem. Eng. J.*, **1976**, 12, 69-75.
2. Anabtawi, M. Z. A.; Abu-Eishah, S. I.; Hilal, N.; Nabhan, M. B. W. Hydrodynamic studies in both bi-dimensional and three-dimensional bubble columns with a single sparger. *Chem. Eng. Process.*, **2003**, 42, 403-408.
3. Akita, K.; Yoshida, F. Gas holdup and volumetric mass transfer coefficient in bubble columns. *Ind. Eng. Chem. Process Des. Dev.*, **1973,** 12, 76-80.
4. Belfares, L.; Cassanello, M.; Grandjean, B. P. A.; Larachi, F. Liquid back-mixing in packed-bubble column reactors: a state-of-the-art correlation. *Catal. Today*, **2001**, 64, 321-332.
5. Bensetiti, Z.; Larachi, F.; Grandjean, B. P. A.; Wild, G. Liquid saturation in cocurrent upflow fixed-bed reactors: a state-of-the-art correlation. *Chem. Eng. Sci.*, **1997**, 52, 4239-4247.
6. Billet, R.; Schultes, M. Advantage in correlating packed column performance. *Inst. Chem. Eng. Symp. Ser. 128*, **1992,** B129–B136.

7. Cassanello, M.; Martínez, O.; Cukierman, A. L. Liquid hold-up and backmixing in cocurrent upflow three-phase fixed-bed reactors. *Chem. Eng. Sci.*, **1998**, 53(5), 1015-1025.
8. Deckwer, W.-D., *Bubble column reactors.* John Wiley & Sons, England, **1992**.
9. Dudukovic, M. P.; Larachi, F.; Mills, P. L. Multiphase catalytic reactors: a perspective on current knowledge and future trends. *Catal. Reviews*, **2002**, 44(1), 123-146.
10. Fair, J. R.; Seibert, A. F.; Behrens, M.; Saraber, P. P.; Olujić, Ž. Structured packing performance – experimental evaluation of two predictive models. *Ind. Eng. Chem. Res.*, **2000**, 39, 1788-1796.
11. Fargues, C.; Mathias, A.; Rodrigues, A. Kinetics of vanillin production from Kraft lignin oxidation. *Ind. Eng. Chem. Res.*, **1996a**, 35, 28-36.
12. Fargues, C.; Mathias, A.; Silva, J.; Rodrigues, A. Kinetics of vanillin oxidation. *Chem. Eng. Technol.*, **1996b**, 19 (2), 127-136.
13. Ferreira, A. G. M.; Ribeiro, I. S. A.; Lobo, L. Q. The surface tension of Kraft black liquor from Eucalyptus. *Silva Lusitana*, **2005**, 13(1), 105-111.
14. Gualito, J. J.; Cerino, F. J.; Cardenas, J. C.; Rocha, J. A. Design method for distillation columns filled with metallic, ceramic, or plastic structured packings. *Ind. Eng. Chem. Res.*, **1997**, 36, 1747-1757.
15. Gianetto, A.; Silveston, P. L., *Multiphase chemical reactors.* Hemispher Publishing Corporation, USA, **1986**.
16. Heilmann, W. V.; Hofmann, H. Proceedings of the Fourth European Symposium Chemical Reactor Engineering, Brussels, Belgium, **1969**, 169.

17. Henriques de Brito, M.; Von Stockar, U.; Bomio, P. Predicting the liquid phase mass transfer coefficient - k_L - for the Sulzer structured packing Mellapak. *Inst. Chem. Eng. Symp. Ser. 128*, **1992,** B137–B144.
18. Henriques de Brito, M.; Von Stockar, U.; Bangerter, A. M.; Bomio, P.; Laso, M. Effective mass-transfer area in a pilot plant column equipped with structured packings and with ceramic rings. *Ind. Eng. Chem. Res.*, **1994,** 33, 647-656.
19. Hikita, H.; Asai, S.; Tanigawa, K.; Segawa, K.; Kitao, M. The volumetric liquid-phase mass transfer coefficient in bubble columns. *Chem. Eng. J.*, **1981**, 22, 61-69.
20. Holman, J. P. *Heat transfer* (SI Metric Edition), McGraw Hill, Singapore, **1989**.
21. Iliuta, I.; Thyrion, F. C. Flow regimes, liquid holdups and two-phase pressure drop for two-phase concurrent downflow and upflow through packed beds: air/Newtonian and non-Newtonian liquid systems. *Chem. Eng. Sci.*, **1997**, 52, 4045-4053.
22. Jordan, U.; Terasaka, K.; Kundu, G.; Schumpe, A. Mass transfer in high-pressure bubble columns with organic liquids. *Chem. Eng. Technol.*, **2002**, 25, 262-265.
23. Kelkar, B. G.; Phulgaonkar, S. R.; Shah, Y. T. The effect of electrolyte solutions on hydrodynamics and back mixing characteristics in bubble columns. *Chem. Eng. J.*, **1983**, 27, 125-133.
24. Khan, A.; Khan, A. A.; Varma, Y. B. G. Flow regime identification and pressure drop in cocurrent gas-liquid upflow through packed beds. *Bioprocess Engineering*, **1997**, 16, 355-360.
25. Khan, A.; Khan, A. A.; Varma, Y. B. G. Prediction of two-phase frictional pressure drop for the concurrent gas and Newtonian liquids upflow through packed beds. *Chem. Eng. Technol.*, **2002**, 25, 51-55.

26. *Kirk-Othmer Encyclopedia of Chemical Technology*; 5th Edition, John Wiley & Sons, **2005**.

27. Kojima, H.; Sawai, J.; Suzuki, H. Effect of pressure on volumetric mass transfer coefficient and gas holdup in bubble column. *Chem. Eng. Sci.*, **1997**, 52, 4111-4116.

28. Kolev, N. *Packed bed columns: for absorption, desorption, rectification and direct heat transfer*. Elsevier, The Netherlands, **2006**.

29. Kumar, A.; Degaleesan, T. E.; Laddha, G. S.; Hoelscher, H. E. Bubble swarm characteristics in bubble columns. *Can. J. Chem. Eng.*, **1976**, 54(6), 503-508.

30. Larachi, F.; Laurent, A.; Wild, G.; Midoux, N. Some experimental liquid saturation results in fixed bed reactors operated under elevated pressure in concurrent upflow and downflow of the gas and the liquid. *Ind. Eng. Chem. Res.*, **1991**, 30, 2404-2410.

31. Larachi, F.; Wild, G.; Laurent, A.; Midoux, N. Influence of gas density on the hydrodynamics of cocurrent gas-liquid upflow fixed bed reactors. *Ind. Eng. Chem. Res.*, **1994**, 33, 519-525.

32. Laso, M.; Henriques de Brito, M.; Bomio, P.; Von Stockar, U. Liquid-side mass transfer characteristics of a structured packing. *Chem. Eng. J.*, **1995,** 58, 251-258.

33. Lau, R.; Peng, W.; Velazquez-Vargas, L. G.; Yang, G. Q.; Fan, L.-S. Gas-liquid mass transfer in high-pressure bubble columns. *Ind. Eng. Chem. Res.*, **2004**, 43, 1302-1311.

34. Letzel, H. M.; Schouten, J. C.; Krishna, R.; van den Bleek, C. M. Gas holdup and mass transfer in bubble column reactors operated at elevated pressure. *Chem. Eng. Sci.*, **1999**, 2237-2246.

35. Macías-Salinas, R.; Fair, J. R. Axial mixing in modern packings, gas and liquid phases: I. Single-phase flow. *AIChE J.*, **1999**, 45(2), 222-239.
36. Macías-Salinas, R.; Fair, J. R. Axial mixing in modern packings, gas and liquid phases: II. Two-phase flow. *AIChE J.*, **2000**, 46(1), 79-91.
37. Mathias, A. L. *Produção de vanilina a partir da lenhina: estudo cinético e do processo.* Ph.D. Dissertation, University of Porto, Portugal, **1993**.
38. Mendelson, H. D. The prediction of bubble terminal velocities from wave theory. *AIChE J.*, **1967**, 13(2), 250-253.
39. Mills, K. C. *Recommended values of thermophysical properties for selected commercial alloys*, Woodhead Publishing, United Kingdom, **2002**.
40. Olujić, Ž.; Kamerbeek, A. B.; de Graauw, J. A corrugation geometry based model for efficiency of structured distillation packing. *Chem. Eng. Process.*, **1999**, 38, 683-695.
41. Olujić, Ž.; Behrens, M. Holdup and pressure drop of packed beds containing a modular catalytic structured packing. *Chem. Eng. Technol.*, **2006**, 29(8), 979-985.
42. Reilly, I. G.; Scott, D. S.; De Brujin, T. J. W.; Piskorz, J. A correlation for gas hold-up in turbulent coalescing bubble columns. *Can. J. Chem. Eng.*, **1986**, 64, 705-716.
43. Saroha, A. K.; Khera, R. Hydrodynamic study of fixed beds with cocurrent upflow and downflow. *Chem. Eng. Process.*, **2006**, 45, 455-460.
44. Shimizu, K.; Takada, S.; Minekawa, K.; Kawase, Y. Phenomenological model for bubble column reactors: prediction of gas hold-ups and volumetric mass transfer coefficients. *Chem. Eng. J.*, **2000**, 78, 21-28.
45. Stiegel, G. J.; Shah, Y. T. Backmixing and liquid holdup in a gas-liquid concurrent upflow packed column. *Ind. Eng. Chem. Process Des. Dev.*, **1977**, 16(1), 37-43.

46. Turpin, J. L.; Huntington, R. L. Prediction of pressure drop for two-phase, two component concurrent flow in packed beds. *AIChE J.*, **1967**, 13(6), 1196-1202.

47. *Ullmann´s Encyclopedia of Industrial Chemistry*; 7th Edition, Wiley-VCH, Verlag GmbH & Co..KGaA, **2003**.

48. Urseanu, M. I., Ellenberger, J.; Krishna, R. A structured catalytic bubble column reactor: hydrodynamic and mixing studies. *Cat. Today*, **2001**, 69, 105-113.

49. Urseanu, M. I.; Guit, R. P. M.; Stankiewicz, A. G.; van Lommen, K. J. H. G. M. Influence of operating pressure on the gas hold-up in bubble columns for high viscous media. *Chem. Eng. Sci.*, **2003**, 60, 1465-1475.

50. van Gelder, K. B.; Westerterp, K. R. Residence time distribution and hold-up in a cocurrent upflow packed bed reactor at elevated pressure. *Chem. Eng. Technol.*, **1990**, 13, 27-40.

51. Wang, G. Q.; Yuan, X. G.; Yu, K. T. A method for calculating effective interfacial area of structured packed distillation columns under elevated pressures. *Chem. Eng. Process.*, **2006**, 45, 691-697.

52. Weber, H. H. *Untersuchungen über die Verweilzeitverteilung in Aufstromkolonnen.* Ph.D. Dissertation, Technischen Hochschule, Damstadt, Germany, **1961**.

53. Wilkinson, P. M.; Haringa, H.; Van Dierendonck, L. L. Mass transfer and bubble size in a bubble column under pressure. *Chem. Eng. Sci.*, **1994**, 49(9), 1417-1427.

54. Woerlee, G. F.; Berends, J.; Olujić, Ž.; de Graauw, J. A comprehensive model for the pressure drop in vertical pipes and packed columns. *Chem. Eng. J.*, **2001**, 84, 367-379.

55. Yang, X.-L.; Euzen, J.-P. Residence time distribution of the liquid in gas-liquid cocurrent upflow fixed-bed reactors with porous particles. *Chem. Eng. Sci.*, **1990**, 45(11), 3311-3317.

56. Yang, X. L.; Wild, G.; Euzen, J. P. Study of liquid retention in fixed bed reactors with concurrent upflow and downflow of gas and liquid. *Int. Chem Eng.*, **1993**, 33(1), 72-84.

57. Zahradnik, J.; Fialova, M.; Kastanek, F.; Green, K. D.; Thomas, N. H. The effect of electrolyte on bubble columns coalescence and gas holdup in bubble column reactors. *Trans. Inst. Chem. Eng.*, **1995**, 73(A), 341-346.

58. Zlokarnik, M. Sorption characteristics of slot injectors and their dependency on the coalescence behaviour of the system. *Chem. Eng. Sci.*, **1979**, 34(10), 1265-1271.

6. Conclusions and suggestions for future work

6.1. Conclusions

In this thesis, the production of vanillin from Kraft lignin oxidation with oxygen was studied in a continuous reactor. Vanillin is a high-added value product with a large spectrum of applications, which makes very attractive the idea of developing a continuous process, integrated as complement into a pulp and paper production plant, to obtain this aromatic compound from lignin-based by-products. It is known that this goal was already achieved by some companies, where nowadays the major example is the Norwegian Borregaard, but the details of these processes are still unavailable to the public knowledge of the scientific community. In fact, the amount of information about vanillin production based on lignin oxidation is very scarce, and the available literature is mainly focused on the use of lignosulphonates that derive from sulphite pulping processes.

Prior to the starting point of this thesis, the Kraft lignin as the source of vanillin production has been researched at the LSRE, where the oxidation kinetics and the optimum reaction conditions were determined (Fargues et al., 1996a; Fargues et al., 1996b; Mathias, 1993; Mathias et al., 1995; Mathias and Rodrigues, 1995). Kraft lignin is obtained in a by-product stream (*black liquor*) of the Kraft pulp process, which is responsible for over 80% of the worldwide pulp production (Ullmann's Encyclopedia,

2003). For this reason, the attention of the work in this thesis was focused on the first step to achieve a complete continuous process – the reaction unit.

Batch experiments of lignin oxidation, with oxygen, were performed in a Büchi AG laboratory autoclave (model BEP280 type II, Switzerland) that includes a 1 litre cylindrical jacketed reactor prepared to handle temperatures up to 200ºC and pressures up to 13 bar. This setup was the same used by Álvaro Mathias with a new data acquisition system developed within this thesis. The purpose of these batch experiments was to determine the vanillin yield obtained with the Kraft lignin kindly supplied by Westvaco Co. (Indulin AT), and compare to the results achieved with different lignins in previous studies, but in similar operating conditions. The results revealed maximum vanillin yields with respect to the lignin mass around 3.5%, which is approximately half of the levels obtained before (Mathias, 1993). It is always important to notice that the reference to these yield values must be the one related to a complete extension of lignin oxidation - 13% obtained using nitrobenzene as oxidant. Since lignin is a natural polymer, its chemical structure can highly differ with the plant source, and also the treatments to recover this polymer from the pulping by-product streams can promote significant structural modifications. These facts can explain the lower vanillin yields achieved in this work, and an important sign of it is a higher lignin mean molecular weight than the one used in Mathias (1993).

Two different mathematical models were developed for the lignin oxidation in the batch reactor – one for isothermal conditions and other for non-isothermal conditions – the latter being an innovation to the work previously reported. These mathematical models were employed to describe batch measurements performed on this thesis and also to other experiments previously reported by Álvaro Mathias (Mathias, 1993). The kinetic study performed at the LSRE was the base for the models, with an

adjustment in two of the original parameter values, due to the different source of raw material. The adjusted parameters were referent to the ratio between the amount lignin oxidized and acid products formed ($Const$), and the activation energy for the lignin oxidation reaction (E_a/R). The experimental data collected allowed to estimate the heat of reaction for the lignin oxidation (ΔH_R^1) in a value of -29687 kJ mol^{-1}.

A complete and operational pilot installation to promote gas-liquid reactions, in a continuous operating mode, was designed and constructed during this thesis. This setup also allows the operation with different flow conditions, for example in semi-batch mode (closed to gas or liquid), and is prepared to work in very strong alkaline media (pH of 14), temperatures up to 170ºC and pressures up to 15 bar. The main piece of equipment of the apparatus is a jacketed bubble column reactor with a working capacity of approximately 8 litres. This reaction unit has an internal diameter of 10 cm, and its main cylindrical body could be used empty or filled with three modules of Mellapak 750.Y structured packing from Sulzer Chemtech (Switzerland).

Experiments of Kraft lignin oxidation and vanillin oxidation were performed in two different reactor configurations – structured packed bubble column reactor (SPBCR) and bubble column reactor (BCR) – to evaluate the performance of the unit and the increase of vanillin yield due to the structured packing internals. In this experimental work, the effect of some operating conditions was studied: the gas flow rate in the range of 250 to 3000 ml_{NTP}/min; oxygen partial pressure of 4 and 5 bar; and the liquid flow rate between 1 l/h and 4.7 l/h. For the lignin oxidation system, the higher value obtained for the vanillin concentration in the exit stream was 0.89 g/l. This result was achieved in an experiment using the SPBCR configuration, and operating with a liquid flow rate of 1 l/h, a gas flow rate of 2000 ml_{NTP}/min, and 5 bar of oxygen partial pressure. This value represents 11.4% of the maximum vanillin yield that can be

achieved from lignin oxidation. Since the lignin used in this thesis is different from the ones previously studied by Álvaro Mathias (Mathias, 1993), it must be pointed out that, most probably, the reference value for the maximum vanillin yield of the supplied Indulin AT would be lower than 13%, which could make the lignin conversion results obtained in this work more optimistic.

A complete mathematical model to describe the systems of vanillin oxidation and lignin oxidation in the continuous reactor was developed. This model is valid for both BCR and SPBCR reactor configurations. The necessary hydrodynamic parameters were also determined based on this model concept that included two compartments in series – axial piston dispersion flow for the column section followed by two small stirred tanks with dead volume for the separation head.

The model was fitted to the experimental results obtained in the BCR reactor configuration, using the oxygen stoichiometric coefficient in the lignin oxidation reaction as the fitting parameter. The value for this parameter was determined as 1.56. The same procedure was made for the lignin oxidation experiments in the SPBCR configuration, using the volumetric mass transfer coefficient ($k_L a$) as the fitting parameter for each experiment. It was verified that the liquid flow rate almost did not affected the value of $k_L a$, but the gas flow rate had a great influence on this mass transfer coefficient. For the lignin oxidation experiments in the SPBCR, the values of $k_L a$ were in the range of 3.80×10^{-4} to 8.05×10^{-4} s^{-1}. One of the main purposes to employ the structured packing was the enhancement of the mass transfer, when compared to the BCR configuration. This objective was achieved, although a very small increase of $k_L a$ was observed (1.35 times).

The influence of some operating conditions, namely the set point of the thermostatic bath, the gas and liquid feed flow rates, and the oxygen partial pressure,

were studied by simulation. The idea was to improve the levels of vanillin yield achieved in the experiments made in the continuous reactor, and to approach them to the ones obtained in the batch reactor for the same lignin source. According to this study, two sets of conditions were determined:

- The first set was obtained for similar conditions to the performed experimental work, using a 50/50 gas mixture of nitrogen and oxygen, except for the gas flow rate that was raised to increase the oxygen mass transfer coefficient ($k_L a$): liquid flow rate of 4 l/h; set point of the thermostatic bath in 433 K during the heating and pressurization, and 423 K during the reaction phase; oxygen partial pressure of 5 bar; total pressure of 10 bar; gas flow rate of 40000 ml_{NTP}/min; and $k_L a$ of 1×10^{-2} s^{-1}. The steady state vanillin concentration in the exit stream was 1.2 g/l, which is 15% of the maximum obtainable yield. This result is approximately 55% of the maximum levels of vanillin concentration obtained in the batch reactor.
- The second set maintained the gas flow rate and total pressure conditions, and to increase even more the oxidative capabilities of the media, it was considered the utilization of pure oxygen: liquid flow rate of 10 l/h; set point of the thermostatic bath of 433 K; oxygen partial pressure of 10 bar; total pressure of 10 bar; gas flow rate of 40000 ml_{NTP}/min; and $k_L a$ of 1.5×10^{-2} s^{-1}. The steady state vanillin concentration in the exit stream was 1.8 g/l, which is 23% of the maximum obtainable yield. This result is approximately 85% of the maximum levels of vanillin concentration obtained in the batch reactor, which represents a significant improvement.

The vanillin yield obtained in the batch experiments performed in this thesis was quite low, limiting strongly the operation of the continuous reactor. The levels of

vanillin yield obtained seems to be limited by the raw material used, possibly inappropriate for this application, and by the low rates of oxygen transfer to the liquid in the developed reaction unit. These two points are crucial for improving the vanillin formation from lignin.

6.2. Suggestions for future work

The suggestions for future work can be divided into three different paths:

Raw material

Like it was verified during this thesis, it could be a very important feature to have a deeper knowledge about the lignin molecule that is intended to use for vanillin production. It could be very interesting that this knowledge should not be limited to the mean molecular weight, but also investigate at the level of chemical structure – types and amounts of functional groups that could deviate the oxygen from the purpose of degrading the lignin molecule; ratio of lignin precursors, determined by NMR techniques, in order to choose a raw material that maximizes the number of appropriate monomers for vanillin production present in the lignin structure.

For each lignin source, it should be advisable to perform some batch reactor tests, to verify the necessity of some adjustments in the original parameters of the lignin oxidation kinetics.

Other aspects to consider about the raw material, in a perspective related to the integration in a pulp mill, could be the study of the chemical composition of the *black liquor* stream, and also the hypothesis of an ultra-filtration prior to the lignin oxidation

reactor to remove the bigger molecules to the burner and use the smaller lignin molecules, easier to degrade, for the vanillin production.

Vanillin quantification

The analytical procedures for the determination of vanillin concentration used in this thesis were based on Mathias (1993). These protocols were difficult to perform and very time consuming. Another issue to improve the work is the inspection of an easier, faster and more precise analytical process for vanillin quantification in the samples of lignin oxidation media.

Reactor unit and its parameters

At this point, one of the most important tasks related to the continuous reactor unit that remain to perform is a deeper experimental study about the hydrodynamics of the SPBCR configuration and its parameters (axial dispersion coefficient, gas and liquid hold-ups). As it was referred in Chapter 5, there is an almost inexistence of studies on bubble column reactors with structured packing internals and operating in up-flow mode, which leaves an open space for investigation.

Since one the main conclusions of this thesis is the necessity of increasing the levels of oxygen mass transfer for the liquid in the continuous reactor, some research could focused in two aspects: increase the $k_L a$ by making it possible to use higher levels of gas flow rate in the present reactor setup, or to discover some kind of packing and/or column internals that could be more efficient for the lignin oxidation system; increasing the levels of oxygen solubility by using higher values of oxygen partial pressure or even promote the application of a pure oxygen gas feed. A possibility could be the application of pure oxygen with a high gas flow rate (up to 4 or 5 l_{NTP}/min), in a

system with total gas recirculation and a makeup to replace the oxygen that is been consumed.

Referring to the oxygen solubility in the lignin oxidation media, due to its extreme importance it should not be excluded the idea of continuously measure the dissolved oxygen in the liquid in a future upgrade to the reactor unit.

6.3. References

1. Fargues, C.; Mathias, A.; Rodrigues, A. Kinetics of vanillin production from Kraft lignin oxidation. *Ind. Eng. Chem. Res.*, **1996a**, 35, 28-36.
2. Fargues, C.; Mathias, A.; Silva, J.; Rodrigues, A. Kinetics of vanillin oxidation. *Chem. Eng. Technol.*, **1996b**, 19 (2), 127-136.
3. Mathias, A. L. *Produção de vanilina a partir da lenhina: estudo cinético e do processo.* Ph.D. Dissertation, University of Porto, Portugal, **1993**.
4. Mathias, A. L.; Lopretti, M. I.; Rodrigues, A. E. Chemical and biological oxidation of *Pinus pinaster* lignin for the production of vanillin. *J. Chem. Tech. Biotechnol.*, **1995**, 64, 225-234.
5. Mathias, A. L.; Rodrigues, A. E. Production of vanillin by oxidation of pine Kraft lignins with oxygen. *Holzforschung*, **1995**, 49, 273-278.
6. *Ullmann´s Encyclopedia of Industrial Chemistry*; 7th Edition, Wiley-VCH, Verlag GmbH & Co..KGaA, **2003**.

Appendix A – Energy balance on the batch reactor

In this appendix is derived an equation to describe the energy balance of the lignin oxidation experiments on the batch reactor system presented in Chapter 3.

The unsteady state energy balance to the system can be written as (Fogler, 1992):

$$\begin{aligned} &energy\ accumulated = heat\ received - work\ done + \\ &energy\ entering\ by\ mass\ flow - energy\ leaving\ by\ mass\ flow \end{aligned} \tag{A.1}$$

Substituting the work term into (A.1) and knowing that:

$$E_i = H_i - PV_i \tag{A.2}$$

it results:

$$\left(\frac{dE}{dt}\right)_{sys} = Q - W_S + \sum F_i H_i\Big|_{in} - \sum F_i H_i\Big|_{out} \tag{A.3}$$

where Q is the heat received by the system from the surroundings; W_S is the shaft work; E_i, H_i, V_i and F_i are, respectively, the total energy, enthalpy of formation, specific volume and molar flow rate of each species.

Using (A.3) to substitute the energy accumulation term:

$$Q - W_S + \sum F_i H_i\Big|_{in} - \sum F_i H_i\Big|_{out} = \sum H_i \frac{dn_i}{dt} + \sum n_i \frac{dH_i}{dt} \tag{A.4}$$

The next step is to expand the terms of mass flow:

$$\sum F_i H_i\Big|_{in} = F_{O2}^{in}\ H_{O2}^{in} \tag{A.5}$$

$$\sum F_i H_i\big|_{out} = \frac{\Delta V_l}{\Delta t}\left(\frac{n_L}{V_l}\ H_L + \frac{n_V}{V_l}\ H_V + \frac{n_D}{V_l}\ H_D + \frac{n_{others}}{V_l}\ H_{others} + \frac{n_{H2O}}{V_l}\ H_{H2O} + \frac{n_{NaOH}}{V_l}\ H_{NaOH}\right) \tag{A.6}$$

The shaft work is assumed to be negligible and the mass balances of the water in the liquid phase, the oxygen in the gas phase, and other products of lignin oxidation are defined by:

$$\frac{dn^l_{H2O}}{dt} = -\frac{\Delta V_l}{\Delta t}\ \frac{n_{H2O}}{V_l} - \frac{dn^g_{H2O}}{dt} \tag{A.7}$$

$$\frac{dn^g_{O2}}{dt} = F^{in}_{O2} - \left(\upsilon_1\ r_1 + \upsilon_2\ r_2\right) V_l \tag{A.8}$$

$$\frac{dn_{others}}{dt} = n\ r_1\ V_l - \frac{\Delta V_l}{\Delta t}\ \frac{n_{others}}{V_l} \tag{A.9}$$

To express the accumulation of moles of water in the gas phase it is used the law of the ideal gases and (3.45):

$$\frac{dP_{H2O}}{dt} = \frac{-B_0}{\left(C_0 + T\right)^2}\ P_{H2O}\ \frac{dT}{dt} \tag{A.10}$$

$$\frac{dn^g_{H2O}}{dt} = \frac{d}{dt}\left(\frac{P_{H2O}\ V_g}{R\ T}\right) = \frac{V_g}{R\ T}\ \frac{dP_{H2O}}{dt} + \frac{P_{H2O}}{R\ T}\ \frac{dV_g}{dt} - \frac{P_{H2O}\ V_g}{R\ T^2}\ \frac{dT}{dt} = \left[\frac{-B_0}{\left(C_0 + T\right)^2} - \frac{1}{T}\right]\frac{V_g\ P_{H2O}}{R\ T}\ \frac{dT}{dt} + \frac{\Delta V_l}{\Delta t}\ \frac{P_{H2O}}{R\ T} \tag{A.11}$$

Knowing that $dH_i = Cp_i dT$, substituting (3.28) to (3.32) and (A.5) to (A.9), into (A.4), and rearranging:

$$Q - r_1 V_l \left(H_V - \alpha H_L + n H_{others} - \upsilon_1 H_{O2}\right) - r_2 V_l \left(H_D - H_V - \upsilon_2 H_{O2}\right) = \\ = \left(H^g_{H2O} - H^l_{H2O}\right) \frac{dn^g_{H2O}}{dt} + F^{in}_{O2} \left(H_{O2} - H^{in}_{O2}\right) + \sum n_i Cp_i \frac{dT}{dt} \quad \text{(A.12)}$$

It was assumed that the oxygen fed to the system suffers enthalpy variations from the ambient to the reaction conditions that are negligible comparing to the other terms in (A.12). Introducing the definitions of heat of reaction and heat of vaporization, and extending the last term to all the species present during lignin oxidation, this equation becomes:

$$Q - r_1 V_l \Delta H_{R,1} - r_2 V_l \Delta H_{R,2} = \\ = \lambda^{H2O}_{vap} \left(\left[\frac{-B_0}{\left(C_0 + T\right)^2} - \frac{1}{T} \right] \frac{V_g P_{H2O}}{R T} \frac{dT}{dt} + \frac{\Delta V_l}{\Delta t} \frac{P_{H2O}}{R T} \right) + \sum n_i Cp_i \frac{dT}{dt} \quad \text{(A.13)}$$

Nomenclature

A_0	parameter on the equation relating vapor pressure to temperature
B_0	parameter on the equation relating vapor pressure to temperature
Cp_i	heat capacity of species or substance i, J mol^{-1} K^{-1} or J kg^{-1} K^{-1}
C_0	parameter on the equation relating vapor pressure to temperature
E_i	total energy of species i, J/mol
F_i	molar flow rate of species i, mol/s
F^{in}_{O2}	molar flow rate of oxygen entering the system, mol/s
H_i	enthalpy of formation of species i, J/mol
H^{in}_{O2}	enthalpy of formation of the oxygen at the system inlet conditions, J/mol
n	"*others*" stoichiometric coefficient on the lignin oxidation reaction
n_i	number of moles of species i, mol

P total pressure, bar

P_i partial pressure of species i, bar

Q heat received by the system from the surroundings, W

r_1 rate of formation of vanillin, mol/s or mol/min

r_2 rate of oxidation of vanillin, mol/s or mol/min

R universal gas constant, l atm mol^{-1} K^{-1}

T reactor temperature, K

V_i specific volume of species i, m^3/mol

V_l volume of the liquid phase inside the reactor, m^3

V_g volume of the gas phase inside the reactor, m^3

W_S shaft work, W

Greek letters

$\Delta H_{R,1}$ heat of reaction of lignin oxidation, J/mol

$\Delta H_{R,2}$ heat of reaction of vanillin oxidation, J/mol

Δt time interval between collection of two consecutive liquid samples, s

ΔV_l volume of liquid taken from the system in each sample collection, m^3

α lignin stoichiometric coefficient on the lignin oxidation reaction

υ_1 oxygen stoichiometric coefficient on the lignin oxidation reaction

υ_2 oxygen stoichiometric coefficient on the vanillin oxidation reaction

λ_{vap}^{H2O} heat of vaporization of water, J/mol

Subscripts

D	vanillic acid
g	gas phase
$H2O$	water
l	liquid phase
L	lignin
$NaOH$	sodium hydroxide
$others$	intermediates that can be formed during lignin degradation
$O2$	oxygen
V	vanillin

Superscripts

g	gas phase
l	liquid phase

References

1. Fogler, H. S. *Elements of Chemical Reaction Engineering* (2nd Edition), Prentice Hall International, USA, **1992**.

Appendix B – Experimental determination of the mean molecular weight of Kraft lignin

The mean molecular weight of the Kraft lignin used in this thesis was experimentally determined by high-performance liquid chromatography (HPLC), more specifically by a GPC (gel permeation chromatography) technique. This technique is the most versatile to determine the molecular mass of polymer samples. It involves the flow through a tubular column of a diluted solution in an organic solvent of the polymer to analyze. The column is packed with particles of a reticulated polymeric gel and the flow is promoted under high pressure conditions.

The GPC technique is based on the principle that the retention time of a polymer chain inside the column depends on the path it takes through the gel. For example, an oligomer of low molecular weight is forced to enter into the pores of the gel, reaching the end of the column through a very sinuous path. On the other hand, a species with high molecular weight is excluded from the gel pores, travelling through a much shorter distance until it exits the column.

B.1. Experimental

HPLC setup

The determination of the mean molecular weight of lignin was performed on a HPLC system from Gilson (Middleton, USA). This system consists on a manometric module (model 805), a pump (model 305) and a UV spectrophotometric detector (model 115). The correspondent system for data acquisition and control is a Gilson 712 HPLC.

It was used a set of chromatographic columns from Polymer Laboratories (Amherst, USA) placed in series to enhance the resolution of the results. This set included a PL gel pre-column with 3 μm packing, followed by a PL gel column with 5 μm packing (type mixed D), and finally two PL gel columns with 3 μm packing (type mixed E).

Experimental procedure

The protocol followed for the determination of the Kraft lignin molecular weight is similar to the one presented in Mathias's thesis (Mathias, 1993) for the same purpose. The Kraft lignin analyzed is called Indulin AT supplied by Westvaco Co. (Virginia, USA). This lignin is derives from the Kraft pulping of the softwood *Pinus spp*.

In a first step, it was prepared an aqueous solution with 60 g/l of Indulin AT and 80 g/l of sodium hydroxide. A sample of 100 μl from this solution was transferred to a glass tube with cap and added 100 μl of HCl 2.5 N. The mixture was agitated during 15 seconds, using a vortex tube agitator at maximum speed. Then, 2.5 ml of tetrahydrofuran (THF) were added and the mixture was agitated in a similar manner during 60 seconds. The final mixture was centrifuged at 1000 rpm, during 5 minutes, developing two distinct phases.

The pump was turned on, feeding the mobile phase (tetrahydrofuran) through the set of columns. With the help of a syringe, the 50 μl injection loop of the HPLC system was filled with organic phase formed in the centrifugation step. Then, the flow of the mobile phase was deviated to the injection loop, dragging the sample through the set of columns, and simultaneously the data acquisition of the UV detector was started up. The conditions of the HPLC analysis are presented in Table B.1.

Table B.1. Operating conditions for the HPLC analysis.

Mobile phase	THF	Q_{MP}	1 ml/min
Temperature	ambient	Injection volume	50 µl
λ_d	254 nm	ΔP_m	126 bar

Calibration curve

In order to build a calibration curve relating molecular mass to the retention time in the columns, it was prepared several solutions of standard polystyrene with different molecular weights (Polymer Laboratories, USA) in tetrahydrofuran solvent. These organic solutions were processed in the HPLC system like the protocol described above and in the same analysis conditions presented in Table B.1. The concentrations of the polystyrene solutions in THF were in the range of 0.3-0.7 % in weight. The resulting calibration curve is presented in Figure B.1.

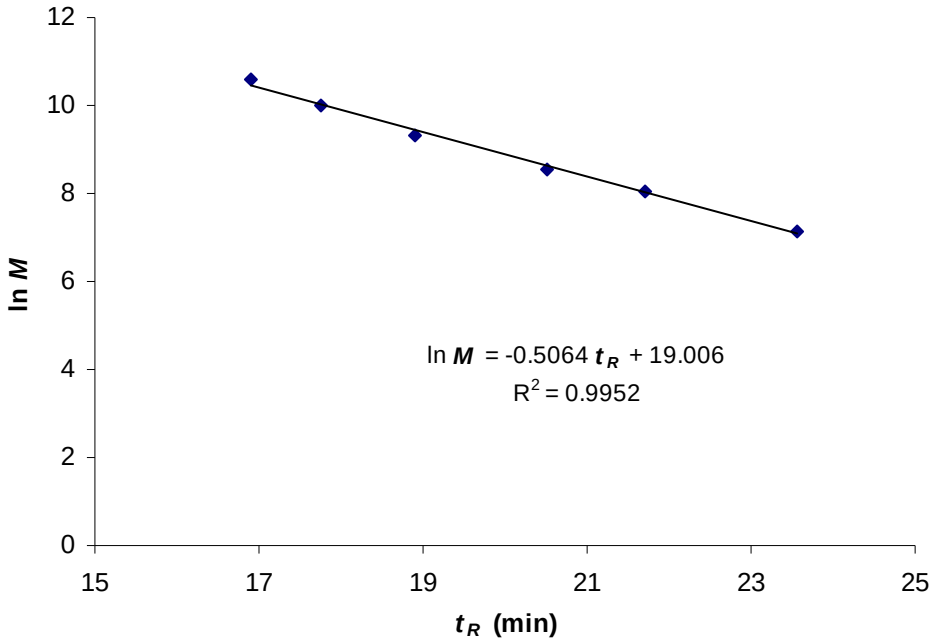

Figure B.1. Calibration curve of molecular weight versus retention time in the HPLC columns. The analysis conditions are in Table B.1.

B.2. Results

The experimental data collected by the acquisition system is the signal of the detector, in mV, as a function of the retention time, in minutes. The system response in the analysis of the Indulin AT sample is presented in Figure B.2.

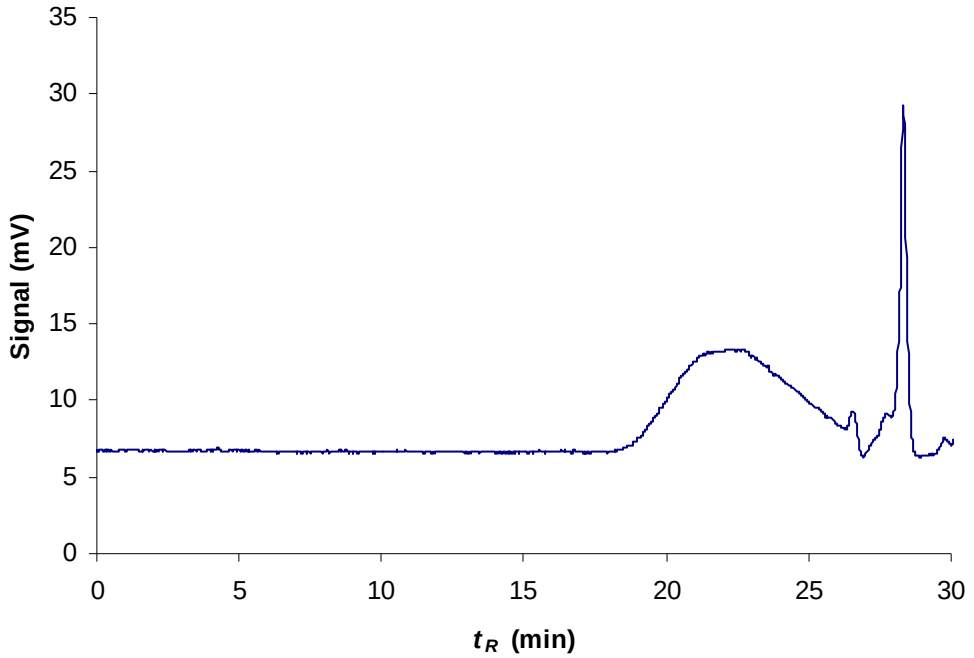

Figure B.2. Curve of the HPLC detector signal versus retention time in the Indulin AT analysis. The conditions of analysis are in Table B.1.

The raw data shown in Figure B.2 must be treated with the purpose of achieving an experimental value for the mean molecular weight of Indulin AT.

First, it was necessary to normalize the curve of the detector signal to obtain the correspondent density function, $P(t_R)$:

$$P(t_R) = \frac{Signal(t_R)}{\int_0^\infty Signal(t_R)dt_R} \tag{B.1}$$

Using the molecular weight dependency on the retention time, described by the calibration curve, the function $P(t_R)$ was transformed in the density function referent to the molecular weight, $P^*(M)$:

$$P(t_R)dt_R = P^*(M)dM \Leftrightarrow P^*(M) = P(t_R)\left|\frac{dt_R}{dM}\right| = \frac{1}{0.5064M}P(t_R) \quad \text{(B.2)}$$

With the function $P^*(M)$ it was possible to calculate the numbered mean molecular weight, $\overline{M}_n$, and the weighted mean molecular weight, $\overline{M}_w$:

$$M_n = \frac{\int_0^\infty P^*(M)\cdot M\cdot dM}{\int_0^\infty P^*(M)\cdot dM} \quad \text{(B.3)}$$

$$M_w = \frac{\int_0^\infty P^*(M)\cdot M^2\cdot dM}{\int_0^\infty P^*(M)\cdot M\cdot dM} \quad \text{(B.4)}$$

The main results obtained in this HPLC analysis are presented on Table B.2.

Table B.2. Final results of the HPLC analysis.

Sample	M_n	M_w	M_w / M_n
Kraft lignin (Indulin AT)	2325	5062	2.18

Nomenclature

Q_{MP} flow rate of the mobile phase

M molecular weight

M_n numbered mean molecular weight

M_w weighted mean molecular weight

t_R retention time in the set of columns

Greek letters

ΔP_m medium pressure drop in the set of columns

λ_d wavelength of the UV detector

References

1. Mathias, A. L. *Produção de vanilina a partir da lenhina: estudo cinético e do processo.* Ph.D. Dissertation, University of Porto, Portugal, **1993**.

Appendix C – Experimental determination of the viscosity and density of the Kraft lignin solutions

C.1. Viscosity of the aqueous Kraft lignin solutions

The objective was to measure the viscosity of the liquid mixture used in the lignin oxidation experiments, performed in the batch and the continuous reactor, and presented in Chapter 3 and 5, respectively.

Equipment

The experimental determination of the viscosity of the Kraft lignin solution was made in a Brookfield viscometer, model LV (Brookfield Engineering Laboratories, USA). The temperature of the lignin solution was controlled by a thermostatic bath (JP Selecta, Spain) with water as the heating fluid. This equipment can perform viscosity measurements to temperatures up to approximately 80ºC.

Experimental procedure

It was prepared 500 ml of an aqueous solution containing 60 g/l of Indulin AT and 80 g/l of sodium hydroxide. This solution was transferred to a beaker of 600 ml and placed in the thermostatic bath.

Once the solution reached a thermal equilibrium, the beaker was placed under the viscometer and its spindle was immersed in the solution. The spindle number 1 was the appropriate for the viscosity range of the sample. The viscometer was turned on and the spindle started to rotate. The viscosity value was read after the rotation speed of the spindle stabilized (it took approximately 1 minute).

This procedure was repeated for three different temperatures of the liquid mixture.

Results

The viscosity of the Kraft lignin solution was measured for three different temperatures and the results are presented in Table C.1.

Table C.1. Viscosity of the Kraft lignin solution.

Temperature (ºC)	Viscosity (cP)	Viscosity (kg m^{-1} s^{-1})
30	4	4×10^{-3}
55	3	3×10^{-3}
75	2.5	2.5×10^{-3}

These results can be used to build a relation between temperature and viscosity based on the Andrade's equation (Poling, Prausnitz and O'Connell, 2001).

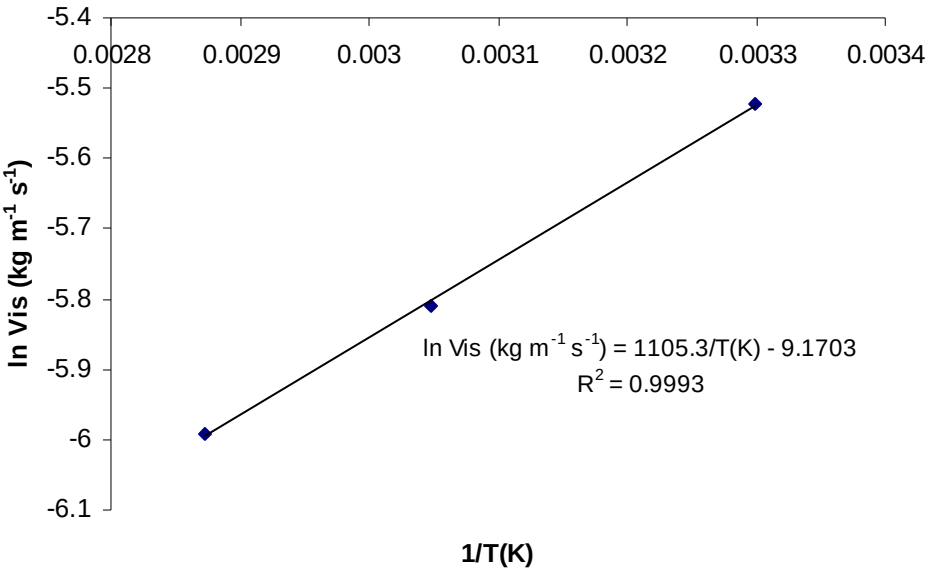

Figure C.1. Results obtained in the viscosity measurements of the Kraft lignin solutions and its dependency with temperature.

With the relation presented in Figure C.1 it can be extrapolated the viscosity of the Kraft lignin solutions in the temperature range of the lignin oxidation experiments.

C.2. Density of the aqueous Kraft lignin solutions

The density of the Kraft lignin solutions used in the lignin oxidation experiments was measured using the pycnometer method.

Experimental procedure

The mass of a 100 ml empty pycnometer was measured in an electronic balance. The pycnometer was filled with the liquid sample and placed in a thermostatic bath to reach a final equilibrium temperature of 30ºC. The mass of the set pycnometer plus liquid sample was also measured in the same electronic balance.

Results

The liquid density was calculated by:

$$\rho_l = \frac{mass\ of\ the\ set - mass\ of\ the\ pycnometer}{pycnometer\ volume} = 1114\ \text{kg m}^{-3}$$

References

1. Poling, B. E.; Prausnitz, J. M.; O'Connell, J. P. *The properties of gases and liquids* (5th Edition), McGraw Hill, USA, **2001**.

Appendix D – Heat capacities of lignin, vanillin and vanillic acid

The heat capacities of lignin, vanillin and vanillic acid used in this work were estimated with the help of the Missenard group additivity method (Poling, Prausnitz and O'Connell, 2001). It was applied a structural model of Kraft lignin presented on Figure D.1 (Knowles, 1998). This molecule and also vanillin and vanillic acid were divided into groups, according to the Missenard method, and predicted their liquid heat capacities for different temperatures. Some of these values are shown on Table D.1 to D.3.

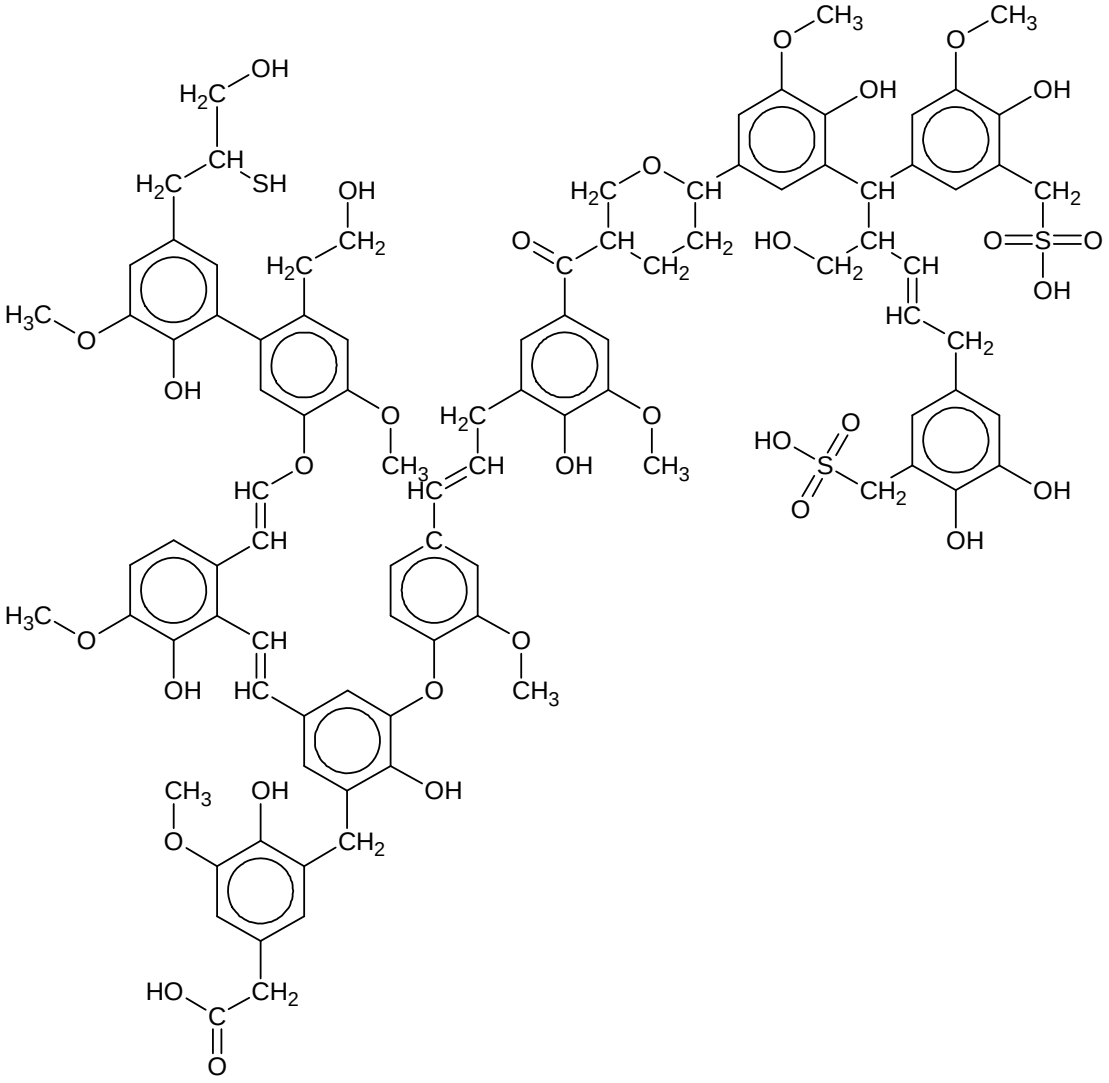

Figure D.1. Structural model of Kraft lignin.

Table D.1. Values used on estimating the heat capacity of Kraft lignin with the Missenard method (Poling, Prausnitz and O'Connell, 2001).

Heat capacity at 50ºC			
Groups	Nº of groups	Individual contribution (cal mol^{-1} K^{-1})	Total contribution (cal mol^{-1} K^{-1})
COOH	1	20	20
H	-28	3.7	-103.6
O	15	7.2	108
CH3	8	10.4	83.2
OH	14	12.5	175
C6H5	10	29.5	295
CH2	14	6.95	97.3
CH	5	6.15	30.75
CtC	4	11	44
CO	1	10.6	10.6
S	3	9.4	28.2
		Cp_{KL} (cal mol^{-1} K^{-1})	788.45
		Cp_{KL} (J mol^{-1} K^{-1})	**3298.95**
Heat capacity at 100ºC			
Groups	Nº of groups	Individual contribution (cal mol^{-1} K^{-1})	Total contribution (cal mol^{-1} K^{-1})
COOH	1	22.5	22.5
H	-28	4.5	-126
O	15	7.4	111
CH3	8	11.55	92.4
OH	14	17	238
C6H5	10	32.5	325
CH2	14	7.4	103.6
CH	5	6.7	33.5
CtC	4	11	44
CO	1	11	11
S	3	9.8	29.4
		Cp_{KL} (cal mol^{-1} K^{-1})	884.4
		Cp_{KL} (J mol^{-1} K^{-1})	**3700.42**

Table D.2. Values used on estimating the heat capacity of vanillin with the Missenard method (Poling, Prausnitz and O'Connell, 2001).

Heat capacity at 25ºC			
Groups	Nº of groups	Individual contribution (cal mol^{-1} K^{-1})	Total contribution (cal mol^{-1} K^{-1})
CO	1	10.4	10.4
H	-1	3.5	-3.5
O	1	7.1	7.1
CH3	1	9.95	9.95
OH	1	10.5	10.5
C6H5	1	28	28
		Cp_V (cal mol^{-1} K^{-1})	62.45
		Cp_V (J mol^{-1} K^{-1})	**261.30**
Heat capacity at 75ºC			
Groups	Nº of groups	Individual contribution (cal mol^{-1} K^{-1})	Total contribution (cal mol^{-1} K^{-1})
CO	1	10.8	10.8
H	-1	4	-4
O	1	7.3	7.3
CH3	1	10.95	10.95
OH	1	14.75	14.75
C6H5	1	31	31
		Cp_V (cal mol^{-1} K^{-1})	70.8
		Cp_V (J mol^{-1} K^{-1})	**296.23**
Heat capacity at 100ºC			
Groups	Nº of groups	Individual contribution (cal mol^{-1} K^{-1})	Total contribution (cal mol^{-1} K^{-1})
CO	1	11	11
H	-1	4.5	-4.5
O	1	7.4	7.4
CH3	1	11.55	11.55
OH	1	17	17
C6H5	1	32.5	32.5
		Cp_V (cal mol^{-1} K^{-1})	74.95
		Cp_V (J mol^{-1} K^{-1})	**313.60**

Table D.3. Values used on estimating the heat capacity of vanillic acid with the Missenard method (Poling, Prausnitz and O'Connell, 2001).

Heat capacity at 25ºC			
Groups	Nº of groups	Individual contribution (cal mol^{-1} K^{-1})	Total contribution (cal mol^{-1} K^{-1})
COOH	1	18.8	18.8
H	-2	3.5	-7
O	1	7.1	7.1
CH3	1	9.95	9.95
OH	1	10.5	10.5
C6H5	1	28	28
		Cp_D (cal mol^{-1} K^{-1})	67.35
		Cp_D (J mol^{-1} K^{-1})	**281.80**
Heat capacity at 75ºC			
Groups	Nº of groups	Individual contribution (cal mol^{-1} K^{-1})	Total contribution (cal mol^{-1} K^{-1})
COOH	1	21.5	21.5
H	-2	4	-8
O	1	7.3	7.3
CH3	1	10.95	10.95
OH	1	14.75	14.75
C6H5	1	31	31
		Cp_D (cal mol^{-1} K^{-1})	77.5
		Cp_D (J mol^{-1} K^{-1})	**324.27**
Heat capacity at 100ºC			
Groups	Nº of groups	Individual contribution (cal mol^{-1} K^{-1})	Total contribution (cal mol^{-1} K^{-1})
COOH	1	22.5	22.5
H	-2	4.5	-9
O	1	7.4	7.4
CH3	1	11.55	11.55
OH	1	17	17
C6H5	1	32.5	32.5
		Cp_D (cal mol^{-1} K^{-1})	81.95
		Cp_D (J mol^{-1} K^{-1})	**342.89**

The molecule model represented on Figure D.1 has a molecular weight of 1876. It was considered that the Indulin AT used in this work has a structure similar to this model, however it is a molecule slightly bigger. A prediction of Cp_L can be obtained by:

$$Cp_L = Cp_{KL} \frac{M_n}{1876} \quad \text{(D.1)}$$

where Cp_{KL} is the estimated heat capacity of the Kraft lignin structural model. It was established a linear relation between Cp_{KL} and T:

$$Cp_{KL} = 8.0812\ T + 688.73 \quad \text{(D.2)}$$

Regarding Cp_V and Cp_D values obtained by the Missenard method, it was also established a relation between the heat capacities and T:

$$Cp_V = 0.6996\ T + 52.54 \quad \text{(D.3)}$$

$$Cp_D = 0.8218\ T + 36.93 \quad \text{(D.4)}$$

References

1. Knowles, D. A. *Chemistry and Technology of Agrochemical Formulations*, Kluwer Academic Publishers, United Kingdom, **1998**.
2. Poling, B. E.; Prausnitz, J. M.; O'Connell, J. P. *The properties of gases and liquids* (5th Edition), McGraw Hill, USA, **2001**.

Appendix E – Heat of formation of vanillin and vanillic acid

The heats of formation of vanillin and vanillic acid in the solid phase, at 25ºC, were estimated using a method based on Benson´s group additivity technique (Salmon and Dalmazzone, 2006). The vanillin and vanillic acid molecules were divided into the appropriate groups presented on Table E.1 and E.2, according to the Benson technique.

Table E.1. Values used on estimating the heat of formation of vanillin with the Benson method (Salmon and Dalmazzone, 2006).

Vanillin heat of formation at 25ºC			
Groups	Nº of groups	Individual contribution (kJ mol^{-1})	Total contribution (kJ mol^{-1})
CO(Cb)(H)	1	-29.2	-29.2
Cb(CO)	1	-110.5	-110.5
Cb(H)	3	3.1	9.3
Cb(O)	2	-67.9	-135.8
O(Cb)(C)	1	-51	-51
C(O)(H)3	1	-41.4	-41.4
O(Cb)(H)	1	-125.9	-125.9
ortho correction	1	-1.2	-1.2
meta correction	1	0	0
		$\Delta H_f^{25^\circ C}$ (kJ mol^{-1})	**-485.7**

Table E.2. Values used on estimating the heat of formation of vanillic acid with the Benson method (Salmon and Dalmazzone, 2006).

Vanillic acid heat of formation at 25ºC			
Groups	Nº of groups	Individual contribution (kJ mol^{-1})	Total contribution (kJ mol^{-1})
CO(O)(Cb)	1	-86.7	-86.7
O(CO)(H)	1	-212.4	-212.4
Cb(CO)	1	-110.5	-110.5
Cb(H)	3	3.1	9.3
Cb(O)	2	-67.9	-135.8
O(Cb)(C)	1	-51	-51
C(O)(H)3	1	-41.4	-41.4
O(Cb)(H)	1	-125.9	-125.9
ortho correction	1	-1.2	-1.2
meta correction	1	0	0
		$\Delta H_f^{25^\circ C}$ (kJ mol^{-1})	**-755.6**

References

1. Salmon, A.; Dalmazzone, D. Prediction of enthalpy of formation in the solid state (at 298.15 K) using second-order group contributions. Part 1. Carbon-hydrogen and carbon-hydrogen-oxygen compounds. *J. Phys. Chem. Ref. Data*, **2006**, 35 (3), 1443-1457.